Australian Centre for Advanced Photovoltaics

UNSW SYDNEY

Annual Report 2023

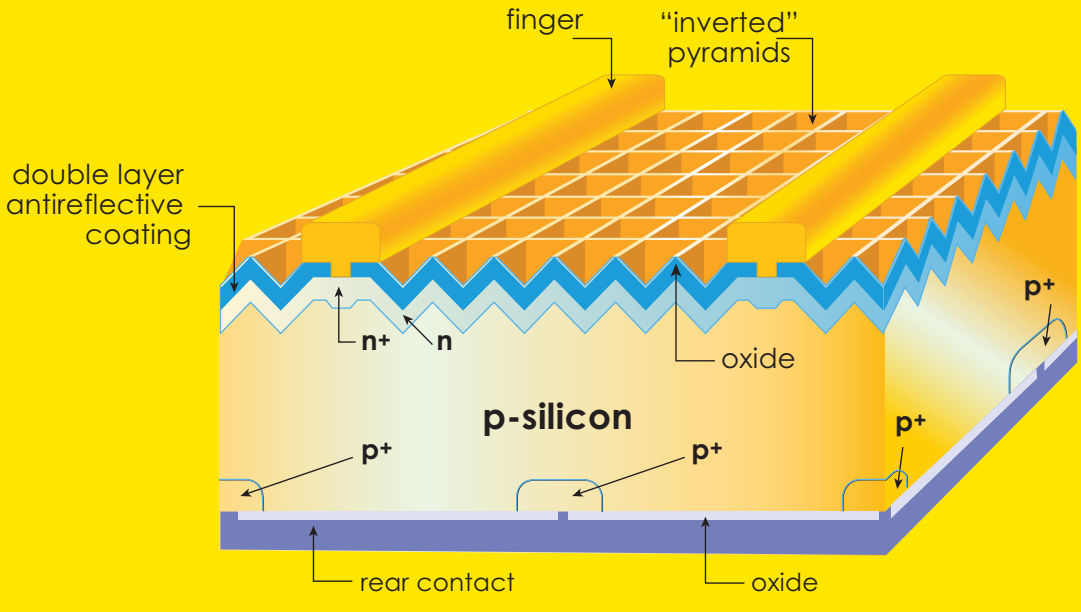

acap.org.au

Acknowledgements

This Project received funding from the Australian Renewable Energy Agency (ARENA).

Written and compiled by
Australian Centre for Advanced Photovoltaics

Edited by
Richard Corkish
PP1: Kean Chern Fong, Moonyong Kim
PP2: Anthony Chesman
PP3: Klaus Weber
PP4: Chandany Sen
PP5: Nathan Chan
PP6: Richard Corkish, Renate Egan, Andrew Blakers

Photos, figures and graphs
Courtesy of Centre staff and students; others as acknowledged in captions.

Cover image
Professor Martin Green, Professor Andrew Blakers, Dr Jianhua Zhao & Dr Aihua Wang received the Queen Elizabeth Prize for Engineering for their development of the PERC Solar Cell.

(LtoR): Professor Martin Green, QEPrize Chairman Lord Browne of Madingley, His Majesty The King, Dr Jianhua Zhao, Dr Masato Sagawa, 2022 awardee, Professor Andrew Blakers, Dr Aihua Wang and Dame Lynn Gladden, Chair of the QEPrize Judges

Photograph: Jason Alden/QEPrize

Queen Elizabeth Prize for Engineering

Contract Number
2013/ASI015

Project title
UNSW, Photovoltaic Strategic Research Initiative, Australian Centre for Advanced Photovoltaics (ACAP) Project

TABLE OF CONTENTS

01 DIRECTOR'S REPORT 2

02 HIGHLIGHTS 4

03 ORGANISATIONAL STRUCTURE AND RESEARCH OVERVIEW 14

04 AFFILIATED STAFF AND STUDENTS 18

05 RESEARCH REPORTS

- Program Package 1 Silicon Materials 24
- Program Package 2 Emerging Materials 54
- Program Package 3 Tandem Solar Cells 88
- Program Package 4 Device To Module 102
- Program Package 5 Manufacturing And Sustainability 116
- Program Package 6 PV Futures And Knowledge Sharing 130

06 COLLABORATIVE ACTIVITIES

- Collaboration Grants 142
- Fellowships 154
- Infrastructure Grants 158

07 FINANCIAL SUMMARY 160

08 PUBLICATIONS 162

ACAP
DIRECTOR'S REPORT

Solar photovoltaics (PV) is transforming our energy system, industries, transport and the way we live. Today, electricity from PV is competitive with residential and commercial electricity pricing at the point of use (on rooftops), where it is widely deployed in Australia today. As a result, PV is now the fastest growing source of new energy generation, with early estimates of over 400 GW installed worldwide in 2023.

In Australia, another 4 GW of solar was installed in 2023, resulting in a total of more than 34 GW of solar installed, retaining Australia's global leadership in installed solar per capita. As a result, 18% of Australia's total electricity demand on the National Electricity Market was met by solar PV in 2023. With wind and pumped hydro, Australia is now meeting close to 40% of its electricity needs from renewables.

While the technology of today works, and we should be deploying it as fast as we can, in doing so, we will continue to learn and improve. At the same time, to drive the zero-emissions economy of the future that will see Australia as a renewable energy superpower, we need to push solar technologies even further and the costs even lower.

In 2022, the Australian Renewable Energy Agency (ARENA) laid out its vision for PV in a White Paper on Ultra Low Cost Solar. By 2030, ARENA wants commercial solar cells to hit 30% efficiency, up from 22% today. It wants large-scale, full-system costs (panels and inverters) to fall by 50% to 30 cents per watt. In achieving these ambitious goals, the cost of electricity would be as low as $15/MWh, opening vast opportunities in green industrial processing, such as green-steel and green-ammonia. The goal is ambitious but achievable.

To help achieve these targets, in 2022, the Australian Federal Minister for Climate Change and Energy, Chris Bowen, announced $45 million in funding to extend the research program at the Australian Centre for Advanced Photovoltaics (ACAP) out to 2030. Now known as ACAP2.0, activities are co-funded by ARENA, UNSW, partner universities, research institutions and industry, with more than 250 Australian researchers already working to achieve the 30:30:30 goals.

The program of work under ACAP2.0 has been renewed to reflect the 30:30:30 goals and Australia's ambition to be a renewable energy superpower. Objectives and tasks include:

- To deliver an improvement in efficiency to over 30%, we need to build on the silicon solar cell, adding a second material to make a tandem cell, that can make the most of the available energy in sunlight;
- To deliver high efficiency tandem solar cells, research is focused on finding the best material combination and on developing the best device structures;
- To ensure emerging solar cell technologies are reliable and durable, ACAP is working on module assembly technologies, answering research questions on the robust interconnection of the individual cells and encapsulating these cells to deliver long operating lifetimes;
- To drive down the cost, we remain focused on the manufacturability of new technologies and are working with industry on scaling up innovation;
- To ensure we can reach the scales needed to deliver terawatts of solar power, we are looking into the materials used to make sure this can be done sustainably, and what to do with solar module technologies when they reach their end of life;
- To accelerate the transition, we aim to provide high quality training opportunities for the next generation of photovoltaic researchers and to share knowledge with stakeholders including energy consumers, industry and policymakers.

This 2023 Annual Report surveys progress and key developments during the year, summarised in the highlight pages and detailed in the following chapters and these contributed to making 2023, once again, an extremely successful year for ACAP.

Over its first decade, ACAP moved effectively to establish a high profile within the international research community. This is evidenced by the string of independently confirmed world records for energy conversion efficiency in efforts led by different nodes and for several different technologies since ACAP's commencement. These include records for rear-junction silicon cells (ANU: 24.4%, 2013), overall sunlight to electricity conversion (UNSW: 40.4%, 2014; 40.6%, 2016), one-sun mini-module (UNSW: 34.5%, 2016), small-area "thin-film" CZTS (Cu_2ZnSnS_4) cells (UNSW: 9.5%, 2016; 11.0%, 2017), > 1 cm^2 CZTS cells (UNSW: 10.0%, 2017), perovskite mini-modules (UNSW: 11.5%, 2016), > 1 cm^2 perovskite cells (UNSW: 18.0%, 2016; 19.6%, 2017; ANU: 21.6%, 2019; 22.6%, 2020) and III-V tandem cells (NREL/UNSW: 32.9%, 2021). In ACAP2.0, performance improvement continues in 2023 with a new benchmark in a high bandgap CZTS solar cell (> 1.5 eV), suitable for the top cell over a silicon bottom cell in a tandem structure, achieved with 11.4% efficiency (UNSW 2023), showing important progress in an emerging material with potential applications in tandem solar cells.

In addition to performance benchmarks, the long tradition of international impact continues. Notably, ACAP leaders Professor Martin Green from UNSW Sydney and Professor Andrew Blakers from the Australian National University were recognised with the award of the 2023 Queen Elizabeth Prize for Engineering. The prize is the leading award internationally for engineering and recognises the pioneering work of professors Green and Blakers, along with solar entrepreneurs Dr Aihua Wang and Dr Jianhua Zhao, who developed the Passivated Emitter and Rear Cell (PERC) solar photovoltaic technology, which has underpinned the exponential growth in high performance, low-cost solar electricity. In addition, ACAP's founding director Scientia

Professor Martin Green was inducted into the United States National Academy of Engineering (NAE) in October 2023 for technical contributions that have enabled the widespread use of silicon photovoltaics and Professor Anita Ho-Baillie, Principal Investigator in ACAP2.0 for The University of Sydney, was elected a Fellow of the UK's Royal Society of Chemistry.

The outstanding work reported under ACAP is made possible through the vision and commitment within ARENA, who recognise the benefit of long-term investment in research. ARENA contribute through the funding for the research program plus formally and informally through participation in informing the research direction, industry partnerships, knowledge sharing and program governance. This support by ARENA, backed by UNSW and our research and industry partners, makes the outstanding research reported here possible.

I'd like to thank and acknowledge the significant effort by ACAP researchers for their contributions to the broad range of progress reported in the following pages. Of note Professor Andrew Blakers, who this year handed leadership of the ANU node of ACAP to Professor Daniel Macdonald. Andrew remains involved with ACAP on the Technical Advisory Committee.

Importantly, I would like to recognise the leadership and vision of Professor Martin Green, founding Centre Director. His leadership in solar research is world-renowned and it remains a great privilege to continue to work with him on the Technical Advisory Committee to ACAP as I take on the role of Executive Director, working alongside Dr Richard Corkish as Chief Operating Officer to deliver the ACAP2.0 Program.

Finally, I am pleased to be able to report that ACAP has taken another major step towards attaining its significant long-term objective of delivering ultra-low-cost solar, by achieving its milestones on time and within budget. I look forward to seeing similar progress in 2024 and subsequent years.

PROFESSOR RENATE EGAN
Executive Director, 2023

2023
HIGHLIGHTS

HIGH IMPACT PAPERS

PA paper by UNSW node authors, Daniel Chen, Michelle Vaqueiro Contreras, Alison Ciesla, Phillip Hamer, Brett Hallam, Malcolm Abbott and Catherine Chan, entitled "Progress in the understanding of light- and elevated temperature-induced degradation in silicon solar cells: A review" was the top-cited article in that leading journal for the period 1 January 2021 – 15 December 2022.

A set of 2023 papers was selected as sufficiently timely and interesting to provide the cover illustration for some of the field's most prestigious journals. One article, including the Chief Investigator for the Monash node team, Udo Bach, with first author Rui Zhi, from the Wuhan University of Technology, and a team of others from the Wuhan University of Technology, the Advanced Energy Science and Technology Guangdong Laboratory and Hubei University of Arts and Science, reported that intragrain planar defects in formamidinium lead iodide ($FAPbI_3$) precursor solution can be strongly reduced by adding phenyl ethylammonium lead iodide (PEA_2PbI_4) and fully eliminated by adding further methylammonium chloride (MACl). As a result, a champion efficiency of 23.69% was achieved, with an improvement of humidity stability. (Zhi, R., Yang, C.-Q., Rothmann, M. U., Du, H.-Q., Jiang, Y., Xu, Y.-Y., Yin, Z.-W., Mo, Y.-P., Dong, W., Liang, G., Bach, U., Cheng, Y.-B. & Li, W. (2023). Direct Observation of Intragrain Defect Elimination in FAPbI3 Perovskite Solar Cells by Two-Dimensional PEA_2PbI_4. ACS Energy Letters 8, 2620-2629. (Figure 2.1(a).)

In another, (Figure 2.1(b)), a UNSW PhD student Eunyoung Choi, with a team of colleagues from UNSW, Korea Research Institute of Chemical Technology (KRICT), Chungnam National University and University of Cambridge, reported that devices incorporating AlO_x on OAI-treated perovskite (OAI/AlO_x) showed enhanced device performance and photo-stability. As a result, the > 24% efficiency devices retained their efficiency over 1000 hours under continuous light illumination. (Choi, E., Lee, J.-W., Anaya, M., Mirabelli, A., Shim, H., Strzalka, J., Lim, J., Yun, S., Dubajic, M., Lim, J., Seidel, J., Agbenyeke, R. E., Kim, C. G., Jeon, N. J., Soufiani, A. M., Park, H. H. & Yun, J. S. Synergetic Effect of Aluminum Oxide and Organic Halide Salts on Two-Dimensional Perovskite Layer Formation and Stability Enhancement of Perovskite Solar Cells. Advanced Energy Materials, 2301717 (Figure 2.1(b).)

In a third cover article, a team from UNSW, University of Sydney, Macquarie University and University of Technology Sydney, reported deposition of perovskite solar cells with 17.1% efficiency on steel. The team believed this to be the highest reported for perovskite cells on steel. (Zheng, J., Ma, F. J., Liao, C., Bing, J., Tang, S., Soufiani, A. M., Chin, R. L., Xue, C., Qu, J., Yang, L., Mahmud, Md A., Sun, Z., Leung, T. L,. Wang, G., Cairney, J. M., Bremner, S., McKenzie, D. R., Huang, S., Ho-Baillie, A. W. Y. (2023). Efficient perovskite solar cell on steel enabled by diffusion barrier and surface passivation. Cell Reports Physical Science 4(9), 101543.)

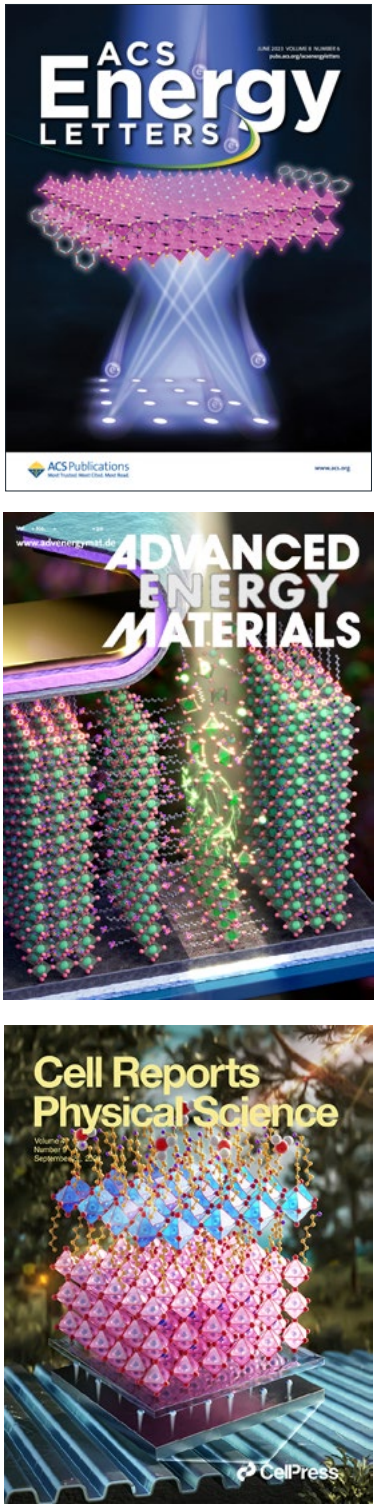

Figure 2.1 (a–c): Cover illustrations for ACAP publication in some of the field's most prestigious journals.

TECHNICAL HIGHLIGHTS

NEW CERTIFIED RECORD EFFICIENCY FOR HIGH-BANDGAP CZTS SOLAR CELLS AT 11.4% (CD-FREE)

In research aimed at revealing the role of Ag alloying in metal precursors in $Cu_2ZnSn(S,Se)_4$ thin films and solar cells, a certified efficiency record of 11.4% was achieved for a 0.2 cm^2 cell. This is a high bandgap kesterite solar cell (> 1.5 eV), suitable for the top cell over a silicon bottom cell in a tandem structure. The addition of silver (Ag) to the kesterite-structured material has led to a significant improvement in the quality of the absorber layer. This facilitated increased grain size, which primarily contributed to the observed improvement in performance. Additionally, a deliberate adjustment of the sulfur (S) distribution to create a gradual change in the bandgap towards the back contact was implemented in the Ag alloyed CZTSSe thin film, which contributed to a higher short-circuit current (J_{SC}) value. These findings provide valuable insights into the detailed mechanisms behind the positive influence of silver on kesterite solar cells and suggest a promising approach for enhancing their overall performance. As a bonus, this device is Cd-free. See section PP2.4.

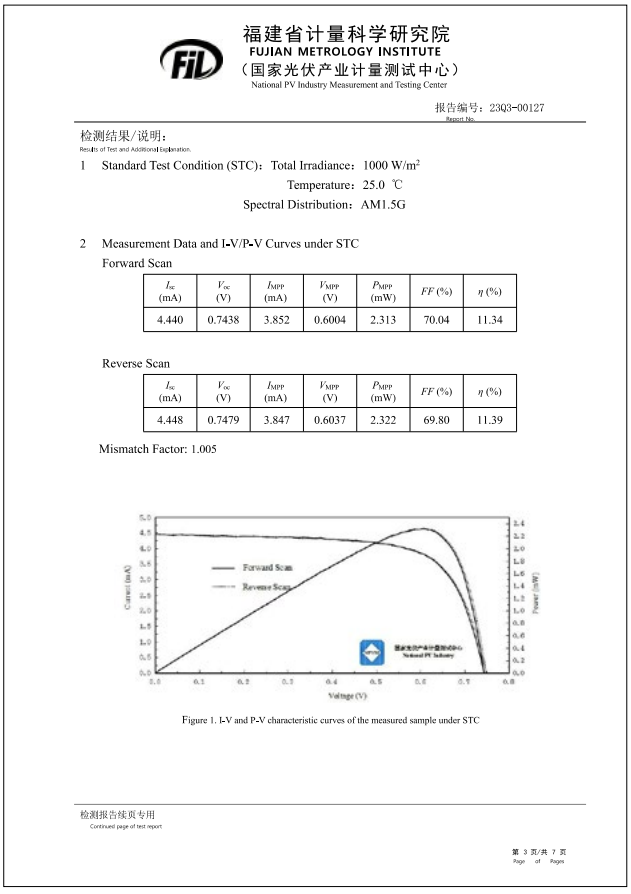

福建省计量科学研究院
FUJIAN METROLOGY INSTITUTE
（国家光伏产业计量测试中心）
National PV Industry Measurement and Testing Center

报告编号：23Q3-00127
Report No.

检测结果/说明：
Results of Test and Additional Explanation.

1 Standard Test Condition (STC)：Total Irradiance：1000 W/m²
Temperature：25.0 ℃
Spectral Distribution：AM1.5G

2 Measurement Data and I-V/P-V Curves under STC

Forward Scan

I_{sc} (mA)	V_{oc} (V)	I_{MPP} (mA)	V_{MPP} (V)	P_{MPP} (mW)	FF (%)	η (%)
4.440	0.7438	3.852	0.6004	2.313	70.04	11.34

Reverse Scan

I_{sc} (mA)	V_{oc} (V)	I_{MPP} (mA)	V_{MPP} (V)	P_{MPP} (mW)	FF (%)	η (%)
4.448	0.7479	3.847	0.6037	2.322	69.80	11.39

Mismatch Factor: 1.005

Figure 1. I-V and P-V characteristic curves of the measured sample under STC

检测报告续页专用
Continued page of test report

第 3 页/共 7 页
Page of Pages

30.3% EFFICIENCY FOR FOUR-TERMINAL PEROVSKITE-SILICON TANDEM SOLAR CELL

A team of researchers from Monash University, The Australian National University (ANU), Flinders University, The University of Sydney and Karlsruhe Institute of Technology (Germany) have achieved a 30.3% efficiency (calculated from the measured performances of the sub-cells) with a perovskite and silicon tandem solar cell. The four-terminal structure allows each sub-cell to be optimised independently, without the requirement of forcing the current to be the same in each.

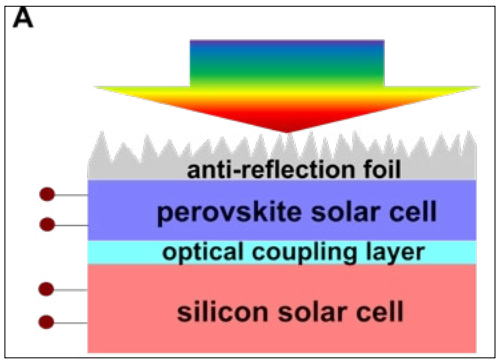

Figure 2.3: Structure of a four-terminal perovskite /silicon tandem solar cell

AWARDS AND PRIZES

SCIENTIA PROFESSOR MARTIN GREEN AND PROFESSOR ANDREW BLAKERS AWARDED THE QUEEN ELIZABETH PRIZE

Figure 2.4: Prof. Martin Green (left), Prof. Andrew Blakers (6th from left), Dr Jinhua Zhao (4th from left) and Dr Aihua Wang (7th from left) receiving the 2023 Queen Elizabeth Prize for Engineering, with Lord John Browne (2nd from left), Dr Masato Sagawa, 2022 winner (5th from left), Prof. Dame Lynn Gladden, Chair of QEPrize Judges, with His Majesty the King.

ACAP leaders Professor Martin Green of UNSW and Professor Andrew Blakers of ANU, along with former colleagues Dr Jianhua Zhao and Dr Aihua Wang, were presented with the 2023 Queen Elizabeth Prize for Engineering by His Majesty King Charles in a ceremony at Buckingham Palace on 12 October 2023 for their invention and refinement of the Passivated Emitter and Rear Cell (PERC) solar cells. This award is considered to be the world's top engineering prize.

Professor Martin Green of UNSW was founding Centre Director of ACAP, a role he held until 2022, and is now a member of its Technical Advisory Committee, Professor Andrew Blakers of ANU was Principal Investigator for the ANU node until 2022 and is now a member of the ACAP Technical Advisory Committee. Former colleagues Drs Zhao and Wang were also researchers at UNSW for 16 years, including the time of the development of PERC. PERC technology, introduced in 1989, revolutionised conventional silicon photovoltaic cell technology and it remains the dominant solar cell technology globally, accounting for over 90% of production in 2023.

VINFUTURE GRAND PRIZE AWARDED TO MARTIN GREEN

In December 2023, Professor Martin Green was awarded the VinFuture Grand Prize in Hanoi for his transformational work in solar energy.

Figure 2.5: Nobel prize winners Stanley Whittingham and Akira Yoshino on the far left and right with Professor Martin Green at the VinFuture Grand Prize ceremony.

LEIGH ANN CONN PRIZE

UNSW's solar pioneer was recognised in December 2023 for leading the development of low-cost, high-efficiency silicon solar cells when he received the prestigious Leigh Ann Conn Prize for Renewable Energy from the University of Louisville.

Figure 2.6: Leigh Ann Conn Prize medallion.

THE WARREN PRIZE AWARDED TO PROFESSOR ANITA HO-BAILLIE

Professor Anita Ho-Baillie, ACAP2.0 Principal Investigator from The University of Sydney won the Royal Society of New South Wales Warren Prize, which recognises research of national or international significance by early- or mid-career engineers and technologists.

Figure 2.7: Professor Anita Ho-Baillie at the ceremony marking award of the Warren Prize by the Royal Society of New South Wales, Australia with Susan Pond, President of the NSW Royal Society.

SCIENTIA PROFESSOR MARTIN GREEN INDUCTED INTO THE US NATIONAL ACADEMY OF ENGINEERING

Figure 2.8: Professor Green being inducted into the US National Academy of Engineering (NAE).

UNSW Sydney's Scientia Professor Martin Green was inducted into the US National Academy of Engineering (NAE) in October 2023 for technical contributions that have enabled the widespread use of silicon photovoltaics. NAE membership honours engineers who have made outstanding contributions to "engineering research, practice, or education, including, where appropriate, significant contributions to the engineering literature" and for "the pioneering of new and developing fields of technology, making major advancements in traditional fields of engineering, or developing/implementing innovative approaches to engineering education". Professor Green acknowledged the importance of the work of his students and colleagues over 49 years of research at UNSW.

PROFESSOR ANITA HO-BAILLIE ELECTED A FELLOW OF THE ROYAL SOCIETY OF CHEMISTRY

The University of Sydney's Professor Anita Ho-Baillie, Principal Investigator in ACAP2.0, was elected a Fellow of the UK's Royal Society of Chemistry. The Royal Society of Chemistry in the United Kingdom has a rich history dating back to 1841 and bestows the title of Fellow upon distinguished researchers who have made substantial contributions to the advancement of the chemical sciences.

In each year from 2019 to 2023, Anita was named a Clarivate Highly Cited Researcher, a title awarded to individuals whose work ranks within the top 1% of citations for a given field, showcasing the highly impactful nature of her research.

Figure 2.9: Anita Ho-Baillie was elected to the UK Royal Society of Chemistry

40TH EUROPEAN PHOTOVOLTAIC SOLAR ENERGY CONFERENCE

Figure 2.10: Soma Zandi was awarded a Student Award at Eu-PVSEC.

Soma Zandi was awarded the prestigious Best Student Presentation Award at the Eu-PVSEC for her outstanding presentation titled "Novel method for the extraction of the implied voltages of silicon wafers and solar cells from luminescence-based measurements". Eu-PVSEC Student Awards were delivered in recognition of the most remarkable and outstanding research work in the field of PV.

BREAKTHROUGH RESEARCH AWARD IN PHYSICAL SCIENCES GOES TO ACAP TEAM

Jianghui Zheng and Md Arafat Mahmdud won The University of Sydney School of Physics Research Award for Breakthrough Research in Physical Sciences, 2023

Figure 2.11: Jianghui Zheng (L) and Md Arafat Mahmud (R) with The University of Sydney School of Physics Research Awards.

ASIA-PACIFIC SOLAR RESEARCH CONFERENCE 2023

Figure 2.12: Luke Sutherland accepting the Wal Read Award. (Photo credit: R. Corkish.)

Luke Sutherland, CSIRO Manufacturing, received the Wal Read Memorial Award for best student oral presentation: "Revolutionizing Scalable Perovskite Solar Cells with Isostatically Deposited Carbon Electrodes".

Figure 2.13: Yansong Wang accepting the Wal Read Award. (Photo credit: Hongying Zhao.)

Yansong Wang, UNSW, received the Wal Read Memorial Award for Best Student Poster: "Multi-Junction GaAs Photodiode Arrays for Biomedical Applications".

Figure 2.14: Gaia Maria Javier received the Muriel Watt Prize at the APSRC 2023. (Photo credit: Hongying Zhao).

Gaia Maria Javier, UNSW, received the Muriel Watt Prize for best oral presentation by a female student: "AI-extraction of spatial photoluminescence and series resistance from electroluminescence images".

Figure 2.15: Haoran Wang received the Monica OliphantPrize at the APSRC 2023. (Photo credit: Hongying Zhao.)

Haoran Wang, UNSW, received the Monica Oliphant Prize for best poster by a female student: "Effects of Soldering Flux on the reliability of TOPCon and HJT Solar Cells".

Figure 2.16: Dang-Thuan Nguyen accepting his award from Renate Egan. (Photo credit: Hongying Zhao.)

Dang-Thuan Nguyen, ANU, received the ACAP Award for Outstanding Student Oral Presentation in PV Devices or Renewable Energy Deployment & Integration (REDI) streams of the 2023 APSRC: "A Research on Perovskite Solar Cells' Tolerance under Proton Radiations".

Figure 2.17: Afsaneh Kashizadeh accepting her award from Renate Egan. (Photo credit: Hongying Zhao.)

The ACAP Award for Outstanding Student Poster Presentation in PV Devices or Renewable Energy Deployment & Integration (REDI) streams of the 2023 APSRC went to Afsaneh Kashizadeh, ANU: "Assessing the material quality of n-type Czochralski silicon wafers grown with melt recharging".

Figure 2.18: David Firnando Silalahi accepting his award from Anna Bruce. (Photo credit: Hongying Zhao.)

The Energies Awards for Outstanding Student Poster in REDI Stream was won by David Firnando Silalahi, ANU: "Indonesia's Vast Marine Solar PV Potential".

Zhuocheng (Ricky) Huang, UNSW, received the Energy Advances Award for Outstanding Poster in PV Device Research: "Modelling PV recycling cost with consideration of learning effect in Australia".

AUSTRALASIAN COMMUNITY FOR ADVANCED ORGANIC SEMICONDUCTORS (AUCAOS) SYMPOSIUM 2023

Figure 2.19: Presentation of the AUCAOS symposium Oral Prize – Student Category by Professor Paul Burn, to Honours student, Euca Brooks (The University of Queensland).

The Australasian Community for Advanced Organic Semiconductors (AUCAOS) Symposium (ACAP is a Platinum Sponsor) convened the organic semiconductor research community of Australia and New Zealand, providing a platform to discuss the latest advancements in computation/theory, the chemistry of novel materials, including processing, film morphology, and spectroscopy, along with device physics and device fabrication/manufacturing/testing.

UNSW ENGINEERING EXCELLENCE AWARDS 2023

ACAP researchers at UNSW node featured strongly in the UNSW Engineering Excellence Awards in 2023.

Figure 2.20: Kaiwen Sun and Rong Deng were among the UNSW Engineering awardees for, respectively, Research Excellence (Early Career Academic) and Women in Engineering.

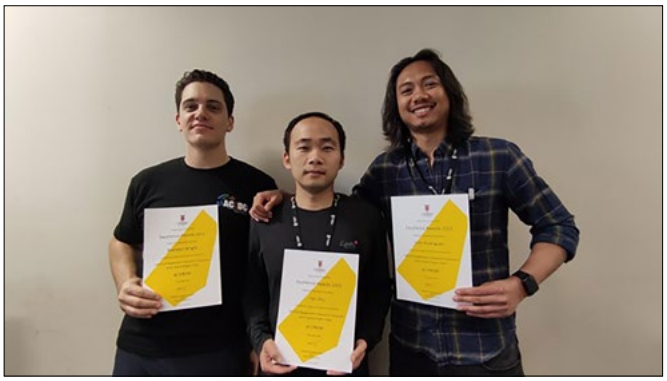

Figure 2.21: The UNSW Engineering Team award went to the Artificial intelligence, Characterisation, Defects, and Contacts (ACDC) Team .

VISITORS AND TOURS

INTERNATIONAL ELECTROTECHNICAL COMMISSION TECHNICAL COMMITTEE 82, SOLAR PHOTOVOLTAIC ENERGY SYSTEMS WORKING GROUP 2 (PV MODULES)

Figure 2.22: IEC Technical Committee 82 outside the ACAP headquarters building on the UNSW campus, 1 November 2023.

MINISTER JENNY MCALLISTER

On 31 January 2023 UNSW welcomed Senator the Hon Jenny McAllister, Assistant Minister for Climate Change and Energy to UNSW. Senator McAllister learnt about UNSW's and ACAP's pioneering solar PV cell and module research during her visit to the Solar Industrial Research Facility.

Figure 2.23: Minister McAllister (centre) with UNSW President and Vice-Chancellor, Attila Brungs,and ACAP Executive Director, Renate Egan.

PEKING UNIVERSITY

A group of students of Sustainability Leadership at Guanghua School of Management, Peking University, working with the Australian Graduate School of Management, toured ACAP facilities at UNSW on14 August 2023.

Figure 2.24: Students of Sustainability Leadership at Guangha School of Management, Peking University visited the Australian Graduate School of Management and ACAP.

NSW SHADOW MINISTER FOR JOBS, INDUSTRY, INNOVATION, SCIENCE AND TECHNOLOGY, MARK COURE

Professor Anita Ho-Baillie, University of Sydney ACAP node, hosted a visit of NSW Shadow Minister for Jobs, Industry, Innovation, Science and Technology, Mr Mark Coure MP in July 2023.

Figure 2.25: ACAP-University of Sydney hosts NSW Shadow Minister for Jobs, Industry, Innovation, Science and Technology, Mark Coure MP.

NEDO, JAPAN

Dr Shigeru Niki, Dr Mitsutoshi Okada and Mr Koki Yanas from the Technology Strategy Centre at the New Energy and Industrial Technology Development Organization (NEDO) visited UNSW ACAP. NEDO is Japan's national R&D agency to both address global energy and environmental challenges and enhance industrial technology. Dr Niki is Director General of the Sustainable Energy Unit. The group discussed existing and future research collaborations, led by Xiaojing Hao, Nicholas Ekins-Daukes and Henner Kampwerth.

Figure 2.26: Dr Shigeru Niki, Dr Mitsutoshi Okada and Mr Koki Yanas from NEDO visited UNSW node of ACAP, hosted by Dani Alexander, CEO of UNSW Energy Institute.

BOARD OF THE CLEAN ENERGY REGULAOR VISIT ACAP AT UNSW

Figure 2.27: UNSW hosts visit from the Board of the Clean Energy Regulator.

UNSW node of ACAP hosted a high-level delegation from the Clean Energy Regulator (CER), timed to coincide with a CER Board Meeting. Visitors included David Parker AM, Chair and CEO, Melanie Herpen, General Manager Human Resources, Security and Facilities, Mark Williamson, Executive General Manager Scheme Support, Michelle Crosbie, Executive General Manager Scheme Operations, Bronwen Shelley, General Counsel and Jonathan Mandl, Team Leader, Planning Performance and Parliamentary Section, as well as Board Members Kate Vidgen, John Kettle.

ORGANISATIONAL STRUCTURE
AND RESEARCH OVERVIEW

The Australian Centre for Advanced Photovoltaics (ACAP) was established in 2013 to develop the next generations of photovoltaic technology and to provide a pipeline of opportunities for performance increase and cost reduction. The founding Australian partners in ACAP are the University of New South Wales (UNSW), the Australian National University (ANU), the University of Melbourne (UoM), Monash University, the University of Queensland (UQ) and CSIRO along with Australian companies and number of international research institutions and industry partners. ACAP has developed a national collaboration that acts as a platform for photovoltaics research in Australia and has provided a pathway for highly visible, structured photovoltaic research both nationally and internationally.

On 24 June 2022 the Minister for Climate Change and Energy, the Hon. Chris Bowen and Member for Kingsford Smith, the Hon. Matt Thistlethwaite, announced the extension of ACAP to 2030 (ACAP 2.0) at the UNSW Kensington Campus. The funding agreement for 2013 – 2030, was executed on 3 January 2023. It nominated, in addition to lead organization, UNSW, the following Project Participants: The Australian National University, The University of Melbourne, CSIRO Manufacturing, Monash University, The University of Queensland, CSIRO Energy and The University of Sydney, with the latter two joining as new partners from 2023.

Fig. 3.1. Minister Chris Bowen and Member for Kingsford Smith, The Hon. Matt Thistlethwaite announce the extension of ACAP to 2030 at the Solar Industrial Research Facility, on the UNSW Kensington Campus.

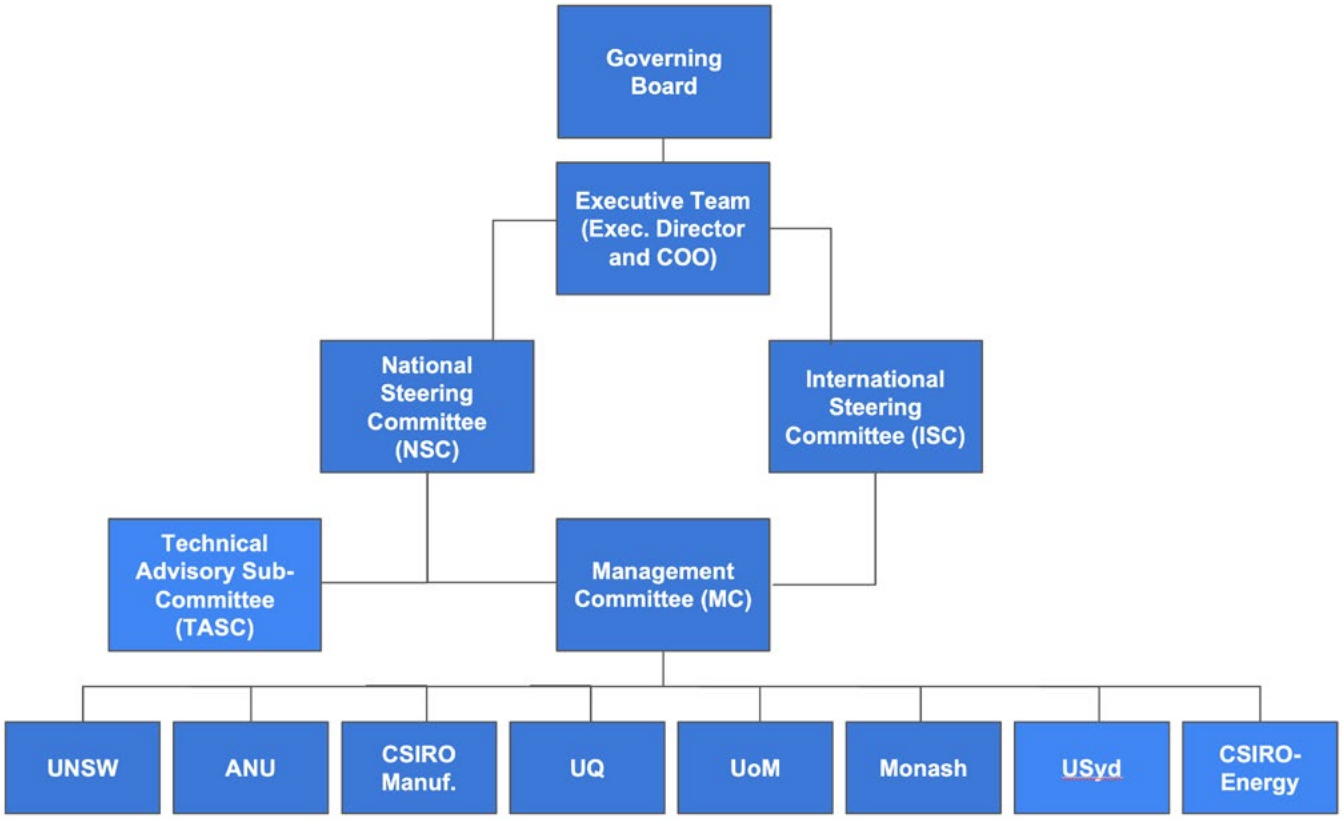

Figure 3.2: Organisational chart. Collaborating industry participants are involved in collaborative research as well as in the Advisory and Steering Committees.

ACAP is driving significant acceleration of photovoltaic development beyond that achievable by partners acting individually, with significant leveraging of past and current funding. This program is supported by the Australian Government through the Australian Renewable Energy Agency (ARENA). The Australian Government, through ARENA, is supporting Australian research and development in solar photovoltaic and solar thermal technologies to help solar power become cost competitive with other energy sources. (The views expressed herein are not necessarily the views of the Australian Government, and the Australian Government does not accept responsibility for any information or advice contained within this report.)

The ACAP2.0 research program is aligned with ARENA's 30/30/30 target of 30% module efficiency and 30 cents per installed watt at utility scale by 2030. The research program changes are reflected in the structure of this report.

Research activities are milestone driven with annual milestone targets established through each year's Activity Plan, in accordance with the Funding Agreement with ARENA. ACAP2.0's new organisational chart is shown in Figure 3.2. The Executive Team report to the Governing Board. The Board has an Independent Chair and membership includes a representative of ARENA as an observer, the ACAP Executive Director plus a representative from no more than three of the Project Participants, selected on a rotating basis.

International activities are coordinated by an International Advisory Committee with membership drawn from ARENA, researcher representatives from several countries, a representative nominated by major industry partners, and the Executive Director of ACAP. The International Advisory Committee is also charged with reviewing and making recommendations on ACAP's research, providing strategic advice to, and assisting the Executive Director with the ongoing management of the joint activities, assisting the ACAP Executive Director to develop cooperative partnerships with international institutions, research bodies and industry, providing feedback on the ACAP Annual Report due to be submitted to ARENA on or around 12 May each year, and specific support for reviews of ACAP.

ACAP's National Steering Committee comprises a representative of ARENA, industrial and academic representatives, The Executive Director, one Principal Investigator from the Recipient and from each Project Participant, and members of the Technical Advisory Subcommittee (TASC) to the National Steering Committee. This Committee provides guidance and support for the Australian Centre for Advanced Photovoltaics (ACAP) by reviewing Centre projects, budgets and plans, and by providing recommendations to the ACAP Executive Director and Management Committee on improvements, opportunities, evaluation of risks and initiatives.

The Technical Advisory Subcommittee to the National Steering Committee's role is to provide technical input to the National Steering Committee and guidance to the Executive Director and Program Package Leads. It will have at least two members, draw on the membership of the National Steering Committee, and may include independent external advisors. The chair of the TASC will be elected by its members.

ACAP's Management Committee is comprised of the Executive Director, the COO, a Principal Investigator employed by and nominated by The University of New South Wales, and a Principal Investigator nominated by each Project Participant. The ACAP Executive Director will chair. This Committee will oversee the planning and operations of ACAP, including recommendations on projects, staff and student exchange and funding, for approval by the National Steering Committee; make decisions in relation to the conduct of approved research projects and communications strategies; approve appointments of and changes to Principal Investigators; the recruitment of new Project Participants; and proposed variations to agreements with Collaborating Organisations.

The ACAP program is (and has been since 2023) organised under six Program Packages (PP1–PP6), each supported by multiple Project Participants and coordinated by expert senior researchers from two or more of the Project Participants.

Program Package 1 (PP1) deals with Silicon Solar Cells, by far the dominant photovoltaic technology commercially, and likely to remain so for at least the next 10 years. They continue to improve in both high performance and lower cost to consumers. Ultra-low-cost solar PV will be achieved from ongoing research, development and deployment in silicon and tandem solar cell technologies. ACAP's Silicon Solar Cells Program Package supports fundamental and applied research that will deliver better, cheaper, and more efficient silicon solar cells. The focus is on areas of improved silicon material, contacts, surfaces and interfaces, high-efficiency devices architectures including bifaciality, performance stability, improved characterisation tools, and silicon-based tandem structures targeting 10c/W module and 30c/W system costs. PP1 will be coordinated by Bram Hoex (UNSW) and Dan Macdonald (ANU).

Program Package 2 (PP2) involves collaborative research into Emerging Materials. This set of research activities focusses on emerging materials and their applications in tandem cell technologies, as well as in applications that will see PV dominate new energy generation over the next decade. Targeted emerging materials are prepared from Earth-abundant and low toxicity feedstocks, require low embedded energy manufacturing, and form the potential for local manufacturing capability. ACAP has world-leading research capabilities across several key emerging photovoltaic classes including metal chalcogenides, perovskites, and organic photovoltaics. ACAP activities in this Program Package will realise these prospective advantages through a focus on emerging materials, processing, defect and device engineering, characterisation, stability, and scalable manufacturing. Coordinators for this topic are Jacek Jaseniek (Monash), Xiaojing Hao (UNSW), Anita Ho-Baillie (The University of Sydney), Anthony Chesman (CSIRO Manufacturing), Paul Shaw (UQ), David Jones (University of Melbourne), Heping Shen (ANU).

Program Package 3 (PP3) addresses Tandem Solar Cells. Tandem cell technologies offer demonstrated prospects of delivering a step change in cell and module efficiency to 30% and beyond. Work in Program Package 3 will focus on bringing together the silicon cells and emerging materials programs in tandem solar cells. The activities will take concepts beyond the research scale, to address the known challenges of combining stable, low-cost, non-toxic and abundant materials in a manufacturable, durable, high efficiency tandem structure. The program targets a commercial tandem cell technology delivering 30% efficiency by 2030. PP3 coordination is overseen by Anita Ho-Baillie (The University of Sydney), Xiaojing Hao (UNSW), Greg Wilson (CSIRO Energy), Klaus Weber (ANU).

The Device to Module Program Package (PP4) focusses on the opportunity to increase performance and reduce cost by optimising the device metallisation, interconnection and module fabrication within a more holistic solar module production framework. Device-to-Module research can deliver benefits at the cell-design level, leading to the reduced use of materials such as silver, enabling large wafers and module sizes, new cell interconnection technologies, light trapping and manufacturing process efficiencies. The learning gained from the growing maturity of the silicon PV industry can be applied to facilitate a faster transition of new, emerging materials and devices from research phase to pilot scale production, with relevance to tandem devices. Coordinators: Marco Ernst (ANU), Anthony Chesman (CSIRO Manufacturing), Benjamin Duck (CSIRO Energy).

Program Package 5 (PP5) investigates the increasingly important area of Manufacturing and Sustainability. With ongoing year-on-year growth of PV manufacturing and deployment, it is essential to identify and address issues that could limit or slow future growth. This Program Package focuses on these issues through the different stages of the PV module lifecycle – manufacturing, use and end-of life. The work program considers supply chain constraints, sustainability, end-of-life management and the possibility of local manufacturing of elements across the solar PV supply chain. Techno-economic analysis, in-field performance analysis, characterisation and optimisation provide a common thread across the full ACAP program to measure, model, assess and validate PV opportunities to inform research directions and support data-driven decision making. Program Package 6 (PP6) involves PV Futures and Knowledge Sharing.

This Program Package includes technology perspectives, commercialisation activities, knowledge sharing and capacity building. ACAP will build on past success in knowledge sharing and communications and extend this to increase engagement, to raise the profile of research outcomes, to participate in the public conversation and to support the development and deployment of ultra-low-cost PV. The knowledge sharing program has been extended to include technology road-mapping and PV futures. ACAP will monitor, model and report on global developments in PV devices, processes, and applications, delivered through a series of authoritative reports with an over-the-horizon view of the future PV industry, facilitating informed decisions.

Targets for PP1–PP6 are established through the Activity Plan for each year.

AFFILIATED
STAFF AND STUDENTS

PROJECT PARTICIPANTS

UNIVERSITY OF NEW SOUTH WALES

Academic Staff and Senior Researchers

Egan, Renate (ACAP Executive Director and node Leader)

Corkish, Richard (ACAP Chief Operating Officer)

Bremner, Stephen

Bruce, Anna

Chan, Catherine Emily

Chang, Nathan

Ciesla, Alison

Conibeer, Gavin

Ekins-Daukes, Nicholas

Green, Martin

Hallam, Brett (p/t)

Hameiri, Ziv

Hamer, Phillip

Hao, Xiaojing

Hoex, Bram

Jiang, Yajie

Kampwerth, Henner

Keevers, Mark

Passey,Rob

Perez-Wurfl, Ivan

Rougieux, Fiacre

Shrestha, Santosh

Sun, Kaiwen

Tayebjee, Murad

Trupke, Thorsten

Uddin, Ashraf

Young, Trevor

ECR and Postdoctoral Fellows

BBorojevic, Nino

Chan, Yuan-Chi

Chen, Qian

Chen, Ran

Cui, Xin

Dehghanimadvar, Mohammad

Deng, Rong

Fletcher,Jack

Gayot, Felix

Gentle, Angus

Haghdadi, Navid

He, Mingrui

Heslop, Simon Francis

Hossain, Md. Anower

Hsiao, Pei-Chieh

Huang, Jialiang

Kim, Moonyong

Kunz, Oliver

Le, Huy Tuan Anh

Li, Caixia

Li, Jianjun (until May 2023)

Liao, Yuanxun

Liu, Mengdi

Liu, Xu

Liu, Ziheng

Ma, Fajun

Nielsen, Michael

Patterson, Robert

Payne, David (Adjunct)

Pearce, Phoebe

Poddar, Shukla

Pollard, Michael

Prasad,Abhnil

Roberts, Michael

Rodriguez, John

Romer, Udo

Samadi, Aref

Sen, Chandany

Shakiba, Ali

Sharma, Abhinav

Sharma, Rama

Song, Ning

Suryawanshi, Mahesh Pralhad

Teymouri, Arastoo

The, Zhi Li

Tong, Jingnan

Vaqueiro Contreras, Michelle

Wang, Li

Wang, Sisi

Wright, Brendan

Wu, Tien-Chun

Yildiz, Baran

Yuan, Xiaojie

Zeng, Yiyu

Zhang, Meng

Zhang, Pengfei

Zhang, Yuchao
Zhou, Zhuangyi
Zhou, Zibo

PhD Students

Abdullah-Vetter, Zubair
Al Kiyumi, Lamees Yaqoob, Mubarak
Baldacchino, Alexander
Buratti, Yoann
Cai, Yalun
Cheng, Yuhao
Choi, Eunyoung
Chowdhury,Tamal
Cong, Jialin
Deng, Shuo
Dipta, Shahriyar Safat
Feng, Ziyue
Furqan, Chaudhry Muhammad
Gottlieb, Hugh Robert
Guo, Xinyao
Hall, Ryan
Hanif, Muhammad
Harrison, Catherine Audrey
Hosseinabadi, Parisa
Howlader, Ashraful Hossain
Javier, Gaia Maria
Kaleem, Akasha
Kasim, Samsudeen
Kim, Eui Ho
Le, Anh Huy Tuan
Lee, Minwoo
Lehmann, Alex
Li, Guo
Lim, Jihoo
Madumelu, Chukwuka
Mo, Alvin Cheuk-Him
Mungra, Mreedula
Mussakhanuly, Nursultan N
Nath, Tanushree Jb
Öström, Ina
Qiu, Tianyun
Radhwi, Haytham
Saghaei, Mahsa
Sakib, Syed Nazmus
Samadi, Aref
Sarsour, Maysa Jehad Jamil
Sazzad, Muhammad Hasnan
Shi, Wenxin
Shim, Hongjae
Song, Hyunsun
Sun, Heng
Sun, Zhenyu
Tan, Xingru
Tarique, Walia
Thomas, Ian
Wang, Ao
Wang, Haoran
Wang, Ruimeng
Wang, Yansong
Wang, Yihao
Wang, Zhimeng
Wu, Xinyuan
Xie, Tong
Yaghoubi Taemeh Alireza
Yang, Zhen
Yuan, Xiaojie
Zhang, Hongrui
Zhang, Lishuang
Zhao, Chenghan
Zhou, Shujie
Zlatinov, Martin Dimitrov

Masters Students

Chew, Zi Lin
Dong, Jiaqi
Fan, Kenneth
Fang, Siyuan
Flores March, Juan Carlos
Fu, Jiexi
Gudi, Sandesh
Jie, Yun
Htun, Kyaw Zin
Hu, Qihuan
Issa, Patric
Joseph, Karan
Katgara, Danishi Yezdi
Katyarmal, Aditi
Kumar, Vijay
Langchen, Zhu
Luo, Yuxuan
Li, Jieyi

Li, Junqi

Liu, Jiarong Lee, Minwoo

Maroun, Joe

Ngo, Thi Uyen Truc

Puspito, Budiningtyas

Rahul, Ashwin

Ren, Ruiyan

Runkai, Liu

Seng, Moonpanha

Shuo, Liu

Tanjung, Aditia Syamputra

The, Zhi Li

Verma, Kanav

Wang, Yuchen

Honours Students

Ahmed, Shaon

al Hanshi, Azzan

Anderson, Jordan

Autthara, Surunchana

Bayanov, Ayrat

Bowen, Olivia Grace

Campbell, Jock

Causley, Samuel

Chai, Jacky

Chen, Xianglin

Chengye, Jia

Chong, Elvis

Cowgill, Louis

Dai Tse, Karlon

Dela Cruz, Roy

Dheerasekara, Ruchinda

Dillon, Michael

Fan, Atkins De Hua

Fan, Kenneth De Cheng

Furrer, George

Gallardo Galan, Roberto

Geller, Joshua

Hanshi, Azzan al

Hassaan, Ibrahim

Ho, Christopher

Hou, Yuyang

Huang, Ricky

Jayasimha, Rohan

Jubor, Zhu

Junhao, Ma

Ketmontri, Ketti

Lan, Jerry

Larcombe, Thomas

Leamon, Elke

Li, Shiyu

Li, Zeyu

Li, Zonglin

Liam Emmett

Lima, Marcel Valencia

Liu, Donny

Luo,Yuxuan

Mellon, Toby

Murphy, Matthew

Nowrungsah, Nichil

O'Kearney, Felix

Ow, Zhong Ming

Paterson, Gabrielle

Qi, Yulun

Raffin, Elizabeth

Raju, Aravind

Ramos, Patrick

Robinson, Nicole

Tran, Benjamin

Wallace, Hugh

Wang, Sijin

Workman, Piper

Wu, Zixi

Yingmei, Zou

Zhang, Weiyi

AUSTRALIAN NATIONAL UNIVERSITY

Academic Staff and Senior Researchers

Macdonald, Daniel (Node Leader)

Black, Lachlan

Blakers, Andrew

Catchpole, Kylie

Chern Fong, Kean

Duong, The

Liu, Anyao

Nguyen, Hieu

Phang, Sieu Pheng

Shen, Heping

Walter, Daniel

Weber, Klaus

ECR and Postdoctoral Fellows

Ahmad, Viqar

Basnet, Rabin

Bui, Anh

Cheng, Cheng

Ernst, Marco

Haggren, Anne

Kang, Di Liang

Liu, Xuesi

Lu, Bin

Mayon, Yahuitl Osorio

Nadolny, Anna

Shehata, Mohamed

Sio, Hang Cheong Kelvin

Tong, Jingnan

Truong, Thien

Weber, Tim

Wenshen, Liang

Zhang, Hualin

PhD Students

Bartholazzi, Gabriel

Broadhurst, Glenn

Chang, Li-Chun

Cheng, Cheng

Cui, Qian

Gaurav, Ashish

Hou, Yihui

Huang, Keqing

Ilkhechi, Noushin

Kashizadeh, Afsaneh

Kodithuwakku, Piyumi Kanchana

Le, Tien

Li, Zhuofeng

Nguyen, Khao

Nguyen, Thuan

Sabah, Sanjida

Silalahi, David

Shehata, Mohamed

Tabi, Grace

Varghese, Anitta

Wang, Jiali

Wang, Wei

Wibowo, Ary

Yang, Zhongshu

MPhil Students

Huang, Zhongrui

Leong, Andrew

Tie, Jirui

Yang, Kaiji

Honours Students

Bond, Arthur

Bradbury, Neil

Chen, Alan

Harding, Matt

Litchfield, Annabel

Martin, Isaac

Medland, James

Scott, Thomas

Thawley, Harry

Travers, Catie

CSIRO MANUFACTURING

Academic Staff and Senior Researchers

Chesman, Anthony (Node Leader)

Angmo, Dechan

Chantler, Régine

Gao, Mei

Scully, Andrew

Vak, Doojin

Weerasinghe, Hasitha

ECR and Postdoctoral Fellows

An, Na Gyeong (visiting)

Kalapparambath Rajendra, Narendra Pai

Kim, Juengeun

PhD Students

Sutherland, Luke

CSIRO ENERGY

Academic Staff and Senior Researchers

Wilson, Gregory (Node Leader)

Duck, Benjamin

Fell, Chris

UNIVERSITY OF MELBOURNE

Academic Staff and Senior Researchers

Jones, David (Node Leader)

Bullock, James

Smith, Trevor

ECR and Postdoctoral Fellows

Ahluwalia, Gagandeep

Corletto, Alexander

Jameel, Mohamed

Lee, Calvin

Masoomi-Godarzi, Saghar

Seyyedhamzeh, Mozdeh

Subbiah, Jegadesian

Yan, Di

PhD Students

Fischer, Karen (joint with KIT)

Kahlil Ahmed, Maria Bibi

Kheirabadi, Hamoon

Novakovic, Sacha

Pan, Yida

Saker-Neto, Nicolau

MONASH UNIVERSITY

Academic Staff and Senior Researchers

Bach, Udo (Joint Node Leader)

Jasieniak, Jacek (Joint Node Leader)

Simonov, Alexandr

ECR and Postdoctoral Fellows

Jie, Zhao

Mozaffari, Naeimeh

Muhamad, Kashif (Kalim)

Nitish, Rai

Rahman, Sharidya

Saripally, Sudhaker Reddy

Sepalage, Gaveshana

Sharma, Manoj

Surmiak, Adam

Wenxin, Mao

PhD Students

Guo, Qianying

Hora, Yvonne

Kessel, Amit

Lam, Jefferson

Luo, Yixuan

Moon, Josh

Nurrosyid, Naufan

Rodriguez, Juan Benitez

Yan, Wenqi

UNIVERSITY OF QUEENSLAND

Academic Staff and Senior Researchers

Burn, Paul (Joint Node Leader)

Shaw, Paul (Joint Node Leader)

ECR and Postdoctoral Fellows

Babazadeh, Mohammad

Bati, Abdulaziz

Gao, Mile

Jin, Hellen

Mallo, Neil

PhD Students

Chu, Ronan

Feng, Yaomiao

Gupta, Satakshi

McAnally, Shaun

Smyth, James

Honours Students

Brooks, Euca

Lindsay, Oliver

Smyth, James

THE UNIVERSITY OF SYDNEY

Academic Staff and Senior Researchers

Ho-Baillie, Anita (Node Leader)

ECR and Postdoctoral Fellows

Bailey, Christopher

Bing, Jueming

Mahmud, Md Arafat

Zheng, Jianghui

PhD Students

Leung, Tik Lun

Liao, Chwenhaw

Tang, Shi

Tao, Runmin

Wang, Guoliang

Yi, Jianpeng

COLLABORATING ORGANISATIONS

AJOU UNIVERSITY

Moon, Sungkon

CHUNGBUK NATIONAL UNIVERSITY

Kim, Dohyung

CHUNGNAM NATIONAL UNIVERSITY

Lim, Jongchul

Yun, Siwon

CUBICPV

Lorenz, Adam

Hunt, Brian

DELPHI LASER/NUTOWN TECHNOLOGIES

Zhao, Yuxing

Carter, Adrian

FEDERAL UNIVERSITY OF SANTA CATARINA (UFSC)

Rüther, Ricardo

GREEN DYNAMICS

Xie, Tong

GYEONGSANG NATIONAL UNIVERSITY

HUNAN RED SOLAR NEW ENERGY SCIENCE AND TECHNOLOGY CO. LTD.

Yi, Hui

KOREA INSTITUTE OF TECHNOLOGY

Seo, DH

KOREA RESEARCH INSTITUTE OF CHEMICAL TECHNOLOGY (KRICT)

Lee, J.-W.

Agbenyeke,R.E.

Kim,C.G.

Jeon,N.J.

Park,H.H.

KYUNG HEE UNIVERSITY

Yun, JH

NATIONAL RENEWABLE ENERGY LABORATORIES

Kopidakis, Nikos

NEOEN AUSTRALIA

Cheylus, Jean-Christophe

OCP

Leeson, Gary

RAYGEN

Lasich, John

RLA POLYMERS-NAN PAO

Tsai, Terry

Chang, Sin

Lord, Frank

SOLARCYCLE

Dias, Pablo

SUNCABLE

Marshall, Luke

SUNDRIVE SOLAR

Allen, Vincent

Hu, David

Lennon, Alison

TINDO SOLAR

Sporne, Robert

TRACTILE

Perkins, Jason

UNIVERSITY OF SURREY

Yun, Jae Sun

VRX SILICA

Maluish, Bruce

PP1
SILICON SOLAR CELLS

PP1.1 SILICON MATERIALS

PP1.1.1 Wafer Fabrication

ANU Team
Prof. Daniel Macdonald, Dr AnYao Liu, Dr Rabin Basnet

ANU Students
Tien Le, Sanjida Sabah, Afsaneh Kashizadeh

UNSW Team
Dr Ran Chen

Partners
LONGi, Jinko Solar

Funding Support
ACAP, ARENA, ANU, UNSW

Aims

As the efficiency of silicon solar cells in mass production continues to increase, the electronic quality of the silicon wafers on which they are made becomes more and more critical. The wafer fabrication activities in PP1.1.1 aim to characterise the quality of Czochralski-grown monocrystalline silicon (Cz-Si) wafers, the dominant type of silicon wafer in the PV industry today. A key focus will be emerging crystal-growth and wafering technologies, such as melt-recharging to allow multiple ingots to be grown from a single crucible, and how these advances impact wafer quality. State-of-the-art industrial silicon wafers will be supplied by leading PV companies including LONGi and Jinko Solar.

Progress

In 2023 we undertook a detailed assessment of the electronic quality of Ga-doped p-type Cz-Si wafers grown at LONGi, one of the world's leading suppliers of silicon wafers. Such p-type wafers are used for the fabrication of PERC cells, currently the largest PV cell technology in production. Our study focused on the impact of melt recharging, in which an ingot is pulled from the molten silicon, and then the melt is replenished, and a second ingot is pulled. Up to nine ingots are pulled in succession using this method, which significantly reduces ingot growth time, energy consumption and costs. However, there is a risk of impurities and contaminants accumulating within the residual melt at the end of each ingot growth, which may affect the wafer quality. Our study was the first reported systematic assessment of the impact of melt recharging on Cz-Si wafer quality.

Nine ingots were grown from a single crucible, as shown in Figure PP1.1.1.1. The ingots were of different lengths, with the final ingot being the longest, as the complete melt was crystallised in this case, leading to a contaminated region at the bottom that is removed and not cut into wafers. Wafers were selected from ingots 1, 4 and 9 to examine any changes in their electronic quality and impurity concentrations.

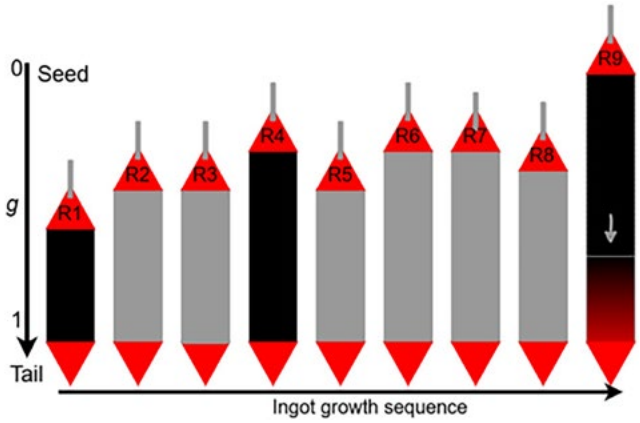

Figure PP1.1.1.1: Schematic diagram of Cz-Si ingots grown with melt-recharging.

Figure P1.1.1.2 shows the dissolved interstitial oxygen concentrations [Oi] along these three ingots, from the seed end (solidified fraction = 0) to the tail end (solidified fraction towards 1). The oxygen concentration increases somewhat from ingot 1 to ingot 9, although the increase is not large. Within each ingot, the oxygen concentration decreases from the seed to the tail end, as expected due to the evaporation of oxygen from the silicon melt.

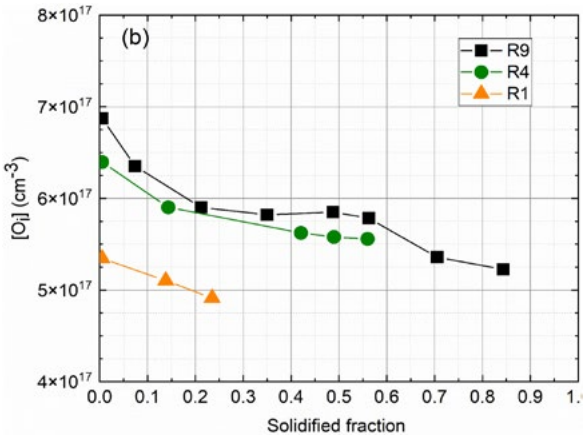

Figure PP1.1.1.2: Dissolved oxygen concentrations in ingots 1, 4 and 9, from the seed end (solidified fraction = 0) to the tail end.

Figure P1.1.1.3 shows the dissolved interstitial Fe concentration [Fei] along each ingot, using the well-known method based on the breaking of iron-acceptor pairs. Again, a small but detectable increase in Fe concentration can be observed in the later-pulled ingots compared to the ingots pulled first. However, this small increase is not expected to be problematic for the fabrication of solar cells. The Fe concentration also increases from the seed end to the tail end within each ingot, as expected due to segregation into the melt, and as modelled using Scheil's segregation law.

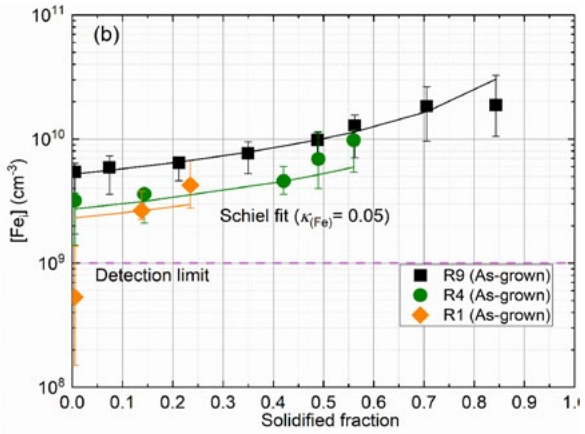

Figure PP1.1.1.3: Dissolved iron concentrations in ingots 1, 4 and 9.

Figure P1.1.1.4 shows the measured carrier lifetimes in the three ingots. Also included are the maximum achievable lifetimes taking into account intrinsic recombination via Auger and radiative processes, and the impact of surface recombination caused by the aluminum oxide passivating layers deposited by atomic layer deposition. The carrier lifetimes in the ingots are only slightly reduced in the subsequently grown ingots, indicating that melt-recharging does not lead to significant accumulation of impurities and defects in subsequently grown ingots. Rather, the number of ingots pulled is more likely limited by mechanical weakening of the crucible itself.

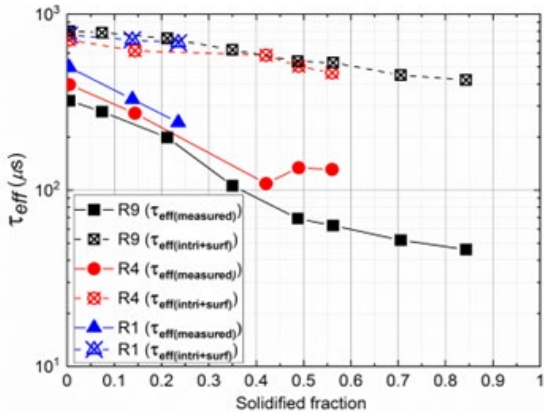

Figure PP1.1.1.4: Effective carrier lifetimes in ingots 1, 4 and 9, and the maximum achievable lifetimes taking into account intrinsic recombination and surface recombination.

Comparison with the maximum achievable lifetimes indicates that, although few additional defects are introduced during the melt recharging, the presence of Fe does partly limit the lifetime in all of these ingots prior to cell fabrication. Fortunately, this Fe contamination is effectively removed by impurity gettering during the phosphorus diffusion used in PERC cell fabrication, as discussed in the following section.

We have recently commenced a similar study on phosphorus-doped n-type silicon ingots grown at LONGi with melt recharging. These wafers are used for higher efficiency solar cells such as TOPCon and Silicon Heterojunction (SHJ) devices. Initial results indicate a very high electronic quality – much higher than their p-type counterparts, and very close to the intrinsic limit. Full results on these n-type recharged ingots will be reported in 2024.

References

Basnet, R., Sun, C., Le, T., Yang, Z., Liu, A., Jin, Q., Wang, Y. & Macdonald, D. (2023). Investigating Wafer Quality in Industrial Czochralski-Grown Gallium-Doped p-Type Silicon Ingots with Melt Recharging. Solar RRL 7 (15), 2300304.

PP1.1.2 Defect Engineering

ANU Team
Prof. Daniel Macdonald, Dr AnYao Liu, Dr Rabin Basnet

ANU Students
Tien Le, Zhongshu Yang

UNSW Team
Dr Ran Chen

UNSW Students
Yalun Cai

Partners
LONGi, Jinko Solar

Funding Support
ACAP, ARENA, ANU, UNSW

Aims

Impurities and defects in silicon wafers can often be removed or mitigated through defect engineering. Metallic impurities, which are often mobile at solar cell processing temperatures, can be extracted to surface layers where they are less harmful to the device, in a process referred to as gettering. Immobile defects such as nano-scale oxygen precipitates can be dissolved through a very high temperature anneal, known as a Tabula Rasa step. Other defects, often related to the presence of hydrogen, may be activated or deactivated during the cell processing steps. The purpose of the activities in PP1.1.2 is to understand these processes and develop effective methods of reducing the impact of impurities and defects in silicon solar cells.

Progress

Following on from the previous section, we have recently studied the response of the p-type Ga-doped Cz-Si wafers from recharged ingots grown at LONGi to phosphorus diffusion gettering (PDG) and Tabula Rasa (TR) treatments. The results are shown in Figure PP1.1.2.1.

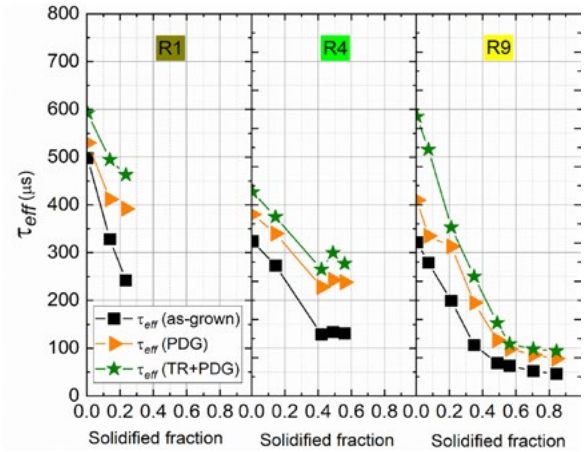

Figure PP1.1.2.1: Carrier lifetimes in ingots 1, 4 and 9, in the as-grown state (no high temperature processing), after phosphorus diffusion gettering, and after Tabula Rasa and phosphorus diffusion gettering.

The carrier lifetimes increased after the gettering step, reflecting the effective removal of the dissolved Fe within the wafers. This would occur naturally during PERC cell fabrication, which requires a phosphorus diffusion step to form the p-n junction. The Tabula Rasa treatment causes a further increase in lifetime when combined with a gettering step. This indicates the dissolution of nano-scale oxygen precipitates in the wafers, which form during ingot cooling. Such Tabula Rasa treatments are not generally used in industry as they require an additional processing step.

We have also recently studied the impact of phosphorus gettering on n-type wafers from another industrial supplier. These results are shown in Figure P1.1.2.2. Again, there is a very clear response to the gettering step, resulting in an increase in lifetime from 1–2 ms to 3–7 ms.

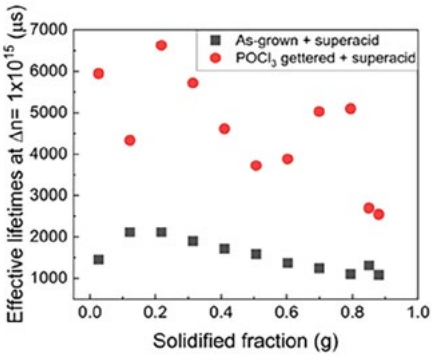

Figure PP1.1.2.2:. Effective lifetimes along an n-type Cz-Si ingot before and after phosphorus diffusion gettering.

This increase causes a significant boost of 10–15 mV in the implied open-circuit voltage of these wafers, as shown in Figure P1.1.2.3. The results show the importance of applying a special pre-gettering step to n-type Cz-Si wafers for the fabrication of silicon heterojunction cells, which otherwise do not provide a gettering mechanism during cell fabrication. Indeed, such a pre-gettering step is now standard in industry for heterojunction cells, which typically achieve open-circuit voltages of 740–750mV.

The observed improvements in lifetime and implied open-circuit voltage after gettering are almost certainly caused by the removal of metallic impurities. However, in this case, it is not possible to directly identify the presence of Fe via the traditional iron-acceptor pairing method, due to the n-type nature of the wafers. However, by measuring the rate at which the lifetime improves during a gettering step, we can estimate the diffusivity of the impurity being removed and compare it to the known diffusivities of common metallic impurities. Doing so, we found that the diffusivity matched that of Fe in silicon very well, as shown in Figure P1.1.2.4. This confirms that the improved lifetimes after gettering in these n-type wafers are indeed caused by the removal of Fe, as was the case for the p-type wafers.

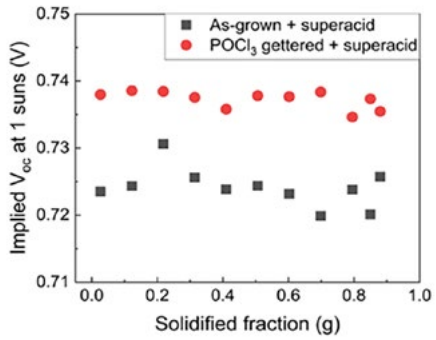

Figure PP1.1.2.3: Implied open-circuit voltages along an n-type Cz-Si ingot before and after phosphorus diffusion gettering.

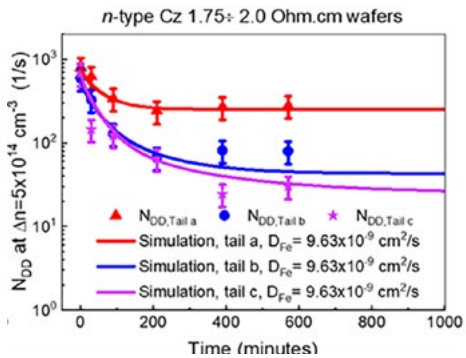

Figure PP1.1.2.4: Measured gettering kinetics in n-type wafers cut from an industrial Cz-Si ingot, and simulated gettering kinetics assuming a diffusivity for the gettered element equal to that of Fe in silicon.

Future work on defect engineering in Cz-Si wafers will focus on the presence of so-called ring defects, caused by nano-scale oxygen precipitates, which often plague n-type Cz wafers, especially from near the top of an ingot where the oxygen concentration is higher. Removing such defects through treatments such as Tabula Rasa steps, or avoiding the ring defects entirely by reducing the oxygen content in the ingots, are both viable strategies for mitigating ring defects in n-type cells.

References

Le, T., Cai, Y., Yang, Z., Chen, R., Macdonald, D. & Liu, A. (2023). Industrial Czochralski n-type silicon wafers: gettering effectiveness and possible bulk limiting defects, submitted to Solar Rapid Research Letters.

PP1.2 SILICON SURFACES AND INTERFACES

PP1.2.1 Doped Tunnel-Oxide Polysilicon

UoM Team
Dr James Bullock, Dr Di Yan

UoM Students
Jesus Ibarra Michel, Yida Pan

ANU Team
Dr Heping Shen, Dr Pheng Phang, Dr Thien Truong

Partner
Jinko Solar

Funding Support
ACAP, ARENA, UoM

Aims

The aim of the work described in this subsection is to reduce costs and improve performance of tunnel-oxide passivated contact (TOPCon) solar cells by: (1). enhancing the doped tunnel-oxide polysilicon process, to achieve lower contact resistivity, reduced optical losses, improved passivation, stability and reliability; and (2). extending the functionalities of doped polysilicon for junction-formation, hydrogenation and patterning capabilities towards novel device applications.

Barrier layers for enhanced thermal stability of doped tunnel-oxide polysilicon contacts

Polycrystalline silicon (poly-Si) passivated junctions/contacts have become a key technology for high efficiency silicon solar cells (Yan et al. 2023a). However, there remain some issues with this technology related to its thermal stability during/after metallisation. For example, significant passivation degradation is observed after printing/firing metal pastes on poly-Si junctions/contacts, particularly for thin poly-Si layers (Yan et al. 2021). Thus, in an industrial setting a thick poly-Si layer, above 100 nm, must be implemented to improve the thermal stability of poly-Si junctions/contacts for the metallisation process. The thick poly-Si layer results in a low short-circuit current density, J_{sc}, due to parasitic absorption. Thus, it is desirable to develop a contact structure which combines a thin poly-Si contact < 30 nm, with low parasitic absorption, with a protective interlayer to prevent/reduce interaction between the metal electrodes and poly-Si layers.

In this activity of PP1.2.1, we explore the use of different "buffer" layers to perform this function. Here we report on titanium oxide, TiO_2, as one of the more successful interlayers between the n-type poly-Si passivated junctions/contacts and the aluminium electrode (Yan et al. 2023b). While screen printing is industry standard, similar passivation degradation has also been shown using thermally evaporated metal electrodes with thin poly-Si contacts. Hence, in this study we use thermal evaporation as a preliminary proxy for screen printing metallisation.

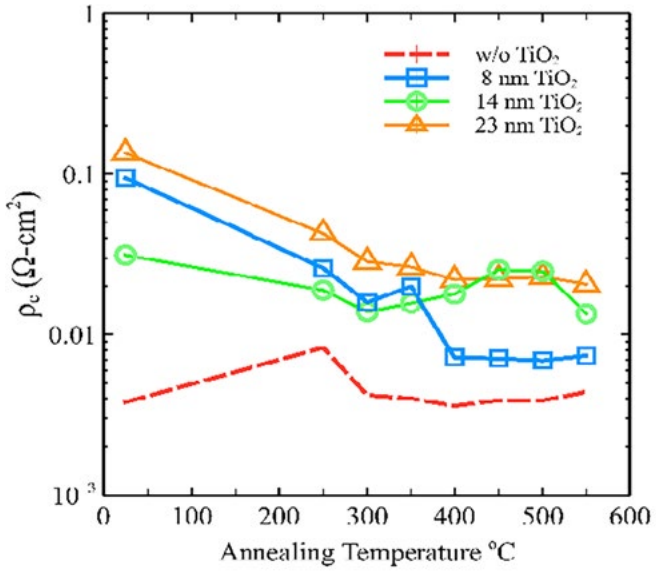

Figure PP1.2.1.1: Contact resistivity ρ_c values of n-type poly-Si contacts with and without the TiO_2 interlayer shown as a function of cumulative annealing steps in air.

Two sets of samples were prepared: passivation samples and contact resistivity ρc samples. Both passivation and contact resistivity samples used a symmetrical structure of LPCVD (low pressure chemical vapour deposition) n-type poly-Si (~50 nm) /SiO_2 (1.5 nm)/ c-Si/SiO2 (1.5 nm) / LPCVD n-type poly-Si (~50 nm). These substrates were prepared by our industrial partner Jinko Solar. The TiO_2 interlayers were deposited by thermal ALD (atomic layer deposition) using titanium tetrakis isopropoxide (TTIP) and H2O precursors at a temperature of 250oC. Three TiO_2 thicknesses, 8 nm, 14 nm and 23 nm, were deposited over the full area of one side of the samples. For passivation samples the TiO_2-deposited side was partially coated with ~200 nm of Al to create adjacent regions with/without Al metallisation. Their passivation quality was examined through photoluminescence (PL) imaging as a function of cumulative high temperature annealing steps at 400°C and 500°C in air. Their corresponding ρ_c was monitored as a function of cumulative annealing steps from 250°C to 500°C on a hotplate in air.

The ρ_c of the contact samples, with 8 nm, 14 nm and 23 nm TiO_2 thicknesses, are shown as a function of cumulative annealing steps in Figure PP1.2.1.1. A reference line for a sample without a TiO_2 interlayer is also included. The samples with the 8 nm TiO_2 interlayer, have a ρ_c two orders of magnitude higher than the samples without an interlayer, at ~100 mΩ-cm^2 in the as-deposited state. With increasing annealing temperature, the ρ_c decreases, reaching a value of ~8 mΩ-cm^2 at an annealing temperature of above 450oC. The samples with thicker TiO_2 have slightly higher ρc values and they decrease with increasing annealing temperature, saturating at a ρ_c of ~20 mΩ-cm2 above 400°C. Thus, while the addition of TiO_2 interlayers leads to an increase in ρ_c, especially for thicker TiO_2 films, the obtained post-annealing ρ_c values are < 20 mΩ-cm^2 which is still sufficiently low for full-area contacts.

PL images of the passivation samples, with 8 nm, 14 nm and 23 nm TiO_2 thicknesses, are shown as a function of cumulative annealing steps in Figure PP1.2.1.2. A reference passivation sample without a TiO_2 interlayer is also included. The Al metallised regions are indicated by green rectangles. For the poly-Si samples without TiO_2, the Al metallised regions have significantly lower PL intensity than the non-metallised regions after annealing at 400oC. This situation is improved for samples with just 8 nm TiO_2 interlayers, which show a PL intensity in the metallised regions that is similar to non-metallised regions after annealing at 400oC. This demonstrates the effectiveness of the interlayer strategy. After an additional 500oC annealing step, both above samples show low PL intensity, indicating poor passivation quality. This is possibly due to the penetration of Al through the poly-Si layers to the c-Si interface which degrades the surface passivation.

Thicker TiO_2 interlayers (i.e. 14 nm and 23 nm) exhibit similar protective behaviour to ~8 nm layers at 400°C. However, at 500°C the added thickness provides additional protection, and some PL intensity is maintained in the Al metallised region. In particular, the sample with the 23 nm TiO_2 interlayer maintains a similar magnitude of PL intensity in regions with/without Al metallisation. Thus, TiO_2 interlayers can effectively reduce the interaction between the poly-Si layer and the Al overlayer.

As presented above, inserting an additional TiO_2 interlayer between the poly-Si layers and Al electrodes can improve thermal stability by limiting the interaction between poly-Si and Al. Based on PL intensity and ρ_c values, we found that thin ~8 nm TiO_2 can work as an effective protective layer for annealing steps at 400°C. With the addition of the TiO_2 interlayer the passivation quality of metallised regions can be maintained, and even slightly improved, after the post-metallisation annealing. This comes at the expense of increased ρc. If stability up to 500oC is required, then thicker TiO_2 interlayers can be used. The use of thicker TiO_2 further increases the ρc to values of ~20 mΩ-cm^2 which is still suitable for full-area contacts.

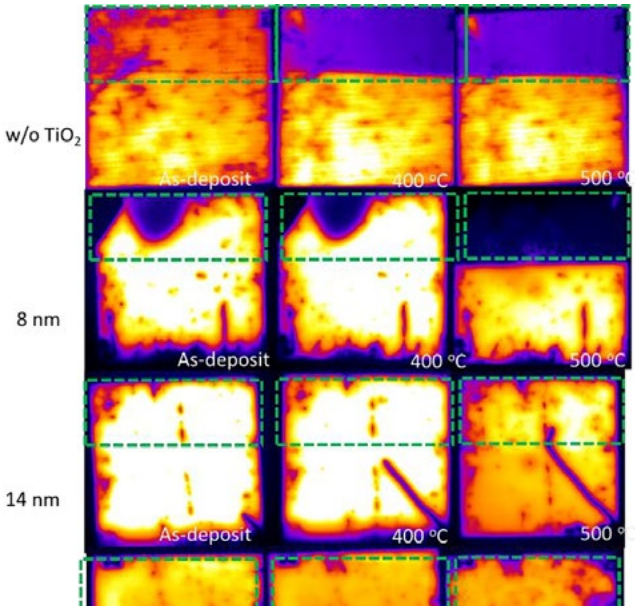

Figure PP1.2.1.2: PL images of n-type poly-Si contacts without TiO_2 (first row) and with 8 nm TiO_2 (second row), 14 nm (third row) and 23 nm TiO_2 (fourth row) before and after cumulative annealing steps.

Highlights and future work

In this study, TiO_2 was utilised as a first proof-of-concept barrier layer. The TiO_2 interlayers were shown to preserve the surface passivation of thin poly-Si layers up to 500°C, while maintaining contact resistivities on the tens of mΩ.cm^2 scale.

In future work, we are trialling other materials, such as conductive metal oxides and nitrides, as protective interlayers between poly-Si and Al electrodes. The optical properties of these materials will also be considered for sunward side applications. In addition, we will extend this TiO_2 interlayer study by using the standard industrial metallisation processes, including firing steps and screen-printed metal pastes.

Physical vapour deposition for doped tunnel-oxide polysilicon contacts

Several methods are available for depositing Si films to create poly-Si passivating contacts, including low-pressure chemical vapour deposition (LPCVD), plasma-enhanced chemical vapour deposition (PECVD), and physical vapour deposition (PVD). Currently, LPCVD is the industry-preferred method due to its throughput, performance and cost advantages. However, its non-directional deposition requires additional etching steps (Yan et al. 2021). PECVD, which offers in situ doping and intermediate directionality (experiencing minor wraparound), has gained considerable attention. Nevertheless, it necessitates extra safety measures due to the use of toxic precursors.

Sputtering, a PVD method, has recently garnered a lot of research interests (Nasebandt et al. 2022; Truong et al. 2023). With its directional and wraparound-free deposition at room temperature, it utilises low-hazard precursors or solid targets, demanding fewer safety measures than LPCVD and PECVD.

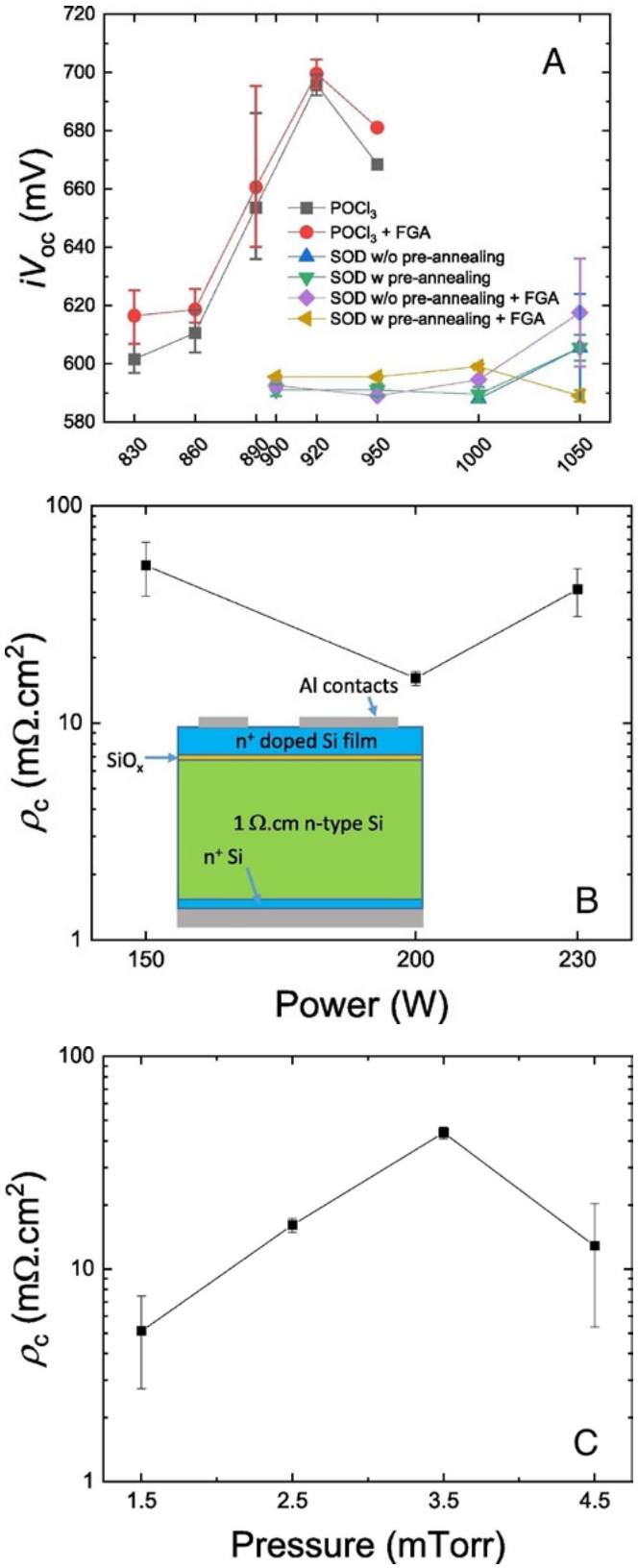

Figure PP1.2.1.3: (A) Performance of ex-situ doped sputtered poly-Si contacts and (B-—C) their contact resistivity with different deposition condition (Truon et al. 2023).

Currently, the doping of sputtered poly-Si contacts can be accomplished via either ex-situ (thermal diffusion) or in situ (co-sputtering) methods. For p+ sputtered poly-Si contacts, both in situ and ex-situ methods yield well-performing contacts with J_0 ~10 fAcm^{-2}, iV_{oc} > 720 mV, and ρ_c < 20 mΩ.cm^2 (Yan et al. 2018; Truong et al. 2020). However, for n+ sputtered poly-Si contacts, in situ diffusion proves challenging due to the absence of a functional n-type sputtering target. Our tests, using various phosphorus targets, revealed that P atoms could not be activated as dopants after sputtering and activation annealing. Therefore, ex-situ doping is the preferred method for forming n+ poly-Si contacts.

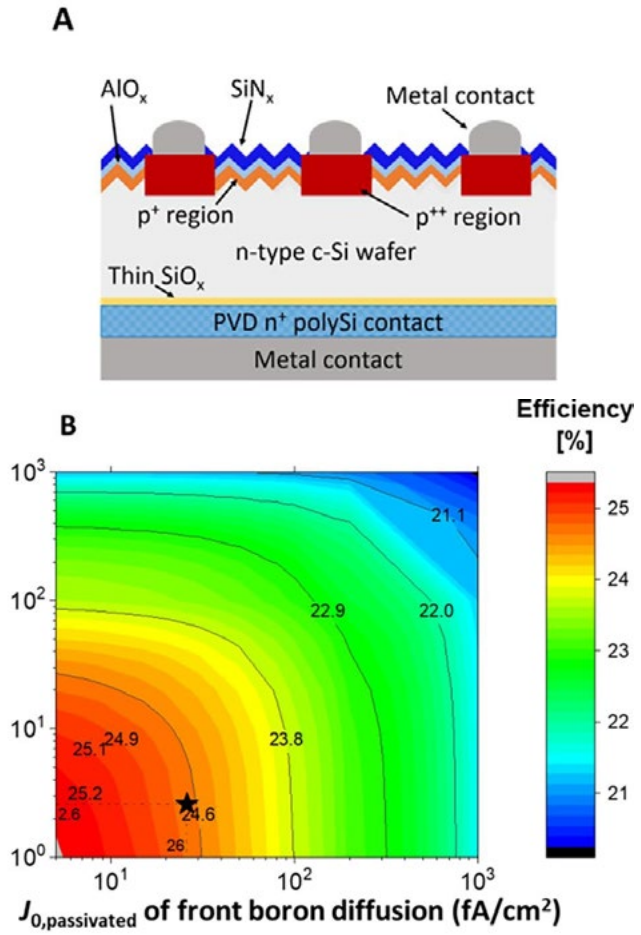

C

V_{oc} (mV)	J_{sc} (mA/cm^2)	FF (%)	η (%)
706	42.39	82.55	24.7

Figure PP1.2.1.3: (A) Performance of ex-situ doped sputtered poly-Si contacts and (B—-C) their contact resistivity with different deposition condition (Truon et al. 2023).

A recent study by Truong et al. (2023) compared two different ex-situ doping methods for n+ sputtered poly-Si contacts involving thermal diffusion using POCl3 and spin-on doping glass. The spin-on doping (SOD) method exhibited significantly lower performance compared to POCl3 diffusion, as illustrated in Figure PP1.2.1.3. This is mainly attributed to the fact that SOD is not a clean process, with a higher probability of contamination. On the other hand, POCl3 diffusion has gettering effects (Liu et al. 2022), making it more effective in contamination mitigation than SOD. Another reason for the difference in performance may be due to crystallinity and diffusion mechanisms (Michel et al. 2023).

The optimal performance for n+ sputtered poly-Si contacts is achieved with J_0 ~2.6 fAcm^{-2}, iVoc = 720 mV, and ρ_c < 10 mΩ.cm^2, as simulated to result in a cell efficiency of 24.7%, as shown in Figure PP1.2.1.4. These values are promising, and there is still room for further optimisation.

Highlights and future work

With a $POCl_3$ diffusion for sputtered n$^+$ poly-Si contacts: an iV_{oc} of ~720mV, a J_0 of 2.6 fAcm^{-2}, and a contact resistivity ρc of less than 10 mΩ.cm2 were achieved. Quokka3 simulations show that cell efficiencies as high as 25% are possible using the optimised passivating contacts.

Building on the outcomes of the Quokka3 simulation, the team is committed to further enhancing the performance of poly-Si contacts and plans to implement these improvements on a full device. This effort aims to demonstrate the substantial potential of the sputtered poly-Si technology.

References

Liu, A., Phang, S. P. & Macdonald, D. (2022). Gettering in silicon photovoltaics: A review. Solar Energy Materials and Solar Cells 234, 111447.

Michel, J. I., Yan, D., Phang, S. P., Zheng, T., Johnson, B. C., Yang, J., Zhang, X., Chen, W., Wan, Y., Truong, T., Stuckelberger, J., Pan, Y., Macdonald, D. & Bullock, J. (2023). Poly-Si passivating contacts prepared via phosphorus spin-on-doping: A comparison between different silicon deposition methods. Solar Energy Materials and Solar Cells 255, 112290.

Nasebandt, L., Min, B., Hollemann, C., Hübner, S., Dippell, T., Peibst, R. & Brendel, R. (2022). Sputtered Phosphorus-Doped poly-Si on Oxide Contacts for Screen-Printed Si Solar Cells. Solar RRL 6, 2200409.

Truong, T. N., Yan, D., Chen, W., Wang, W., Guthrey, H., Al-Jassim, M., Cuevas, A., Macdonald, D. & Nguyen, H. T. (2020). Deposition pressure dependent structural and optoelectronic properties of ex-situ boron-doped poly-Si/SiOx passivating contacts based on sputtered silicon. Solar Energy Materials and Solar Cells 215, 110602.

Truong, T., Kang, D., Wang, E.-C., Wang, J., Phang, S. P., Macdonald, D. & Stuckelberger, J. (2023). Ex-situ phosphorus-doped polycrystalline silicon passivating contacts for high-efficiency solar cells by physical vapour deposition. Solar Energy 255, 285-291.

Yan, D., Cuevas, A., Michel, J. I., Zhang, C., Wan, Y., Zhang, X. & Bullock, J. (2021). Polysilicon passivated junctions: The next technology for silicon solar cells? Joule 5, 811-828.

Yan, D., Cuevas, A., Phang, S. P., Wan, Y. & Macdonald, D. (2018). 23% efficient p-type crystalline silicon solar cells with hole-selective passivating contacts based on physical vapor deposition of doped silicon films. Applied Physics Letters 113(6). *https://doi.org/10.1063/1.5037610*

Yan, D., Cuevas, A., Stuckelberger, J., Wang, E.-C., Phang, S. P., Kho, T. C., Michel, J. I., Macdonald, D. & Bullock, J. (2023a). Silicon solar cells with passivating contacts: Classification and performance. Progress in Photovoltaics: Research and Applications 31, 310-326.

Yan, D., Michel, J. I., Pan, Y., Phang, S. P., Macdonald, D., Shen, H., Duan, L., Catchpole, K., Yang, J., Zheng, P., Zhang, X., Jin, H. & Bullock, J. (2023b). Improving the Stability of Polycrystalline Silicon Passivated Contacts Using Titanium Dioxide. 2023 IEEE 50th Photovoltaic Specialists Conference (PVSC), 1-3.

PP1.2.2 Advanced Hetero-Contacts

ANU Team
Dr Lachlan Black, Prof. Daniel Macdonald

ANU Students
Mohamed Shehata, Gabriel Bartholazzi

UNSW Team
Dr Michael Nielson, Dr Alexander Baldacchino, A/Prof. Murad Tayebjee, Prof. Bram Hoex

UNSW Students
Alvin Mo

UoM Team
Dr James Bullock, Dr Di Yan

UoM Students
Jesus Ibarra Michel

Partner
Jinko Solar

Funding Support
ACAP, ARENA, ANU, UNSW, UoM

Aims

This Program Package aims to develop advanced hetero-contact materials and structures in order to overcome the limitations of existing contact technologies for silicon solar cells. Current focuses include the development of optically transparent passivating contacts based on metal oxide materials, investigation of low-damage sputtering methods for transparent conductive oxide layers, and development of passivating tunnel interlayers for singlet fission devices

Transparent Passivating Contacts

Effective suppression of contact recombination losses via so-called passivating contacts is essential for realising high efficiency silicon solar cells. Existing Si-based passivating contacts, based either on hydrogenated amorphous silicon (a-Si:H) or polycrystalline silicon (poly-Si), are highly effective electrically, but have limited optical transparency due to their relatively narrow bandgaps, resulting in significant parasitic absorption losses when these contacts are placed on the front side of a solar cell. This results in an unavoidable trade-off between high current and high voltage at a cell level, or necessitates complex processing to form local contacts, which adds cost and introduces additional transport losses. Passivating contacts based on alternative wide bandgap materials such as metal oxides offer the potential to overcome this trade-off, if their electrical properties can be improved to match those of Si-based contacts. This project aims to realise effective passivating contact structures combining excellent passivation and contact properties with high optical transparency, by exploring the application of alternative wide bandgap materials in this role.

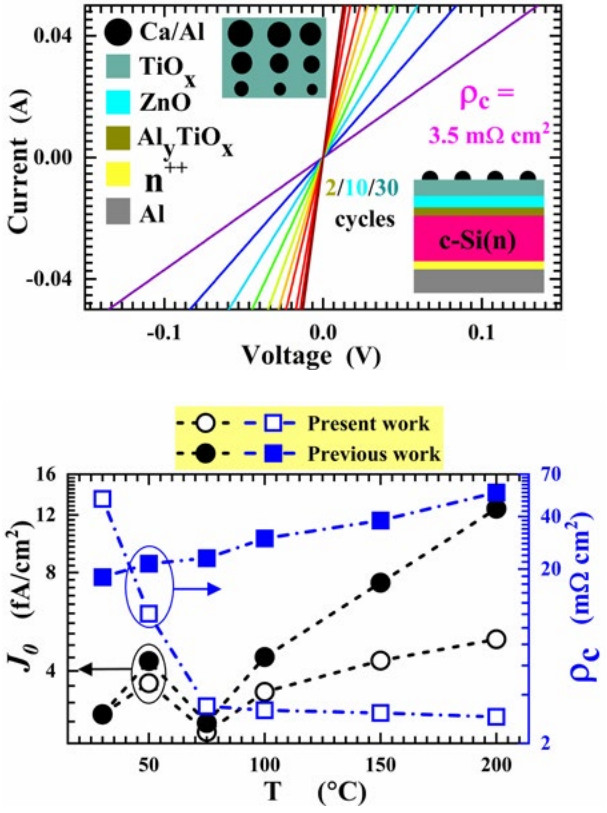

Figure PP1.2.2.1: Top: Current-voltage curves measured for an $AlTiO_x/ZnO/TiO_2$ electron-selective passivating contact as a function of contact diameter in a Cox–Strack contact resistivity test structure. The inset shows the stack structure and the resulting contact resistivity ρc extracted from the measurements. Bottom: Surface recombination parameter J_0 and contact resistivity ρ_c vs. deposition temperature for $AlTiO_x/ZnO/TiO_2$ (labelled "Present work") and $AlTiO_x/TiO_2$ (labelled "Previous work") stacks (Shehata et al. 2023a).

We have previously demonstrated outstanding passivation and contact performance for electron-selective passivating contacts employing a novel $AlTiO_x/TiO_2$ stack structure prepared by atomic layer deposition (ALD). These contacts exhibited record passivation performance for electron-selective contacts based on transparent materials, with passivation comparable to state-of-the-art Si-based contacts. This work was reported by Shehata et al. (2022).

Building on this work, we have now developed a new structure which maintains the passivation performance while reducing the contact resistivity by an order of magnitude. In this structure, some of the $AlTiO_x$ thickness is replaced by ALD ZnO to form an $AlTiO_x/ZnO/TiO_2$ structure. As shown in Figure PP1.2.2.1, this structure shows passivation performance (in terms of the surface recombination parameter J_0) comparable to or better than the original $AlTiO_x/TiO_2$ stack, but with greatly reduced contact resistivity of 2–4 mΩ cm² compared to > 20 mΩ cm² with the previous structure, as well as a reduced sensitivity of both contact resistivity and J_0 to deposition temperature. This work has been reported by Shehata et al. (2023a)..

In our initial work on these stacks in Shehata et al. (2022, 2023a), we hypothesised that their excellent passivation might result from passivation of the interface by chlorine atoms (Cl) originating from the $TiCl_4$ precursor used for ALD of the TiO_2 layer. This mechanism had been hypothesised also by other authors for single TiO_2 layers deposited from $TiCl_4$, however, direct evidence of the role of Cl in passivation had not previously been reported. As a follow-up to our initial work, we therefore chose to investigate this proposed passivation mechanism, seeking to provide direct evidence of the role of Cl in silicon surface passivation.

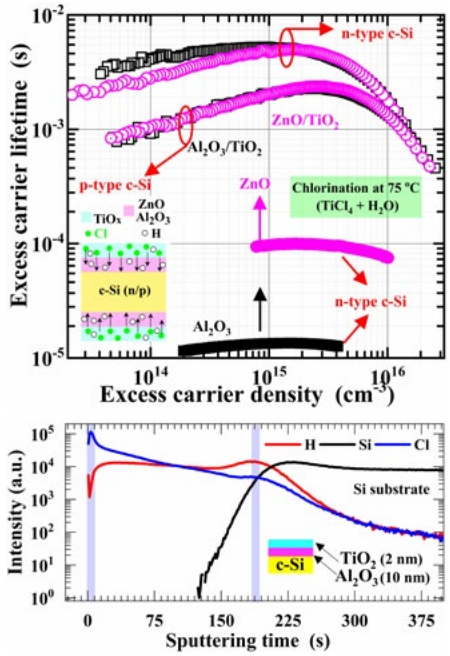

Figure PP1.2.2.2: Top: Effective carrier lifetime of Si wafers passivated by 1 nm of either ZnO or Al_2O_3, both before and after capping by 2 nm of TiO_2 deposited from $TiCl_4$ + H_2O. Deposition of all layers occurred at 75°C and no post-deposition annealing was applied. Bottom: Compositional profile of H, Cl and Si obtained by time-of-flight secondary ion mass spectrometry (ToF-SIMS) for an Al_2O_3 (10 nm) / TiO_2 (2 nm) structure (Shehata et al. (2023b).

Using purpose-designed experiments, we have now experimentally verified the critical role of chlorine in the passivation mechanism of these stacks. TiO_2 capping layers were deposited on ZnO and Al_2O_3 interlayers of varying thickness, and the resulting changes in passivation were correlated with measurements of the Cl and H distribution in the stack using SIMS, as illustrated in Figure PP1.2.2.2. Capping of either ZnO or Al_2O_3 interlayers by TiO_2 at low temperatures was found to result in outstanding passivation performance, while SIMS clearly showed that Cl was diffusing to and accumulating at the Si interface, where it presumably passivates dangling bonds in a similar way to hydrogen. Remarkably, this diffusion and passivation was found to occur at very low temperatures (75°C). This is in contrast to hydrogen diffusion and passivation, which typically requires annealing at temperatures of ~400°C. This work has been reported in Shehata et al. (2023b).

Besides the application of these TiO_2-based stacks as electron-selective contacts, we have also explored their application as tunnelling interlayers for hole-selective contacts. In this role, we seek to benefit from their excellent surface passivation properties while keeping their overall thickness low to maintain the hole-selectivity of the contact stack. As an initial demonstration of this approach, we have successfully demonstrated $AlTiO_x/TiO_2$ stacks as a passivating tunnel interlayer for Cu_2O hole-selective contacts. As shown in Figure PP1.2.2.3, both the passivation and contact resistivity of Cu_2O contacts improve with the addition of the interlayer. Indeed, in both cases, record low values are achieved for this material, depending on the interlayer thickness. This work has been reported in Bartholazzi et al. (2023).

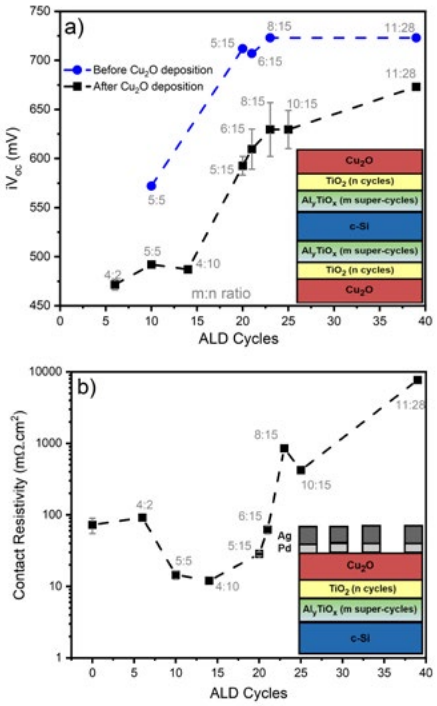

Figure PP1.2.2.3: Top: Implied open-circuit voltage for Si wafers passivated by a stack of $AlyTiO_x/TiO_2$, both before and after capping with a Cu_2O hole-selective layer, as a function of the total number of $AlyTiO_x/TiO_2$ super-cycles/cycles. Labels beside each data point indicate the ratio m:n of Al_yTiO_x super-cycles to TiO_2 cycles. Bottom: Corresponding contact resistivity measured for $Al_yTiO_x/TiO_2/Cu_2O$ hole-selective contact stacks (Bartholazzi et al. 2023).

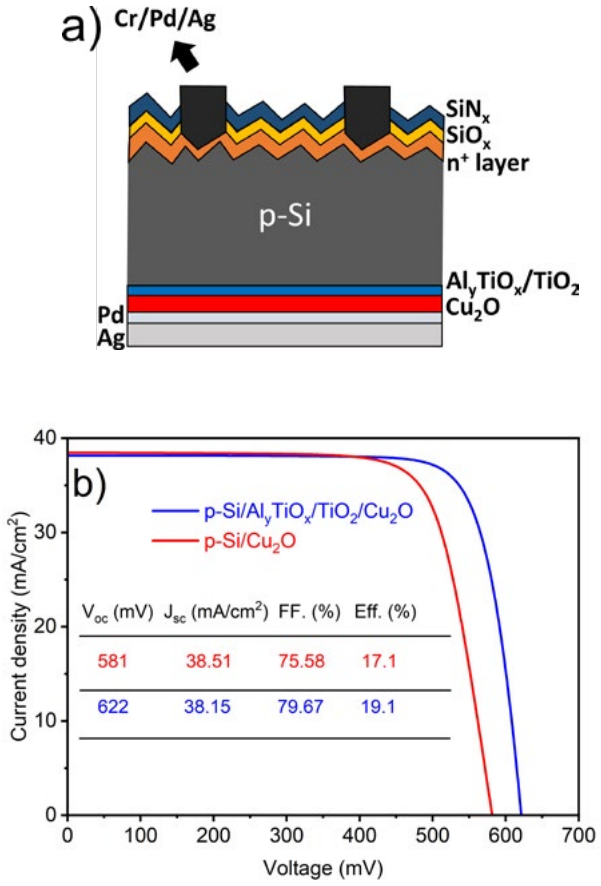

Figure PP1.2.2.4: Top: Schematic structure diagram of proof-of-concept cells with rear-side $Al_yTiO_x/TiO_2/Cu_2O$ hole-selective contact. Bottom: Corresponding J-V curves and cell parameters for this cell, with and without the Al_yTiO_x/TiO_2 interlayer stack (Bartholazzi et al. 2023

The resulting optimised contact was demonstrated as a rear contact in proof-of-concept p-type silicon solar cells (see Figure 1.2.2.4), resulting in an efficiency of 19.1%, compared to 17.1% for control devices without the $AlTiO_x/TiO_2$ interlayer. While the absolute efficiency of both devices was limited by non-ideal front-side optics (resulting in low short-circuit current), the benefit of the improved rear contact properties was amply demonstrated, with an increase of ~40 mV in the open-circuit voltage as well as a ~4% absolute increase in fill factor compared to the control.

Low-Damage Sputtering of TCOs

Magnetron sputtering is the standard deposition method for transparent conductive oxides in industrial applications. For example, indium tin oxide is utilised in the production lines of silicon heterojunction solar cells and for emerging technologies such as perovskite and tandem Si-perovskite cells. Magnetron sputtering usually involves high energy particle collisions with the substrate and causes significant surface damage. This project aims to develop low-damage, room temperature magnetron sputtering approaches. This is achieved by using hollow cathode targets and a gas flow sputtering mechanism, which is performed at high pressure/flow to reduce the energy of colliding particles and to carry the sputtered atoms to the substrate. Additionally, we explore the impact of different sputtering parameters including (but not limited to) pressure and excitation sources.

We have carried out room temperature sputtering using three different approaches as shown in Figure PP1.2.2.5. We compare the different properties of the films and the damage done to c-Si with thin/fragile passivating layers on top (Michel et al. 2023). The sputtered layers were indium tin oxide (ITO) and hydrogenated indium oxide (IO:H) and the excitation sources we have used so far are radio-frequency (13.56 MHz) and pulsed DC.

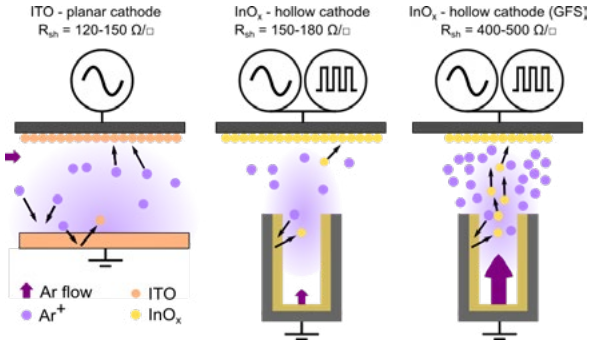

Figure PP1.2.2.5: TCO deposition diagram including hollow cathode (HC) and gas flow sputtering (GFS) approaches for low-damage sputtering.

We have measured the electrical and chemical properties of ITO and InO_x (via hollow cathode) and found them to be comparable, as shown in Figure PP1.2.2.6. The bulk resistivity and hall parameters are in the range of expected numbers for applications in high efficiency photovoltaics and the metallic-to-oxidised indium ratio for the films is similar to the ITO reference.

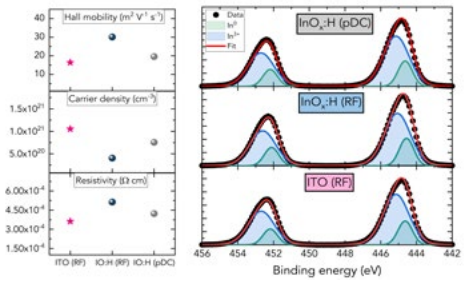

Figure PP1.2.2.6: Electrical and chemical properties of ITO and InOx. Left: Hall mobility, carrier density and resistivity of the three films. Right: Indium 3Dd core levels of the three films, showing very similar stoichiometry

A part of this work has involved the development of the InO_x gas flow sputtering recipe. To find suitable conditions for the gas flow sputtering mode we studied the effect of Ar flow rate and pressure on the deposition rate of the films. Figure PP1.2.2.7 shows the deposition rate as a function of Ar flow rate and process pressure for an RF excitation source. A large dependence of the deposition rate on the Ar flow rate, is observed when the pressures are 60 and 80 mtorr, meaning that the sputtered particles are delivered to the substrate by the gas and without a strong flow there is no deposition rate. Corresponding R_{sh} values (for 40–50 nm films) are also added for the data points. The films deposited via gas flow sputtering generally show higher R_{sh} values as compared to the ITO and InO_x references (at a pressure of 1 mtorr), which show Rsh <180 Ω/□.

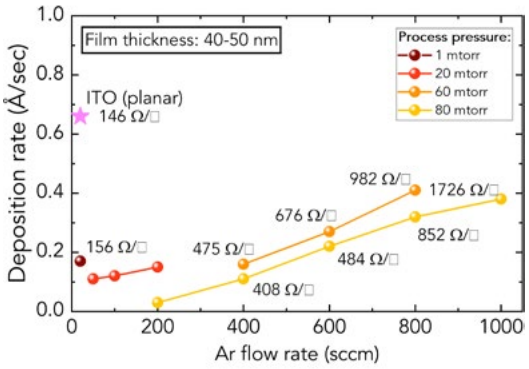

Figure PP1.2.2.7: Deposition rate as a function of the Ar flow rate for different process pressures featuring both ITO and InO_x with different target geometries.

Finally, we have recently tested our low-damage sputtering recipes in actual passivating structures to evaluate the impact. These test structures consist of symmetrical SiO_x/poly-Si (n^+) passivating contact structures deposited on c-Si and yielding minority carrier lifetimes higher than 1 ms. The thickness of the poly-Si film in these structures is 10 nm, which makes them very sensitive to the interface damage caused by sputtering. A summary of these experiments is shown in Figure PP1.2.2.8, where the damage after sputtering on half of the sample is evaluated by photoluminescence images. These promising results show the lower damage or the highest recovery in passivation observed with hollow cathode and gas flow sputtering as compared to the conventional planar target sputtering.

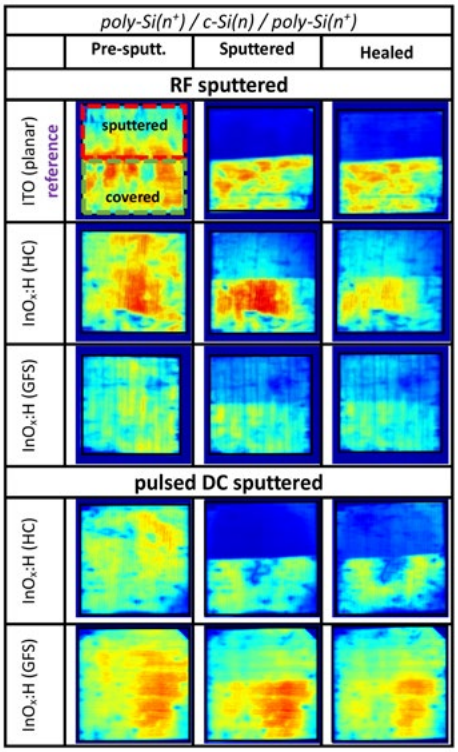

Figure PP1.2.2.8: Photoluminescence images of symmetrical c-Si/SiO_x/poly-Si(n^+) passivating structures during different sputtering process steps.

Future work involves optimising the gas flow sputtering recipes to yield lower resistivities so that we can employ the films in actual solar cell devices. Additionally, we have started tests using our high power impulse magnetron sputtering (HiPIMS) source which allows for higher ionisation of atoms and a film with better properties at room temperature.

Interlayers for Singlet Fission

Conventional silicon-based single-junction solar cells are approaching their fundamental efficiency limit. A major barrier to surpassing this limit is thermalisation loss. Addressing this challenge could lead to significant breakthroughs. While tandem solar cells have been developed as a solution to this problem, our research introduces an innovative, cost-effective and highly efficient alternative: singlet fission (SF) sensitised silicon solar cells. This approach requires only the deposition of a singlet fission layer atop a silicon substrate. Singlet fission is advantageous as it generates two photoelectrons (triplets) from a single high-energy photon. These photoelectrons can then be injected into the silicon to generate an electric current. However, a critical concern with this design is the high recombination velocity at the interface between the singlet fission layer and the silicon, leading to premature recombination of photoelectrons originating from the SF layer before they can be effectively harvested.

In our project, we are developing an interlayer between the SF layer and the silicon substrate to passivate the silicon surface and enhance the transfer of triplets. We have investigated various interlayer materials and thicknesses to optimise this process.

In 2019, a research group from MIT pioneered the development of an interlayer for sensitised SF silicon solar cells (Einzinger et al. 2019). Their innovation employed HfO_xN_y with a thickness of approximately 8 Å. To achieve this ultra-thin, uniform layer, atomic layer deposition (ALD) was utilised. However, the resultant cell performance in this study was suboptimal, indicating that further refinement of the interlayer is necessary. Our project focuses on the discovery of new materials and engineering of the interlayer, now designated as the passivating exciton transport layer (PETL).

A primary challenge in developing PETL is balancing the layer's thickness: while a thicker layer (~10 nm) is beneficial for passivation, a thinner layer is required for efficient exciton (triplets and singlets) tunnelling, and optimal thickness varies with different materials.

The most straightforward approach to assess interlayer performance (or triplet injection efficiency) is through external quantum efficiency (EQE) measurements, particularly by observing an EQE enhancement in the short wavelength region. However, this necessitates fabricating a complete cell for EQE measurement. More critically, it does not allow differentiation between the effects of passivation and triplet injection on the observed EQE boost. Consequently, we have developed an optical setup to assess triplet injection performance independently of full device fabrication – magnetic field photoluminescence (MPL) measurement.

Before delving into MPL, it is pertinent to understand singlet fission. In this process, a high energy photon excites a molecule from its ground state to a singlet excited state, which then shares its energy with a neighbouring molecule, producing two triplets through singlet fission in the SF layer. In our study, tetracene is employed as the SF material. As this is a spin-allowed process, the total spin of the molecules remains zero before and after singlet fission. These triplets are then injected into the silicon substrate.

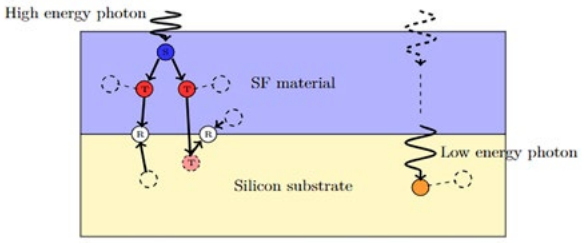

Figure 1.5: Schematic diagram of SF sensitized silicon based solar cell without interlayer

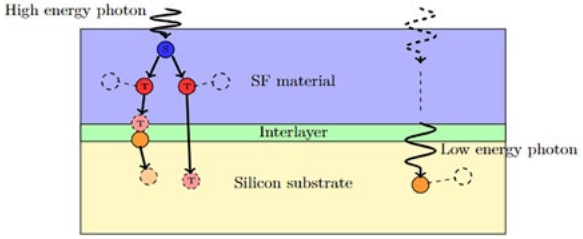

Figure 1.6: Schematic diagram of SF sensitized silicon based solar cell with interlayer

Figure PP1.2.2.9: Schematic diagram of SF sensitised silicon-based solar cell working principle, (a) without interlayer, and (b) with interlayer

The population dynamics of singlets and triplets are significantly influenced by the presence of a magnetic field, as illustrated in Figure PP1.2.2.10. An increase in the magnetic field strength results in an augmented population of singlets, concomitantly reducing the population of triplets. This phenomenon can be attributed to the magnetic field's influence in restricting the separation of triplet pairs. The magnetic field essentially acts as a modulating factor, altering the balance between singlet and triplet states, as evidenced by the observed changes in their respective populations under varying magnetic field intensities.

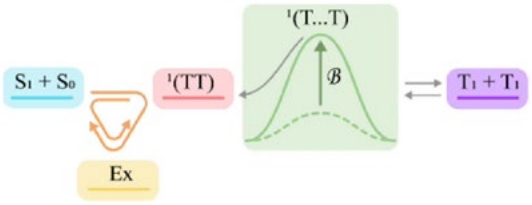

Figure PP1.2.2.10: State dynamic of singlet fission in the presence of a magnetic field.

When evaluating the alterations in silicon photoluminescence in the presence of a magnetic field (denoted as MPL_{Si}), it becomes possible to determine the nature and extent of either triplet or singlet injection into the silicon. A key indicator in this measurement is the direction of change in MPL_{Si} under high magnetic field conditions. Specifically, a positive change in MPL_{Si} at elevated magnetic field strengths suggests an increase in singlet contributions to silicon PL. Conversely, a negative MPL_{Si} change under similar conditions is indicative of enhanced triplet contributions to silicon PL. Given our focus on optimising triplet injection, our research aims to achieve a negative MPL_{Si} change, highlighting the successful augmentation of triplet populations in the silicon substrate.

In our study, we focused on changes in MPL_{Si} within a high magnetic field range (1,500–3,300G). By plotting these changes as a function of interlayer thickness for different PETL materials, as shown in Figure PP1.2.2.11, we can analyse their effectiveness. The graph reveals that certain PETL materials facilitate triplet transfer, indicated by a negative MPL_{Si} change. As previously mentioned, the optimal thickness is marked by a peak in the graph. Thicknesses below this peak did not passivate effectively, whereas thicknesses above it restricted the triplets from tunnelling through the layer.

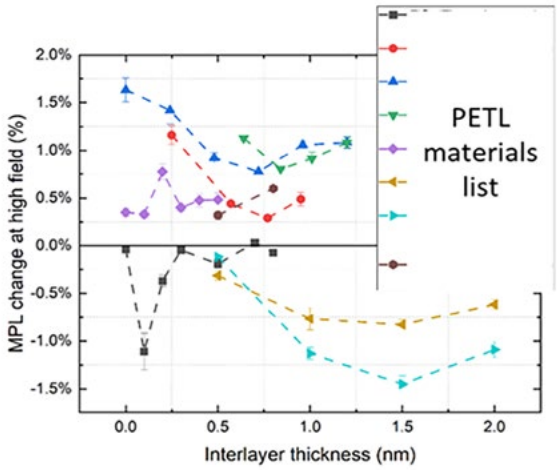

Figure PP1.2.2.11: The effect of applied magnetic field on photoluminescence depends on the interlayer thickness for different PETL materials.

A significant achievement of our research is the discovery of three new PETL materials that demonstrate potential in facilitating triplet injection. Notably, we have identified the thickest PETL materials to date that show evidence of triplet injection at a thickness of 1.5 nm. This is also the first instance of observing enhanced triplet injection in p-type silicon substrates. These materials are currently undergoing intellectual property (IP) registration and are therefore confidential. Additionally, we have conducted bichromatic MPL_{Si} and time-resolved photoluminescence (TRPL) measurements. These tests further confirm the effectiveness of these PETL materials as interlayers in promoting triplet injection.

References

Shehata, M. M., Phang, P., Basnet, R., Yin, Y., Kremer, F., Bartholazzi, G., Andersson, G. G., Macdonald, D. H. & Black, L. E. (2022). Outstanding Surface Passivation for Highly Efficient Silicon Solar Cells Enabled by Innovative Al_y TiO_x /TiO_x Electron-Selective Contact Stack. Solar RRL 6, 2200550.

Shehata, M. M., Bartholazzi, G., Macdonald, D. E. & Black, L. E. (2023a). Engineering Silicon Interfaces with Transparent $AlyTiO_x$/ZnO/TiO_2 Stack Exhibiting Exceptional Passivating Contact Performance. Advanced Energy Materials 13.

Shehata, M. M., Macdonald, D. E. & Black, L. E. (2023b). Dramatic Reduction of Silicon Surface Recombination by ALD TiO_x Capping Layer from $TiCl_4$ and H_2O: The Role of Chlorine. ACS Applied Materials & Interfaces.15(39) 46504 *https://doi.org/10.1021/acsami.3c09083*

Bartholazzi, G., Shehata, M. M., Basnet, R., Samundsett, C., Macdonald, D. H. & Black, L. E. (2024). Novel Interlayer Boosting the Performance of Evaporated Cu2O Hole-Selective Contacts in Si Solar Cells. Solar RRL 8, 2300727.

Michel, J.I., Yan, D., Chen, W. & Bullock, J. (2023). Towards low-damage transparent conductive oxide sputtering for high-efficiency photovoltaics. 2023 Asia-Pacific Solar Research Conference. Melbourne 5–7 December 2023. (and manuscript in prep).

Einzinger, M., Wu, T., Kompalla, J. F., Smith, H. L., Perkinson, C. F., Nienhaus, L., Wieghold, S., Congreve, D. N., Kahn, A., Bawendi, M. G. & Baldo, M. A. (2019). Sensitization of silicon by singlet exciton fission in tetracene. Nature 571, 90-94.

PP1.2.3 Advanced Dielectrics

ANU Team
Prof. Daniel Macdonald, Dr Lachlan Black, Dr Marco Ernst

ANU Student
Cole Johnson

Partners
Eindhoven University of Technology (Netherlands)
SunPower Corporation (USA)

Funding Support
ARENA, ANU

Aims

This project aimed to explore the practical use of innovative multifunctional dielectric layers based on phosphorus oxide (PO_x) in order to minimise surface recombination and simplify the manufacturing of high efficiency silicon solar cells.

Highly efficient silicon solar cells often employ local contacts to reduce recombination at contact points, achieving some of the highest efficiencies in laboratory settings. The challenge lies in translating these advancements into the industry, replacing complex photolithographic techniques with cost-effective, high-throughput methods for local contact creation.

Collaborating with the Eindhoven University of Technology, the ANU identified phosphorus oxide (PO_x) as a promising passivation material for silicon cells. PO_x exhibited comparable or superior performance compared to currently used materials in mass production. Given that phosphorus is a dopant in silicon, PO_x also holds potential for local contact formation through laser doping – an established industrial process.

This project investigated the utilisation of phosphorus oxide (PO_x) as an insulating layer within high efficiency silicon solar cells. The goal was to mitigate efficiency loss due to surface recombination and simplify production processes through localised laser contact formation. The integration of multifunctional dielectric layers, like PO_x, could streamline processing, ultimately reducing the cost of producing high efficiency silicon solar cells. The overarching aim was to advance this promising technology for future commercial applications.

Progress

Initially demonstrated on flat silicon surfaces, PO_x-based dielectric stacks have now also been demonstrated on textured silicon surfaces. Textured surfaces are found on the front side of commercial silicon solar cells and may or may not have a heavily doped phosphorus emitter. Crucially, PO_x-based stacks on such surfaces have proven to significantly reduce surface recombination losses compared to the industry-standard SiO_x/SiN_x passivation stacks (see Figure PP1.2.3.1). Their applicability in commercial solar cell manufacturing is reinforced by proven compatibility with a standard SiN_x capping layer and the high temperature firing process.

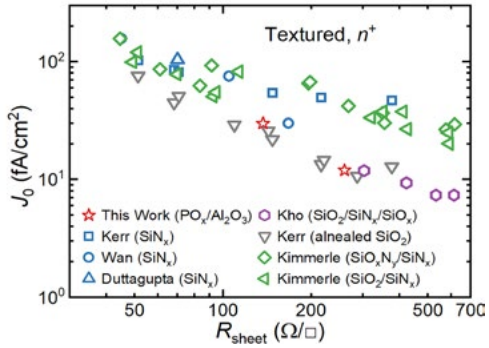

Figure PP1.2.3.1: Surface recombination parameter J_0 vs. sheet resistance for n^+ diffused, textured silicon surfaces passivated by PO_x/Al_2O_3 stacks in this work. This data is compared to conventional passivation layers such as SiN_x and SiO2/SiN_x, as well as state-of-the-art (non-industrial) 'annealed' SiO2 and $SiO_2/SiN_x/SiO_x$ (ONO) stacks (Melskens et al. 2021).

The durability of PO_x passivation was examined by accelerated environmental testing at the specialised facilities of our industry partner SunPower. Additionally, a focused investigation into its stability under ultraviolet light was conducted. These studies have helped to identify potential degradation mechanisms and avoidance strategies.

Analysis of the chemical structure and composition of PO_x-based stacks uncovered notable intermixing between the PO_x layer and Al_2O_3 capping layer during annealing treatments at elevated temperatures (refer to Figure PP1.2.3.2). These treatments are essential for activating the advantageous electrical properties of the stacks, and the observed structural changes provide insights into the microstructural origins of these properties.

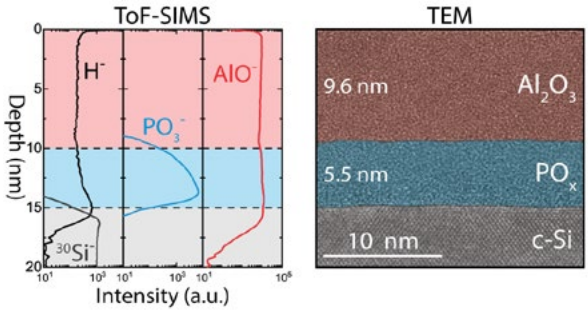

Figure PP1.2.3.2: Left: Compositional profile obtained by time-of-flight secondary ion mass spectrometry (ToF-SIMS). Right: Corresponding cross-sectional transmission electron microscopy image of PO_x/Al_2O_3 stacks after annealing (Theeuwes et al. 2021).

We explored two alternative capping layers for PO_x and investigated six PO_x-based ternary compounds to understand their passivation properties. This has resulted in, among other outcomes, an enhanced comprehension of the crucial role played by the capping layer, revealing a multi-faceted nature surpassing our initial expectations. Additionally, we gained knowledge about the chemical origin of the positive fixed charge in PO_x, a critical factor influencing its passivation quality.

The capacity to form local electrical contacts through laser processing of silicon surfaces coated with PO_x-based dielectric stacks has been successfully demonstrated. Optimised laser processing enables the simultaneous removal of the dielectric stack while introducing phosphorus into the silicon substrate. As phosphorus functions as an n-type dopant in silicon, this process allows the creation of local n^+ emitter regions that align automatically with the laser processed contact openings. This alignment facilitates the formation of contacts by low electrical resistance (Figure PP1.2.3.3). While previously hypothesised, experimental verification has now been achieved. This breakthrough presents exciting prospects for streamlining the manufacturing processes of high-efficiency silicon solar cells.

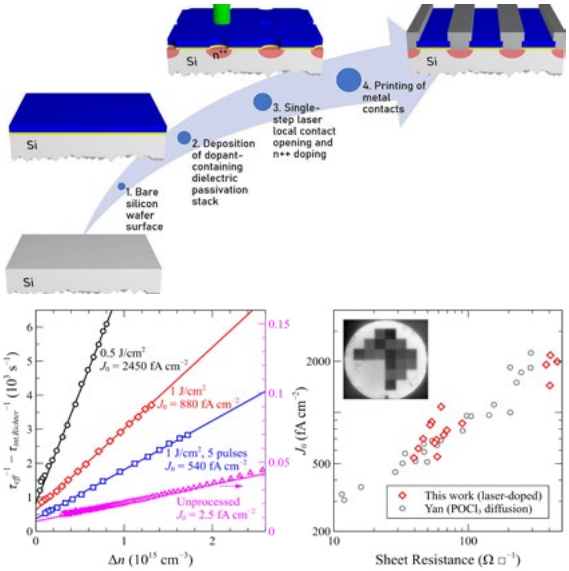

Figure PP1.2.3.3: Top: Schematic representation illustrating the formation of laser-doped contacts from a dopant-containing dielectric layer. Bottom left: An example demonstrating the extraction of the surface recombination parameter J_0 for planar silicon surfaces after laser doping from PO_x/Al_2O_3 with varying laser parameters. Bottom right: Summary of J_0 vs. sheet resistance for laser-doped regions formed from PO_x/Al_2O_3 stacks, in comparison to results obtained with a standard thermal diffusion process. The inset features a photoluminescence image of a PO_x/Al_2O_3 -passivated silicon wafer with an array of square regions processed using different laser settings (Black et al. 2020).

The initial demonstration of laser processed point-contact formation from PO_x/Al_2O_3 stacks focused on large-area laser processed regions (approximately 1 cm × 1 cm). However, for practical implementation in solar cell devices, it is preferable to minimise the contact area, typically achieved through small-area point contacts (e.g. 20 µm × 20 µm). Consequently, a systematic investigation was undertaken to explore the formation of small-area laser processed point contacts. This investigation considered the influence of laser processing parameters and subsequent annealing treatments on contact recombination and resistive losses. The verification of successful point-contact formation is depicted in Figure PP1.2.3.4, and optimal laser settings have been determined to minimise both contact recombination and resistivity.

In contrast to large-area laser processed regions, small point contacts introduce edge recombination losses due to laser-induced defects, leading to a notable increase in overall recombination losses. Consequently, a systematic investigation of various annealing treatments was conducted, resulting in the successful identification of a novel low-temperature annealing process capable of passivating the majority of laser-induced defects (see Figure PP1.2.3.4). This discovery is a crucial prerequisite for ensuring the viability of such contacts for application in silicon solar cells.

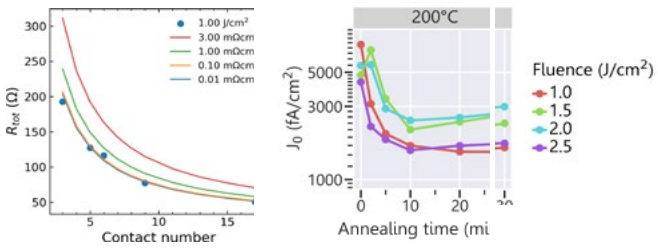

Figure PP1.2.3.4: Left: Measurement of contact resistivity for point contacts formed through laser processing of POx/Al2O3 stacks. Right: Recovery of surface recombination parameter J0 for laser processed point contacts during annealing at 200°C. (Ernst et al. 2022).

The resulting optimised contact properties were demonstrated to be compatible with an efficiency potential of 24.4% for n-PERL silicon solar cells featuring PO_x passivation and laser processed point contacts. This assessment was based on cell simulations utilising properties for other device components (bulk and front side) that were previously measured for cells fabricated in our laboratory.

References

Black, L. E., Ernst, M., Theeuwes, R., Melskens, J., Macdonald, D. & Kessels, W. M. M. (2020). Self-aligned local contact opening and n+ diffusion by single-step laser doping from PO_x/Al_2O_3 passivation stacks. Solar Energy Materials and Solar Cells 217. (*https://doi.org/10.1016/j.solmat.2020.110717*).

Ernst, M., Black, L. E., Theeuwes, R., Macdonald, D. & Kessels, W. M. M. (2022). Simultaneous laser local contact opening and n+ doping from PO_x/Al_2O_3 passivation stacks for high-efficiency PERL solar cells. 8th World Conference on Photovoltaic Energy Conversion, Milan, Italy, 26–30 September 2022.

Melskens, J., Theeuwes, R. J., Black, L. E., Berghuis, W.-J. H., Macco, B., Bronsveld, P. C. P. & Kessels, W. M. M. (2021). Excellent passivation of n-type silicon surfaces enabled by pulsed-flow plasma-enhanced chemical vapor deposition of phosphorus oxide capped by aluminum oxide. physica status solidi RRL 15. (*https://doi.org/10.1002/pssr.202000399*).

Theeuwes, R. J., Melskens, J., Black, L. E., Beyer, W., Koushik, D., Berghuis, W. J. H., Macco, B. & Kessels, W. M. M. (2021). PO_x/Al_2O_3 stacks for c-Si surface passivation: Material and interface properties. ACS Applied Electronic Materials 3. (*https://doi.org/10.1021/acsaelm.1c00516*).

PP1.3 SILICON ADVANCED DEVICES AND FABRICATION TECHNOLOGIES

PP1.3.1 Advanced Fabrication Technologies

UoM Team
Dr James Bullock, Dr Di Yan

UoM Students
Yida Pan

ANU Team
Dr Di Kang

ANU Student
Jiali Wang

Partners
Jinko Solar

Funding Support
ACAP, ARENA, UoM

Aims

The tunnel oxide passivated contact (TOPCon) approach, which utilises a stack consisting of a doped polysilicon (poly-Si) layer and a thin SiO_x layer, has already achieved excellent passivation/cell results (Yan et al. 2023, 2021). However, it is challenging to utilise full-area poly-Si contacts, particularly on the solar cell's front side, due to parasitic absorption. As such, one of the approaches to advance the TOPCon architecture is to develop processes for localised poly-Si doping under the front contacts or use in an interdigitated back contact (IBC) structure with partial poly-Si contacts, both of which can greatly reduce the parasitic absorption. However, the complex processes used to form the patterned doping (i.e. photolithography, laser contact opening) make it difficult for industry adoption, and thus simplified approaches for patterning of poly-Si layers would need to be developed (Michel et al. 2023).

In this activity of PP1.3.1, we aim to develop a simple approach to localised p^+poly-Si regions, which utilise a deposited pure boron layer to act as a dopant source during a subsequent high temperature anneal. Unlike traditional ex-situ doping, which uses BBr_3/BCl_3 as the doping sources, the boron layer, deposited by electron-beam evaporation, will allow a single-sided doping and precise control both spatially and in terms of dose by simply varying the boron deposition region and thickness.

Progress

To start we confirm that the boron layers can effectively introduce active boron dopants into the poly-Si layer. Figure PP1.3.1.1 shows ECV measurements for samples with 50 nm poly-Si thickness annealed at a temperature of 950°C for 10 minutes. It can be seen from the ECV profiles that in both cases the intrinsic poly-Si layer has been doped and that a thicker boron layer results in a slightly higher boron dose. The main difference between the two films is the formation of a very high boron concentration of ~5 × 10^{20} cm^{-3} at the surface within the boron/capping layer region. We believe this is the result of the formation of a boron rich layer (BRL). In other results (not shown), we found the presence of the capping layer to be helpful in increasing the active boron concentration within the poly-Si layer and c-Si substrate.

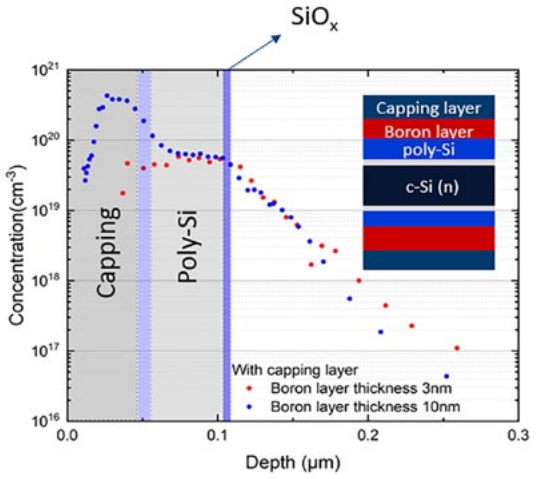

Figure PP1.3.1.1: ECV profile of two 50 nm p+poly-Si samples, doped using a solid boron source (3 nm – red and 10 nm – blue) by annealing at 950oC for 10 minutes.

Based on these results, additional poly-Si thicknesses (100 nm and 150 nm) were also introduced to study the effect of the poly-Si thickness. We performed a survey varying drive-in temperature and time for these different films. Table PP1.3.1.1 compiles the best contact recombination and resistivity results achieved for these 50 nm, 100 nm and 150 nm poly-Si films to date. It is found that for all poly-Si thicknesses the best performance was obtained using a 3 nm boron layer. However, there appeared to be no clear trend in the best furnace conditions. The best result was obtained for 150 nm poly-Si films, using a 950°C anneal for 60 minutes which produced an iV_{oc} (implied V_{oc}) of ~704 mV with a low ρc of ~2.7 mΩcm^2.

Table PP1.3.1.1: Summary of best results for 50 nm, 100 nm and 150 nm e-beam boron p+poly-Si contacts.

	pol-Si thickness		
	50 nm	100nm	150nm
Boron layer thickness (nm)	3	3	3
Furnace condition	1000°C for 10 minutes	950°C for 10 minutes	950°C for 60 minutes
τ_{eff} (μs)	730	523	842
iV_{oc} (mV)	696	698	704
J_0 (fA/cm2)	22	21	21
ρ_c (mΩcm2)	175	4.95	2.7

We also compare the excess carrier dependent effective lifetime τeff of the best results in Figure PP1.3.1.2. The strong injection dependence behaviour seen in all three plots is a common feature of p$^+$poly-Si passivated contacts on n-type substrates which has been attributed to various factors including B-O complex defects near the surface, edge recombination, and damage to the SiO_x layer during boron in-diffusion.

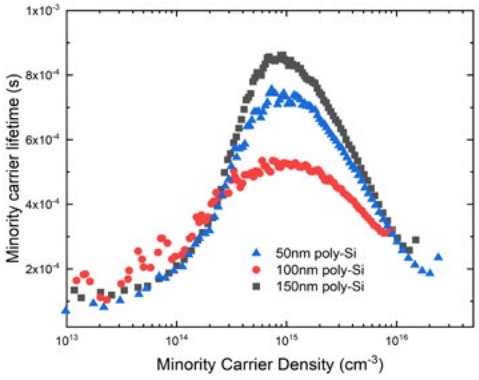

Figure PP1.3.1.2: Excess carrier dependent effective lifetime τeff for the best results obtained with each poly-Si thickness.

Finally, a simple demonstration of patterning using selective area deposition of the e-beam boron layer is provided in Figure PP1.3.1.3. As shown in the device cross-section on the left side, a 50 nm poly-Si film was used with a full area boron/capping layer stack on the rear side and a patterned (TLM or Cox and Strack) boron/capping layer on the front. The pattern was formed by evaporating through a shadow mask. These samples were then annealed at 950°C for 10 minutes in line with the conditions provided in Table PP1.3.1.1. The two PL images provided on the right side of Figure PP1.3.1.3 show clearly brighter regions associated with where the boron/capping layers have been deposited. This simple demonstration confirms that localised area doping can be achieved with this approach.

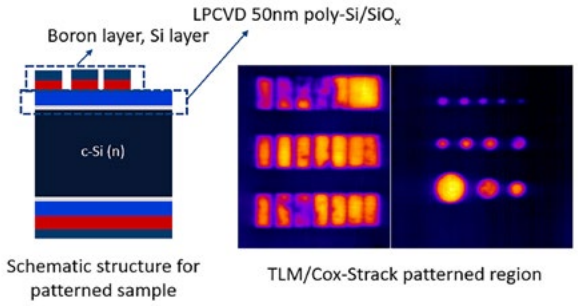

Figure PP1.3.1.3: Demonstration of patterned region doping using e-beam evaporation of the boron/capping layer stack through a TLM/Cox and Strack patterned shadow mask.

So far, we have demonstrated that boron films and capping layers, deposited by electron-beam evaporation, can serve as a dopant source to fabricate localised p^+ poly-Si passivating contacts (Pan et al. 2023) To date the best iV_{oc} value of ~704 mV was achieved, alongside a low ρ_c of ~2.7 mΩcm^2 using an intrinsic 150 nm poly-Si film as the starting point. We have demonstrated that this simple approach can be used with a shadow mask to fabricate patterned p^+poly-Si contacts that are compatible with industrial manufacturing. We are currently in the process of fabricating/testing a more extensive set of sample structures and conditions within this parameter space. We are also in the process of taking more specialised measurements, for example cross-sectional transmission electron microscopy with elemental mapping.

References

Yan, D., Cuevas, A., Stuckelberger, J., Wang, E.-C., Phang, S. P., Kho, T. C., Michel, J. I., Macdonald, D. & Bullock, J. (2023). Silicon solar cells with passivating contacts: Classification and performance. Progress in Photovoltaics: Research and Applications 31, 310-326. doi:10.1002/pip.3574

Yan, D., Cuevas, A., Michel, J. I., Zhang, C., Wan, Y., Zhang, X. & Bullock, J. (2021). Polysilicon passivated junctions: The next technology for silicon solar cells? Joule 5, 811-828. *https://doi.org/10.1016/j.joule.2021.02.013*

Michel, J. I., Yan, D., Phang, S. P., Zheng, T., Johnson, B. C., Yang, J., Zhang, X., Chen, W., Wan, Y., Truong, T., Stuckelberger, J., Pan, Y., Macdonald, D. & Bullock, J. (2023). Poly-Si passivating contacts prepared via phosphorus spin-on-doping: A comparison between different silicon deposition methods. Solar Energy Materials and Solar Cells 255, 112290.

Pan, Y., Kang, D., Yan, D., Wang, J., Zheng, P., Yang, J., Zhang, X. & Bullock, J. (2023). Ex-situ Doping of Polysilicon Hole Contacts via Electron-Beam Boron Evaporation. 2023 Asia-Pacific Solar Research Conference. Melbourne 5–7 December 2023.

PP1.3 SILICON ADVANCED DEVICES AND FABRICATION TECHNOLOGIES

PP1.3.2 Device Simulation

ANU Team
Prof. Daniel Macdonald, Dr Sieu Pheng Phang, Dr Di Kang, Dr Er-Chien Wang, Dr Kelvin Sio, Dr Josua Stuckelberger, Dr Kean Fong

ANU Student
Mr Zhongshu Yang\

UNSW Team
Dr Fa-Jun Ma, Dr Shaozhou Wang, Dr Chuqi Yi, Prof. Ziv Hameiri, A/Prof. Stephen Bremner, Prof. Xiaojing Hao, Prof. Bram Hoex

Partners
Jinko Solar, Nanchang University

Funding Support
ACAP, ARENA, ANU, UNSW

Aims

As the efficiency of silicon solar cells increases ever steadily in mass production, device simulations become more important to understand the primary losses and identify the bottlenecks to the solar cell efficiency. Commercial software packages like Sentaurus, Atlas, APSYS and COMSOL are still employed in the photovoltaic community. While these commercial tools offer a generic approach and theoretically can handle various solar cell technologies, practical implementation often reveals dramatic differences in device setups for different types of solar cells, even when using the same simulator. This situation presents challenges for users. New users often encounter a steep learning curve when attempting to become proficient with these versatile simulators, while experienced users frequently find themselves reinventing solutions for specific solar cell configurations. Consequently, there is a lack of synergy in the photovoltaic community when it comes to unified multi-dimensional solar cell simulations, presumably due to the inherent difficulties in unifying simulations across diverse solar cell technologies.

We aim to develop a framework to support process/optical/electrical simulations simultaneously by editing 11 variables in a plain text file, obviating the need for in-depth knowledge of the above commercial tools. The simulation results provide more in-depth understanding of the operation of high efficiency solar cells and provide guidance for further improvements.

Progress

From 2009 to 2015, our research focus primarily revolved around device simulations related to various silicon-based solar cells such as full-area aluminium back surface field solar cells, PERC, all-back-contact and HJT solar cells. With these simulations, we aimed to deepen our

understanding of the operation and behaviour of these solar cells to make informed design and optimisation decisions. Additionally, we focused on optimising material choices and device structures to achieve higher power conversion efficiency. Optical simulations were also conducted to improve light trapping schemes. From 2015 onwards, our research expanded to encompass a broader range of solar cell technologies. This included solar cell types like TOPCon, carrier selective contacts, Cu_2ZnSnS/Se_4, perovskite, III-V, tandem cells, etc. We employed numerical simulations to investigate and optimise the performance of these diverse solar cell architectures. Furthermore, we leveraged numerical simulations to simulate and understand various characterisation techniques commonly used in solar cell research. These techniques included current density-voltage (J-V) characteristics, quantum efficiency (QE) measurements, quasi-steady-state photoconductance (QSSPC) measurements for effective lifetime assessment, Suns-open circuit voltage (Suns-V_{oc}) measurements, capacitance-voltage (C-V) measurements, photoluminescence analysis, electroluminescence, etc.

Our simulations were conducted using a range of simulators, including Sentaurus, PC1D, Quokka3, AFORS-HET and SCAPS-1D. Throughout these simulations, we systematically explored and examined all the pertinent settings required for multi-dimensional process, electrical and optical simulations of solar cells. From a high-level perspective, we discovered a commonality in the simulation steps shared across these different tools. In Figure PP1.3.2.1, we summarised the 11 simulation steps involved in typical multi-dimensional process, optical and electrical simulations, according to their rough sequence in a simulation workflow.

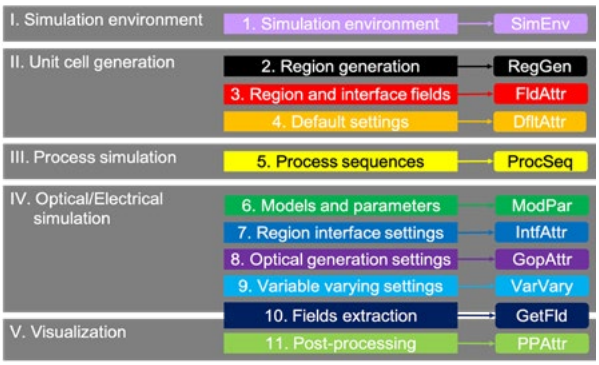

Figure PP1.3.2.1: Typical multi-dimensional solar cell simulations may be divided into five stages with 11 sequential simulation steps that are well represented by 11 corresponding variables.

These 11 simulation steps may be categorised into five distinct stages as follows:

I. The initial stage focuses on setting up the general simulation environment.

II. In this stage, the simulator generates the required unit cell and introduces relevant fields.

III. The unit cell goes through a sequence of process steps including diffusion, implantation and more.

IV. Here, models are specified, parameters are set for regions and interfaces, and variables are varied as needed for the simulation.

V. The final stage involves post-processing and visualisation of simulation results.

Combinations of these steps are sufficient for carrying out typical multi-dimensional solar cell simulations. Yet, not all the steps are required for many simulations. To the best of our knowledge, we are the first to formalise the 11 simulation steps and document this simulation workflow, thereby providing a structured framework for conducting simulations of solar cells. This structured framework has proven to be a pioneering contribution, offering clarity and consistency in typical multi-dimensional solar cell simulations. It has streamlined the simulation process, fostering more efficient research and development endeavours in the field.

Two high efficiency silicon solar cell architectures were selected as case studies for the framework, namely interdigitated back contact heterojunction (HJT) solar cells and front and back contact TOPCon solar cells.

Interdigitated back contact HJT solar cell

The HJT solar cell with interdigitated back contacts has been reported to achieve an impressive power conversion efficiency of 26.3% (Yoshikawa et al. 2017). Based on the revealed details in this reference and reasonable assumptions, both optical and electrical simulations with 11 sets of variables were performed to replicate the reported reflection, QE and light J-V curves using the developed UniSolar framework (https://github.com/mfjamao/Unified-Solar-Cell-Simulation) as a demonstration. For optical simulations, a cross-sectional representation of the unit cell with a textured top surface and a simplified bottom (neglecting thin-film layers) is depicted in Figure PP1.3.2.2(a). From the reference, a layer of a-Si provides the top surface passivation. For best chemical passivation, this layer should be a-Si:H(i). While the specifics of the ARC stack were not disclosed in the reference, it is very likely that hydrogenated silicon nitride (SiN_x:H) was deposited atop a-Si:H(i). In addition to light trapping, this SiN_x:H layer serves as a hydrogen source and provides the necessary field-effect passivation to complement the a-Si:H(i) layer. The exact thickness of the top a-Si:H(i) layer cannot be determined through optical simulations according to Figure PP1.3.2.2(b). Various simulations were conducted with a-Si:H(i) thickness ranging from 1 to 9 nm, yielding comparable results indicated by curves 2 to 6. Since the thickness of the top a-Si:H(i) layer was reported to be 6 nm on the world record 26.81% HJT solar cell (Lin et al. 2023). We decided to set the top a-Si:H(i) thickness to 6 nm for the subsequent electrical simulations.

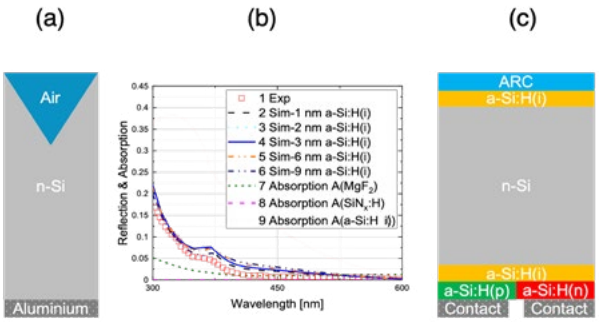

Figure PP1.3.2.2: A silicon HJT solar cell with interdigitated back contacts (Yoshikawa et al. 2017): (a) Unit cell for optical simulation; (b) simulated and measured reflection curves plus absorption in each top thin-film layer when a-Si:H(i) is 6 nm; and (c) unit cell for electrical simulations.

Figure PP1.3.2.3 indicates that measured QE and light J-V characteristics can be reasonably reproduced with the previous assumed parameters. Curve 5 in Figure PP1.3.2.3(a) is calculated by removing reflection and absorption in ARC, which is the theoretical upper limit of the external QE. Strikingly, curve 5 closely aligns with the measured external QE, suggesting that the internal QE within the silicon substrate and the top a-Si:H(i) layer is close to 100%, up to a wavelength of 1000 nm. This observation challenges the conventional assumption that most photo-generated electron-hole pairs are rapidly recombined within a-Si:H(i). This assumption is primarily rooted in the understanding that a-Si:H(i) is very defective, leading to SRH lifetimes as low as picoseconds. Curve 4, on the other hand, is computed by further subtracting the absorption in 6 nm a-Si:H(i) from curve 5. The difference between curve 4 and the measured QE below 600 nm is remarkable, suggesting effectively suppressed recombination due to efficient charge carrier separation and injection into the substrate, which was already characterised by photoluminescence (Paduthol et al. 2018).

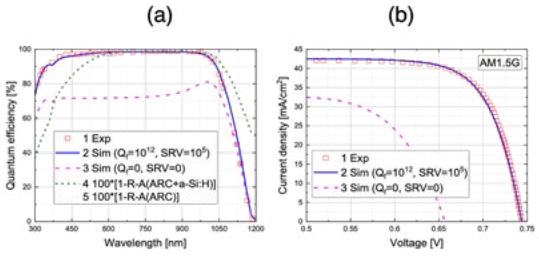

Figure PP1.3.2.3: (a) Measured and simulated QE; and (b) light J-V of silicon HJT solar cell with interdigitated back contacts for two scenarios: SiN_x:H and perfect chemical passivation with zero fixed charge density.

The negligible recombination observed in a-Si:H(i) can be attributed to the field-effect passivation of SiN_x:H. SiN_x:H possesses a high-density fixed positive charge, which induces a strong electric field within a-Si:H(i) as well as the surface region of the substrate. The induced electric field in a-Si:H(i) facilitates charge carrier separation and hole transport towards the substrate. This field-effect prevents photo-generated carriers from recombining rapidly within a-Si:H(i), even in the presence of high-density defects, and reduces the interface recombination between SiN_x:H and a-Si:H(i) to negligible levels. In essence, SiN_x:H's field-effect passivation plays a crucial role in suppressing recombination and outweighs the adverse impact of high-density traps within the a-Si:H(i) layer. It is worth noting that SiN_x:H not only provides field-effect passivation to a-Si:H(i) but also extends its passivation to the top a-Si:H(i)/Si interface. When field-effect passivation is absent (i.e. fixed charge Q_f is zero), external QE is significantly lower, as exemplified by curve 3 in Figure PP1.3.2.3(a). This QE reduction is due to increased recombination occurring at the top a-Si:H(i)/Si interface. These observations are further supported by the results presented in curve 3 of the light J-V simulation in Figure PP1.3.2.3(b). These results emphasise the critical role of applying strong field-effect passivation to the top a-Si:H(i) layer. Essentially, SiN_x:H provides strong field-effect passivation, both within the top a-Si:H(i) layer and at its interface with the substrate. This insight highlights the significance of proper field-effect passivation in optimising the performance of this solar cell.

Front and back contact TOPCon solar cell

Working in collaboration with the R&D team at Jinko Solar, we have previously detailed the characterisation and simulation of a high efficiency large area TOPCon solar cell with an independently certified efficiency of 24.8%. Control samples were carefully planned and processed in parallel with the cell fabrication, in order to measure various parameters as inputs for the simulation. The primary limitations to the cell efficiency were identified as recombination at the front boron diffusion and parasitic absorption in the rear poly-Si passivating contacts. Simulations also indicated that thinner metal fingers would increase the cell efficiency, by enabling a reduction in both recombination and shading. All three aspects have been further optimised since then, leading to a strongly improved certified solar cell efficiency of 25.4% at Jinko Solar. We have since updated the model for this state-of-the-art large-area silicon solar cell (Zheng et al. 2023).

In terms of the optical improvements, the updated screen-printing and poly-Si processes have enabled a reduction in the thickness of the poly-Si from 125 nm to 90 nm, without degradation to the surface passivation or contact resistivity. The resultant reduction in the parasitic absorption and improvements to the short-circuit current density (J_{SC}) are clearly demonstrated in the comparison of long wavelength EQE (external quantum efficiency) of solar cells with 90 nm and 125 nm poly-Si (see Figure PP1.3.2.4 below), corresponding to an overall increase of about 0.1 mA cm^{-2}. The higher reflectance and path-length enhancement factor (Z-factor) in the long wavelength region are also consistent with the reduction in parasitic absorption. The remaining free carrier absorption in the rear poly-Si is estimated to still account for

a loss of 0.25 mA cm^{-2} and remains an important avenue for further improvements. The finger width for the front metal grid has also been reduced from 35 µm to 25 µm through optimisation of the screen-printing process.

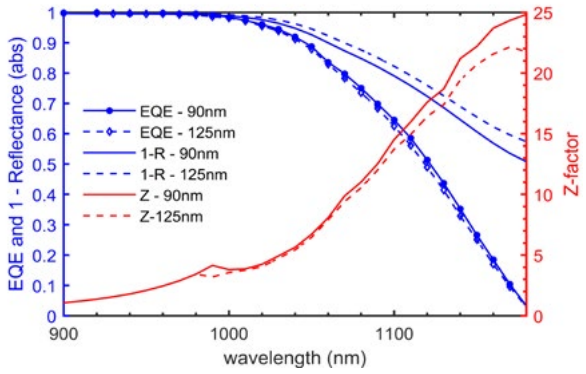

Figure PP1.3.2.4: Optical analysis comparing silicon solar cells with 90 nm and 125 nm poly-Si layer thickness, showing the measured EQE, 1 – reflectance, and the path-length enhancement factor (Z-factor). The EQE measurement was performed independently by ISFH CalTeC, and normalised to factor out the effect of grid shading. The Z-factor is extracted from the measured EQE, fitted front surface reflectance in the long wavelength, and the simulated collection efficiency of the cell from Quokka3.

On the front surface, the implementation of selective boron diffusions improved the overall front surface passivation. By selectively increasing the doping concentration under the metal contact, the enhanced shielding effect of the boron diffusion can reduce the overall recombination at the metal contact while simultaneously reducing the contact resistivity. Selective doping also allows lighter doping within non-contacted regions, enabling a reduction in Auger recombination and overall surface recombination. The combined effect of heavier doping under the contacts, and lighter doping within the non-contacted regions can improve the overall V_{OC} and FF of the cell. Using the previous model for the 24.8% cell as a baseline, the updated cell parameters were fitted from the average I-V performance of the solar cells after the various optimisations to cell processes. Firstly, the lighter boron diffusion in the passivated regions between the metal fingers, combined with the optimisation of the rear surface morphology and poly-Si passivating contacts resulted in an average increase in V_{OC} of about 2 mV. The improvements were assumed to be equally distributed between the front and rear surface, resulting in a slightly reduced front $J_{0\text{-passivated}}$ of 5 fA cm^{-2} and improved rear surface $J_{0\text{-passivated}}$ of 2 fA cm^{-2}. Next, the implementation of heavier boron diffusions in the contact region along with the reduction in finger contact width provided an average increase in V_{OC} of about 6 mV, along with a slight improvement in FF. The improvements were correlated with a reduction in $J_{0\text{-contact}}$ to 500 fA cm^{-2} and a reduced front contact resistivity of 0.5 mΩ·cm^2. The J_{SC} of the simulated cell is matched to the measured value, while the V_{OC}, fill factor and cell efficiency are 718 mV, 83.6% and 25.36% respectively. In comparison, the measured VOC, fill factor and cell efficiency are 719.1 mV, 83.7% and 25.41% respectively. The updated simulation is used as a baseline reference for analysis of potential further improvements.

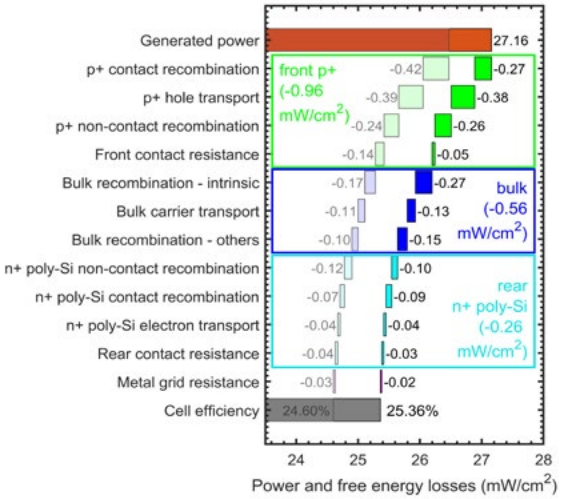

Figure PP1.3.2.5: Free energy loss analysis of the champion cell, based on simulation results. The total recombination and resistive losses are 1.78 mW cm^{-2}. The total free energy loss for the front surface, bulk and rear surface were 0.96, 0.56 and 0.26 mW cm^{-2} respectively. The free energy loss analysis from our previous work has been included in a lighter shade for comparison.

The free energy loss analysis, after accounting for optical losses, shows a reduction in the front surface contact recombination in comparison to the previous champion cell. As a result, lateral current transport within the front boron diffusion is now the most significant loss mechanism. Overall, the front surfaces still contribute to more than half of the total free energy losses. Bulk recombination has also been slightly increased, but bulk losses from intrinsic recombination remain stronger compared to the non-intrinsic bulk recombination channels, suggesting that further gains from wafer bulk will require a shift towards higher resistivity wafers to decrease intrinsic recombination. Rear surface electrical losses remain minimal, reflective of the excellent passivation quality of the phosphorus-doped n$^+$ poly-Si passivating contacts.

Despite the further optimisation of the front boron diffusions and the reduction of the front contact fractions through the reduction of the electrode finger width, the front surface electrical losses remain the primary limiting factors for the cell efficiency in the state-of-the-art large-area solar cell. Figure PP1.3.2.5 suggests that the recombination losses from the contact and non-contact regions are comparable to resistive losses from lateral carrier transport, and both recombination and resistive losses have to be improved to deliver strong gains in cell efficiency. This can be achieved by improving the surface J_0, reducing the R_{sheet}, or decreasing the finger pitch, noting that any changes have to be balanced against other potential trade-offs.

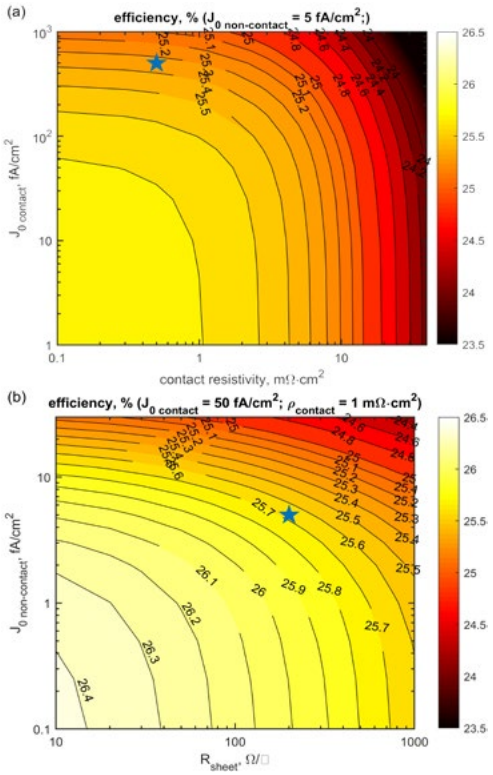

Figure PP1.3.2.6: Contour plots of simulated cell efficiency for (a) $J_{0\ contact}$ vs. contact resistivity and (b) $J_{0\ contact}$ vs. sheet resistance for the front p⁺ layer. The non-contact parameters for (a) are based on the baseline cell parameters, while the contact parameters for (b) are assuming an effective front p⁺ passivating contact with J_0 contact of 50 fA cm⁻² and contact resistivity of 1 mΩ·cm². The baseline parameters for the measured cell are included as blue stars for reference.

The application of passivating contacts to the front surface is a promising pathway to reduce the front surface recombination. However, any variations to the contact resistivity and sheet resistances (for front junction devices) also have to be carefully balanced. Figure PP1.3.2.6(a) shows a contour plot of the simulated solar cell efficiency when varying the electrical properties of the front p⁺ contacts, as a function of the passivation in the y-axis and contact resistivity in the y-axis. Figure PP1.3.2.6(b) shows the corresponding plot for p⁺ non-contact regions between the metal grids, assuming the implementation of an effective passivating contact for the p⁺ contacts, with sheet resistance as the x-axis and $J_{0\text{-}passivated}$ as the y-axis.

Figure PP1.3.2.6(a) shows that the contact resistivity of the front p⁺ contact has to be limited to approximately below 8 mΩ·cm² to improve the overall cell efficiency, even for the best case scenario where the contact recombination can be effectively passivated with $J_{0\ contact}$ of < 10 fA cm⁻². In comparison to the application of passivating contacts on the rear surface, front surface passivating contacts are more sensitive to the contact resistivity, because the contact fractions are generally lower due to the requirement to balance the optical shading against the contact resistivity and contact recombination. Assuming that effective passivating contacts can be realised for the p⁺ contacts, Figure PP1.3.2.6(b) shows that the sheet resistance and the passivation quality of the non-contact region are both important parameters that have to be considered for further improving the cell performance. For the current cell architecture and cell properties, a near ideal surface J_0 of 0.1 fA cm⁻² without further improving lateral conduction would result in an efficiency gain of up to 0.3% absolute. Simultaneously reducing the sheet resistance to 10 Ω/□ would deliver a further gain of more than 0.4% absolute in cell efficiency, driven by improvements in both J_{SC} and FF.

References

Yoshikawa, K., Kawasaki, H., Yoshida, W., Irie, T., Konishi, K. Nakano, K., et al. (2017). Silicon heterojunction solar cell with interdigitated back contacts for a photoconversion efficiency over 26%. Nat Energy 2, 17032.

Lin, H., Yang, M., Ru,. X, Wang, G., Yin, S., Peng, F., et al. (2023). Silicon heterojunction solar cells with up to 26.81% efficiency achieved by electrically optimized nanocrystalline-silicon hole contact layers. Nat Energy 8, 789-799.

Paduthol, A., Juhl, M. K., Nogay, G., Löper, P. &Trupke, T. (2018). Measuring carrier injection from amorphous silicon into crystalline silicon using photoluminescence. Progress in Photovoltaics: Research and Applications 26, 968-73.

Zheng, P., Phang, S.P., Yang, J., Wang, Z., Chen, J., Wang, E.C., Stuckelberger, J., Sio, H.C., Zhang, X., Macdonald, D. & Jin, H. (2023). Polysilicon Passivating Contacts in Mass Production: the Pursuit of Higher Efficiencies. IEEE JPV 14, 80-84. DOI: 10.1109/JPHOTOV.2023.3329642.

PP1.3 SILICON ADVANCED DEVICES AND FABRICATION TECHNOLOGIES

PP1.3.3 ADVANCED DEVICES

UoM Team
Dr James Bullock, Dr Di Yan

UoM Students
Jesus Ibarra Michel

UNSW Team
Prof. Ziv Hameiri

UNSW Student
Anh Huy Tuan Le

ANU Team
Prof. Daniel Macdonald, Dr AnYao Liu, Dr Sieu Pheng Phang

Funding Support
ACAP, ARENA, UoM

Aims

Despite the widespread industrial success of poly-Si and a-Si-based passivating contacts, dealing with the optical losses associated with external doped silicon contacts remains a challenge. One of the aims of PP1.2/1.3 is to find and integrate wide bandgap metal compound materials as prospective candidates to replace doped silicon at the electron contact of solar cell devices (Michel et al. 2023a). This has the potential to reduce optical losses and simplify the fabrication process.

Progress

We have trialled several wide bandgap ionic metal compound materials as electron contacts on c-Si Michel et al. 2023a). Based on their low work functions, and tendency to form dipoles at the interface with other materials, these interlayers can facilitate downwards band bending at the c-Si surface and enhance the conductivity for electrons (Michel et al. 2023a). Figure PP1.3.3.1 shows the specific contact resistivity ρ_c values measured for a variety of thermally evaporated thin (i.e. ~2 nm) films on n-type c-Si with a top aluminum (Al) electrode. The pink bars show new materials that have been tested during this project and that have not been reported before as suitable electron contacts for c-Si. As a reference, we have added the direct contact between n-Si and Al. We see an improvement of one to three orders of magnitude ρ_c when the ionic interlayers are added (Muñoz et al. 2021).

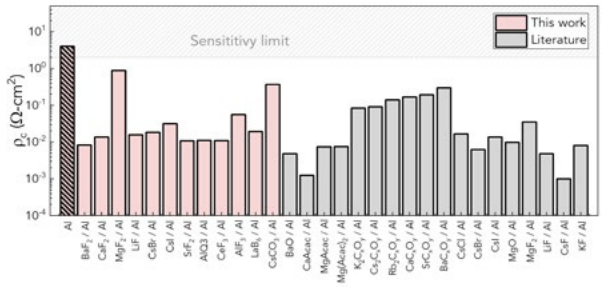

Figure PP1.3.3.1: Compilation of e-contact wide gap materials tested on n-Si based on our work and the broader literature.

From the large pool of materials, we picked cesium bromide (CsBr) as a promising candidate due to its good thermal and ambient stability and its comparatively better performance when paired with additional passivating interlayers. During this project we have found that due to the lack of surface passivation of ionic films on c-Si, additional dedicated passivating layers are required. We added a thin (2–5 nm) TiO_x film deposited via atomic layer deposition at low temperature and built a TiO_x/CsBr/Al stack as our final electron contact. Figure PP1.3.3.2 shows the minority carrier lifetime at the metallised regions in this structure as a function of post-annealing temperature for two different TiO_2 thicknesses. We have found that the passivation performance drops but then recovers after annealing at temperatures > 200ºC. Also, we observe overall higher lifetimes for the thicker TiO_x. Similarly, the ρ_c is also plotted and improves with increasing temperature. The gains in passivation by the thicker TiO_x film are compromised by a higher contact resistance.

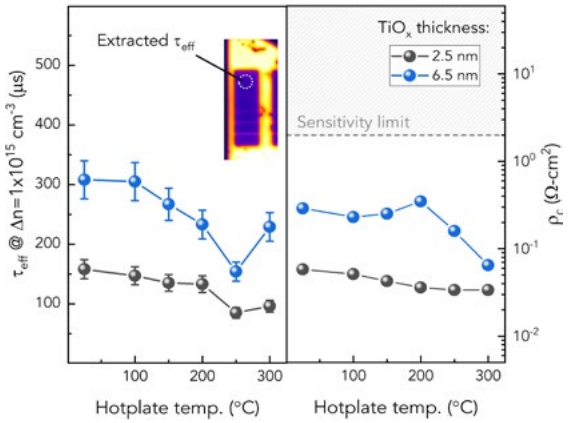

Figure PP1.3.3.2: Evolution of minority carrier lifetime at the metallised regions and specific contact resistivity as a function of annealing temperature for TiO_x/CsBr/Al contact structures.

Finally, we have employed our TiO_x/CsBr/Al as a full-area stack at the rear side of a front boron diffused solar cell and obtained an efficiency of 20.5% after a post-annealing step at 250ºC. The one-sun current-voltage curve and the schematic of this device are shown in Figure PP1.3.3.3.

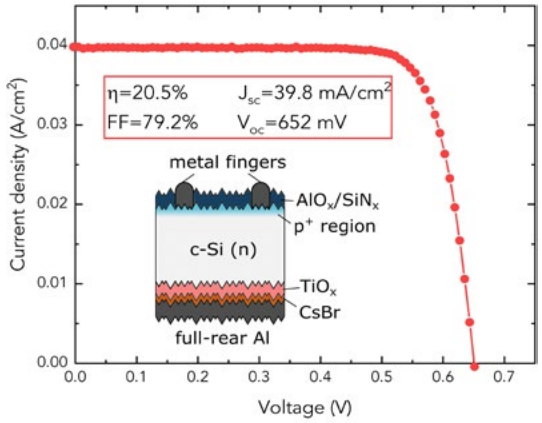

Figure PP1.3.3.3: Current-voltage curve of a solar cell device measured at 1.5 AMG standard conditions employing a full-area TiO_x/CsBr/Al stack at the rear side with a conventional front boron diffusion.

The next steps of this project involve combining these electron contact stacks with transparent conductive oxides to enable their use at the front side of solar cell devices and take more advantage of their transparency. Also, we have started to work on other types of metal oxides with different scalable deposition techniques (e.g. solution processed) to achieve similar goals.

References

Michel, J. I., Le, A. H. T., Yan, D., Berghuis, W.-J., Korte, L., Liu, A., Phang, S. P., Chen, W., Macdonald, D., Macco, B., Hameiri, Z. & Bullock, J. (2023a). Electron contact interlayers for low-temperature-processed crystalline silicon solar cells. Progress in Photovoltaics: Research and Applications n/a. DOI: https://doi.org/10.1002/pip.3768.

Ibarra Michel, J., Dréon, J., Boccard, M., Bullock, J. & Macco, B. (2023). Carrier-selective contacts using metal compounds for crystalline silicon solar cells. Progress in Photovoltaics: Research and Applications 31, 380-413. doi:10.1002/pip.3552.

Muñoz, D., Richter, A., Carroy, P., Valla, A., Bullock, J., Ibarra, J. & Roux, C. (2021)In Evaporated contacts, Silicon Solar Cell Metallization and Module Technology, Chapter 5, Eds: Thorsten Dullweber, T.& Tous, L. Institution of Engineering and Technology.

PP1.4.1 Optical and Electrical Characterisation & PP 1.4.2 Imaging and Microscopy

ANU Team
Anh Bui, Khoa Nguyen, Daniel Macdonald, Hieu Nguyen

Aims

This project aims to utilise an advanced optical characterisation cluster for photovoltaic (PV) research activities at the Australian National University (ANU) ACAP node and collaborators to investigate the fundamental properties of a photovoltaic device.

The cluster consists of the following tools:

- IMA hyperspectral luminescence imaging (ANU)
- Tandem Modulum (Fraunhofer Institute for Solar Energy Systems) Progress

We have conducted a spatial resolved analysis of the photoluminescence (PL) spectra of individual sub-cells within perovskite silicon tandem solar cells. This investigation is performed through the utilisation of a hyperspectral imaging system.

The aim of this spectral measurement is to gain a comprehensive understanding of the characteristics of each sub-cell within the tandem solar cell structure. By employing hyperspectral imaging, we are able to capture detailed spectral information of each sub-cell, providing insights into the optoelectrical properties of a device.

For the spectral measurements of the perovskite top cell, an excitation is performed using a 532 nm laser. To capture the luminescence signal, an sCMOS camera is employed with a 541 nm long-pass filter placed in front of the camera. This filter effectively blocks the reflection of the laser, which could potentially cause damage to the camera. The luminescence signal is detected from 600 to 900 nm with a step size of 2 nm.

For the spectral measurements of the silicon bottom cell, an excitation is performed using an 860 nm laser. To capture the luminescence signal, an InGaAs camera (Alizé™ 1.7) is employed with a 900 nm long-pass filter placed in front of the camera. This filter effectively blocks the reflection of the laser, which could potentially cause damage to the camera. The luminescence signal is detected from 950 to 1350 nm with a step size of 2 nm.

Figure PP1.4.1.1 displays the PL spectra of the top and bottom cells. From the PL spectra, a suitable bandpass filter and laser source can be selected to capture the appropriate PL signal of each sub-cell. This ensures the maximisation of the signal-to-noise ratio and minimises the impact of other emission sources. For instance, it is not recommended to use a light source with an excitation wavelength shorter than 800 nm to stimulate the bottom cell, as it may partially stimulate the top cell.

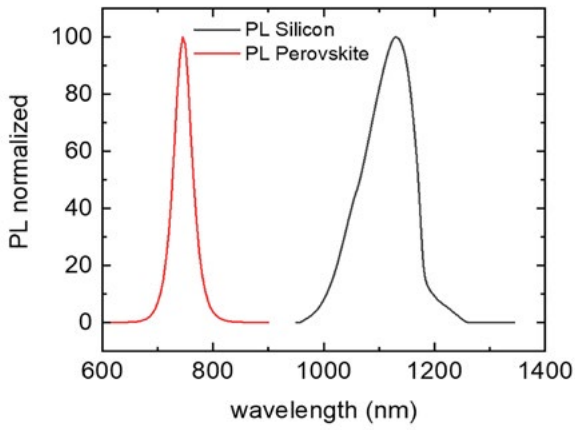

Figure PP1.4.1.1: PL spectra of perovskite and silicon sub-cells in a tandem device.

In the next step, utilising the spectrally resolved data, we carefully chose a suitable filter for capturing PL images of each sub-cell in the perovskite silicon tandem solar cell. Subsequently, an absolute calibration was performed to convert relative PL images into implied open-circuit voltage (iV_{oc}) images, facilitating the exploration of local performance variations in the device. This analysis allows us to establish a benchmark for the fabrication process. The detailed calibration process is outlined below.

Figure PP1.4.1.2 displays the schematic of the measurement system. The perovskite silicon tandem solar cell can be excited, sub-cell-selectively, using a 450 nm laser for the perovskite top cell and an 808 nm laser for the silicon bottom cell. The PL images are acquired using a silicon CCD camera. By employing the generalised Planck law (Wurfel 1982), the detected PL intensity can be described by the following formula:

$$I_{PL} = \int SF \times SR(E) \times C \times E^2 \times A(E) \times exp\left(\frac{-E}{kT}\right) \times exp\left(\frac{iV_{OC} \times q}{kT}\right) dE \qquad (1)$$

Here, A(E) is the energy-dependent absorptivity, k is the Boltzmann constant, T is the sample's absolute temperature, and C is a physical constant. SR(E) is the spectral response of the entire system, determined by a calibrated tungsten-halogen light source. SF is a scaling factor accounting for the fraction of the emitted light detected by the system. SR(E) and SF are fixed for a given experimental setup.

The iV_{OC} can be calculated by Equation 2:

$$iV_{OC} = \frac{kT}{q} \times \ln\left(\frac{I_{PL}}{SF \int \times SR(E) \times C \times E^2 \times A(E) \times exp\left(\frac{-E}{kT}\right) dE}\right) \qquad (2)$$

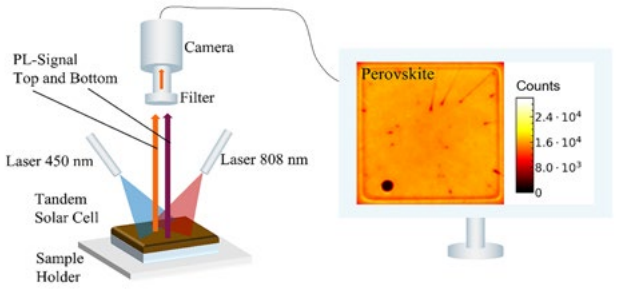

Figure PP1.4.1.2: Schematic of tandem PL imaging system and the demonstration.

Figure PP1.4.1.3 displays the calibration process. Initially, we measure the transmissivity of the objective and bandpass filter, extracting the quantum efficiency of the camera from the supplier datasheet to calculate the SR(E) of the system. Subsequently, utilising the extracted SR(E) value, we employed a calibrated light source lamp (ISS-5P-SR-FS from Gigahertz-Optik) with a known spectrum and spatially uniform photon flux. This enables the calculation of an SF. Finally, employing SF, SR(E), and measuring A(E) and PL intensity, the iV_{oc} image can be calculated using Equation 2.

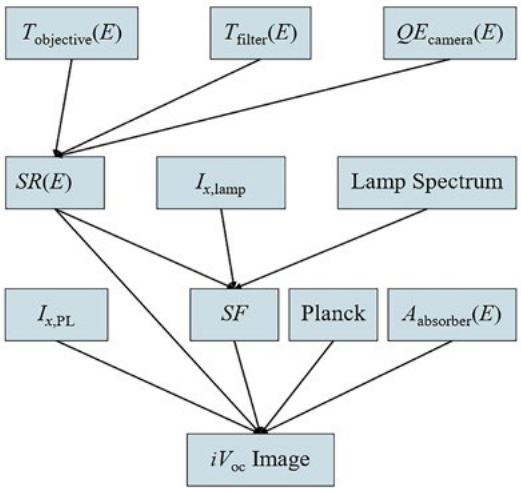

Figure PP1.4.1.3: Graphical algorithm to acquire an iV_{OC} image.

Figure PP1.4.1.4(a) and PP1.4.1.4(b) display the iV_{OC} images of seven silicon bottom cells and perovskite top cells on one substrate, respectively. Additionally, Figure PP1.4.1.4(c) and PP1.4.1.4(d) shows the spatially resolved iV_{OC} of two cross-sections of the silicon iV_{OC} image in Figure PP1.4.1.4(a) and two cross-sections of the perovskite iV_{OC} image in Figure PP1.4.1.4(b), respectively. While most parts of the presented tandem solar cells are well performing and homogeneous, the chosen cross-sections cover local inhomogeneities. Natural inhomogeneity is the presence of fingers and busbars, shading the PL signal from the solar cell and hindering the local iV_{OC} determination. While this cannot be circumvented, other defects of the cell can be prevented by changes in the manufacturing routine. As Figure PP1.4.1.4(c) depicts, a line-shaped defect in the silicon bottom cell leads to a local decrease in iV_{OC} by approximately 50 mV compared to other well-performing parts of the cells for both cross-sections. Several inhomogeneities are visible in the perovskite sub-cell in Figure PP1.4.1.4(d). Cross-section 3 features a very local defect decreasing iV_{OC} by approximately 93 mV. Cross-section 4 features a larger patterned inhomogeneity resulting in a loss of approximately 50 mV across a larger region compared to the well-performing parts of cross-section 4. More details on the calibration procedure and the applications of the method are given in the team's article (Fischer et al. 2023).

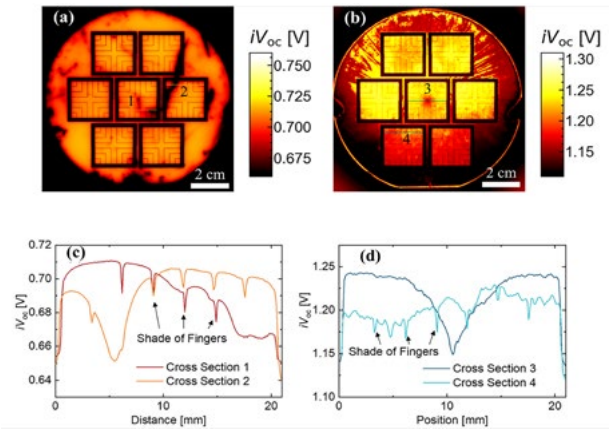

Figure PP1.4.1.4: (a), (b) iV_{oc} images of the silicon bottom cells and the perovskite top cells of tandem devices, respectively, which reveal local losses. (c), (d) Cross-sections of the iV_{oc} images in (a) the silicon and (b) the perovskite sub-cell, respectively.

Highlights

- Demonstration of the method for absolute calibration for the tandem PL imaging system.
- Prediction of the performance loss of perovskite silicon in the tandem solar cells.

Future Work

Based on the results of the iV_{oc} calibration, the team will continue to extract different parameters including:

- Pseudo-fill factor, which represents the maximum achievable fill factor without the influence of series resistance and serves as an indicator for the optimisation process.
- Ideality factor and activation energy of recombination: these two parameters can serve as indicators for understanding the recombination mechanism within the device.

References

Fischer, O., Bui, A. D., Schindler, F., Macdonald, D., Glunz, S. W., Nguyen, H. T. & Schubert, M. C. (2023). Versatile implied open-circuit voltage imaging method and its application in monolithic tandem solar cells. Progress in Photovoltaics: Research and Applications. https://doi.org/10.1002/pip.3754.

Wurfel, P. (1982). The chemical power of radiation. Journal of Physics C: Solid State Physics 15, 3967-3985.

PP1.4.3 Interface and Surface Analysis

ANU Team
Dr Lachlan Black, Prof. Daniel Macdonald

ANU Students
Mr Mohamed Shehata, Mr Gabriel Bartholazzi

Partners
University of Warwick

Funding Support
ACAP, ARENA, ANU

Aims

Understanding surface and interface properties is key to engineering passivation and contact structures that can enable high efficiency solar cells. Within this Program Package we investigate the application of techniques such as capacitance–voltage, impedance spectroscopy, Kelvin probe, and surface photovoltage measurements, to characterise the electronic and energetic properties of silicon surfaces and interfaces in test structures and devices and correlate these with solar cell performance.

Progress

Impedance spectroscopy (IS) is a powerful characterisation technique that is commonly applied to organic, perovskite and thin-film solar cells. However, it has not been widely applied to solar cells based on crystalline silicon (c-Si), and particularly not to modern, high efficiency silicon devices. We have recently demonstrated the application of the IS technique to a 21.25% efficient c-Si solar cell featuring a SiO_x/poly-Si rear passivating contact, as illustrated in Figure PP1.4.3.1. This type of cell architecture is structurally similar to that of current high efficiency industrial devices. The investigated cell was measured over a wide range of frequencies under illuminated open-circuit conditions and under different DC biases in darkness. The resistive and capacitive components associated with the p^+–n junction and at the n^+-poly–n low–high junction, which cannot be resolved by standard DC measurements, are readily distinguished by the IS method. These parameters allowed for the determination of junction time constants and lifetimes. We found that the lifetimes derived from IS measurements performed under open-circuit illuminated conditions were in excellent agreement with the carrier recombination lifetime under illumination. Our findings demonstrate that IS is a promising technique to explore various dynamic properties of high efficiency c-Si solar cells. This work was reported in (Shehata et al. 2023).

We have also begun exploring various applications of the new, ACAP-funded, KP Technology UHV Φ4 Kelvin probe system installed at ANU. This system has the capability to measure a wide range of energetic properties of semiconductors and other materials, including work function, ionisation potential / valence band energy, surface band bending and bandgap, via Kelvin probe, surface photovoltage spectroscopy and photoemission yield spectroscopy techniques. It is capable of measurements under vacuum or ambient conditions at temperatures up to 500°C, with spatial resolution provided via a motorised sample stage.

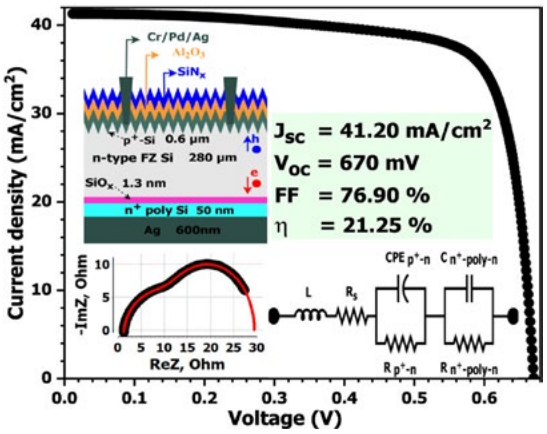

Figure PP1.4.3.1: Impedance spectroscopy was used for the first time to investigate a silicon solar cell with a poly-Si rear passivating contact. Main plot shows the J-V characteristics of the investigated device. Insets show the cell structure, example impedance plot, and equivalent circuit used to fit impedance data (Shehata et al. 2023).

One recent application of this system has been to measure the spatial variation of work function in advanced hetero-contact structures based on metal oxides. For example, we have recently shown improved passivation and contact performance for C_u2O hole-selective layers on silicon, following the insertion of a thin ALD Al_yTiO_x/TiO_2 stack as a passivating tunnel interlayer. Work function measurements reveal that this improvement is correlated with a significant increase of work function, as well as an improvement in spatial uniformity, as illustrated in Figure PP1.4.3.2. This helps to explain the beneficial effect of the interlayer. This work was reported by Bartholazzi et al. (2024).

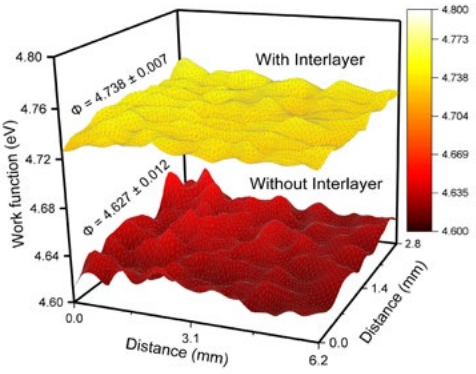

Figure PP1.4.3.2: Spatial variation in work function for evaporated Cu_2O thin films on silicon, with and without an ALD Al_yTiO_x/TiO_2 interlayer (Bartholazzi et al. 2024).

In another application of this system, we have taken advantage of its ability to measure work function simultaneously with in situ annealing with a temperature ramp. As shown in Figure PP1.4.3.3, we have tracked changes in the work function of silicon surfaces with HfO_2 passivation layers of various thickness as a function of annealing temperature in vacuum up to ~500°C. All films were found to exhibit a substantial reduction in work function at temperatures coincident with

the onset of passivation in lifetime samples annealed ex-situ in air. This sharp change in work function was also found to be correlated with the crystallisation threshold of the HfO_2 films. This work was reported by (Wratten et al. 2023).

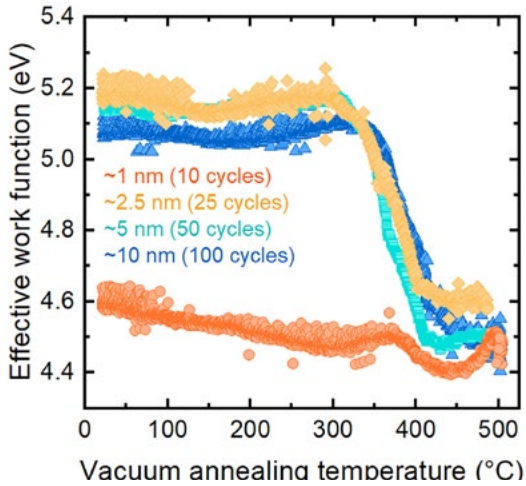

Figure PP1.4.3.3: Work function of ALD HfO_2 thin films of varying thickness (number of cycles) deposited on a silicon surface, as a function of temperature during a ramped anneal in vacuum (Wratten et al. 2023).

References

Shehata, M. M., Truong, T. N., Basnet, R., Nguyen, H. T., Macdonald, D. H. & Black, L. E. (2023). Impedance spectroscopy characterization of c-Si solar cells with SiO_x/ Poly-Si rear passivating contacts. Solar Energy Materials and Solar Cells 251, 112167. (*https://doi.org/10.1016/j.solmat.2022.112167*)

Bartholazzi, G., Shehata, M. M., Basnet, R., Samundsett, C., Macdonald, D. H. & Black, L. E. (2024). Novel Interlayer Boosting the Performance of Evaporated Cu_2O Hole-Selective Contacts in Si Solar Cells. Solar RRL 8, 2300727. (*https://doi.org/10.1002/solr.202300727*).

Wratten, A., Pain, S. L., Yadav, A., Khorani, E., Niewelt, T., Black, L., Bartholazzi, G., Walker, D., Grant, N. E. & Murphy, J. D. (2023). Exploring hafnium oxide's potential for passivating contacts for silicon solar cells. Solar Energy Materials and Solar Cells 259, 112457. (*https://doi.org/10.1016/j.solmat.2023.112457*)

[1] (*https://doi.org/10.1016/j.solmat.2023.112457*)

PP1.4.4 Simulation and Modelling

Lead Partner
ANU

Team
Dr Hieu Nguyen, Prof. Daniel Macdonald

ANU Student
Khoa Nguyen

Funding Support
ACAP, ANU

Aims

The goal of this project is to propose a model that investigates the interaction between sub-cells, specifically focusing on the luminescent coupling effect, in a monolithic perovskite/silicon tandem solar cell. Subsequently, the impact of the luminescent coupling effect on energy yield will be explored to determine optimised parameters for each sub-cell, including bandgap and thickness.

Progress

The model for luminescent coupling in a monolithic perovskite/ silicon tandem solar cell

We have proposed a simulation model to estimate the ratio of the re-emitted photon escaping from the rear and front side of the high bandgap perovskite top-cell $R_{rear/front}$ using SunSolve – a commercial software hosted by PV Lighthouse. The software integrates ray tracing capabilities with a transfer-matrix-based coherent thin-film simulator. Since SunSolve is designed to analyse incident light from the external side of a layer stack, our simulations are divided into two segments, each focusing on the layer stack above and below the perovskite layer.

The absorption profiles are computed utilising the SunSolve Power software, which incorporates both the transfer-matrix and ray tracing methods. In this approach, the thin layer is considered a coherent layer and is treated using the transfer-matrix method. Conversely, the thick layer, characterised by a complex morphology, is analysed as an incoherent layer, and its properties are resolved using the ray tracing method, as illustrated in Figure PP1.4.4.1(a). The emitted photons within the perovskite absorber are treated as isotropic, possessing an energy equivalent to the bandgap (refer to Figure PP1.4.4.1(b)). Consequently, the data indicates that a significant portion of re-emitted photons, escaping from the perovskite top cell, undergo recycling by the bottom cell. This observation underscores the noteworthy impact of the luminescence coupling effect on monolithic tandem solar cells, as depicted in Figure PP1.4.4.1(c).

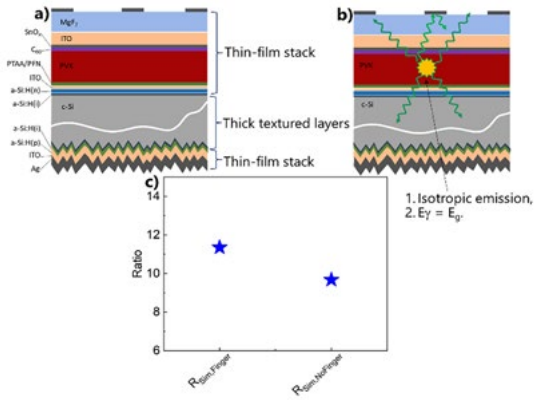

Figure PP1.4.4.1: (a) Schematic of the cell structure; (b) illustration of the emitted photon in the perovskite absorber; and (c) results for the ratio of emitted photons escaping from rear and front sides of the perovskite top cell in the monolithic perovskite/silicon-heterojunction tandem solar cell.

The role of the luminescent coupling in the energy yield of a monolithic tandem solar cell

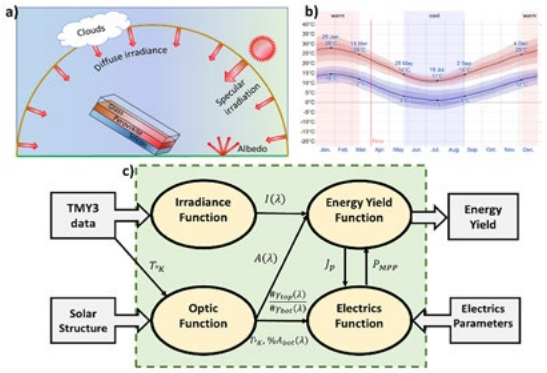

Figure PP1.4.4.2: (a, b) The illustration of the possible factors that can affect the EY in a working condition. (c) Schematic of the EY modelling.

An energy yield (EY) modelling is proposed to optimise the device architecture for different locations. In contrast to power conversion efficiency (PCE), energy yield (EY) takes into consideration environmental factors, including dynamically changing irradiation conditions and ambient temperature (see Figure PP1.4.4.2(a,b). Moreover, this model incorporates the consideration of the luminescence coupling effect (LC).

The irradiance module computes spectrally and angular-resolved direct and diffuse irradiance spectra using typical meteorological data (TMY3) obtained from the National Renewable Energy Laboratory (NREL). This is achieved through the integration of the Simple Model of Atmospheric Radiative Transfer of Sunshine (SMARTS) and a cloud model. The combination of these models allows for the derivation of hourly resolved irradiance data from the TMY3 data set. Subsequently, the optic model calculates spectrally and angularly resolved absorptance, transmittance and reflectance for each layer within the tandem structure. This is achieved through a combination of the transfer-matrix method, series expansion of the Beer-Lambert law, and geometrical ray tracing applied to various geometrical structures. Furthermore, the optic module incorporates the impact of temperature by accounting for the temperature dependencies of both optical and electrical characteristics.

By combining the irradiance data and absorptivity values for each sub-cell, the maximum power output of the tandem cell can be computed. Subsequently, the annual yield is determined by integrating over hourly data throughout the year. The results reveal a significant enhancement in output power with and without the luminescence coupling (LC) effect, as illustrated in Figure PP1.4.4.3(a). Moreover, there is a discernible difference in the optimisation of absorber thickness, depicted in Figure PP1.4.4.3(b) and (c). Additionally, variations in typical irradiance at different locations contribute to a noteworthy impact on the thickness optimisation, as shown in Figure PP1.4.4.3(d, e and f).

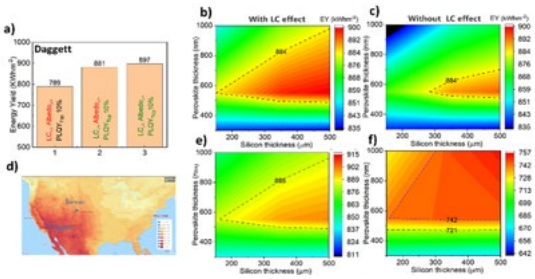

Figure PP1.4.4.3: (a) EY results from irradiance data at Daggett under different scenarios. (c, d) Optimisation of the thickness of each sub-cell with and without the effect of LC. (d) Locations of two different investigated areas and their optimisation strategies for each location, respectively (e, f).

Finally, the impact of the bandgap of the perovskite top cell is another significant factor influencing thickness optimisation. A higher bandgap leads to an increase in the thickness of the perovskite top cell and a reduction in the silicon bottom cell. However, it is worth noting that if the bandgap of the perovskite is excessively high, achieving the optimal thickness for the absorber becomes challenging.

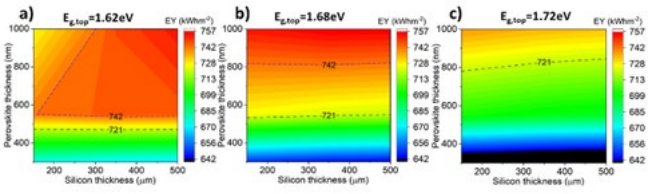

Figure PP1.4.4.4: Optimisation of the thickness of each absorber at different top-cell bandgaps: (a) 1.62 eV, (b) 1.68 eV and (c) 1.72 eV.

Highlights

- Estimate the luminescent coupling (LC) effect between sub-cells in a monolithic perovskite/tandem solar cell using the optic model.
- Optimise the cell structure under different working conditions, considering various factors such as constantly changing irradiation conditions, ambient temperature, angle of incidence, and luminescent coupling, based on the energy yield (EY) model.

Future Work

The ANU team will keep working to validate and improve the model to match global predictions. They are also aiming to create a user-friendly interface that quickly gives the necessary information for optimising solar cell configurations.

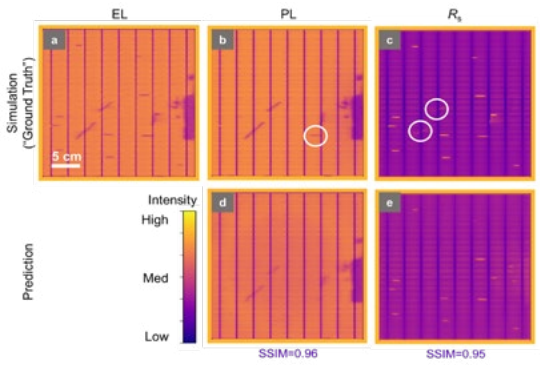

Figure PP1.4.5.1: Results of separating spatially resolved photoluminescence and resistance for identifying defects.

Boost computational efficiency of sharpness correction of conventional photoluminescence imaging tools

We addressed the inadequate throughput performed by conventional point-spread function (PSF) correction tools, such as LumiTools (Payne et al. 2017). We developed a convolutional neural network (CNN) model that employs a three-layer encoder-decoder structure for rapid PSF correction. As shown in Figure PP1.4.5.2, the trained model effectively enhanced the sharpness of raw images (with peak signal-to-noise ratio PSNR = 38.5, SSIM = 0.97), and the inference time required for PSF corrections was 10 times shorter compared to LumiTools.

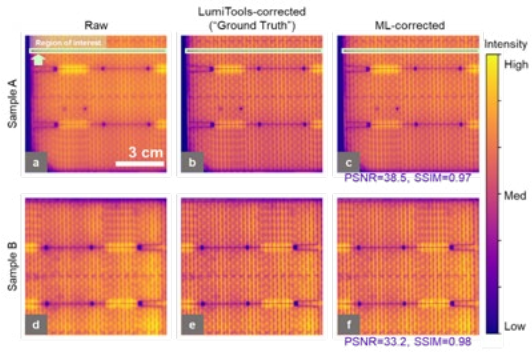

Figure PP1.4.5.2: Representative results from the validation set: (a) and (d) are the raw images; (b) and (e) are the LumiTools-corrected images (ground-truth); (c) and (f) are the ML-corrected images (model predictions).

Advance multi-class defect classification for electroluminescence and infrared images

Our progress involved automating the image processing pipeline, starting from raw images through adaptive thresholding, region of interest (ROI) identification, module edge detection, to module cropping. We then extracted statistical and texture-based features, such as contrast and homogeneity, to detect anomalies. The features were further clustered using K-means (as shown in Figure PP1.4.5.3) and principal component analysis (PCA). Lastly, we validated the classification results on two types of EL image data sets using Kullback-Leibler (KL) divergence, demonstrating the capability to identify a range of defects.

PP1.4.5 Machine Learning

UNSW Team
Prof. Ziv Hameiri, Dr Brendan Wright, Dr Tien-Chun Wu, Dr Ali Shakiba, Dr Rama Sharma

UNSW Students
Mr Zubair Abdullah-Vetter, Ms Gaia Maria Javier

Funding Support
ARENA, ACAP

Aims

Our research aims to leverage machine learning (ML) capabilities for automating photovoltaic (PV) cell performance diagnosis, focusing on (a) image-based module defect characterisation, and (b) electrical signal-based module efficiency estimation.

For image-based characterisation, we aim to (a) identify defects by separating key spatially resolved electrical features from electroluminescence (EL) images; (b) boost the computational efficiency of sharpness correction of conventional photoluminescence (PL) imaging systems by ten times; and (c) advance multi-class defect classification for both EL and drone-captured infrared (IR) images.

For signal-based characterisation, we aim to (a) estimate the inherent degradation state of modules in utility-scale solar farms; (b) extract different modes of operation from the daily profile of inverter output; (c) extract electrical parameters from spectral responses of current for estimating internal quantum efficiency (IQE) of modules; and (d) predict long-term degradation of modules using 10% of historical input data.

Progress

Identify defects by separating key spatially resolved electrical features from electroluminescence images

We adapted a U-Net (Ronneberger et al. 2015) model to extract spatially resolved PL features that highlight recombination features directly related to the implied open-circuit voltage (iV_{oc}), and series resistance (R_s) from simulated EL images by Griddler. The results are shown in Figure PP1.4.5.1. For PL prediction, the model accurately reproduced cracks and regions with high recombination, resulting in a structural similarity (SSIM) score of 0.96. For the R_s prediction, the model successfully identified finger breaks.

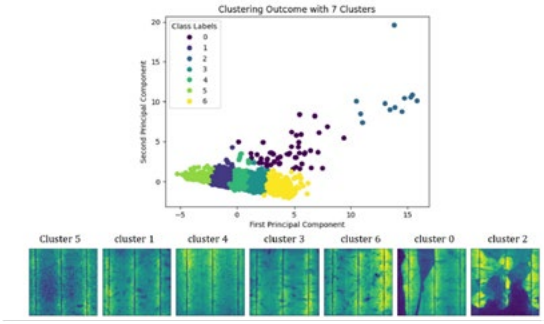

Figure PP1.4.5.3: (Top) K-means clustering of 3,780 EL modules into seven clusters. (Bottom) Examples of images classified into those seven cluster categories.

Extract different modes of operation from the daily profile of inverter output

We developed an ML pipeline to extract different modes of operations for inverters in a utility-scale PV plant. The pipeline leverages a beta variational autoencoder (VAE) (Higgins et al. 2016) with 1D convolutional layers, to extract intricate features from a latent representation learned from the electrical and meteorological data. The latent representation was compressed with t-distributed stochastic neighbour embedding (t-SNE) and clustered with a density-based clustering algorithm to extract different modes of operation. Figure PP1.4.5.4 shows a visualisation using a 2D t-SNE embedding of the latent factors. The model is capable of discerning clear-sky days from cloudy days, communication blackouts, as well as the direct impact of the plane of array (POA) irradiance on the generated DC power.

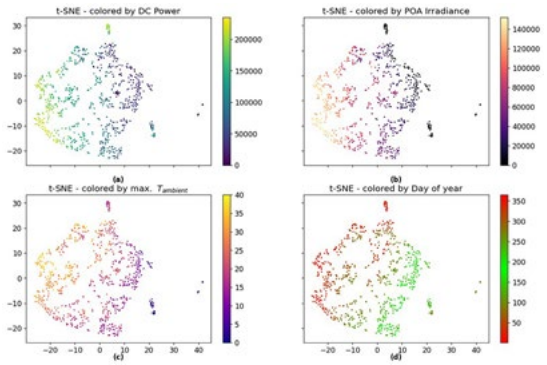

Figure PP1.4.5.4: Embedding of the transformed daily profiles in the latent factors with the t-SNE algorithm coloured by the daily aggregated DC power and POA irradiance, and the maximum daily temperature.

Extract electrical parameters from spectral responses of current for estimating internal quantum efficiency of modules

We developed a random forest (RF)- and convolutional neural network (CNN)-based pipeline to extract electrical parameters from spectral responses measurements (IQE) from gallium arsenide (GaAs) solar cells. SolCore was used to generate a training data set of 40,000 GaAs solar cells. We varied the following parameters in the simulation: the diffusion length of the minority carriers of the emitter (L_e) and bulk (L_h), and the surface recombination velocity of those regions (S_p and S_n, respectively). Our modelling pipeline integrated an array of RF models with a chain regression technique (Pedregosa et al. 2011). Further improvements were performed by calculating the IQE derivative array and applying PCA for training the RF and CNN models to predict the parameters, as shown in Figure PP1.4.5.5. The root mean square error (RMSE) values (in the range of 0.02–0.08) showed that the method achieved very accurate estimations for all four parameters.

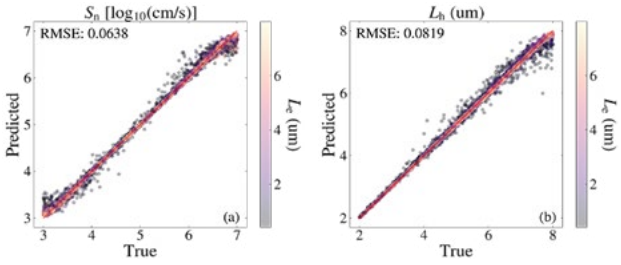

Figure PP1.4.5.5: Predicted vs. true plots are presented in the chain order: L_e, S_p, S_n, and L_h. The colour bars represent the true values of the corresponding parameter in the same region of the solar cell.

Predict long-term degradation of modules using 10% of historical input data

We employed a latent ordinary differential equation neural network (ODENN) framework to predict multiple diverse trends of PV module performances throughout a 1,500-hour accelerated damp heat (DH) test. The performance parameters trained and predicted by the ODENN model were the open-circuit voltage (V_{oc}), the mean pixel intensity of the EL images, module efficiency, and two-diode saturation current density (J_{02}). At inference time, only the first 10% (0–144 h) of the measured four parameters collected during the DH test were entered as inputs to the model. As shown in Figure PP1.4.5.6, the mean absolute percentage errors (MAPE) of the parameter predictions fall in the range of 0.2%–23%.

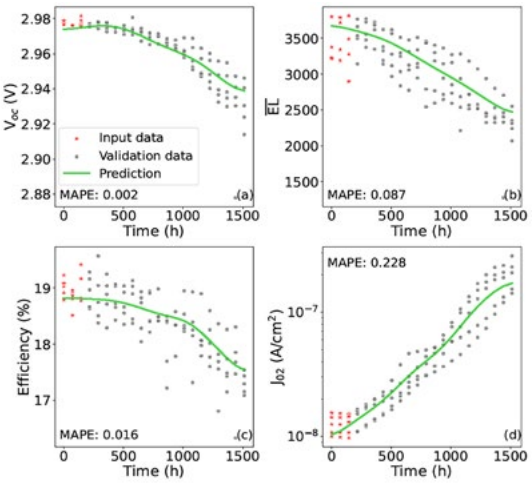

Figure PP1.4.5.6: Representative test samples with their measured and the predicted trends versus time for (a) V_{oc}, (b) mean EL intensity, (c) efficiency, and (d) J_{02}.

References

Ronneberger, O., Fischer, P., & Brox, T. (2015). U-Net: Convolutional networks for biomedical image segmentation. arXiv.

Payne, D. N. R., Vargas, C., Hameiri, Z., Wenham, S. R. & Bagnall, D. M. (2017). An advanced software suite for the processing and analysis of silicon luminescence images. Computer Physics Communications 215, 223-234.

Higgins, I., Matthey, L., Pal, A., Burgess, C. P., Glorot, X.,

Botvinick, M. M., Mohamed, S. & Lerchner, A. (2016). beta-VAE: Learning Basic Visual Concepts with a Constrained Variational Framework. International Conference on Learning Representations.

Pedregosa, F. . (2011). Scikit-learn: machine learning in python. J. Mach. Learn. Res., 12, 2825-2830. (*https://dl.acm.org/doi/10.5555/1953048.2078195*).

PP2
EMERGING MATERIALS

OVERVIEW

Program Package 2 (PP2) encompasses research into a range of next generation cell technologies, spanning organic photovoltaics (OPVs), Earth-abundant kesterite materials, and perovskite solar cells (PSCs). The Program Package examines all aspects of these classes of solar cells, including fundamental material properties, material synthesis, incorporation into devices and their optimisation for enhanced efficiency and lifetime, and scale-up using industrially relevant production methods.

Research in PP2 occurs across all ACAP nodes, and 2023 saw substantial advances across all work packages. In some instances, the efficiency of lab-scale devices is approaching that of conventional Si solar cells, and improvements in the scalable manufacturing indicate these technologies are rapidly approaching commercialisation in initially niche applications where a premium is placed on their potentially unique form factor.

PP2.2 ORGANIC PHOTOVOLTAICS

Research Teams
University of Queensland: Prof. Paul Burn, Dr Paul Shaw, Dr Hui Jin, Dr Neil Mallo

University of Melbourne: A/Prof. David Jones, Dr Jegadesan Subbiah, Dr Calvin Lee

UNSW: A/Prof. Ashraf Uddin, Prof. Gavin Conibeer, Prof. Bram Hoex, A/Prof. John Stride, Prof. Mahbub Hassan

Research Students
University of Queensland: Shaun McAnally, Ronan Chu, Satakshi Gupta, James Smyth, Oliver Lindsay, Euca Brooks

University of Melbourne: Jacob Yin, Maria Bibi Khalil Ahmed

UNSW: Leiping Duan, Habibur Rahman, Shahriyar Safat Dipta, Walia Binte Tarique, Ashraful Hossain Howlader, Yanxiang Wang, Jiawei Hu

Academic Partners
Prof. Ian Gentle (The University of Queensland), Prof. Jan Behrends (Free University of Berlin), Prof. Anna Köhler (University of Bayreuth), Dr Alexander Colsmann (Karlsruhe Institute of Technology), Prof. Akshay Rao (Cambridge University), Prof. Anita Ho-Baillie (University of Sydney), Dr Md Arafat Mahmud (University of Sydney), Prof. Yingping Zou (Central South University, Changsha)

Funding Support
ACAP, ARENA, ARC, UQ, UoM, UNSW

The continued research and development of organic photovoltaic (OPV) devices has led to materials with better absorption and donor-acceptor energy offsets, which has resulted in record certified power conversion efficiencies (PCEs) of > 19% (Chen et al. 2023). This achievement mainly relies on using high performance non-fullerene acceptors (NFA). Due to the rapid development of new molecules and the variety of their chemical structures, understanding how the different NFA

materials affect optoelectronic and device properties is far from complete and is primarily explored in this scheme. Simplifying the synthesis of polymeric donors and NFAs provides an effective channel for scaling up future materials. Similarly, the development of materials that can be used in a single-component organic solar cell would result in simpler device architectures. Using industrially relevant solvents to fabricate OPV devices would reduce production costs and provide a clear pathway towards commercialisation.

For ease of reading, this program has been divided into two broad sections: Organic Photovoltaic Materials and Organic Photovoltaic Devices.

PP2.2.1 ORGANIC PHOTOVOLTAIC MATERIALS

Aims

The materials development program has had the following aims:

- Establish the relationship between molecular structure, dipole moment and dielectric constant of organic semiconductor materials that can be used in homojunction devices.
- Design new singlet fission (SF) materials that are energy-matched to silicon.
- Develop a high-throughput screening protocol for evaluating new SF materials.
- Design device architectures for inclusion of SF materials.

Progress

The effect of fluorinated benzothiadiazole units on the dielectric constants of organic semiconductor materials

An ongoing study on organic semiconductor small molecules composed of glycolated cyclopentadithiophene donors and fluorinated benzothiadiazole (BT) acceptors has been completed. A series of eight compounds were compared (structures shown in Figure PP2.2.1) in which the influence of fluorination, end group (aldehyde or dicyanovinyl) and conjugation length on the dielectric constants at different frequencies was studied. For all the materials, the inclusion of one or more fluorinated BT units increased the value of the low-frequency dielectric constants. However, at the higher optical frequency, the dielectric constants decreased upon fluorination. This was attributed to electronic repulsion between the fluorine

and adjacent acceptor resulting in a twisted conformation, which decreased the conjugation length. An increased conjugation length has been shown in some cases to lead to larger high optical frequency dielectric constants. The dimer with a fluorinated BT unit and a dicyanovinyl acceptor group had dielectric constants of 10.2 at 0.1 MHz and 4.0 at 10^{14} Hz. While it has been proposed that efficient free charge generation is possible for materials with a dielectric constant of over 10, the fluorinated dimer performed poorly in homojunction devices, supporting the theory that it is the optical frequency dielectric constant that is of greater relevance to the spontaneous dissociation of excitons into free charges.

Energy-level tuning in SF materials via biradical character destabilisation

Singlet fission (SF)–enhanced solar cells are an alternative to traditional tandem devices, however, they may be enabled by significantly simpler implementation. Singlet fission allows effective use of high energy photons, i.e. photons with energy twice the silicon bandgap, to generate two excited states from a single absorbed photon.

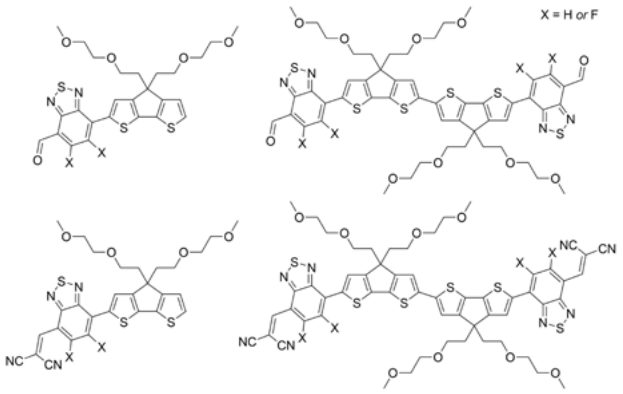

Figure PP2.2.1: The structures of the eight compounds prepared to study the effect of fluorination, conjugation length and the acceptor group on low and optical frequency dielectric constants.

One of the more promising classes of SF-capable materials are the diketopyrrolopyrroles (DPPs) as they have long been used in the paint and organic electronic industries and are characterised by ideal material properties such as high charge mobilities, good stabilities and broad absorption spectra. DPPs were first reported to undergo SF in 2016, where two derivatives were found to possess rapid triplet formation rates and high triplet quantum yields (TQYs). Of note was that the T_1 triplet energy levels for both SF-capable derivatives were found to be around 1.0 eV, below that of the silicon bandgap and thus incompatible with Si PV systems.

To rectify this, we pursue a molecular engineering strategy that modifies DPP chromophores so that their T_1 energy levels are raised to match that of the Si bandgap, while still maintaining a sufficient T_1- S_1 energy gap for efficient, exothermic SF. DPP chromophores are known to be captodatively stabilised biradicaloids in the ground state where the stabilisation of the biradical character serves to depress the S_0/T_1 energy gap. Here our work destabilises the biradical character to increase the energy gap and raise $E(T_1)$, and does so via the introduction of sterically bulky chloro- or methyl- groups on the flanking thiophene moiety to force an out-of-plane twist relative to the lactam core (Figure PP2.2.2, DPPC and DPPM respectively). This work was conducted in collaboration with the University of Cambridge, University of Queensland and the Free University Berlin and recently published (Lee et al. 2023).

In this work we show that our molecular engineering approach was indeed able to increase the energy of the S_1 and T_1 energy levels of diketopyrrolopyrrole derivatives such that the energy-level requirements for exothermic SF and energy transfer to silicon are met. Time-resolved photoluminescence studies show that our silicon-matched materials are SF active in the solid state, forming a correlated triplet pair $^1(TT)$ – a crucial intermediate in the SF process – as observed through Herzberg-Teller emission from $^1(TT)$ at both 77 K and room temperature. This observation was itself a notable phenomenon, as only a handful of studies report $^1(TT)$ emission yet we demonstrate that this is an important tool for probing both singlet fission behaviour as well as quantifying energy levels. Transient electron paramagnetic resonance studies, however, show that the correlated triplet pair does not readily separate into the unbound triplets, which is a requirement for energy harvesting by silicon. The fact that the triplet pair do not separate into free triplets is attributed to the intermolecular crystal packing within the thin films. Nevertheless, these results demonstrate a promising route for energy-tuning silicon-matched SF materials.

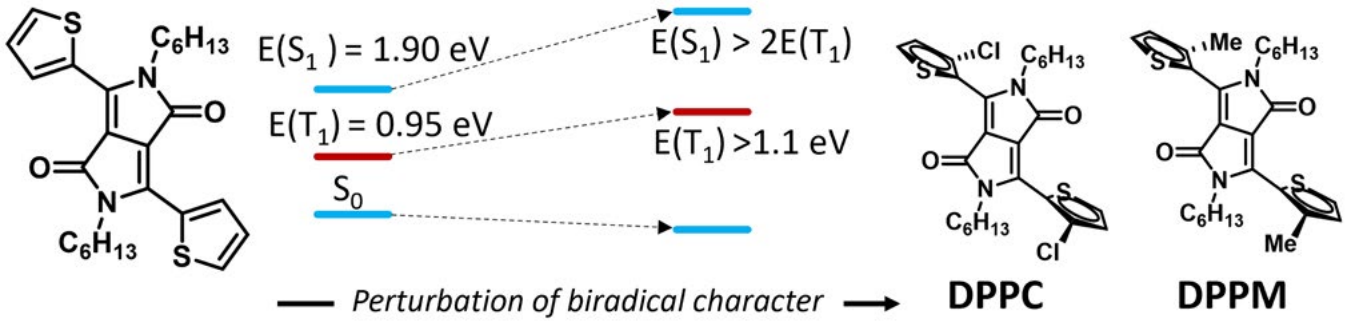

Figure PP2.2.2: Energy level modifications in a diketopyrrolopyrrole chromophore to achieve energetic compatibility with a silicon semiconductor.

Turning on SF in bridged SF chromophores

There are many proposed SF chromophores with calculated triplet energy levels matched to silicon that do not support SF due to poor intermolecular orbital overlap in the solid state. One such chromophore, related to DPPM and DPPC above, is the phenyl substituted diketopyrrolopyrrole (PDPP) (see Figure PP2.2.3). We have proposed that by inclusion of a secondary functional element, which is a bridge between two chromophores, we can modify the crystal packing, allowing appropriate orbital overlap between SF chromophores and allow SF to be turned on.

In this work we proposed the use of pyrene as a bridging element, as (i) there should be good conjugation through the pyrene, (ii) the pyrene molecules can π-stack providing a secondary driver for self-assembly to modify crystallisation, and (iii) can be linked through the 1,6- or the 2,7- positions to examine structure-property relationships. In addition, we can change the PDPP alkyl side chain to further examine the effect of substituents on crystal packing, and SF behaviour.

Two analogous pairs of PDPP dimers have been synthesised, using an octyl or 2-ethylhexyl substituted PDPP substituted in the 1,6- or the 2,7- positions in the pyrene (see Figure PP2.2.3). In initial studies, time-resolved photoluminescence studies show that our silicon-matched materials are SF active in the solid state, forming a correlated triplet pair ^{1}(TT) – a crucial intermediate in the SF process – as observed through Herzberg-Teller emission from ^{1}(TT) at both 77 K and room temperature. This observation was itself a notable phenomenon, as only a handful of studies report ^{1}(TT) emission yet we demonstrate that this is an important tool for probing both singlet fission behaviour as well as quantifying energy levels.

Spectroscopic screening program for singlet fission materials

Our material screening program utilising relatively simple spectroscopic techniques was developed due to bottlenecking in our materials development workflow – our efforts in the design and synthesis of potential candidates for singlet fission–capable chromophores were outstripping the capabilities of our collaborators to perform the in-depth spectroscopic analysis required to verify that our materials were indeed undergoing singlet fission. To reduce the burden on our collaborators, we developed a facile screening process (Figure PP2.2.4) that we could perform in-house using commercial, benchtop spectroscopic instruments. Each step of this three-part process would necessitate that certain unambiguous criterion be met before proceeding on to the next. This process affords multiple time-saving benefits: (1) it allows us to quickly disregard materials that do not possess the fundamental markers for singlet fission, (2) it allows us a quicker feedback process on design criteria for next generation materials, (3) it circumvents the need to access in-demand, bespoke equipment in dedicated spectroscopic laboratories to perform relatively simple characterisation, and (4) it allows us to deliver materials to our collaborators with key spectroscopic information already in hand to facilitate their in-depth analysis.

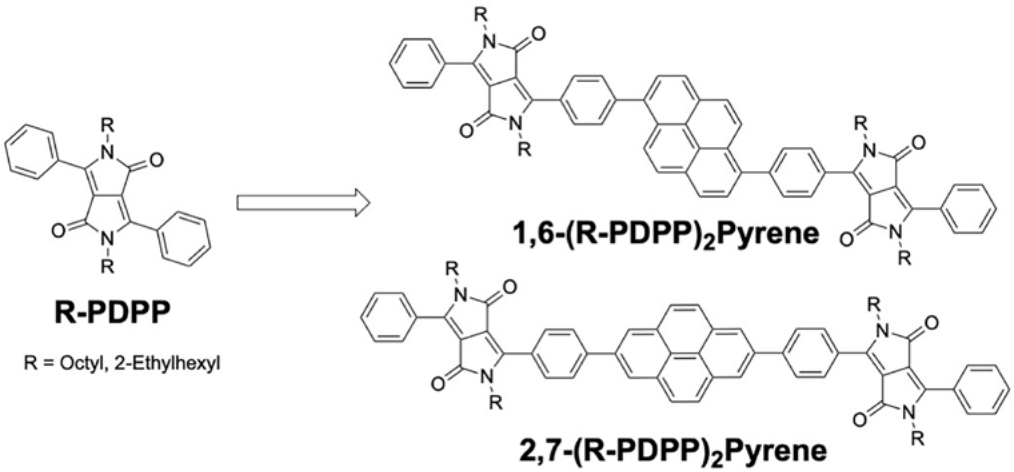

Figure PP2.2.3: Bridged phenyl-diketopyrrolopyrrole chromophores to control crystal packing and turn on singlet fission in the solid state.

Our screening process utilises three key spectroscopic techniques – (1) time-resolved single-photon counting (TCSPC) studies, (2) photoluminescence quantum yield (PLQY) measurements, and (3) nanosecond transient absorption (ns-TA) measurements. To perform these measurements we utilise two off-the-shelf benchtop instruments – the Edinburgh Instruments FS5 spectrophotometer with integrating sphere module, and a Magnitude Instruments enVISTA broadband transient spectrometer.

The first step of this process involves the comparison of emission decay rates of a material in both solution and solid state through TCSPC studies, with the rationale that the solid-state packing of chromophores would "switch on" singlet fission and therefore create additional, non-emissive exciton deactivation pathways not accessible in the solution state. This would manifest as both significantly quenched prompt fluorescence and a multi-exponential fit (with time constants in the order of < 1 ns) for the solid-state emission decay, with both results forming the first criteria in our screening process.

Following on from this, in our second step via PLQY measurements we quantify the degree of fluorescence quenching present in the solid state of a candidate material relative to the solution state. While our materials typically possess high PLQYs in the solution state (> 70%), the criterion for this step is for these PLQYs to be quenched to < 5% in the solid state, thereby suggesting that additional non-emissive relaxation pathways (i.e. singlet fission) are accessible.

The third step in this process aims to quantify the presence of long-lived dark states, i.e. correlated or free triplet species, as lifetimes for these species in the order of > 10^{-7} seconds are required for efficient triplet transport and harvesting. Using ns-TA studies of solid-state films of candidate materials, we ideally identify both the ground-state bleach features as well as any photo-induced absorption features using relatively low-resolution but wide-spectrum scans. Fitting these features to decay curves with time constants in 10^{-7} to 10^{-6} second regimes fulfils the third and final criterion of our screening, with the overall process able to furnish us not only with candidate materials with the capability to form long-lived dark species upon photo-excitation, but also provide us with the approximate spectral regions of interest for our collaborators to focus their spectroscopic efforts on in follow-up studies.

Using this process, to date we have produced 10 materials of interest which we have subsequently passed on to our partner institutions to perform in-depth characterisation, including shorter-timeframe transient absorption studies to quantify the photo-excitation pathways involved, as well as transient electron paramagnetic resonance studies to determine the nature of any triplet species produced.

Highlights

- Fluorinated solar cell materials with high dielectric constants were synthesised. Characterisation of these materials indicates that it is the value of the dielectric constant at high frequencies that governs spontaneous charge generation.
- Evidence of singlet fission observed in phenyl substituted diketopyrrolopyrrole, enabling singlet fission materials that are energy-matched with silicon.
- Protocol established for the rapid screening of potential single fission materials.

Future Work

- Continued development of organic semiconductors with intrinsic charge generation, including high dielectric constant materials.
- Identify potential SF materials for detailed study using ultra-fast spectroscopy.
- Incorporate SF materials into devices.

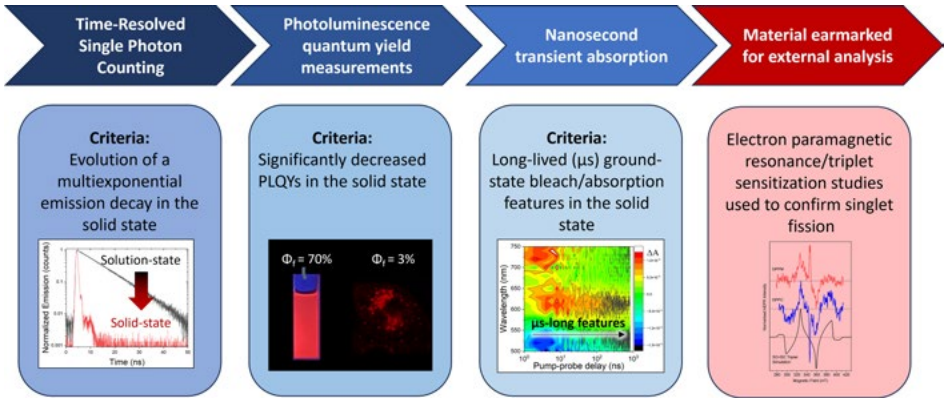

Figure PP2.2.4: Spectroscopic techniques involved in our high-throughput material screening process and desired outcomes (inset).

PP2.3 PEROVSKITES

Research Team

ANU Team
Prof. Klaus Weber, Dr Heping Shen, Dr Daniel Walter, Dr Viqar Ahmad, Keqing Huang, Dr The Duong, A/Prof. Thomas White, Prof. Kylie Catchpole

UNSW Team
Prof. Xiaojing Hao, Prof. Ziv Hameiri, Dr Xu Liu, Dr Meng Zhang, Dr Ziheng Liu, Dr Mingrui He, Prof. Martin Green

University of Melbourne Team
A/Prof. David Jones, Dr Jegadesan Subbiah

University of Queensland Team
Prof. Paul Burn, Dr Paul Shaw, Dr Abdulaziz Bati, Dr Wei Jiang, Dr Neil Mallo

CSIRO Team
Dr Mei Gao, Dr Doojin Vak, Dr Dechan Angmo, Dr Hasitha Weerasinghe, Dr Andrew Scully, Ms Régine Chantler, Dr Anthony Chesman

University of Sydney Team
Prof. Anita Ho-Baillie, Dr Md Arafat Mahmud, Dr Jianghui Zheng, Dr Jueming Bing

Research Students
ANU: Keqing Huang, Grace Tabi, Thuan Nguyen
UNSW: Yihao Wang, Minwoo Lee, Jihoo Lim, Yuru He, Nursultan Mussakhanuly, Ziyue Feng.
University of Queensland: Ronan Chu, Satakshi Gupta, Yaomiao Feng
University of Sydney: Shi Tang, Chwenhaw Liao, Guoliang Wang, Tik Lun Leung, Jianpeng Yi

Academic Partners
EPFL (Switzerland), Helmholtz-Zentrum Berlin (HZB), Pennsylvania State University, Southwest Petroleum University, University of Cambridge, University of Technology Sydney, University of Surrey, Prof. Ian Gentle (University of Queensland), National Taiwan University, National Synchrotron Radiation Research Center (Taiwan)

Funding Support
ACAP, ARENA, ARC, UQ, UoM, UNSW, UoS, ACAP, King Abdullah University of Science and Technology (KAUST) through the Ibn Rushd Postdoctoral Fellowship Award (ASRB)

Aims

- Develop strategies to fabricate stable and efficient perovskite solar cells.
- Passivation of perovskite and electron transport layers for efficient perovskite solar cell fabrication.
- Assessment of new fluorinated additives, including organic cations in a capping layer for 3D/2D perovskite heterojunctions.
- Develop strategies to synthesise highly crystalline electron transport layers.
- Develop bismuth-based lead-free perovskite solar cells.
- Improve performance of wide bandgap perovskite solar cells for tandem cells.
- Achieve > 25% of power conversion efficiency.
- Achieve less than 10% relative reduction in efficiency after 10,000 hours of storage.
- Develop a 10 cm^2 five-cell mini-module.
- In-house development of a five-cell mini-module capable of recovering more than 90% of its MPP current after shading one cell for 30 minutes.

Progress

Double-sided surface passivation of the perovskite layer for efficient solar cells

Interfacial passivation has been regarded as an effective strategy to enhance the performance of perovskite solar cells (PSCs) by modifying defect trap states between perovskite and charge transport layers. Here, we used 1,4-diazabiyclo octane (DABCO) to passivate the perovskite/electron transport layer (ETL) and 1,8-diaminonaphthalene (DAN) to passivate the perovskite/hole transport layer (HTL). This demonstrated that using DABCO and DAN to passivate the SnO and perovskite layers, respectively, to suppress the interface defects from perovskite and metal oxide films, can effectively decrease non-radiative recombination and extend the carrier recombination lifetime to boost PSC device performance. Earlier, we reported that ETL passivation using DABCO and device performance were optimised by varying the concentration of DABCO solutions. Here, we have used perovskite layer passivation together with ETL passivation to improve the performance of perovskite solar cells.

PSCs were fabricated using regular geometry (Figure PP2.3.1(a)) using the precursors of $CsFaPbI_3$ with 10 mol% excess $PbCl_2$, followed by thermal annealing at 150°C in ambient conditions. Figure PP2.3.1(b) shows the J-V curves of the perovskite solar cells with various surface passivation. Earlier, we optimised the PSC with a 5 mM DABCO solution passivated ETL surface, which shows optimum device performance, and here we used the same condition along with perovskite top layer passivation using a DAN solution. As shown in Table PP2.3.1, the double-sided passivated perovskite devices exhibit the best device performance of 21.9% compared to other perovskite devices.

The photovoltaic parameters for all devices with and without ETL passivation using a DABCO solution are shown in Table PP2.3.1. The control device without surface passivation demonstrates a PCE of 19.2%, whereas the device with the 5 mM exhibits the best performance of 20.6%. The electrical impedance spectroscopy (EIS) (Figure PP2.3.1(c)) characterisation was carried out to study charge carrier transport properties of PSCs with and without a double-sided passivation layer, with devices with double-sided passivation exhibiting a lower impedance of 4.5 kΩ compared to the device without surface

passivation which shows a higher impedance of 21 k Ω. This means a more effective charge extraction and lower recombination loss at the interface of ETL/perovskite, which facilitates enhanced device performance. The surface morphology of the passivated perovskite layer is characterised by atomic force microscopy, and the height and phase, with decreased roughness, are shown in Figure PP2.3.2.

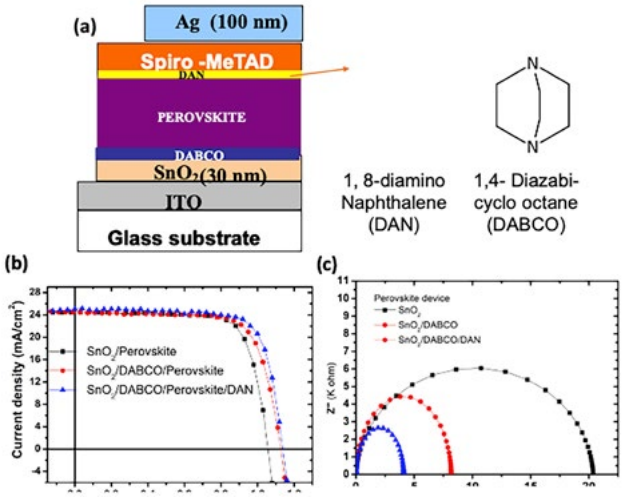

Figure PP2.3w.1: (a) Schematic diagram of a perovskite solar cell and the molecular structure of DABCO and DAN; and (b) J-V curves and (c) EIS plot of the PSCs with various passivation layers.

Table PP2.3.1: Photovoltaic parameters of perovskite solar cells with single- or double-sided passivation layers.

ETL/Perovskite	J_{sc} ($mAcm^{-2}$)	V_{oc} (V)	FF (%)	PCE (%)
ITO/SnO_2	24.4	1.08	73	19.2
ITO/SnO_2/DABCO	24.5	1.12	76	20.6
ITO/SnO_2/DABCO/ Perovskite/DAN	24.9	1.14	78	21.9

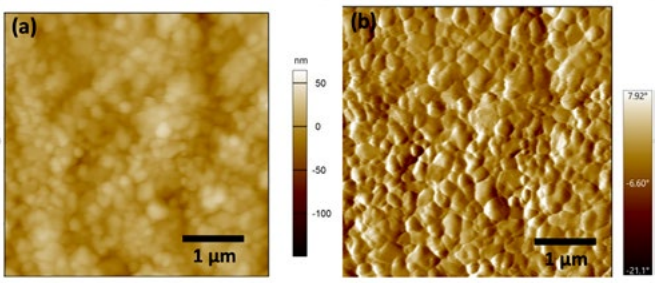

Figure PP2.3.2: (a) AFM height and (b) phase image of the surface passivated perovskite layer.

Caesium bismuth iodide-based lead-free perovskite solar cells

The development of environmentally friendly Pb-free perovskite solar cells is in high demand owing to limitations in the practical application of Pb-based perovskite solar cells. Therefore, lead-free perovskite materials are getting much attention as an alternative to the $APbX_3$ system because of the toxicity and bioaccumulation of lead in the ecosystem. In recent years, air-stable bismuth halide perovskites have attracted much attention. However, the performance of bismuth-based solar cells lags behind lead halide perovskites in terms of device performance due to poor control of the formation of perovskite film quality. In this work, UoM researchers investigated the solar cell device performances of $Cs_3Bi_2I_9$ and $CsBi_3I_{10}$ perovskites synthesised via the LARP (Ligand-assisted Re-precipitation) method, in which Dimethylformamide (DMF) has been used as a "good" solvent and toluene as a "poor" solvent. This method is considered one of the most cost-effective and simple methods to synthesise high quality perovskite materials under ambient conditions.

The synthesis of $Cs_3Bi_2I_9$ and $CsBi_3I_{10}$ was performed by the LARP approach, and the schematic representation of the LARP process is shown in Figure PP2.3.3(a). The precursor materials are highly soluble in DMF, while at the same time, the products $Cs_3Bi_2I_9$ and $CsBi_3I_{10}$(CBI10) are not soluble in toluene (since toluene is a poor solvent for $Cs_3Bi_2I_9$ and $CsBi_3I_{10}$). Due to good solubility, the precursors were dissolved in DMF, and then this solution mixture was transferred into the "poor" solvent (toluene) to obtain the desired product. The XRD pattern of both $Cs_3Bi_2I_9$ and $CsBi_3I_{10}$ are shown in Figure PP2.5.3(b) and the observed XRD pattern for both perovskite $Cs_3Bi_2I_9$ and $CsBi_3I_{10}$ (CBI_{10}) well matches with the reference pattern, which confirms the formation of the same material. The characteristic absorption peak at 488 nm has been observed in the UV-Vis spectrum of $Cs_3Bi_2I_9$ (Figure PP2.3.3(c)). The range of visible light absorption has been found to extend up to 623 nm. Compared to $Cs_3Bi_2I_9$, the bandgap of CBI_{10} has been reduced to 1.72 eV (shown in Figure PP2.3.3(d)), which causes extended light absorption.

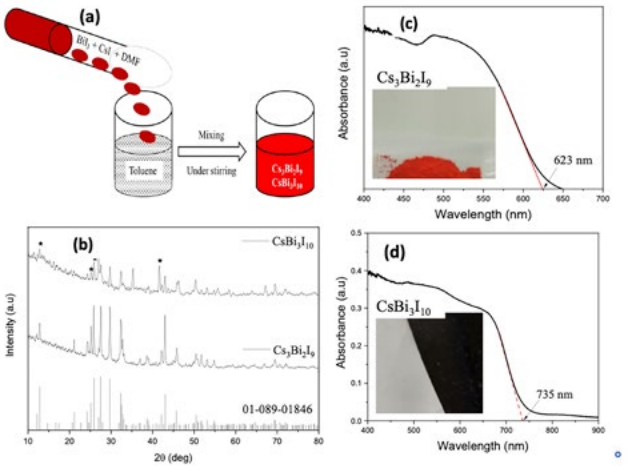

Figure PP2.3.3: (a) Schematic representation of LARP process to synthesise $Cs3Bi_2I_9$ and $CsBi_3I_{10}$ perovskites; (b) XRD pattern of $Cs3Bi_2I_9$ and $CsBi_3I_{10}$ perovskites; (c) absorption spectra of $Cs3Bi_2I_9$ and (d) $CsBi_3I_{10}$ respectively.

The prepared perovskites were fabricated into solar cell devices with the device structure of ITO/NiO/Perovskite layer/$PC_{61}BM$/BCP/Ag as shown in Figure PP2.3.4(a). J-V measurements of the perovskite solar cell devices fabricated with $Cs_3Bi_2I_9$ and $CsBi_3I_{10}$ (before and after annealing) have been depicted in Figure PP2.3.4(b), and the J-V parameters are shown in Table PP2.3.2. The device structure adopted in this work is ITO/NiO/Perovskite layer/PC61BM/BCP/Ag. As shown in Figure PP2.3.4(b), the device fabricated with $Cs_3Bi_2I_9$ delivered a power conversion efficiency (PCE) of 0.7% with a fill factor (FF) of 47, V_{OC} of 0.62 V, and J_{SC} of 2.3 $mAcm^{-2}$. The poor performance of the device might be due to the discrete nature of the $[Bi_2I_9]_3$–bioctahedra, as well as bulk recombination, even though $Cs_3Bi_2I_9$ has a long charge carrier lifetime. The device fabricated with CBI10 before annealing delivered a PCE of 0.15% with FF of 34, V_{OC} of 0.40 V and J_{SC} of 1.1 $mAcm^{-2}$. The poor performance of the device is due to the absence of perovskite structure formation.

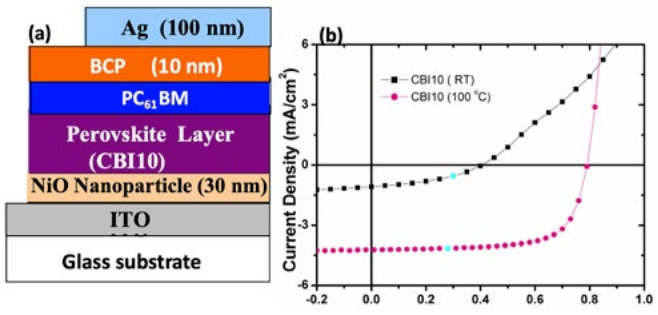

Figure PP2.3.4: (a) Schematic diagram of a perovskite solar cell; and (b) J-V plot of CBI10-based perovskite device with and without annealing.

Table PP2.3.2: Photovoltaic parameters of CBI10-based perovskite solar cell with and without annealing.

Perovskite Layer	J_{SC} ($mAcm^{-2}$)	V_{OC} (V)	FF (%)	PCE (%)
CBI10-RT	1.1	0.40	34	0.15
CBI10-100°C	4.2	0.79	69	2.3

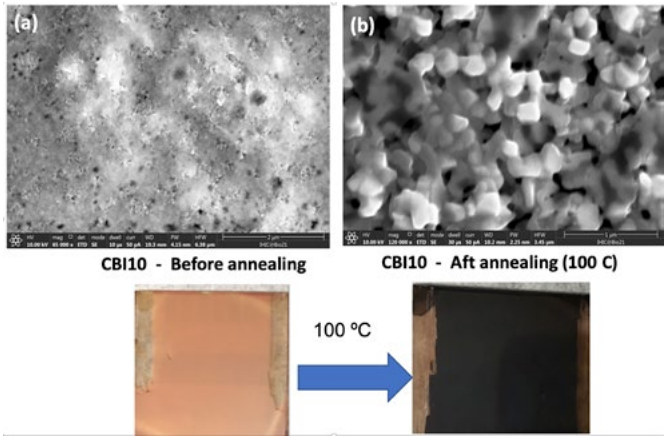

Figure PP2.3.5: (a) SEM images of CsBi3I10 film before and (b) after annealing at 100°C; and (c) the photograph of the corresponding perovskite film before and after annealing showing crystal formation.

Finally, the device fabricated with CBI10 annealed at 100°C showed the best performance efficiency of 2.3% with an improved FF of 69, V_{OC} of 0.79 V and J_{SC} of 4.2 $mAcm^{-2}$. Upon annealing at 100°C, the CBI10 film changes colour from orange-red to blackish (Figure PP2.3.5(c)) with compact and large-grain morphology. Compared to $Cs_3Bi_2I_9$, the enhanced performance of the CBI10 perovskite-based device is due to improved surface morphology and perovskite crystal formation upon annealing (Figure 2.3.5(a) and 2.3.5(b)), which reduces the interface energy barrier and efficient interfacial charge extraction.

Strategies for improving ETL and perovskite layer quality

In order to improve the PCE and stability of PSCs, the poor quality of electron transport layers (ETLs), which is regarded as one of the main reasons for PSCs' performance and degradation, must be resolved. By analysis, we found the poor quality of ETLs originates from their crystallinity. The poor crystallinity negatively impacts device efficiency and stability, due to its inefficient electron transport capacity and unexpected stress and defects at the interface, which leads to degradation of perovskites. To tackle this issue, we developed a novel technology to manipulate the crystallinity of ETLs and thus simultaneously improved the device efficiency and stability. The up-to-date cell (0.14 cm2) fabricated with target ETLs demonstrated an efficiency of up to 25.1% under reverse scanning conditions, as shown in Figure PP2.3.6(a).

Moreover, we found that the notorious phase segregation and/or phase transition issue of FAPbI3-based perovskite materials at low temperatures could be overcome. We developed innovative strategies to synthesise robust perovskite absorbers and improve the stability of associated perovskite solar cells. Unencapsulated devices fabricated with robust perovskite absorbers can maintain high efficiencies over one year (> 9000 hours, still under tracking) as shown in Figure PP2.3.6(a

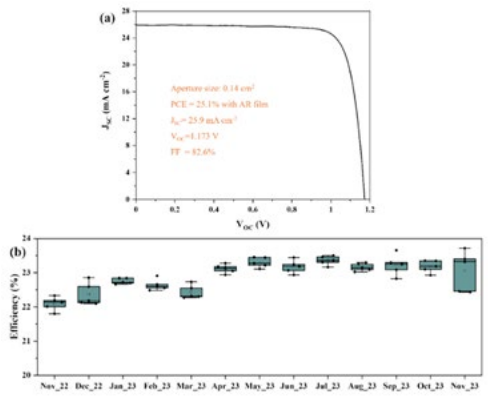

Figure PP2.3.6: (a) J-V curve of up-to-date champion target cell fabricated by target high-crystalline electron transport layers (Testing condition: Ambient air, 40–60% RH, 25–30°C). (b) Performance evolution of perovskite devices fabricated by target robust perovskite absorbers stored in N2 desiccator (RH < 10%) over one year.

In order to better understand the degradation mechanisms and therefore accelerate the development of stability improvement strategies, we conducted an analysis of the underlying driving forces responsible for segregation. We found that the heat-induced reversal of segregation could be due to dynamic disorder-induced localisation of polarons and thermal disorder-induced strain (TDIS), where both drivers could coactively reduce the impact of light-induced strain (LIS). The reversal of segregation constantly quenched PL signal. The stronger the quenching the more prominent was the reversal of segregated ions (Figure PP2.3.7(a–d)), indicating the interplay between light intensity and temperature. Furthermore, respective charge-carrier lifetime reduced from ~950 ns at 25°C to ~800 ns at 40°C and further to ~330 ns as the temperature increased to 80°C, consistent with the steady-state PL quenching (Figure PP2.3.7(e)) and excess carrier density decreased (Figure PP2.3.7(f)). Such changes in carrier dynamics were ascribed to dynamic disorder-induced localisation of polarons.

Temperature-dependent transient mid-infrared spectroscopy (TRIR) confirmed the localisation of polarons at elevated temperatures but with a reduced population of polarons (possibly due to a reduction in excess carrier density). According to Emin's large polaron model, the changes in absorption spectra indicate dynamic disorder-induced localisation of polarons. Since the polaron population decreased due to reduced excess carrier density, the LIS gradient within the perovskite lattice (otherwise responsible for segregation) also could decrease.

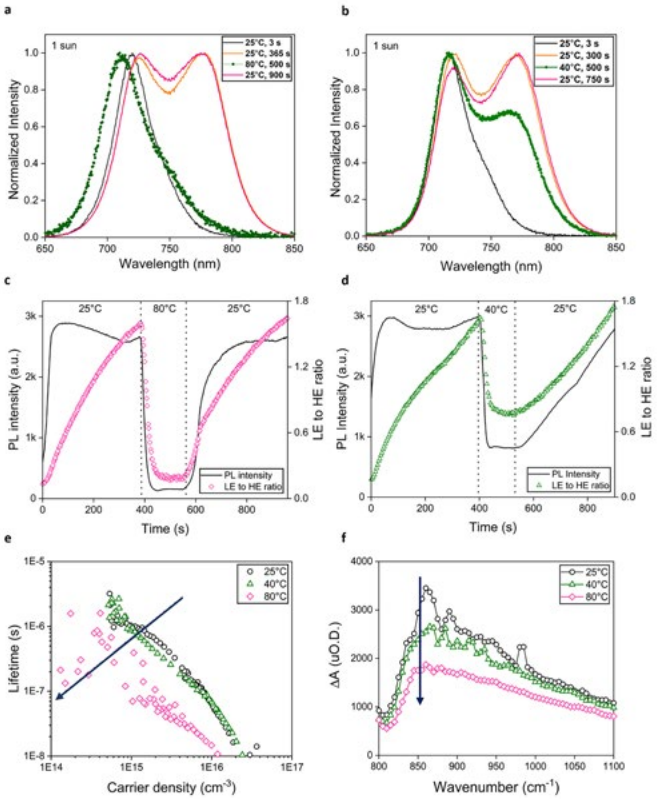

Figure PP2.3.7: Selected normalised temperature-dependent PL spectra with the remixing temperature of (a) 80°C and (b) 40°C. Change in the high-energy (HE) PL peak intensity and in the ratio of low-energy (LE) peak intensity to the HE peak intensity over time. (c) Sample heated to 80°C under one-sun illumination intensity, (d) sample heated to 40°C under one-sun illumination intensity. (e) Calculated charge carrier lifetime and excess carrier density from 2D TRPL (the blue line with an arrow represents excess carrier density under one-sun equivalent illumination intensity at the respective condition). (f) Temperature-dependent, time-resolved mid-IR (TRIR) absorption spectra of $Cs_{0.05}FA_{0.65}MA_{0.30}Pb(I_{0.70}Br_{0.30})_3$ samples scanned at different temperatures 50 ns after bandgap excitation.

To evaluate structural changes contributing to segregation and reversal, we further conducted in situ temperature-dependent XRD measurements, both in the dark and under illumination at ~0.1 Wcm^{-2} intensity. Upon light soaking, all diffraction peaks decreased in intensity with a simultaneous peak broadening and uniformly shifted to a lower 2θ angle compared with pristine mixed-halide phase (28.38° to 28.29°), implying loss of crystallinity, increased disorder, and light-induced expansion of the perovskite lattice, respectively (Figure PP2.3.8(a–b)). More importantly, a shoulder appears at 28.06°, indicating the segregation of the initial mixed phase into two crystalline phases.

Since I-rich perovskites have a larger lattice constant than Br-rich perovskites, the emergence of the peak at a lower angle could correspond to the presence of I-rich domains. Heating the sample to 80°C during illumination attenuates the shoulder at 28.06°. Moreover, all diffraction peaks shifted to an even lower 2θ angle as the lattice expanded further with increased FWHM. Broadened diffraction peaks imply the presence of thermally activated structural disorder, consistent with Mid-IR examinations. As the perovskite lattice thermally expands, the strain on the lattice tends to increase. Therefore, unlike the reversal of segregation in the dark and at room temperature conditions due to entropy-driven relaxation of the lattice strain, under illumination, entropy-driven reversal of segregation seems to be assisted with a vastly strained perovskite framework, confirmed by a shift of the individual diffraction peaks. In contrast, upon in situ heating to 40°C, the shoulder corresponding to I-rich domains remains nearly unchanged. In addition, the shift in the peak position is not significant, indicating a minor change in the lattice constant and strain at moderate temperatures.

To quantify the response of the perovskite lattice to different conditions, the relative change of the lattice parameters and strain was obtained using a Pawley fit to the corresponding XRD diffraction peaks. We find that the lattice exhibits higher expansion and greater strain disorder due to the combined effects of illumination and heating than the influence of each condition individually for a certain illumination intensity. The changes in lattice properties due to only thermal disorder are consistent with the shifts of the diffraction peaks towards the lower angle. Interestingly, the TDIS at 40°C (~0.151%) is comparable to LIS generated under one-sun illumination intensity (~0.141%). However, the TDIS value at 80°C (0.227%) exceeds that imposed by the one-sun illumination. Therefore, we speculate that at 40°C and one-sun illumination, with a lattice strain of 0.188%, LIS could contribute more to the total strain (0.188%) than TDIS, leading to dominant enthalpy. Therefore, halide ions reversal was less pronounced (see Figure PP2.3.8(b)). However, upon illumination at 80°C, the main contributor to the greater strain (0.250%) could be due to TDIS, spreading across the lattice and disrupting LIS gradients (as LIS decline due to a decrease in polaron density observed in 2D TRPL/TRIR analysis). Therefore, the enthalpic driving force of segregation could be counterbalanced.

The perovskite framework is likely to be more ordered at low temperatures. So, the effect of LIS would be more significant because distortions influence their surroundings more strongly. In contrast, the strain induced by polarons could have a minor influence at higher temperatures because the disorder caused by thermal fluctuations could mask the changes in structure caused by LIS. This enhanced understanding of the underlying driving forces responsible for segregation and thermally activated reversal could provide a pathway for designing stable and efficient perovskites under real-world operating conditions.

Absolute methylammonium (MA)-free perovskite attracts great interest due to its superior stability over MA-containing perovskite. However, it is more challenging to prepare high quality MA-free perovskite films with the gas-quenching method, which is a mass-production compatible technique that has been widely adopted in pilot lines of perovskite photovoltaics. We provide a systematical study on the precursor engineering of MA-free perovskite ($FA_{0.9}Cs_{0.1}PbI_3$), revealing the effect of the pyrrolidone-based ligands including 2-pyrrolidone (NP), N-methyl-2-pyrrolidone (NMP), N-ethyl-2-pyrrolidone (NEP) and N-octyl-2-pyrrolidone (NOP) on the film preparation as well as the device fabrication of MA-free perovskite solar cells. By using NP as a ligand, a smoother buried interface and a rougher top interface of the device can be obtained (Figure PP2.3.9). The improved interface maximises the utilisation rate of incident light and improves the current density of the devices, showing greater potential in preparing high quality gas-quenched MA-free perovskite films and devices compared to NMP and other pyrrolidone-based ligands.

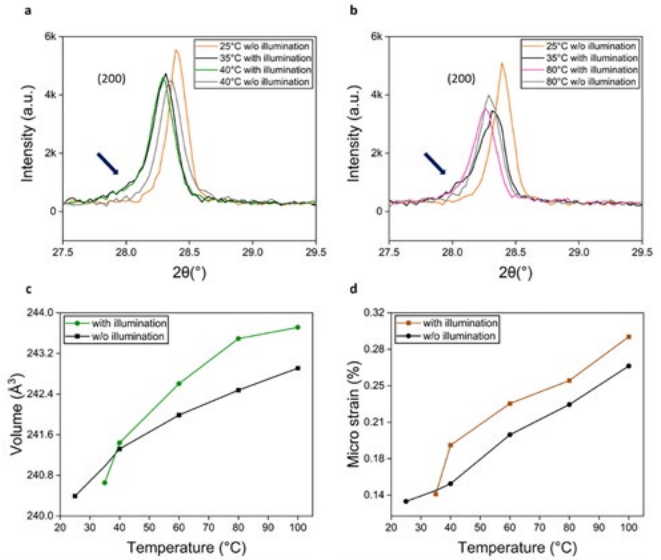

Figure PP2.3.8: Temperature-dependent XRD pattern of (200) plane, measured on a $Cs_{0.05}FA_{0.65}MA_{0.30}Pb(I_{0.70}Br_{0.30})3$ perovskite thin film in the following order: under dark, under illumination only (~0.12 W/cm²), under illumination with heating to (a) 40°C, (b) 80°C, and at an elevated temperature only without illumination, respectively. (c) Lattice parameters and (d) extracted stain.

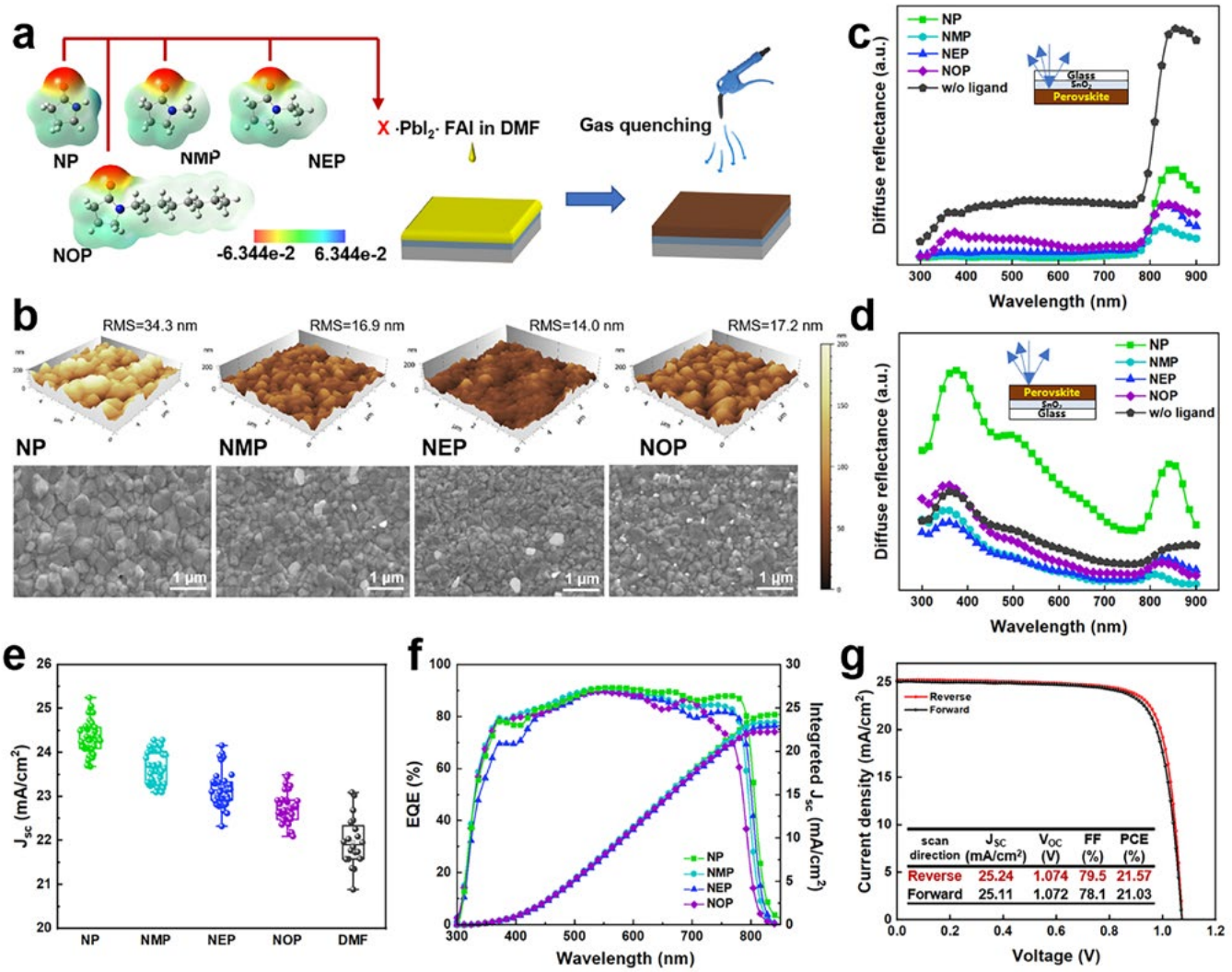

Figure PP2.3.9: (a) ESP mapping of pyrrolidone-based ligand molecules and schematic of preparation of $FA_{0.9}Cs_{0.1}PbI3$ perovskite thin films by gas quenching, X indicates ligands; (b) AFM topographic maps and SEM images of gas-quenched $FA_{0.9}Cs_{0.1}PbI3$ perovskite film prepared with various pyrrolidone-based ligands; (c) glass-incident and (d) film-surface-incident diffuse reflectance spectra of $FA_{0.9}Cs_{0.1}PbI3$ perovskite prepared with different pyrrolidone-based ligands; (e) statistical box chart of the photocurrent density of the PSCs fabricated with different ligands and without ligands; (f) EQE spectra of PSCs fabricated with different ligands; (g) J-V curves and photovoltaic parameters of best performing device fabricated with NP.

Improved encapsulation techniques for enhanced device performance

Ensuring reliable encapsulation is critical in extending the device lifetime of metal halide perovskite solar cells (PSCs) for their commercialisation. However, the performance loss resulting from the encapsulation process has been an obstacle to realising the excellent performance of PSCs in practical applications. We revealed that the encapsulation-induced performance loss is highly related to the tensile strains imposed on the functional layers of the device while exposing PSCs directly to the deformed encapsulant for the first time (Figure PP2.3.10). Therefore, a barrier-strategy for the encapsulation of PSCs is developed by employing a non-adhesive barrier layer to isolate the deformed encapsulant from the PSC functional layer, achieving a strain-free encapsulation for the PSCs. As a result, the encapsulated device with a barrier layer effectively reduced the relative performance loss from 21.4% to 5.7%, and dramatically improved the stability of the device under double 85 environment condition. This work provides an effective barrier strategy to mitigate the negative impact of encapsulation on the performance of PSCs as well as insight into the underlying mechanism of the accelerated degradation of PSCs under encapsulation-induced strains.

For the inverted structure, different substrate optimisation strategies have been investigated to fabricate stable, reproducible and efficient inverted PSCs. A 23.9% efficiency inverted structure PSC (without antireflection coating) has been achieved. The improvement is from enhanced light harvesting after substrate optimisation, a better working function uniformity with HTLs optimisation, aligned energy levels through the whole device after introducing the multi-interfacial-layers and buried interface passivation (Figure PP2.3.11). The low reproducibility issue of high performance inverted p-i-n perovskite solar cells has been solved without losing efficiency and stability.

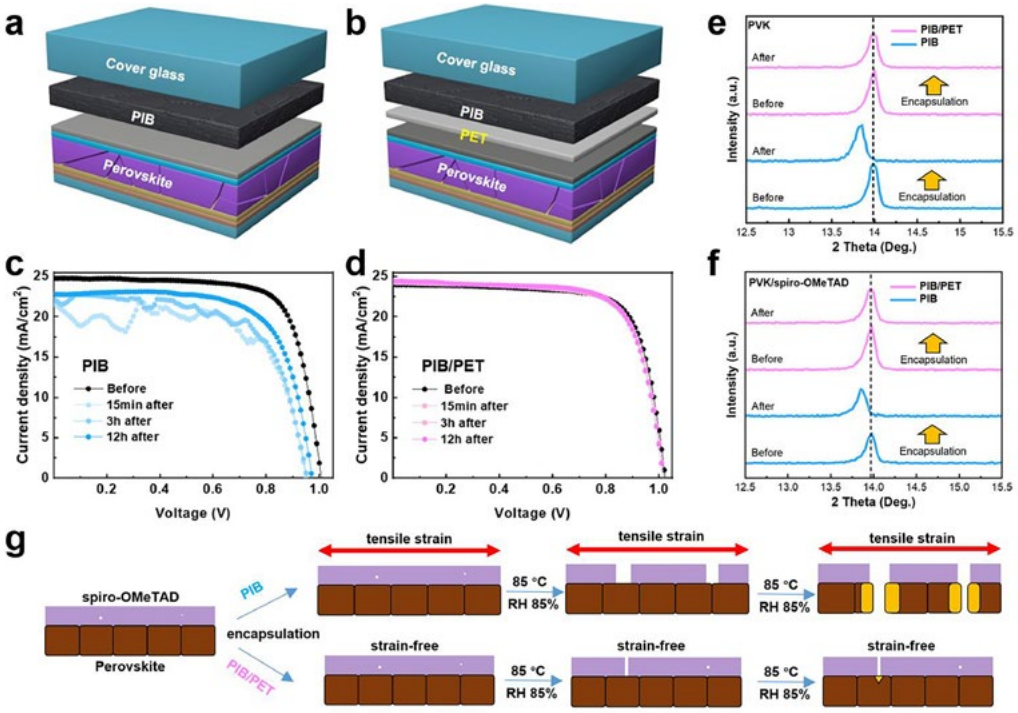

Figure PP2.3.10: (a) Schematic diagram of encapsulation structure of PIB encapsulation and (b) PIB/PET encapsulation; (c) J-V curves of PIB device and (d) PIB/PET device before and after encapsulation for various times of 15 minutes, 3 hours and 12 hours; (e) XRD patterns of the perovskite films and (f) perovskite films coated with spiro-OMeTAD in two encapsulation structures before and after lamination. (g) Schematic diagram of the proposed mechanism on improving stability with barrier strategy encapsulation.

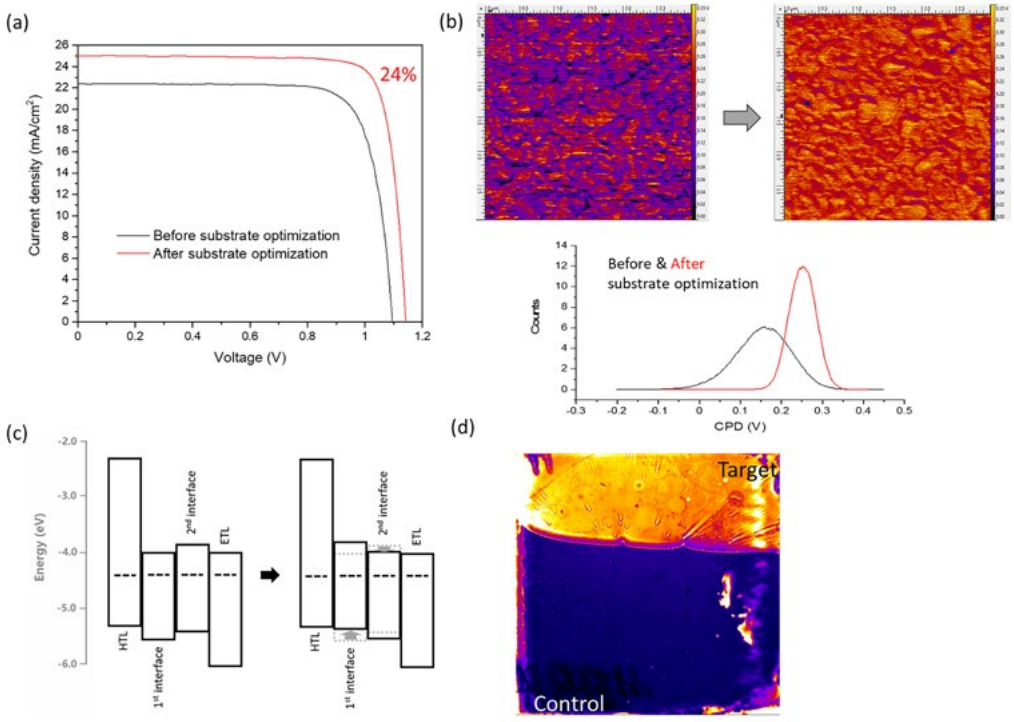

Figure 2.3.11: (a) Efficiency improvement after substrate optimisation. (b) Working function uniformity improvement with HTL optimisation. (c) Band alignment improvement with multi-interfacial-layers optimisation. (d) Passivation (PL improvement) with multi-interfacial-layers optimisation.

High efficiency, stable single-junction perovskite solar cells

The ANU team successfully demonstrated highly efficient perovskite solar cells with the following cell structure: Glass/FTO/SnO_2/Perovskite/Spiro-OMeTAD/Au. Efficiencies of over 25% have been achieved based on perovskites with a bandgap of 1.53 eV. The corresponding I-V curve is shown in Figure PP2.3.12, and the photovoltaic metrics are detailed in Table PP2.3.3.

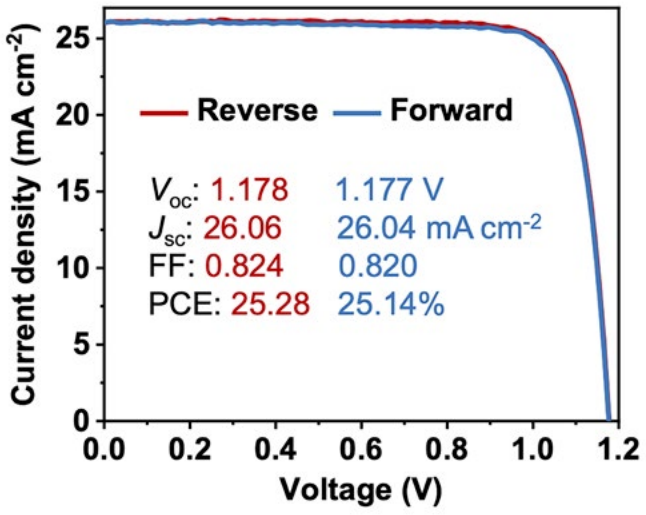

Figure PP2.3.12: J-V curves of the champion n-i-p PSC.

The cells exhibit remarkable stability, retaining 98% of their initial efficiencies even after 11,208 hours of storage in dry air (approximately 5% relative humidity), as illustrated in Figure PP2.3.13. The initial average efficiency stands at 23.25%.

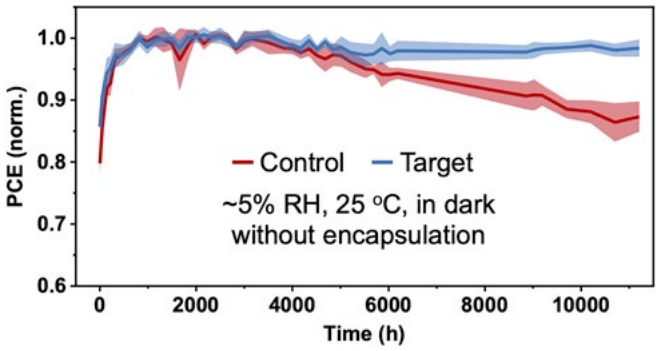

Figure PP2.3.13: Long-term stability of the unencapsulated PSCs (five cells for each condition) stored in dry air (relative humidity of ~5% and ~25°C).

Development of perovskite mini-modules

We successfully demonstrated perovskite mini-modules through laser scribing perovskite substrates. The first step in the development of the mini-module was laser scribing the FTO (fluorine-doped tin oxide) glass substrates for 100 µm cuts. Figure PP2.3.14 shows a 100 µm scribe of FTO on a glass substrate (also known as P1 scribe).

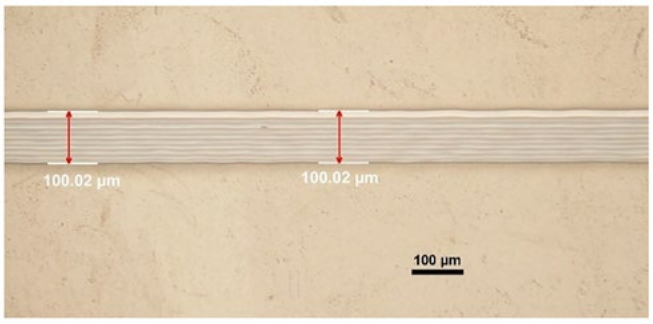

FigurePP 2.3.14: Laser scribing of FTO on glass substrates (P1 step).

After scribing P1, the perovskite mini-module was developed similar to the small-area cell preparation. The mini-module was developed as an n-i-p module and subsequent electron transport, perovskite and hole transport layers were deposited (details in Flourinated Materials section below).

After deposition of the hole transport layer, the mini-module substrate was again laser scribed (100 µm width) to separate out the cells in the module (known as P2 scribe). The P2 scribed substrate had 100 nm of gold deposition as the final step after which a third laser scribe was done to separate out the gold in each cell within the mini-module (known as P3 laser scribing step). The pump fluence used for P2 and P3 steps was 236 mJ cm^{-2}. Figure PP2.3.15 shows the laser scribed P1, P2 and P3 from one of the cells in the mini-module.

The mini-module was able to achieve 14% power conversion efficiency (PCE) with V_{oc} being 5.25 V, a fill factor of 55% and a J_{sc} of 16.1 mA cm^{-2}. Figure PP2.3.16. shows the J-V characteristics of the mini-module.

Compact and mesoporous titania were employed as the electron transport layer in the n-i-p structure. The perovskite absorber consisted of a dual cation composition (caesium and formamidinium). Spiro-OMeTAD was used as an evaporated hole transport layer. Gold was used as the top electrode.

Table PP2.3.3: Performance data of the champion n-i-p PSC.

Device Geometry/ Annealing	J_{sc} (mAcm^{-2})	V_{oc} (V)	FF (%)	PCE (%)
n-i-p -150°C (Reverse scan)	26.06	1.178	82.3	25.28
n-i-p-150°C (Forward scan)	26.04	1.177	82.0	25.14

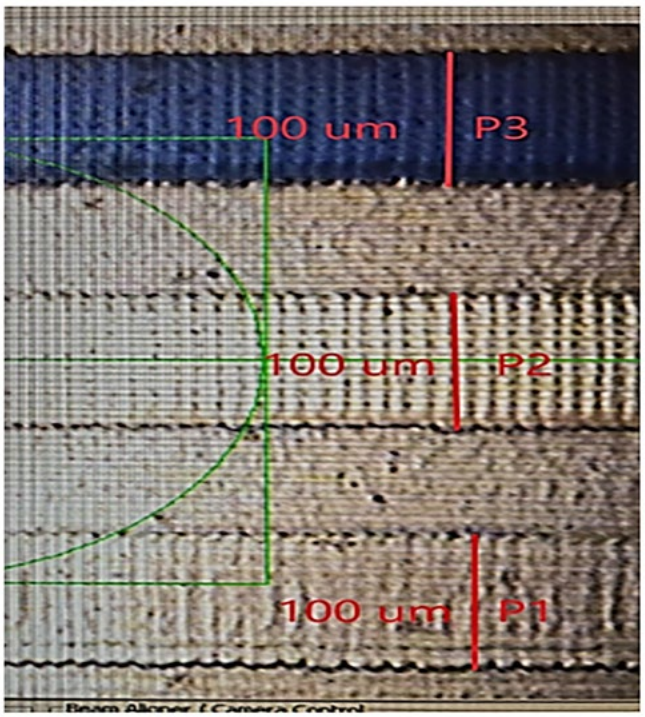

Figure 2.3.15: Laser scribing of P1, P2 and P3 on a mini-module

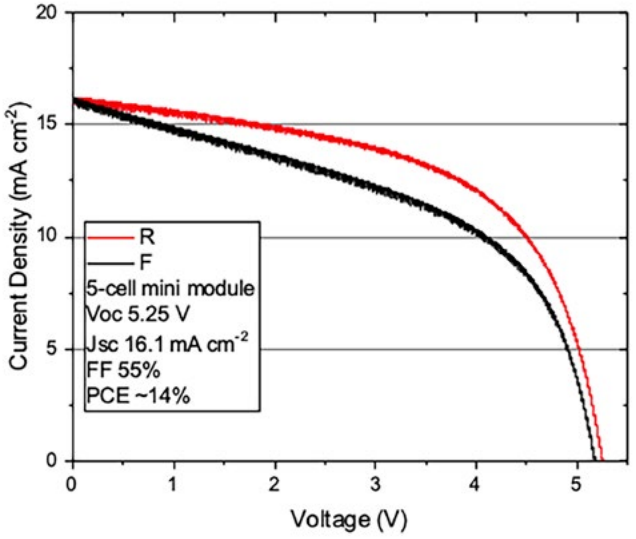

Figure 2.3.16: J-V characteristics of the five-cell mini-module.

Fluorinated materials for PSCs

As the efficiencies of 3D-based perovskite solar cells surpass 26%, there is a growing emphasis on enhancing their long-term stability for widespread manufacturing and deployment. The instability of PSCs has been linked to both intrinsic and external factors, including ion migration, exposure to oxygen and moisture, and thermal stress. Various strategies have been explored to enhance device stability, including the introduction of additives, the implementation of charge-selective layers, and the optimisation of interfaces. Two-dimensional PSCs, specifically quasi-2D Ruddlesden–Popper structures denoted by the general formula $(RNH_3)_2(A)_{n-1}BnX_{3n+1}$, where RNH_3 generally represents bulky ammonium cations and n indicates the number of layers, have demonstrated enhanced stability compared to their 3D counterparts. However, pure 2D perovskite layers can impede charge transport, resulting in poor device performance compared to 3D systems. The incorporation of fluorinated spacer cations is of particular interest due to their hydrophobic characteristics.

In previous work we have shown that the length of the alkyl linker between the 2,3,4,5,6-pentafluorophenyl head and ammonium tail can have a strong effect on the device performance. In the study it was found that small amounts of the additive with a methylene unit between the fluorinated head and ammonium salt gave methylammonium lead triiodide (MAPI) inverted PSCs with enhanced performance. However, larger additive amounts decreased the efficiency.

To elucidate the reason behind the change in performance we carried out time-resolved studies to understand the impact of the additive on the charge carrier dynamics. Using steady-state photoluminescence (PL) measurements at different temperatures we found that small amounts of additive (0.32 and 1.0 mol%) impeded the phase transition process that occurs in MAPI, which was indicative that the additive was located in the bulk of the film. Importantly, the exciton binding energy was found not to change significantly, suggesting that exciton formation and dissociation processes are not affected.

To gather further information about the effect of the additive on the photophysical properties of the MAPI films, transient absorption and reflectivity measurements were performed to determine the lifetime of the charge carrier recombination processes. For the transient absorption measurement where the transmitted laser pulse probes the entire film, the lifetime of the charge decay process was similar for the neat films as well as for the films with additives indicating that the charge recombination process occurs at a similar timescale in the bulk of the film. In contrast, for transient reflectivity measurement, which only probes the surface of the films, the films with the additive showed a slower decay process when the additives were present. The results indicated that the additive was concentrated at the surface, with the longer-lived excited state leading to the situation where more charge carriers are available and hence the enhanced device performance.

Building upon these insights and considering that the most effective devices composed of 3D perovskite films typically contain a mix of halide anions, we introduced a fluorinated organic cation salt additive, specifically $FEABr:Cl_{50:50}$ (50:50 combination of bromide and chloride counter anions) deposited onto the surface of MAPI to form a 3D/2D perovskite film. The selection of these two anions is based on the observation that ammonium bromide salts, when integrated into the perovskite film, can enhance device photovoltage, while chloride salts contribute to increased grain size through slower nucleation.

Furthermore, based on our work showing that treating metal oxide charge extraction layers with additives can enhance hole extraction in inverted PSCs, we also investigated treating the tin(IV) oxide electron transporting layer with the $FEABr:Cl_{50:50}$ additive to modify its properties. The dual utilisation of this novel fluorinated additive resulted in perovskite films with larger average grain size, extended carrier lifetime, and more efficient charge collection relative to the control films. Optimised n-i-p devices, with a 0.2 cm^2 aperture, exhibited a remarkable power conversion efficiency (PCE) exceeding 23% with negligible hysteresis. Unencapsulated devices also demonstrated enhanced operational

stability at the maximum power point (MPP) under continuous light illumination at 80 ± 5°C in humid conditions.

Finally, in preparation for scaling devices with additive we have developed a blading coating system with a fully adjustable air knife that is suitable for use in a glovebox environment.

Mixed-A-cation perovskites from lead acetate precursors

Lead acetate ($PbAc_2$) was shown in 2015 to produce methylammonium lead perovskites with increased performance and easier fabrication. Despite this early success, the $PbAc_2$ route was never applied to produce the mixed-A-cation perovskites, which have dominated the perovskite field since 2014. Our team identified the side reactions which impeded the synthesis of mixed-A-cation perovskites from $PbAc_2$ and proposed a new synthesis route, using ammonium salts as halide salts, resulting in more efficient, easier to manufacture and more stable perovskite solar cells compared to the traditional PbI_2-route (Figure PP2.3.17).

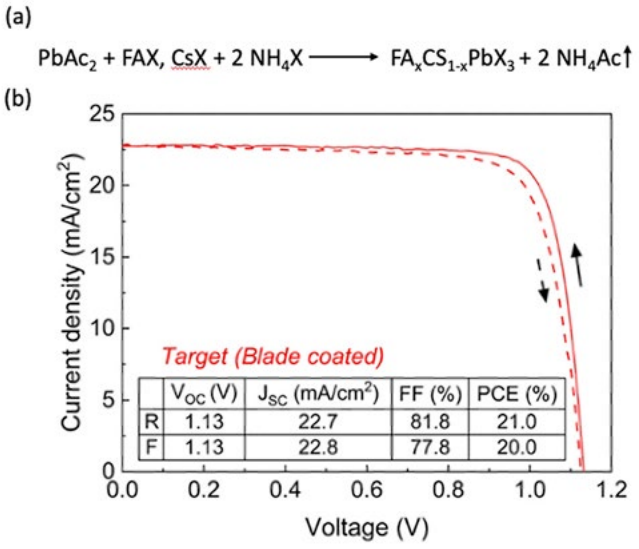

Figure PP2.3.17: Lead halide perovskite from lead acetate precursors. (a) Reaction equation for the synthesis of formamidinium caesium perovskite from lead acetate. (b) Current density-voltage characteristic of a $FA_{0.83}Cs_{0.17}Pb(I_{0.9}Br_{0.1})3$ solar cell fabricated from lead acetate precursor.

Back-contact perovskite solar cells (bcPSCs)

Despite multiple technical advantages over conventional sandwich configurations, bcPSCs still lag behind record-performing sandwich architectures. Recently our team was able to further narrow the performance gap between these two architectures through the introduction of guanidinium thiocyanide into the perovskite precursor solution (Figure PP2.3.18). This resulted in a perovskite growth with preferred out-of-plane crystal orientation, increased charge carrier mobility and lifetimes, increasing the energy conversion efficiency to 11.2%.

Intermediate phase engineering

Our team has used dimethylammonium chloride as an additive to promote and control the formation of perovskite intermediate precursor phases in the absence of the complexing solvent DMSO (Figure PP2.3.19). This enabled us to tune the grain size, texturing, crystal orientation and crystallinity of the resulting formamidinium caesium perovskite film. More importantly it resulted in an improved stability, with a median T80 lifetime of 1190 hours under simulated sunlight at 65°C in air, under open-circuit conditions.

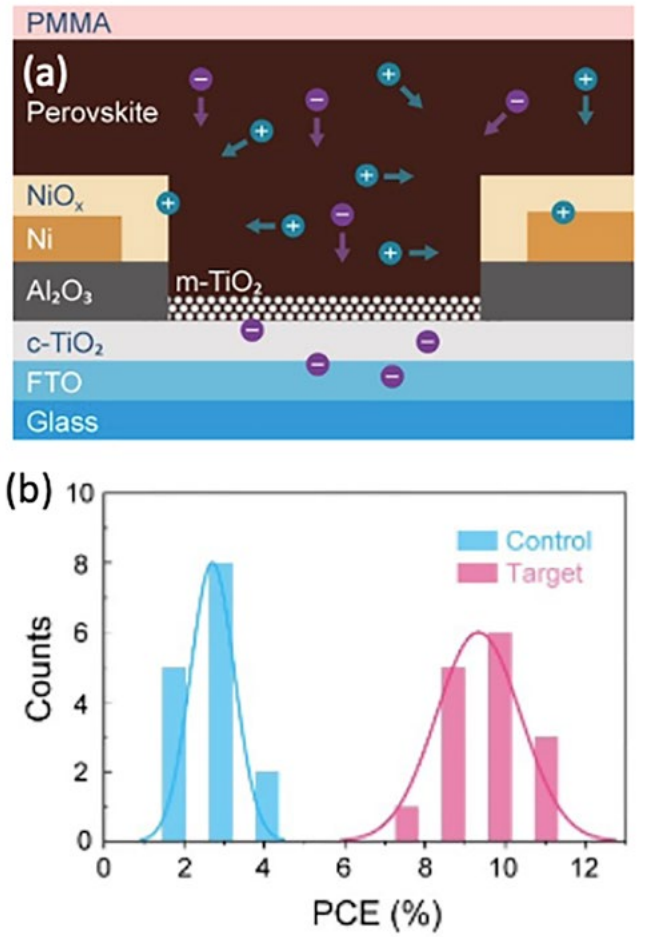

Figure PP2.3.18: Back-contact perovskite solar cells. (a) Cross-sectional diagram of a back-contact perovskite solar cell. (b) Statistics of device power conversion efficiency (PCE) under simulated sunlight (AM1.5, 1000 Wcm^{-2}). $MAPbI_3$ with 0 (control) and 0.125 (target) mole fraction addition of guanidinium thiocyanate.

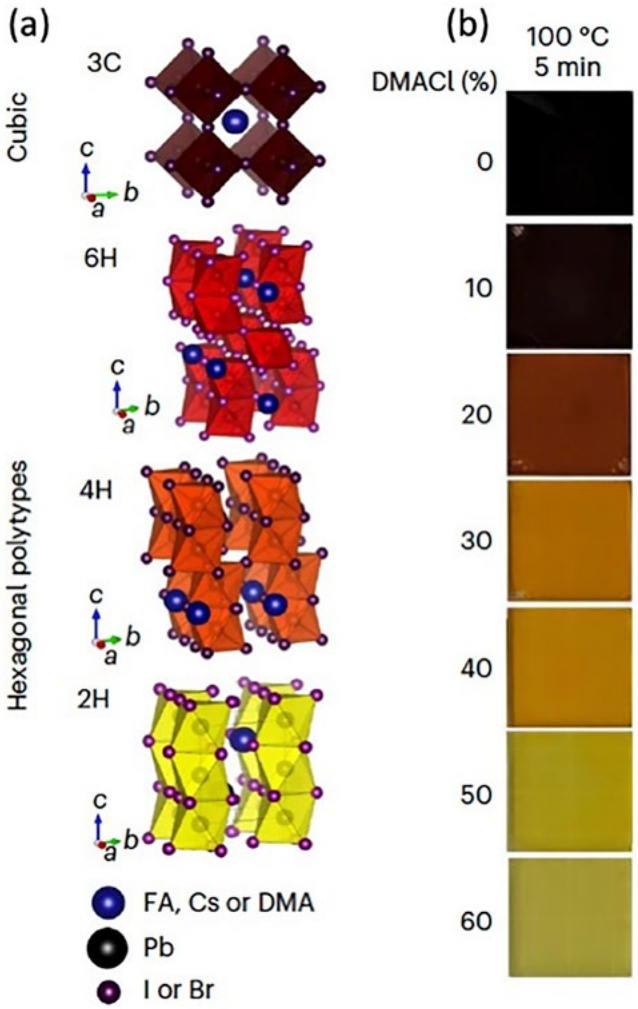

Figure PP2.3.19: Impact of dimethylammonium chloride addition to the precursor solution on the formation of intermediate phases of $FA_{0.83}Cs_{0.17}Pb(Br_{0.2}I_{0.8})_3$. (a) Unit cells of the hexagonal lead halide perovskite and respective intermediate phases. (b) Photographs of perovskite films spin-coated with various amounts of dimethylammonium chloride after five minutes annealing at 100°C. Percentages of additives are expressed in respect to lead.

Inorganic 2D perovskites

Metal halide perovskite materials demonstrate immense potential for photovoltaic and electronic applications. While tremendous progress has been made on three-dimensional (3D) perovskites, layered perovskites either in 2D (Figure 2.3.20) or quasi-2D form have additional advantages such as outstanding stability, structural flexibility while retaining tunable bandgap, and electronic confinement effect.

Research at the University of Sydney has involved the development of a Ruddlesden–Popper (RP) phase, Dion–Jacobson (DJ) phase, the alternating cations in the interlayer space (ACI) phase perovskites in the form of single crystals or thin films for the demonstrations of photodetectors (Liao 2022), field effect transistors and solar cells. More details for the latter will be included in 2024's report. For the work on 2D Ruddlesden–Popper (RP) lead halide perovskites, while most reports have described layered perovskites separated by A-site-substituted organic spacers, with the general formula of $A_{n+1}B_nX3_{n+1}$ (n = 1, 2, …), we reported an X-site-substituted RP. In particular, the first inorganic-cation pseudohalide 2D phase perovskite single crystal at the time of reporting. The $Cs_2Pb(SCN)_2Br_2$ single crystal was synthesised by the antisolvent vapour-assisted crystallisation (AVC) method at room temperature (Figure PP2.3.20 and Figure PP2.3.21). It exhibits a standard single-layer (n = 1) Ruddlesden–Popper structure described in the space group of Pmmn (#59) and has a small separation (d = 1.69 Å) between the perovskite layers. The SCN^- anions are found to bend the 2D $Pb(SCN)_2Br_2$ framework slightly into a kite-shaped octahedron, limiting the formation of a quasi-2D perovskite structure (n > 1). This 2D single crystal exhibits a reversible first-order phase transformation to 3D $CsPbBr_3$ (Pm3m #221) at 450 K. At the time of reporting, it has the lowest exciton binding energy for 2D perovskites (n = 1). Also importantly, the $Cs_2Pb(SCN)_2Br_2$ single crystal is moisture and room temperature stable. Key to this stability is the amount of $Pb(SCN)_2$ precursor used in the synthesis, which needs to be four times higher than the estimated stoichiometry to successfully suppress the formation of 3D $CsPbBr_3$ at room temperature. A $Cs_2Pb(SCN)_2Br_2$ single-crystal photodetector was demonstrated with respectable responsivity of 8.46 mA/W and detectivity of $\approx 1.2 \times 10^{10}$ Jones at a low bias voltage of 0.5 V.

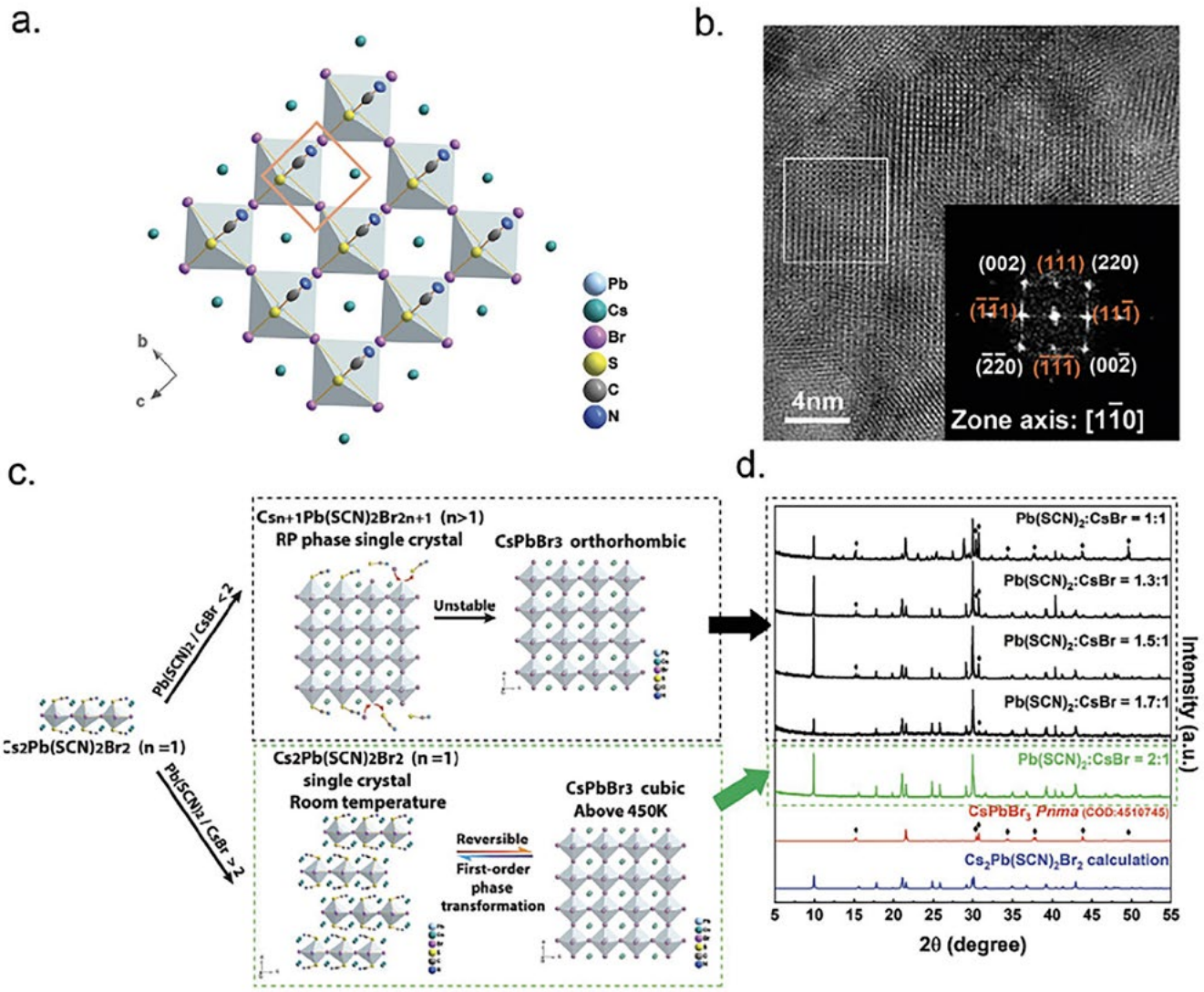

Figure PP2.3.20: $Cs_2Pb(SCN)_2Br_2$ crystal structure and synthetic route. (a) Crystal along the [100] direction generated by single-crystal XRD. The orange square outline shows the $Cs_2Pb(SCN)_2Br_2$ unit cell. (b) HRTEM image and inset: FFT electron diffraction image of $Cs_2Pb(SCN)_2Br_2$ single crystal along the [1,1,0] zone axis. (c) Illustrations of the effect of different $Pb(SCN)_2$/CsBr ratios on the resultant $Cs_2Pb(SCN)_2Br_2$ structure, the single-layered RP phase crystal pile-up strategy, and reversible phase transformation from $Cs_2Pb(SCN)_2Br_2$ orthorhombic phase to $CsPbBr_3$ orthorhombic phase. (d) Powder XRD pattern of different stoichiometric ratios of $Pb(SCN)_2$ and CsBr, $CsPbBr_3$ Pnma space group (COD# 4510745), and $Cs_2Pb(SCN)_2Br_2$ calculation data from the single-crystal XRD measurement. Figures from (Liao 2022).

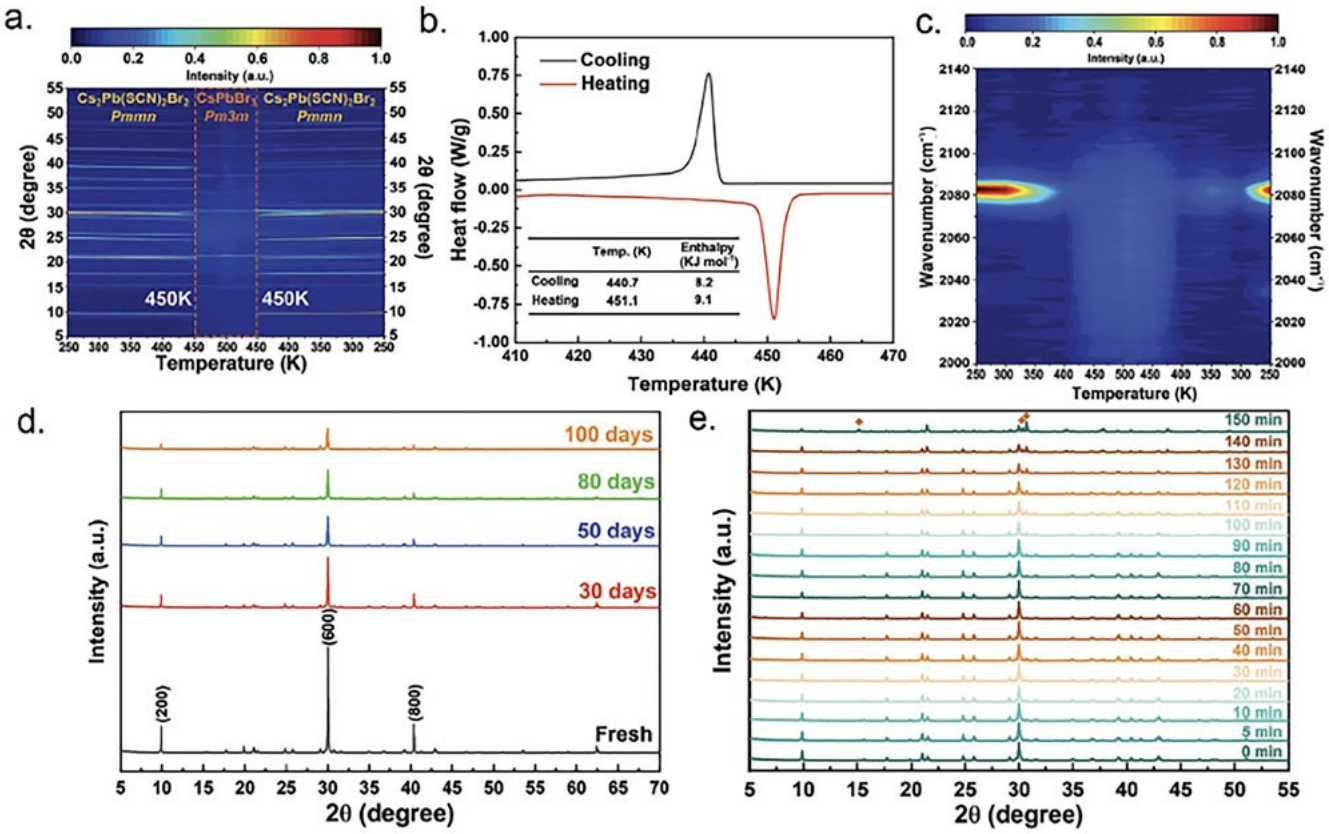

Figure 2.3.21: Phase transformation, ambient and water stability of $Cs_2Pb(SCN)_2Br_2$ single crystal. (a) Pseudocolour map of temp–pXRD between 250 and 500 K. (b) DSC thermograms of $Cs_2Pb(SCN)_2Br_2$ single crystal cycled between 410 and 470 K showing a reversible phase transformation. (c) Pseudocolour map of temp–Raman spectra between 250 and 500 K. (d) Powder XRD pattern of $Cs_2Pb(SCN)_2Br_2$ showing stability after 100 days of ambient storage (T ≈ 25°C and RH ≈ 70%). (e) Powder XRD of samples from single-crystal water sprayed every 10 minutes for 150 minutes in total. The $CsPbBr_3$ orthorhombic pXRD peaks are marked in the 150-minute pXRD pattern. Figures from (Liao 2022).

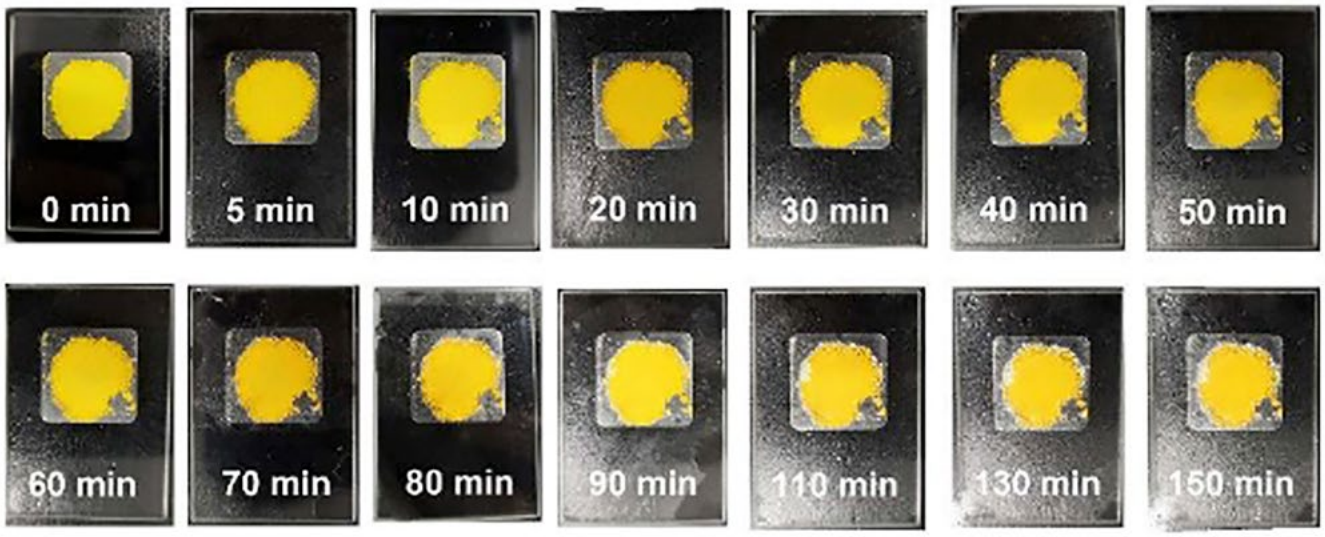

Figure 2.3.22: Photos of a $Cs_2Pb(SCN)_2Br_2$ single crystal under water stability testing by spraying every 10 minutes. The $Cs_2Pb(SCN)_2Br_2$ single crystal remains stable for up to 150 minutes (Liao 2022).

Highlights

- A novel double-sided surface passivation layer using DABCO and DAN, has been explored for the fabrication of an efficient perovskite solar cell. High performance perovskite solar cell was demonstrated with a PCE of 21.9%..
- Perovskite mini-module was able to recover 91% of its MPP current after shading of one cell for 30 minutes.
- Inverted perovskite solar cells reached 23.9% efficiency.
- Revealed mechanism of thermally activated reverse halide segregation.
- 25.28% efficiency with low bandgap perovskite (1.53 eV) was achieved in n-i-p single-junction perovskite solar cells.
- 98% of the initial efficiencies was retained after more than 10,000 hours of storage in dry air (~5% relative humidity and ~25°C). The cells had a starting efficiency of 23.25% and were not encapsulated.
- 85.5% of the initial efficiency was maintained after 1000 hours of operation under one-sun illumination without encapsulation.
- Reported the first inorganic-cation pseudohalide 2D phase perovskite single crystal. The single crystal can be synthesised at room temperature, has the lowest exciton binding energy for 2D perovskites and has been shown to be moisture stable, withstanding water sprays unprotected for 150 minutes.

Future Work

- Efficient and stable perovskite solar cells using bi-functional passivation materials for interface and bulk passivation.
- Explore the mechanism of surface passivation and degradation studies using the surface characterisation technique.
- Lead-free perovskite solar cells with various antioxidant additives and passivation layers.Target stable perovskite solar cells with 25% efficiency under heat-light stress.
- Target over 1 cm^2 inverted perovskite solar cells with efficiency beyond 23%, MPP stability over 1000 hours.
- Develop more efficient and stable hole transport materials to replace spiro-OMeTAD to further enhance the cell performance and stability.
- Development of larger area multi-cell mini-modules.
- Investigate the effect of other fluorinated additives on the optoelectronic and device properties of different perovskite materials.
- Investigate the effect of varying the anion on the optoelectronic and device properties of different perovskite materials.
- Explore the scalability of the additive containing perovskite films.
- Development of Dion–Jacobson (DJ) phase perovskites and alternating cations in the interlayer space (ACI) phase perovskites demonstrating improved stability for electronic and solar cell applications.

References

Bati, A. S. R. , Zhong, Y. L., Burn, P. L., Nazeeruddin, M. K., Shaw, P. E. &, Batmunkh, M. (2023). Next generation applications for integrated perovskite solar cells., Communications Materials. 2023. 4, 2.

Bati, A. S. R., Jiang, W., Chu, R., Mallo, N., Burn, P. L., Gentle, I. R., and & Shaw, P. E. (2023). Fluorinated Cation-based 2D Perovskites for Efficient and Stable 3D/2D Heterojunction Perovskite Solar Cells. ACS Applied Materials & Interfaces. 10.1021/acsami.3c13609.

Bati, A. S. R., Myagmarsereejid, P., Fronzi, M., Fan, K., Liu, P., Zhong, Y. L., Burn, P. L., Gentle, I.R., Shaw, P.E. and & Batmunkh, M. (2023). Atomically Doped 2D Black Phosphorus for Efficient and Stable Perovskite Solar Cells. Small Structure. 2300334.

Liao, C.-H., Chen, C.-H., Bing, J., Bailey, C., Lin, Y.-T., Pandit, T. M., Granados, L., Zheng, J., Tang, S., Lin, B.-H., Yen, B.-H., McCamey, D. R., Kennedy, D. R., Chueh, D. R., & Ho-Baillie, A. W. Y. (2022). Inorganic-Cation Pseudohalide 2D Cs2Pb(SCN)2Br2 Perovskite Single Crystal. Advanced Materials. 34, 2270054.

Liao, C.-H., Mahmud, M. A., & Ho-Baillie A. W. Y. (2023). Recent progress in layered metal halide perovskites for solar cells, photodetectors, and field-effect transistors. Nanoscale, 15, 4219- – 4235.

McMeekin, D., et al. (2023). Intermediate-phase engineering via dimethylammonium cation additive for stable perovskite solar cells. Nature Materials, 22, 73-83.

Mussakhanuly, N. (2023). Thermal Disorder-Induced Strain and Carrier Localisation Activate Reverse Halide Segregation., Advanced Materials, Accepted.

Peng., J., et al. (2002). Centimetre-scale perovskite solar cells with fill factors of more than 86 per cent. Nature, 601, 573.

Sun, X., et al. (2023). The effect of pyrrolidone-based ligands in gas-quenching fabrication of FA0.9Cs0.1PbI3 perovskite films and solar cells., J. Alloys Compd. 960, 170670.

Vijaya, S., Subbiah, J., Jones, D. J &, Sambandam, A. (2023). LARP-assisted synthesis of CsBi3I10 perovskite for efficient lead-free solar cells. RSC Advances 13, 9978-9982.

Zhang, Y., et al. (2023). Barrier Strategy for Strain-Free Encapsulation of Perovskite Solar Cells., J. Phys. Chem. Lett., 14 (48), 10754-10761.

Zhao, B., et al. (2023). Enhanced Carrier Diffusion Enables Efficient Back-Contact Perovskite Photovoltaics. Angew. Chem. Int. Ed. 62, e202218174.

Zhao, K., et al. (2023). Efficient and stable formamidinium–caesium perovskite solar cells and modules from lead acetate-based precursors. Energy Environ. Sci. 16, 138-–147.

Zhao, P., Subbiah, J., Zhang, B., Hutchison, J., Ahluwalia, G., Mitchell, V. D., Ghiggino, K. P. &, Jones, D. J. (2023). Advanced Materials Interfaces. 202313.

PP2.4 METAL CHALCOGENIDES

Lead Partner
UNSW

UNSW Team
Prof. Xiaojing Hao, Scientia Prof. Martin Green, Prof. Nicholas (Ned) Ekins-Daukes, Dr Jialiang Huang, Dr Kaiwen Sun, Dr Jianjun Li, Dr Xin Cui, Dr Mingrui He

UNSW Students
Heng Sun, Xiaojie Yuan, Ao Wang, Guojun He, Jialin Cong, Chen Qian

Industry Partner
Baosteel

Other Partners
Catalonia Institute for Energy Research (IREC), LONGi Solar, IBM, Nanyang Technological University (), National Renewable Energy Laboratories (NREL), Corning Research & Development Corp., University of Sydney, Tsinghua University, Chonnam National University, East China Normal University

Funding Support
ARENA, ACAP, ARC, Baosteel

Aims

All successfully commercialised non-concentrating photovoltaic technologies to date are based on silicon or chalcogenides (semiconductors containing Group VI elements, specifically Te, Se and S). The successful chalcogenide semiconductor materials, CdTe and Cu(In,Ga)Se_2 (CIGS), can be regarded as "synthetic silicon" where the balance between atoms in these materials is providing the same average number of valence band electrons as in silicon, resulting in the same tetrahedral coordination (Figure PP2.4.1) (Walsh et al. 2012).

Cd is toxic while Te and In are among the 12 most scarce elements in Earth's crust. These factors can be expected to limit the long-term potential of the established chalcogenide technologies based on CdTe and CIGS. The work at ACAP looks at alternatives based on elements in the Periodic Table with similar properties but involving only Earth-abundant, non-toxic elements.

A kesterite Cu_2ZnSnS_4 (CZTS) compound semiconductor has emerged, as a promising candidate for thin-film solar cells. Analogous to the chalcopyrite structure of CIGS, CZTS shares similar optical and electrical properties. CZTS has a bandgap of around 1.5 eV, and a large absorption coefficient of over 10^4 cm^{-1}. Notable is that the bandgap of the CZTS family can be tuned to span from 1.5eV to beyond 2.25 eV, above that of the highest efficiency III-V cells. This makes the material suitable for tandem cells. For thin-film solar cells, energy conversion efficiencies up to 14.9% and 11.4% have been achieved so far for CZTSSe and CZTS solar cells by Chinese Academy of Sciences (CAS) and UNSW, respectively (Green et al. 2023).

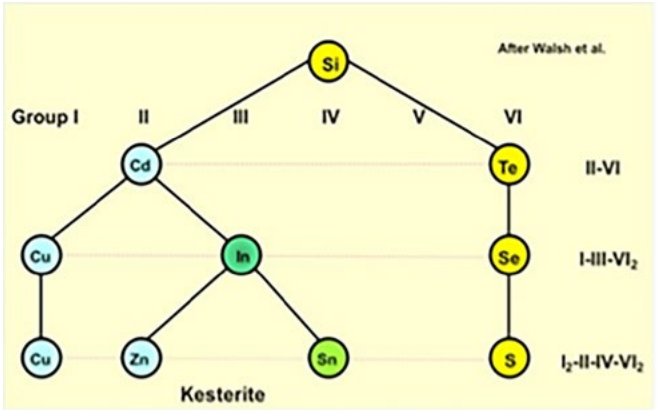

Figure PP2.4.1: The schematic of "Synthetic Si" showing how the CZTS is derived.

ACAP's work in the CZTS area takes the sputtering fabrication direction, a low-cost, high-throughput and up-scalable manufacturing process which has been used in the commercialised high performance CIGS solar cells. In this regard, CZTS offers realistic potential to achieve the efficiency levels required for transferring lab-scale processes to commercialisation in the short term as being fully compatible with current CIGS production lines. Using kesterite materials less than two microns thick, cells can be light and flexible if grown on a flexible substrate, which has wide applications in areas such as building integrated photovoltaics (BIPV), transport vehicles, unmanned aerial vehicles (UAVs), and Internet of Things (IoT), harvesting light and reducing greenhouse gas emissions. Work in this strand includes the development of high efficiency CZTS solar cells on soda–lime glass and flexible stainless steel.

Progress

Ge incorporation for phase evolution intervention

An effective Ge incorporation strategy is introduced to minimise defects and control phase evolution during CZTS crystallisation (Wang et al. 2023b). We find the critical time point requiring external intervention during sulfurisation is when the kesterite grains are about to form. A thin Ge layer on top of the well-mixed precursor is shown to effectively suppress the initial formation of kesterite phases, thereby limiting excessive nucleation centres (Figure PP2.4.2). Fewer grain seeds and the potential interaction of Ge and Na facilitate grain merging, thus resulting in less grain boundaries (Figure PP2.4.3). At the same time, the incorporation of Ge leads to the forming of CZTS grains at higher temperatures, which in turn enhances interior grain quality and reduces defect density (Figure PP2.4.4). A small amount of Ge remaining in the final CZTS film may further reduce the defect concentration. As a result, the defect-induced non-radiative recombination is inhibited, enabling the band-to-band transition to dominate (Figure PP2.4.5). Relieving the recombination path results in over 800 mV V_{OC} and a record V_{OC}/V_{OC}^{SQ} of 63.2%, contributing to 10.7% efficiency champion Cd-free CZTS solar cells (Figure PP2.4.6).

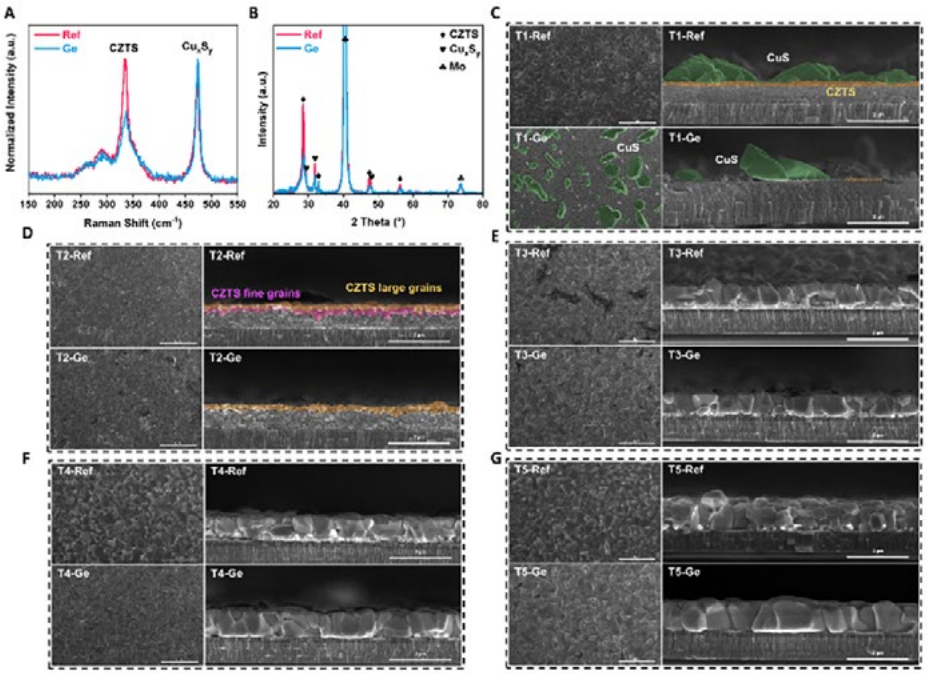

Figure PP2.4.2: (a) Normalised Raman spectra and (b) XRD patterns of Ref and Ge samples at T1. (c–g) Cross-section and plane-view SEM images of Ref and Ge samples from T1 to T5. At T1, the CuS phase and CZTS grains are colour-coded as transparent green and orange, respectively. Later in T2, the CZTS large grains on the surface of the film are coloured with the same transparent orange colour, while the underlying CZTS small grains that appeared in the Ref sample are coloured pink.

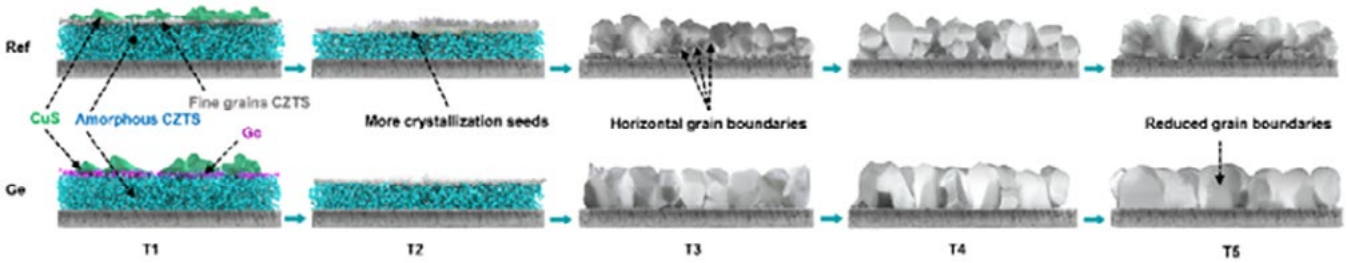

Figure PP2.4.3: Schematic illustration of how Ge affects kesterite phase evolution and morphology during sulfurisation annealing.

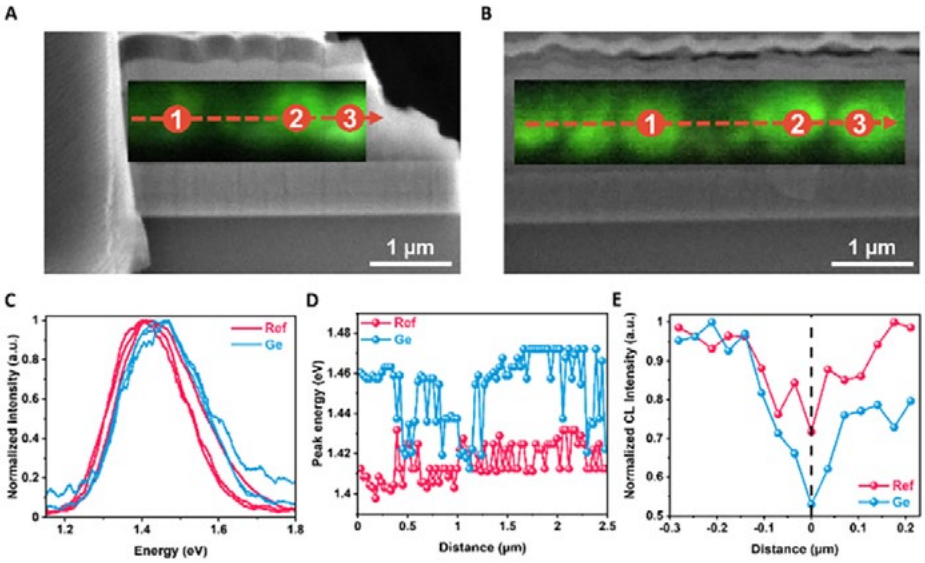

Figure PP2.4.4: CL mapping of (a) Ref and (b) Ge devices with three grains of interest are marked. CL lines scan is implemented in the direction indicated by arrows. (c) CL spectra of three marked grains in Ref and Ge. (d) CL peak energy line-scan from grain 1 to 3 for two samples. (e) Normalised CL peak energy line-scan of Ref and Ge films at the grain boundary region between grain 2 and 3.

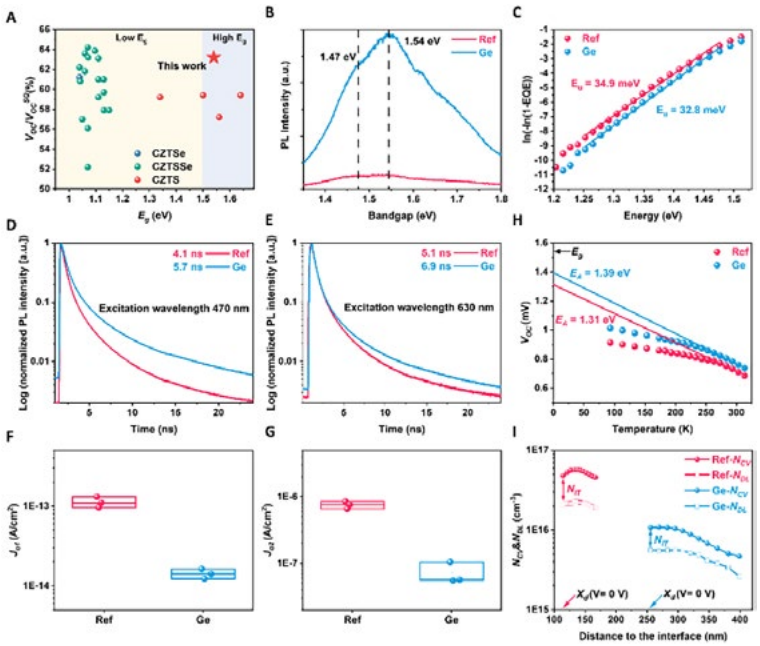

Figure PP2.4.5: (a) V_{OC} deficit determined by V_{OC}/V_{OC}^{SQ} for reported high performance kesterite solar cells. The Ge incorporation device in this work is represented by an asterisk. (b) Room temperature PL spectra of Reference (Ref) and Ge devices. (c) Urbach tail energy EU of Ref and Ge cells derived from EQE. Normalised TRPL curves of Ref and Ge solar cells with a laser excitation wavelength of (d) 470 nm and (e) 630 nm. Fitted recombination current density (f) J_{01} and (g) J_{02} of Ref and Ge solar cells from Suns-V_{OC} measurement. Three representative cells on each sample are presented. (h) Temperature-dependent V_{OC} curves and fitted activation energy EA of Ref and Ge solar cells. The bandgap of 1.54 eV for the Ge cell is indicated. (i) CV and DCLP profiles of Ref and Ge solar cells. The depletion width X_d is obtained from where V = 0, and the interface defect density N_{IT} is calculated from the difference between carrier density results of CV and DLCP at this point.

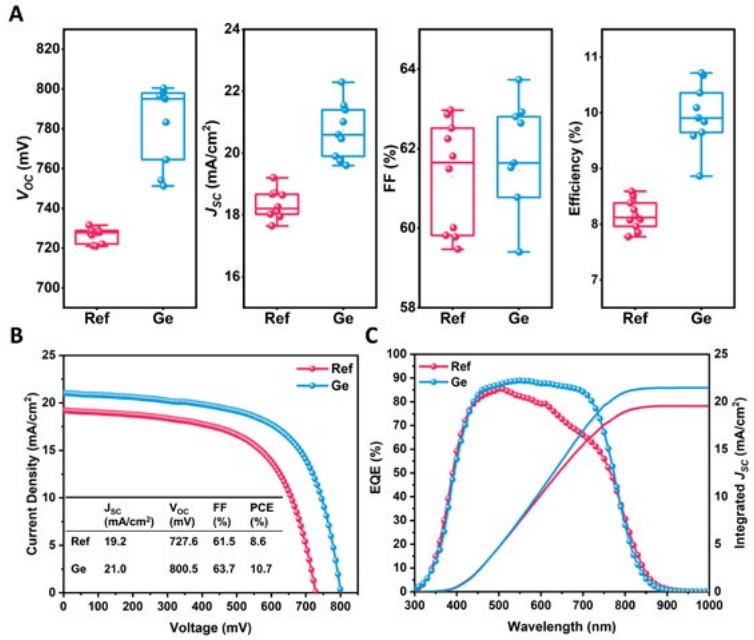

Figure PP2.4.6: (a) Statistic performance distribution of Ref and Ge solar cells on each 2.5 cm × 2.5 cm sample. (b) Current density-voltage (J-V) curves of the most efficient Ref and Ge devices. The photovoltaic parameters of the champion solar cells are indicated. (c) EQE spectra of Ref and Ge cells with integrated J_{SC} curves. The integrated J_{SC} (19.6 and 21.5 mA cm^{-2}) is slightly higher than the value measured from J-V due to the absence of metal grid shading.

Li-enhanced liquid-phase promoted grain growth for highly efficient Cu_2ZnSnS_4 solar cells

Small grain size and near-horizontal grain boundaries are known to be detrimental to the carrier collection efficiency and device performance of pure-sulfide Cu_2ZnSnS_4 (CZTS) solar cells (Li et al. 2022; Yuan et al. 2022). However, forming large grains spanning the absorber layer while maintaining high electronic quality is challenging, particularly for pure sulfide CZTS. Herein, a Li-enhanced liquid-phase-assisted grain growth (LGG) based on our previous LGG process is proposed to further enlarge the grain size of the CZTS absorber (Yuan et al. 2022). By introducing a suitable amount of Li into the previously reported Ge-alloyed CZTS (CZTGS) nanoparticle layer at the bottom of the sputtered precursor, a larger grain size can be obtained when compared to samples with the CZTGS nanoparticle layer (Figure PP2.4.7), thus further increasing bulk minority carrier lifetime and improving the carrier collection efficiency (Figure PP2.4.8). The remaining liquid phase layer at the rear interface in the Li-CZTGS modified sample indicates a similar grain growth procedure to the previous CZTGS modified sample. The introduced Li can induce the formation of a Li-S liquid phase via the remaining Li at above 350oC, facilitating the LGG process for growing larger grains (Figure PP2.4.9). The modified morphology further increases the short-circuit current density, enabling 10.53% efficient green Cd-free CZTS devices (Figure PP2.4.10). This work unveils the mechanism of Li introduction in growing large CZTS grains, advancing the morphology control of sulfide-based kesterite solar cells.

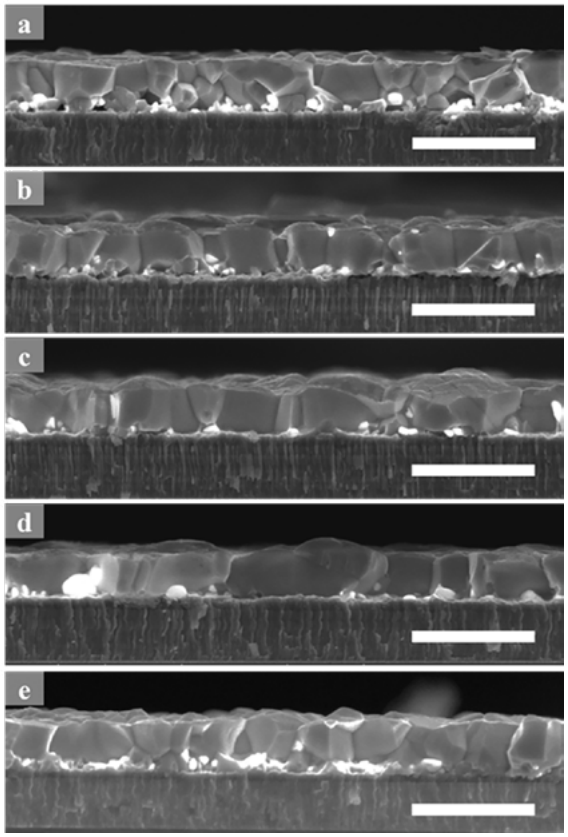

Figure PP2.4.7: Cross-sectional SEM images of (a) the reference CZTS and CZTGS-modified CZTS after sulfurisation annealing with different Li/(Li+Cu) ratio in CZTGS: (b) 0, (c) 0.07, (d) 0.15 and (e) 0.24. The unit of the scale bars is 2 μm.

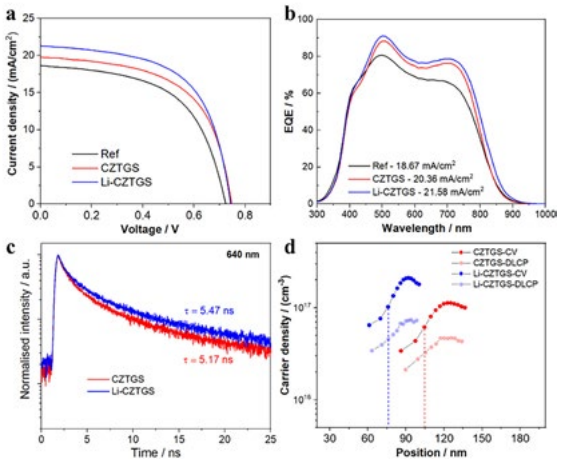

Figure PP2.4.8: (a) Illuminated J-V curves (AM 1.5, total area) and (b) EQE curves of representative reference, CZTGS-modified and Li-CZTGS modified devices. The integrated J_{SC} was calculated from EQE and AM 1.5 spectra. (c) TRPL decay curves of the double exponential function model at excitation wavelengths of 640 nm; and (d) CV-DLCP plots for the CZTGS and Li-CZTGS modified devices.

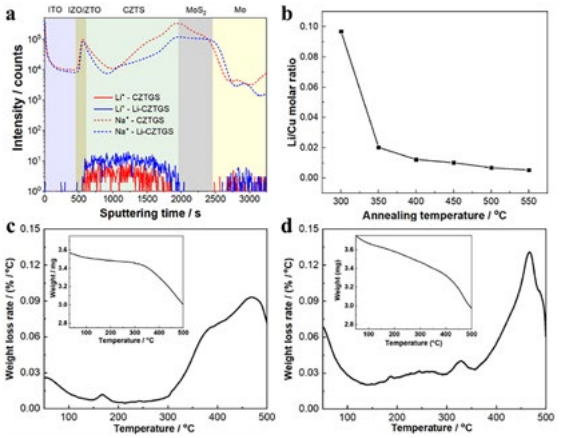

Figure PP2.4.9: (a) TOF-SIMS depth profile of Li and Na in CZTGS and Li-CZTGS devices. The divided layers are dependent on the profiles of other major elements in both devices (b) Li/Cu molar ratio of one-layer Li-CZTGS nanoparticle film at different sulfurisation temperatures (300oC is for the precursor sample before the sulfurisation), DTG and TGA (insets) curves of (c) CZTGS and (d) Li-CZTGS nanoparticle layers.

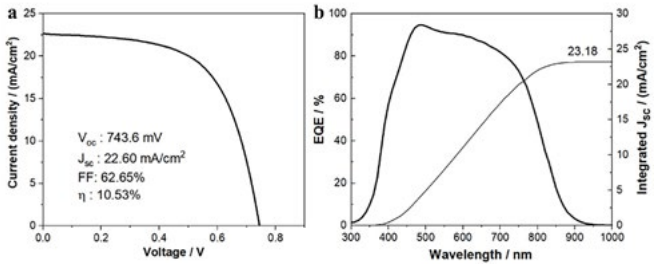

Figure PP2.4.10: Illuminated J-V curves (AM 1.5) and (b) EQE curves of the best Li-CZTGS-modified device with ARC. The integrated J_{SC} was calculated from EQE and AM 1.5 spectrum.

Revealing the role of Ag alloying in metal precursors in $Cu_2ZnSn(S,Se)_4$ thin films and solar cells

The addition of silver (Ag) to the kesterite bulk has led to a significant improvement in the quality of the absorber layer, resulting in the achievement of a certified new record efficiency. In this study, we investigated the mechanisms responsible for the enhancing effect of Ag on kesterite solar cells by combining Ag with the precursor and subsequently subjecting it to selenisation. It was observed that introducing Ag into the precursor expedited the formation of a liquid phase with copper selenide ($Cu_{2-X}Se$) during the initial stages of kesterite thin-film development. As a result, this liquid phase facilitated the growth of grains, leading to an increased grain size, which primarily contributed to the observed improvement in performance. Additionally, a deliberate adjustment of the sulfur (S) distribution to create a gradual change in the bandgap towards the back contact was implemented in the Ag alloyed CZTSSe thin film, which contributed to a higher short-circuit current (J_{sc}) value. Exploring the formation pathway of Ag-alloyed CZTSSe revealed the appearance of a ZnS phase near the back surface during the intermediate stages of kesterite formation. It is plausible that sulfur remained in proximity to the near back surface, influencing the bandgap grading. These findings provide valuable insights into the detailed mechanisms behind the positive influence of silver on kesterite solar cells and suggest a promising approach for enhancing their overall performance.

Plasma-enhanced atomic layer deposition of ZnMgO for efficient CZTS solar cells

We demonstrate the deposition of a ZnMgO window layer of controlled thickness, composition and electro-optical properties by atomic layer deposition (ALD) (Figure PP2.4.12) (Cui et al. 2023). We also employed in situ ellipsometry to monitor the growth behaviour, optical properties and to predict the composition of the ZMO films by a modified rule of mixtures (ROM) model, thereby facilitating the accurate control and tunability of material properties in real time (Figure PP2.4.13). The amorphous ZnMgO deposited at low temperature down to 100°C using plasma-enhanced ALD showed superior smoothness than high temperature plasma-enhanced ALD and comparable doping density with high temperature thermal ALD but a much lower electron affinity (Figure PP2.4.14). The overall charge carrier recombination at the CZTS/ZnSnO/ZnMgO region was reduced due to the optimised ZnMgO conduction band minimum, thus reducing the V_{OC} and fill factor loss for a CZTS solar cell (Figure PP2.4.15). In addition, the thinner and larger bandgap ZnMgO was believed to reduce the parasitic absorption, improving the J_{SC} and boosting the efficiency to 10% (Figure PP2.4.16).

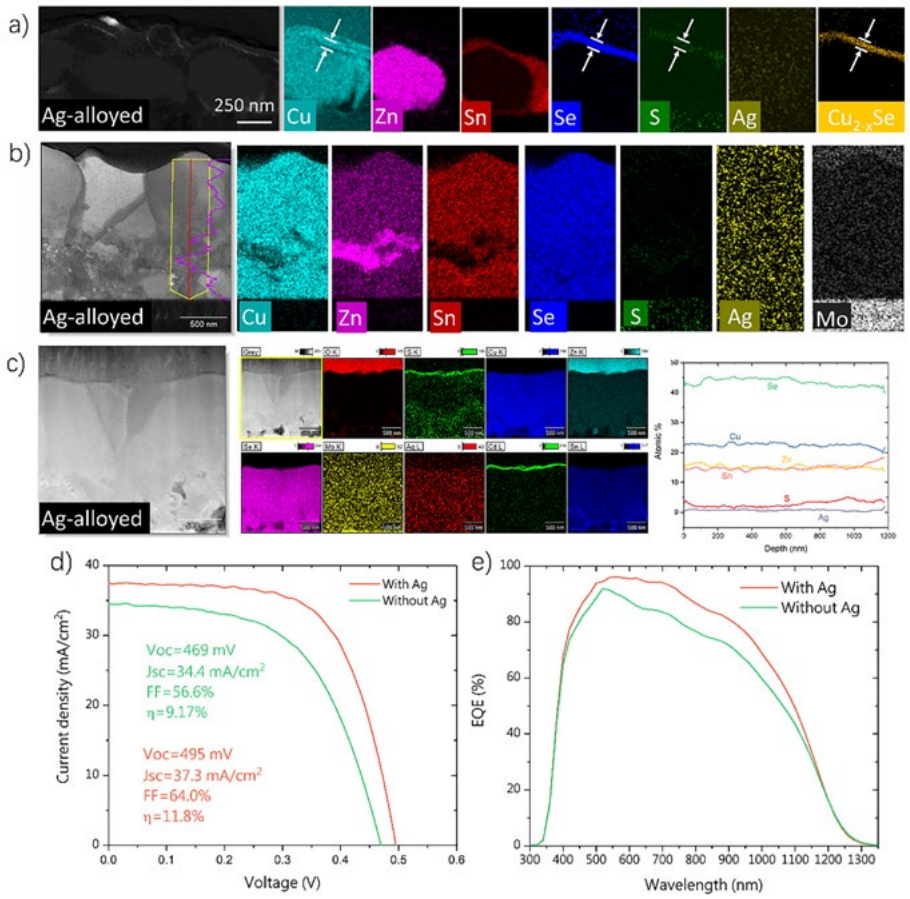

Figure PP2.4.11: Cross-sectional high-angle dark-field transmission electron microscopy (HADDF-TEM) images and corresponding energy-dispersive X-ray spectroscopy (EDS) elemental mapping of: (a) Ag-alloyed CZTSSe thin film just reaching 520°C; (b) Ag-alloyed CZTSSe thin film annealed at 520°C for 1 minute; (c) Ag-alloyed CZTSSe solar cell; (d) current-voltage (I-V) curve; and (e) external quantum efficiency (EQE) of CZTSSe solar cells with and without Ag incorporation.

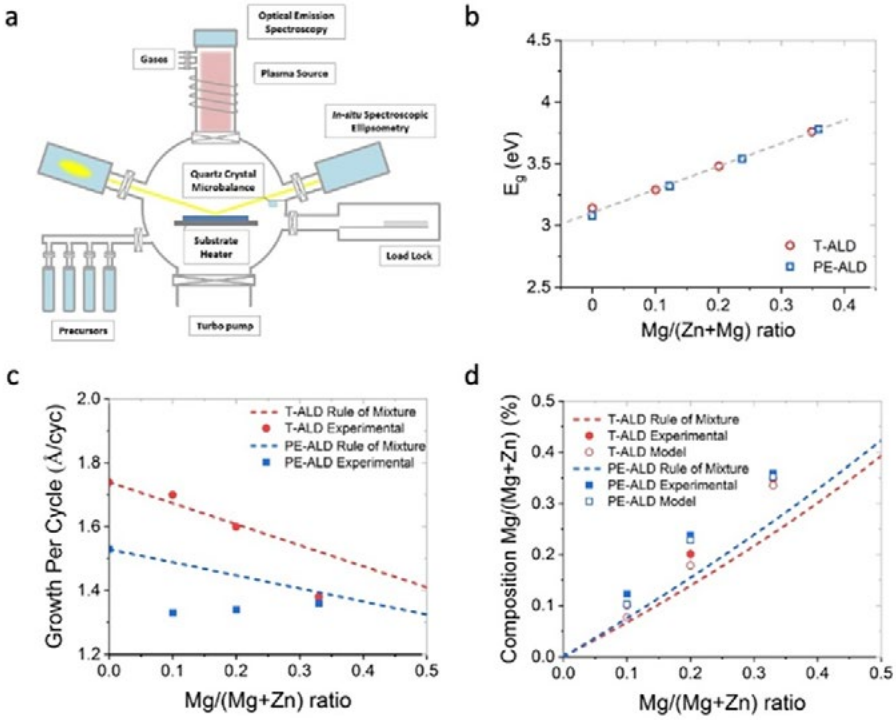

Figure PP2.4.12: (a) Schematic representation of the Fiji G2 ALD system with in situ spectroscopic ellipsometry used for the thermal ALD and PE-ALD deposition in this work. (b)The growth behaviour of ZnMgO film via T-ALD and PE-ALD at 150°C. (c) Variations in growth per cycle (GPC, dot and square) of ZMO films as a function of the ALD sub-cycle ratio compared to the trends calculated from the rule of mixture (dashed line). (d) Experimental composition (dots and squares) determined from ICP-OES of the ZMO films as a function of ALD sub-cycle ratio compared to the trends calculated from the rule of mixture (dashed line) and modified model (open circles and squares).

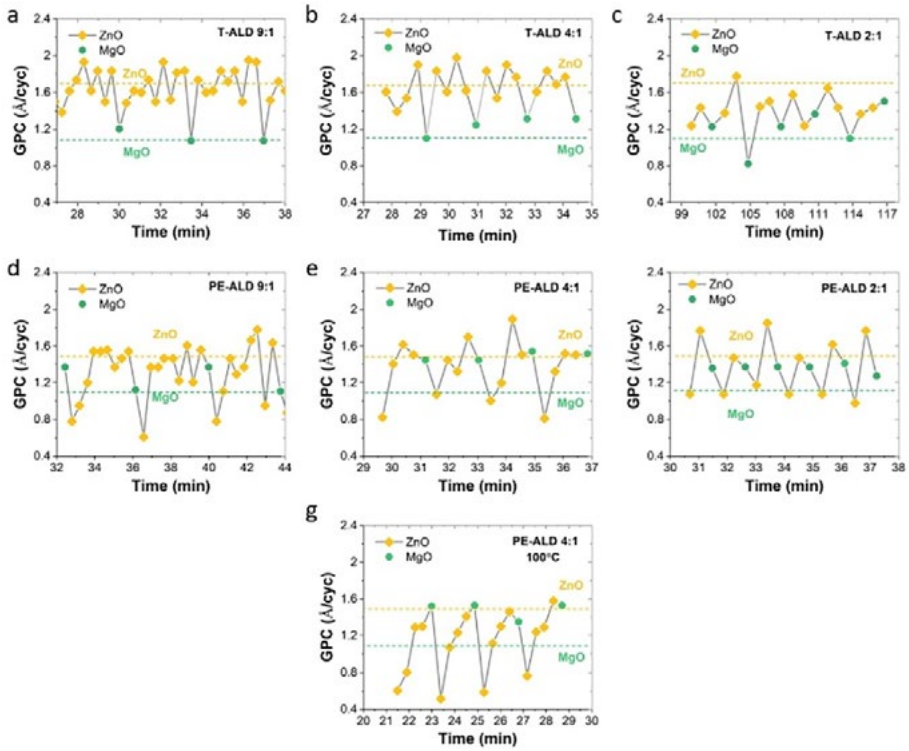

Figure PP2.4.13: GPC of consecutive ZnO and MgO sub-cycles using (a —c) T-ALD and (d–g) PE-ALD as measured by in situ ellipsometry. The dashed lines indicate the GPC for pure ZnO and MgO.

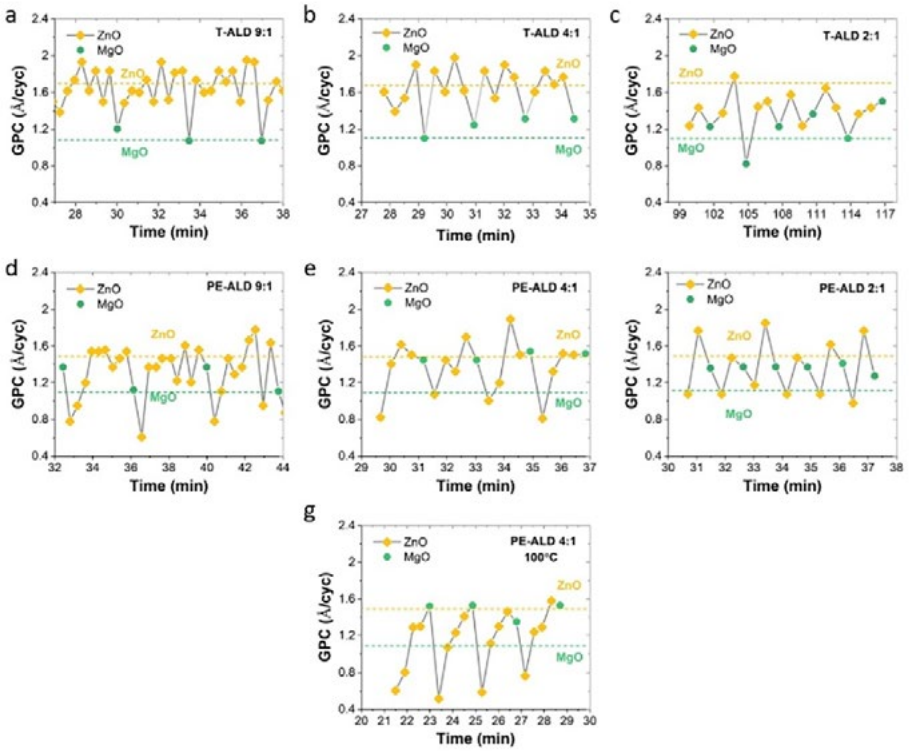

Figure PP2.4.14: Atomic force microscope (AFM) morphology of various ZMO thin films deposited through (a–c) T-ALD at 150°C, (d–f) PE-ALD at 150°C and (g) PE-ALD at 100°C.

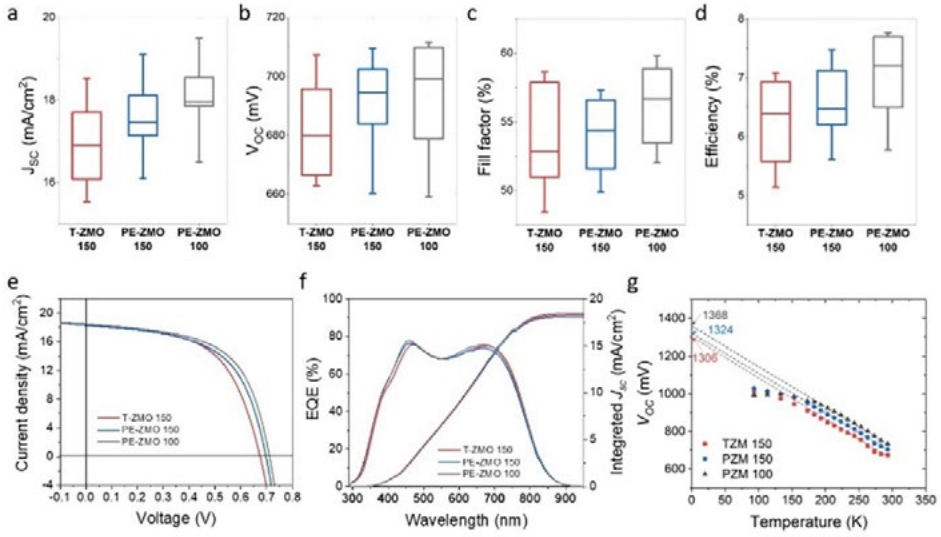

Figure PP2.4.15: (a–d) Box-plots of the photovoltaic parameters of CZTS cells, (e) J-V characteristics, (f) EQE and (g) V_{oc} as a function of temperature (T) for the best CZTS device with ZMO window layer deposited from T-ALD and PE-ALD at different temperatures, the Zn:Mg pulse ratio was kept as 4:1. Ten CZTS solar cells were fabricated per experimental condition.

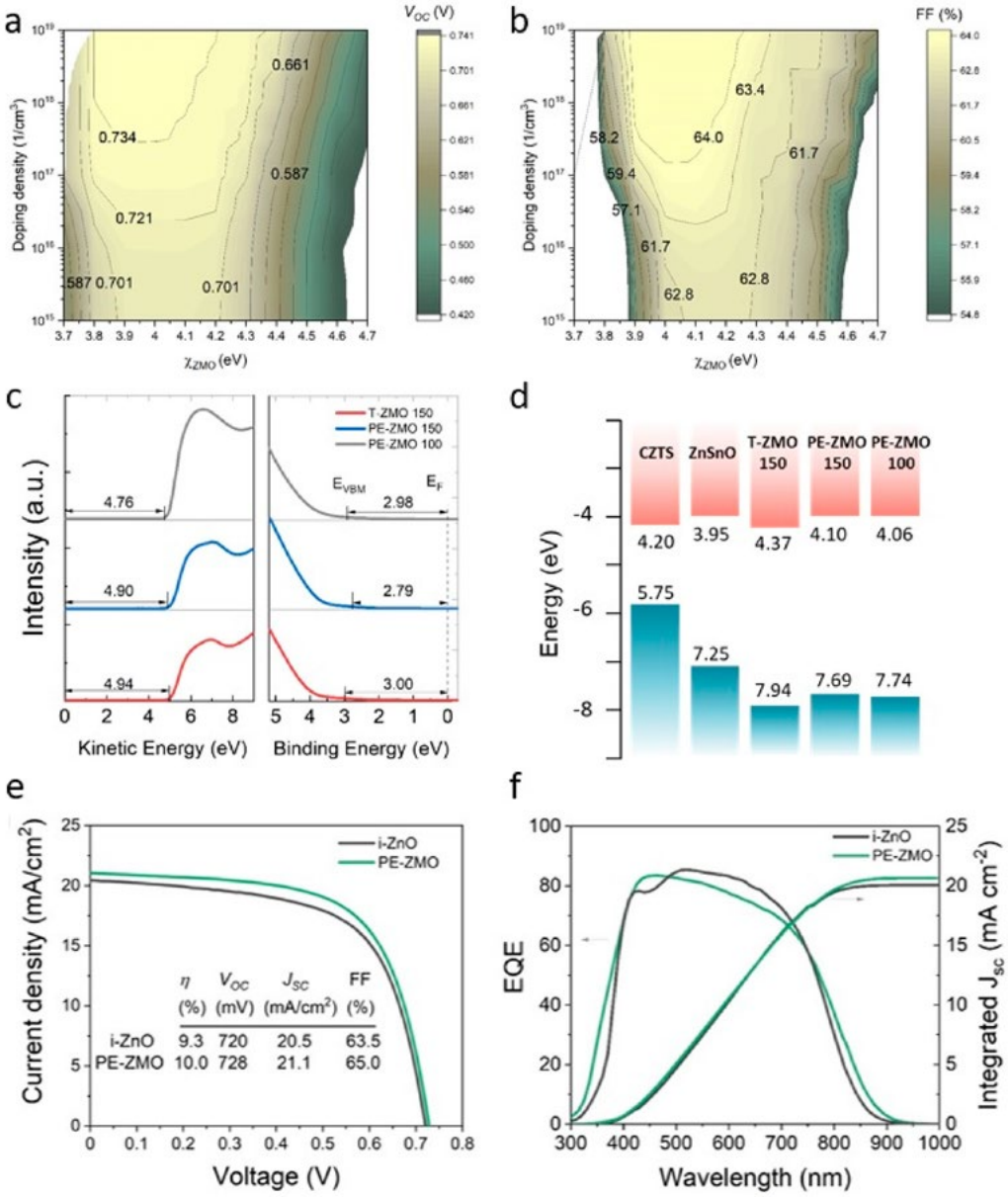

Figure PP2.4.16: Calculated contour plots of (a) open-circuit voltage, (b) fill factor for CZTS/ZnSnO/ZnMgO devices with the variation of ZMO properties, (c) UPS spectra and (d) band diagram of ZnMgO thin films synthesised from T-ALD and PE-ALD at different conditions. (e) J-V characteristics and (f) EQE of the champion CZTS/ZTO/PE-ZMO solar cell with an antireflection coating by using a PE-ZMO window layer with Zn:Mg pulse ratio of 4:1 deposited at 100°C.

Highlighted progress for high bandgap chalcogenide $CuInGaS_2$ solar cells

Pure sulfide $Cu(In,Ga)S_2$ (CIGS) has emerged as one of the most promising options for a tandem top cell due to its tunable bandgap from 1.5 eV to 2.4 eV, and its potential for high efficiency, eco-friendliness, low cost and excellent stability. In continuation of last year's research, we have conducted further research on improving the performance of CIGS solar cells. In this report, we highlighted our research progress on this material. We previously developed a potassium cyanide (KCN)-free and H_2S-free CIGS solar cell with 11.6% baseline efficiency, followed by studying the effects on the ZnSnO buffer layer and achieved an efficiency of 14.0%. This year, we have developed a novel method, aiming to further reduce the recombination by introducing cation alloying into CIGS. The results showed that the best device performance was possible using 16.0% (Ag/(Cu+Ag) Ag-alloying, achieving a 12.24% efficiency without antireflection coatings (ARC) (Figure PP2.4.17). We can conclude that Ag accumulates at the front interface and forms certain grading, which mainly drives the conduction band minimum lower (Figure PP2.4.18).

It is possible that the conduction band offset (CBO) has been minimised, leading to a significantly improved heterojunction quality. The device performance has been greatly improved, especially on V_{OC} and FF, with the V_{OC}-deficit significantly decreasing from 792 mV to 702 mV, compared to the sample with 16.0% Ag-alloying with the sample without Ag-alloying. This facilitation can be attributed to improved heterojunction quality which shows the smallest J_{02} (Table PP2.4.1).

Subsequently, we developed a high temperature sulfurisation annealing profile to further minimise the V_{OC}-deficit. Higher temperatures (> 600°C) facilitated crystallinity and grain growth according to SEM results (Figure PP2.4.19). XRD results were consistent with SEM as the intensity and full width at half maximum (FWHM) improved with increasing temperature (Figure PP2.4.20). More importantly, SIMS analysis revealed a sharper Ga-gradient profile towards the Mo-SLG (Figure PP2.4.21), which may result in reduced recombination within the bulk. Finally, we achieved the lowest V_{OC}-deficit of 671 mV with 625°C sulfurisation profile, which is 31 mV lower than the result we mentioned above.

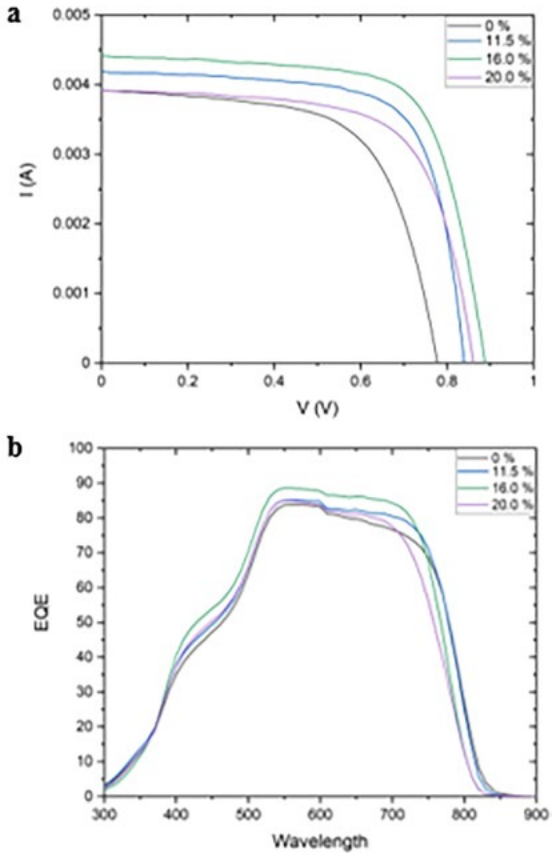

Figure PP2.4.17: (a) Current density-voltage (J-V) curves; and (b) EQE spectra of the most efficient CIGS device with amount of Ag-alloying.

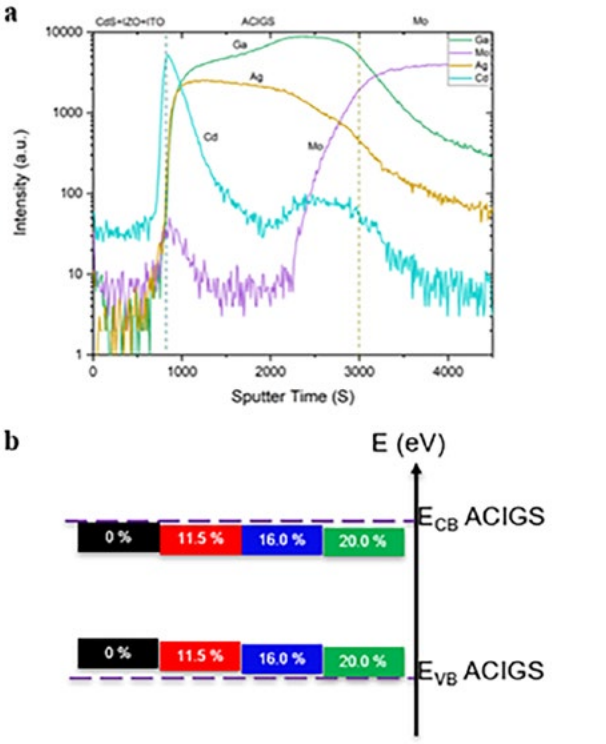

Figure PP2.4.18: (a) Secondary ion-mass spectrometry (SIMS) of 20.0% Ag-alloying CIGS; and (b) schematic band diagram of different Ag-alloyed CIGS.

Table PP2.4.1: Detailed device performance and J_{02} obtained from Suns-V_{OC}.

Sample	J_{SC} ($mAcm^{-2}$)	V_{OC} (mV)	FF (%)	Eff (%)	Eg(eV)	V_{oc} Deficit (mV)	J_{02} (A/cm^2)
0%	17.50	777.22	63.13	8.59	1.57	792.78	1.687 E-7
11.5%	18.69	838.90	70.65	11.08	1.57	731.1	2.366 E-8
16.0%	19.70	887.97	69.98	12.24	1.59	702.03	5.600 E-9
20.0%	17.50	860.41	66.90	10.08	1.59	729.59	1.743 E-8

Table PP2.4.2: Detailed device performance with bandgap obtained from EQE.

Sample	J_{sc} (mAcm^{-2})	V_{oc} (mV)	FF (%)	Eff (%)	Eg(eV)	V_{oc} Deficit (mV)
600 C	18.18	822.18	56.96	8.52	1.53	707.82
625 C	18.74	878.30	72.04	11.86	1.55	671.70
650 C	19.70	887.97	69.98	12.24	1.59	702.03

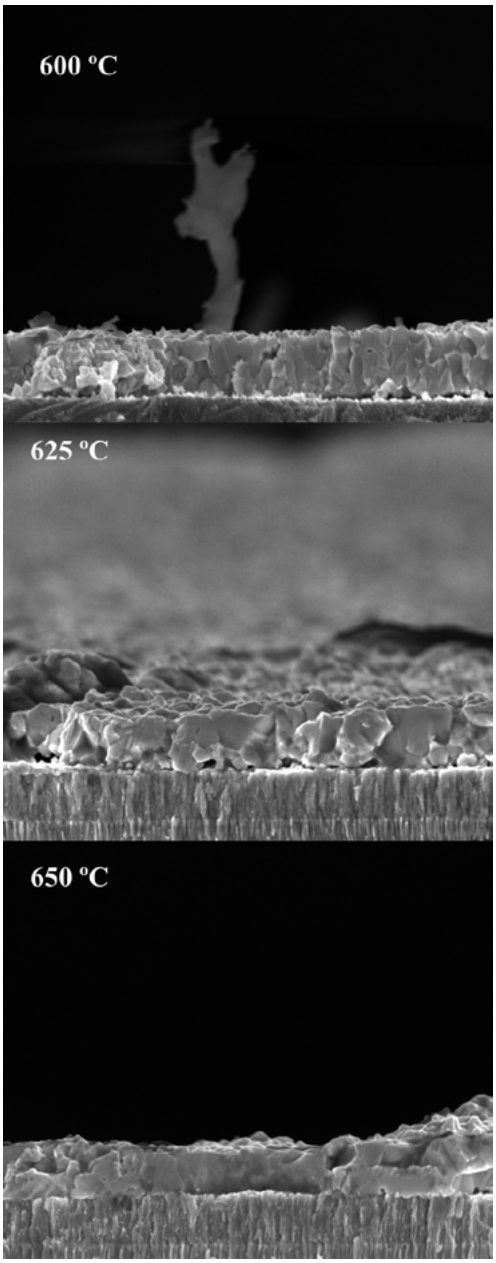

Figure PP2.4.19: SEM images of different high temperature sulfurisation processes.

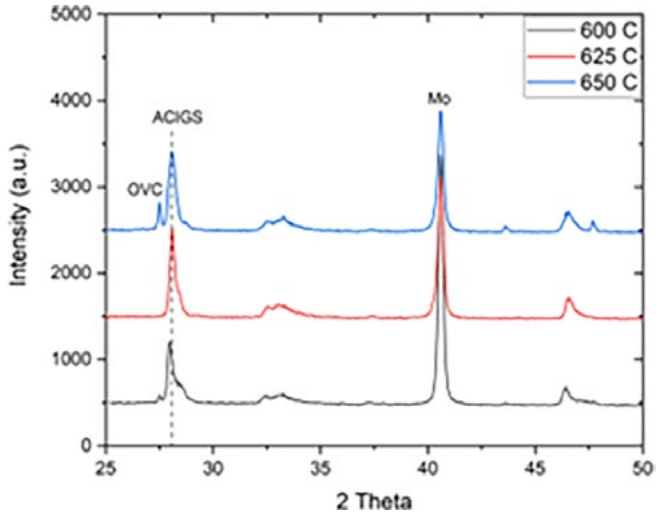

Figure PP2.4.20: XRD results of different high temperature sulfurisation processes.

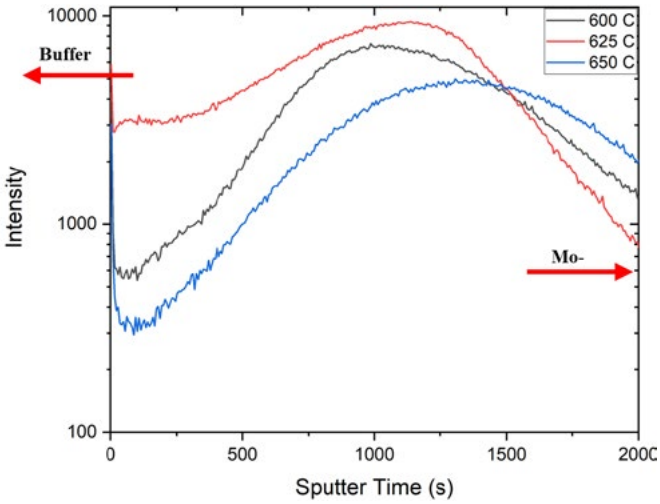

Figure PP2.4.21: SIMS Ga-profile of different high temperature sulfurisation processes.

Bifacial and semitransparent $Sb_2(S,Se)_3$ solar cells for single-junction and tandem photovoltaic applications

Thin-film solar cells are expected to play a significant role in the space industry, building integrated photovoltaic (BIPV), indoor applications, and tandem solar cells, where bifaciality and semitransparency are highly desired. $Sb_2(S,Se)_3$ has emerged as a promising new photovoltaic (PV) material for its high absorption coefficient, tunable bandgap, and non-toxic and Earth-abundant constituents. However, high efficiency $Sb_2(S,Se)_3$ solar cells exclusively employ monofacial architectures, leaving a considerable gap towards large-scale application in aforementioned fields.

In 2023, we demonstrated the first application of $Sb_2(S,Se)_3$ in a single-sided bifacial and semitransparent structure by employing indium-doped tin oxide (ITO) as the back contact capping on the MnS hole-transporting layer (HTL) (Figure PP2.4.22) (Qian et al. 2023). The analysis of carrier kinetics on this bifacial and semitransparent solar cell (BSSC) with front (FTO side) and rear illumination (ITO side) respectively (Figure PP2.4.23) implies distinct electron travelling paths before being collected. The distinctive ultra-thin fully depleted absorber layer (≈350 nm) fabricated by the hydrothermal method enables carrier transport via drifting instead of diffusing towards the HTL/electron-transporting layer (ETL), significantly suppressing the bulk recombination and improving the bipolar transport properties and bifaciality. Consequently, a PCE of 7.41% and 6.36% was achieved under front and rear illumination, respectively (Figure PP2.4.24). In comparison, the conventional gold-based monofacial and opaque solar cell (MOSC) achieved a PCE of 9.50% and 0.70% in respective aforementioned conditions. It also exhibits excellent capability of absorbing incident light with sequentially increased tilt angles within a 2π period, implying good adaptability to real-world applications, whereas the MOSC has stricter requirements for incident angles (Figure PP2.4.25).

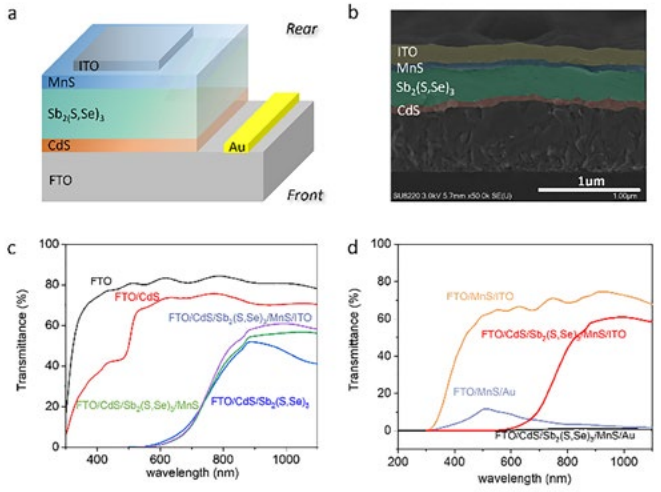

Figure PP2.4.22: (a) Schematic configurations of the $Sb_2(S,Se)_3$ BSSC and MOSC, and (b) cross-sectional SEM image of the BSSC. (c) Transmittance after every sequent deposition step. (d) Transmittance of the BSSC, MOSC and their corresponding back contacts deposited on FTO-coated glass.

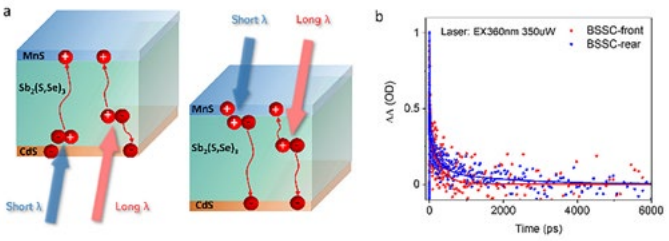

Figure PP2.4.23: (a) Schematic diagram of the carrier generation, transport, and collection process under front illumination (left) and rear illumination (right), respectively, and (b) kinetic study of photo-generated carriers with front and rear illumination, respectively in BSSCs.

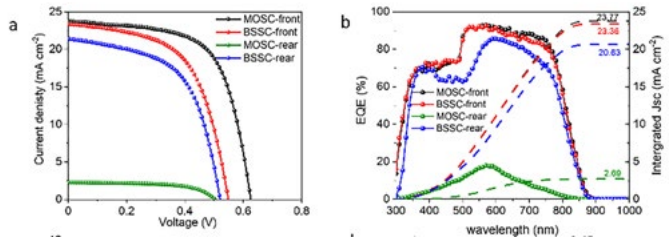

Figure PP2.4.24: (a) J-V curve, (b) EQE response of $Sb_2(S,Se)_3$ MOSCs and BSSCs with front and rear illumination, respectively.

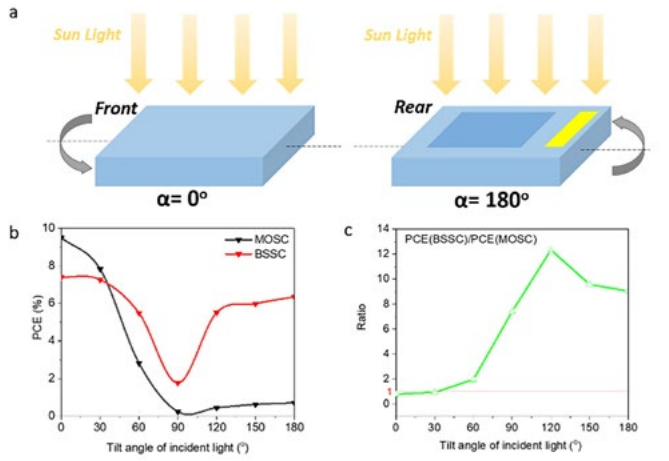

Figure PP2.4.25: (a) Schematic diagram for measuring PV performance against rotation angles. (b) PCE of MOSCs and BSSCs, and (c) their corresponding ratios against tilt angles of incident light.

Highlights

- A Ge incorporation strategy was developed to alleviate the non-radiative V_{OC} loss by manipulating the phase evolution during the critical kesterite phase formation stage.
- New certified record efficiency for CZTS solar cells (also Cd-free) at 11.4% was achieved.
- A Li-enhanced liquid-phase-assisted grain growth strategy is introduced to further enlarge the grain size and improve the carrier collection efficiency of CZTS solar cells.

- The function and consumption of Li addition in the grain growth of CZTS was unveiled.
- A high efficiency CZTS solar cell with in-house measurement over 11% efficiency was achieved.
- A champion 10.0% efficient PE-ZMO device was demonstrated with a device structure of Mo/CZTS/ZnSnO/ZnMgO/ITO.
- A bifacial and semitransparent $Sb_2(S,Se)_3$ solar cell was fabricated by a TCO/n-i-p/TCO structure. PCEs of 7.41% and 6.36% were achieved under front illumination and back illumination, respectively.
- An $Sb_2(S,Se)_3$/silicon tandem solar cell with a PCE of 11.66% was demonstrated.

Future Work

Future work in 2024 will focus on the investigation of the loss mechanism of different metal chalcogenide solar cells and integration of our already developed effective strategies to further improve the device performance. The cost analysis of different technologies will be studied to evaluate the commercialisation potential.

References

Cui, X., Sun, K., Huang, J., Sun, H., Wang, A., Yuan, X., Green, M., Hoex, B. & Hao, X. (2023). Low-Temperature Plasma-Enhanced Atomic Layer Deposition of ZnMgO for Efficient CZTS Solar Cells. ACS Materials Letters 5, 1456-1465.

Green, M. A., Dunlop, E. D., Yoshita, M., Kopidakis, N., Bothe, K., Siefer, G. & Hao, X. (2023). Solar cell efficiency tables (version 62). Progress in Photovoltaics: Research and Applications 31, 651-663.

Li, J., Huang, J., Ma, F., Sun, H., Cong, J., Privat, K., Webster, R. F., Cheong, S., Yao, Y., Chin, R. L., Yuan, X., He, M., Sun, K., Li, H., Mai, Y., Hameiri, Z., Ekins-Daukes, N. J., Tilley, R. D., Unold, T., Green, M. A. & Hao, X. (2022). Unveiling microscopic carrier loss mechanisms in 12% efficient Cu2ZnSnSe4 solar cells. Nature Energy 7, 754-764.

Li, J., Sun, K., Yuan, X., Huang, J., Green, M. A. & Hao, X. (2023). Emergence of flexible kesterite solar cells: progress and perspectives. NPJ Flexible Electronics 7, 16.

Qian, C., Sun, K., Cong, J., Cai, H., Huang, J., Li, C., Cao, R., Liu, Z., Green, M., Hoex, B., Chen, T. & Hao, X. (2023). Bifacial and Semitransparent Sb2(S,Se)3 Solar Cells for Single-Junction and Tandem Photovoltaic Applications. Advanced Materials 35, 2303936.

Sun, K., Huang, J., Li, J., Yan, C. & Hao, X. (2022). Recent progress in defect engineering for kesterite solar cells. Science China Physics, Mechanics & Astronomy 66, 217302.

Walsh, A., Chen, S., Wei, S.-H. & Gong, X.-G. (2012). Kesterite Thin-Film Solar Cells: Advances in Materials Modelling of Cu2ZnSnS4. Advanced Energy Materials 2, 400-409.

Wang, A., He, M., Green, M. A., Sun, K. & Hao, X. (2023a). A Critical Review on the Progress of Kesterite Solar Cells: Current Strategies and Insights. Advanced Energy Materials 13, 2203046.

Wang, A., Huang, J., Cong, J., Yuan, X., He, M., Li, J., Yan, C., Cui, X., Song, N., Zhou, S., Green, M. A., Sun, K. & Hao, X. (2023b). Cd-Free Pure Sulfide Kesterite Cu2ZnSnS4 Solar Cell with Over 800 mV Open-Circuit Voltage Enabled by Phase Evolution Intervention. Advanced Materials, n/a, 2307733.

Yuan, X., Li, J., Huang, J., Yan, C., Cui, X., Sun, K., Cong, J., He, M., Wang, A., He, G., Mahboubi Soufiani, A., Jiang, J., Zhou, S., Stride, J. A., Hoex, B., Green, M. & Hao, X. (2022). 10.3% Efficient Green Cd-Free Cu2ZnSnS4 Solar Cells Enabled by Liquid-Phase Promoted Grain Growth. Small 18, 2204392.

Publications

Cui, X., Sun, K., Huang, J., Sun, H., Wang, A., Yuan, X., Green, M., Hoex, B. & Hao, X. (2023). Low-Temperature Plasma-Enhanced Atomic Layer Deposition of ZnMgO for Efficient CZTS Solar Cells. ACS Materials Letters 5, 1456-1465.

Li, J., Huang, J., Ma, F., Sun, H., Cong, J., Privat, K., Webster, R. F., Cheong, S., Yao, Y., Chin, R. L., Yuan, X., He, M., Sun, K., Li, H., Mai, Y., Hameiri, Z., Ekins-Daukes, N. J., Tilley, R. D., Unold, T., Green, M. A. & Hao, X. (2022). Unveiling microscopic carrier loss mechanisms in 12% efficient Cu2ZnSnSe4 solar cells. Nature Energy 7, 754-764.

Li, J., Sun, K., Yuan, X., Huang, J., Green, M. A. & Hao, X. (2023). Emergence of flexible kesterite solar cells: progress and perspectives. NPJ Flexible Electronics 7, 16.

Qian, C., Sun, K., Cong, J., Cai, H., Huang, J., Li, C., Cao, R., Liu, Z., Green, M., Hoex, B., Chen, T. & Hao, X. (2023). Bifacial and Semitransparent Sb2(S,Se)3 Solar Cells for Single-Junction and Tandem Photovoltaic Applications. Advanced Materials 35, 2303936.

Sun, K., Huang, J., Li, J., Yan, C. & Hao, X. (2022). Recent progress in defect engineering for kesterite solar cells. Science China Physics, Mechanics & Astronomy 66, 217302.

Wang, A., He, M., Green, M. A., Sun, K. & HAO, X. (2023a). A Critical Review on the Progress of Kesterite Solar Cells: Current Strategies and Insights. Advanced Energy Materials 13, 2203046.

Wang, A., Huang, J., Cong, J., Yuan, X., He, M., Li, J., Yan, C., Cui, X., Song, N., Zhou, S., Green, M. A., Sun, K. & Hao, X. (2023b). Cd-Free Pure Sulfide Kesterite Cu2ZnSnS4 Solar Cell with Over 800 mV Open-Circuit Voltage Enabled by Phase Evolution Intervention. Advanced Materials, 2307733.

Yuan, X., LI, J., Huang, J., Yan, C., Cui, X., Sun, K., Cong, J., He, M., Wang, A., He, G., Mahboubi Soufiani, A., Jiang, J., Zhou, S., Stride, J. A., Hoex, B., Green, M. & Hao, X. (2022). 10.3% Efficient Green Cd-Free Cu2ZnSnS4 Solar Cells Enabled by Liquid-Phase Promoted Grain Growth. Small 18, 2204392.

PP2.6 SCALE-UP AND PRINTING

Lead Partner
CSIRO

Research Team
Dr Mei Gao, Dr Doojin Vak, Dr Dechan Angmo, Dr Hasitha Weerasinghe, Dr Andrew Scully, Ms Régine Chantler, Dr Anthony Chesman

Student
Luke Sutherland

Other Partner
Monash University

Funding Support
ARENA, ACAP, ARC, Baosteel

Aims

Advances in the efficiency and lifetime of solar cells that incorporate emerging materials must be accompanied by the development of large-scale, industrially relevant production methods to enable their translation to the marketplace. Furthermore, cost-prohibitive materials, such as silver or gold electrodes, need to be replaced with efficient substitutes if these technologies are to be economically viable.

The main topic of this study is the use of carbon-based solution-processible electrodes that can offer low fabrication costs, can be adapted to scalable roll-to-roll (R2R) deposition, and exhibit a suitable work function and conductivity for charge extraction. However, optimising the charge transport layer (CTL)/carbon interface without damaging the underlying functional layers is a persistent challenge. To address this, we demonstrate a scalable lamination technique that gives a CTL/carbon interface that is engineered to deliver performance on par with vacuum-deposited electrodes.

Progress

Cold isostatic pressing (CIP) has been reported for the fabrication of perovskite solar cells (PSCs). CIP involves submerging a sample into a chamber of ambient-temperature fluid, either liquid or gas, which is then isostatically pressurised as shown in Figure PP2.6.1. The CIP technique mitigates the risk of stress concentrations for depositing printed electrodes and permits the use of very high pressures (> 200 MPa) to enhance the CTL/electrode interface contact and facilitate efficient charge transfer. For flexible PSCs, whole rolls with thousands of devices can be sealed and pressed in a single cycle, while rigid PSCs can be efficiently stacked for maximum throughput. By using an isostatic press, we fabricate research-scale (0.16 cm^2) carbon-based PSCs (C-PSCs) with a record power conversion efficiency (PCE) of up to 20.8% (Figure PP2.6.2). The unencapsulated C-PSCs significantly outperform the Au-electrode control devices after 1000 hours of accelerated operational stability testing (ISOS-L-1). Furthermore, we demonstrate flexible, roll-to-roll (R2R) printed C-PSCs with efficiencies of up to 15.8%.

To further showcase the advantages of uniformly distributed pressure using the CIP lamination technique, we progressed to fabricating large-area, C-PSCs. The uniform pressure distribution enables the fabrication of large-area C-PSCs with record efficiencies of 19.8% and 16.9% for 0.95 cm^2 and 5.5 cm^2 cells, respectively (Figure PP2.6.3). While performance gaps are evident in research-scale C-PSCs compared to their evaporated electrode counterparts, these differences become significantly more pronounced for large-area cells of approximately 1 cm^2 and greater.

These findings underscore the critical role of interface contact in enhancing C-PSC performance, and the results pave the way for developing low-cost, efficient and reliable PSCs. Further work to fabricate 100 cm^2 modules using the same method will be pursued in 2024.

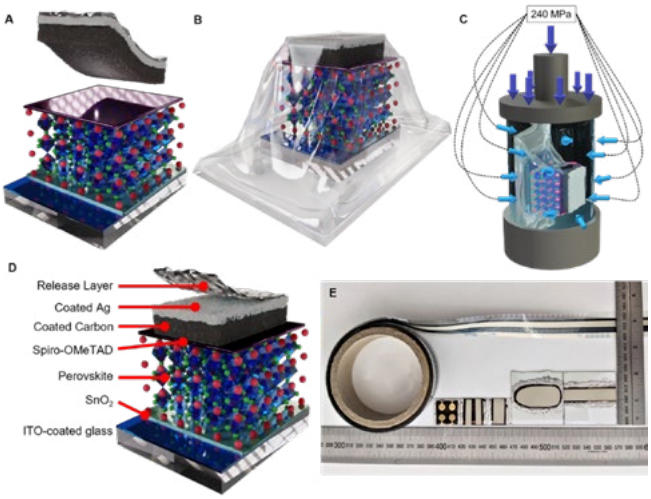

Figure PP2.6.1: Illustrations describing the CIP lamination process and photos of devices fabricated in this work. (A) Illustration of PSC up to the HTL and the coated bilayer electrode on a release layer. (B) Vacuum sealing of the PSC stack and electrode. (C) Isostatic pressing of the sealed device stack in water. (D) Final C-PSC device architecture after removing the release layer by peeling after the electrode lamination process. (E) Image showing the resulting C-PSCs and one PSC with an evaporated Au electrode.

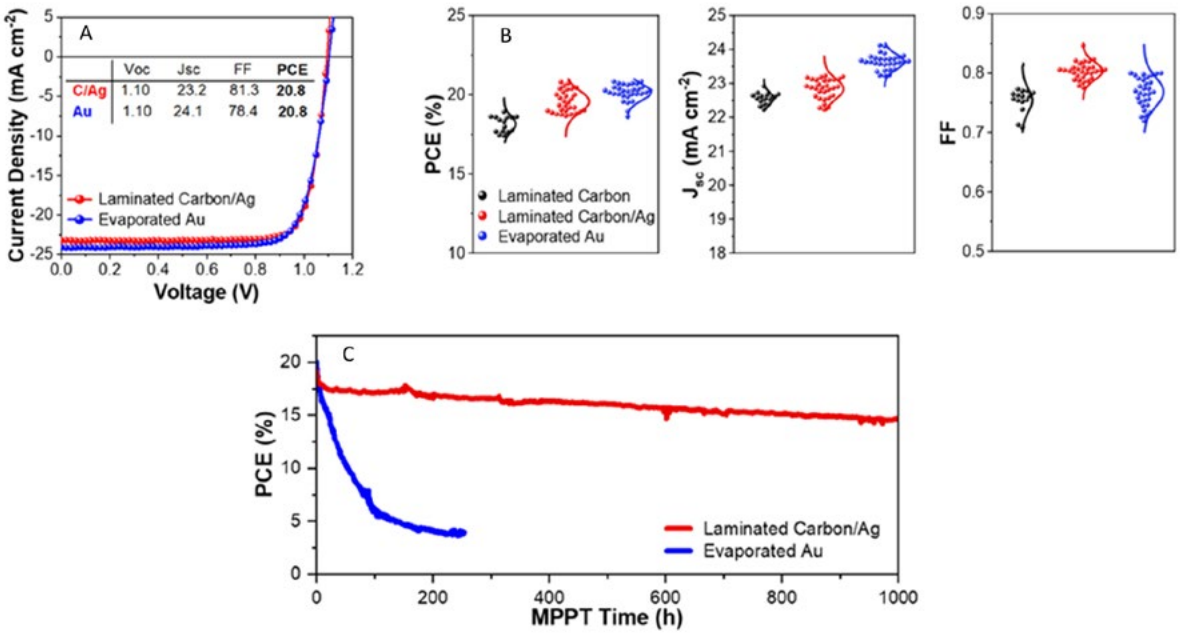

Figure PP2.6.2: Photovoltaic performance of the optimised C-PSCs. (A) J-V curves comparing the C-PSC with the best control device with an evaporated Au electrode. (B) Box plots of the device PCE, J_{sc}, and FF, comparing 15 carbon-only C-PSCs, 30 carbon/Ag C-PSCs and 30 evaporated Au PSCs. (C) MPP tracking stability performance of unencapsulated devices (one-sun illumination, 11% RH, 30°C), comparing the laminated electrode with evaporated Au.

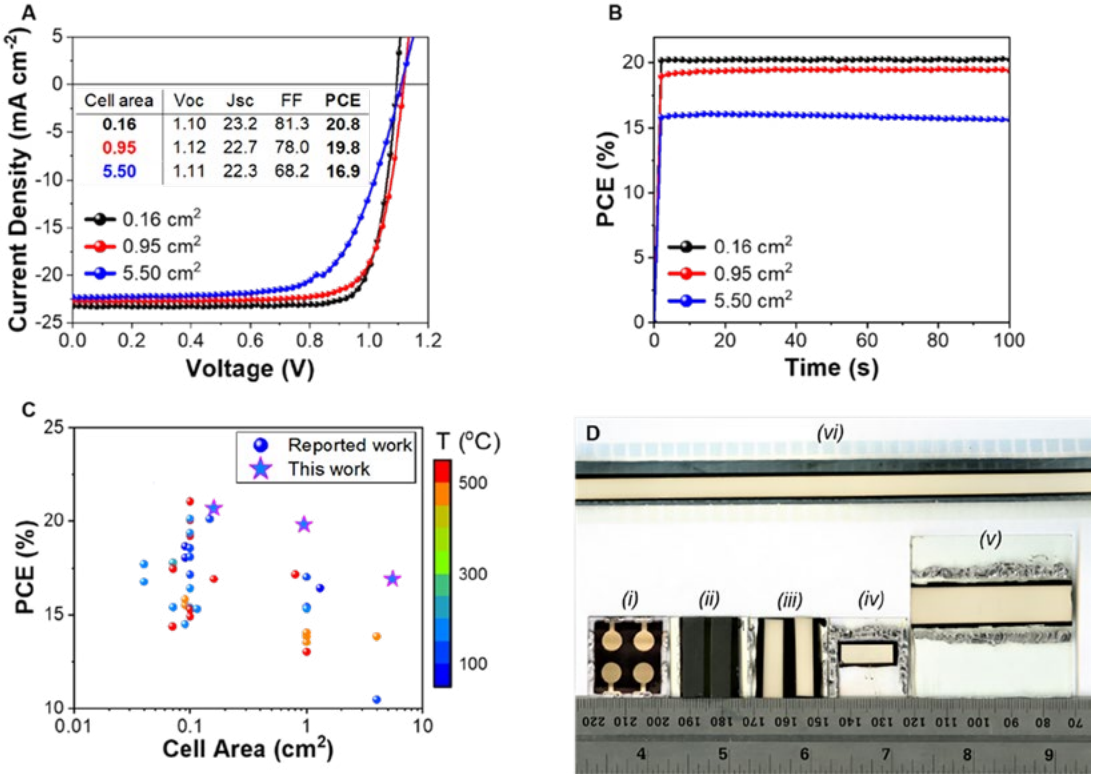

Figure PP2.6.3:. Photovoltaic performance of large-area C-PSCs. (A) J-V curves in reverse scan direction of devices with varying active area with the inset table providing the detailed photovoltaic parameters. (B) Short-term MPP tracking under one-sun illumination comparing the research-scale (0.16 cm²) cells with the large-area C-PSCs. (C) Summary of the best performing planar, monolithic C-PSCs in the literature with the dot-colour representing the maximum temperature used for the device fabrication. (D) Image showing the six device configurations highlighted in this work, including (i) research-scale Au PSC, (ii) research-scale C-PSC with carbon-only electrode, (iii) research-scale C-PSC with coated carbon/Ag electrode, (iv) large-area (~1 cm²) C-PSC with laminated electrode, (v) large-area (5.5 cm²) C-PSC with laminated electrode, and (vi) strip of flexible R2R-fabricated C-PSCs with laminated electrode.

Highlights

- A solvent-free method for depositing carbon electrodes was demonstrated.
- The method was shown to be scalable and was used in the fabrication of devices with an area of 5.5 cm^2.
- The devices showed excellent performance and outperformed analogous devices with gold electrodes.

Future Work

- The CIP process will be upscaled to allow for the fabrication of module-sized (100 cm^2) devices.

References

Sepalage, G. A., Weerasinghe, H., Rai, N., Duffy, N. W., Raga, S. R., Hora, Y., Gao, M., Vak, D., Chesman, A. S. R., Bach, U. & Simonov, A. (2002). Advanced Materials Technologies 7, 2101148.

Sutherland, L. J., Vak, D., Gao, M., Peiris, T. A. N., Jasieniak, J. J., Simon, G. P. & Weerasinghe, H. (2022). Vacuum-Free and Solvent-Free Deposition of Electrodes for Roll-to-Roll Fabricated Perovskite Solar Cells. Advanced Energy Materials 12, 2202142.

PP3
TANDEM SOLAR CELLS

OVERVIEW

In tandem solar cells, two or more solar cells based on different materials and with different optical properties are stacked on top of one another. Each solar cell absorbs a specific part of the solar spectrum and efficiently converts it into electrical power. In this way it is possible to significantly increase the conversion efficiency of solar cells compared to single- junction cells. Efficiencies of nearly 45% are theoretically possible, compared to about 32% for single junction cells. Tandem cells are considered the most promising route to continue significantly reducing the cost of solar electricity into the future, and to achieve ARENA's target of 30% module efficiency and 30c/W installed PV cost by 2030.

Many different types of tandem cells, based on different material combinations and different architectures, are possible. In this Project Package the focus will be on the most prospective tandem cells.

The scope of the work packages summarised below is very broad, and it is not anticipated that there will be activities on all packages and sub-packages every year. Instead, the partners will identify several critical areas of research where they can have the greatest global impact, given capabilities and resources.

PP3.1 Perovskite Tandems

The aim of this work package is to develop perovskite tandems with either silicon or alternative material bottom cells that will achieve > 30% efficiency, and to develop manufacturable approaches to deliver these high efficiency tandem technologies.

Cell durability has improved to maintain 96% of peak efficiency after 530 hours in wetting conditions and 94% after 2200 hours in the air. Cells also maintained 93% of peak efficiency after ~2000 hours under one-sun open-circuit conditions and 90% after 1000 hours at the maximum power point, respectively. Moreover, > 24% efficient single-junction and > 19% inverted perovskite solar cells were achieved, and 27% efficiency mechanically stacked perovskite/Si tandems.

Ongoing work targets the fabrication of encapsulated perovskite cells that achieved efficiencies of over 25% and maintain 20% efficiency at 85% relative humidity, 85°C, and continuous one-sun illumination.

PP3.2 III-V on Silicon Tandems

By stacking top cells on silicon, the inherent efficiency advantages of tandem designs can be harnessed to substantially improve on current silicon performance through the addition of thin layers of high performance materials. The III-V materials system is one of the promising top-cell candidates, with a proven track record of high performance, long-term stability, and an existing deep knowledge base in terms of material properties and fabrication techniques.

The leading techniques for III-V/silicon tandem cells are through direct growth, wafer bonding, mechanical stacking and spectrum splitting.

PP3.3 Chalcogenide on Silicon Tandems

As an alternative to inorganic III-V materials, chalcogenide semiconductors are another group of promising photovoltaic materials for silicon-based tandems with high efficiency potential, low-cost potential, and demonstrated long-term stability. This work package will progress the development of metal chalcogenides to target > 20% efficiency semitransparent high bandgap chalcogenide cells, and 30% efficiency chalcogenide/silicon tandem cells, using manufacturing sequences compatible with silicon production lines and through the direct growth of top-cell and alternative cost-effective tri-chloro-acetic (TCA) bonding technologies.

PP3.4 Tuned Bottom Silicon Devices

The aim of this work package is the demonstration of highly tuned bottom silicon devices and development of enabling technologies, guided by a detailed technology roadmap based on current technology projections and state-of-the-art device simulations.

Tandem PV with a bottom silicon cell is projected to enter the PV market within the next five years and occupy a ~5% market share within the next 10 years (ITRPV 2021). The suitability of silicon devices as the bottom cell is driven by both economic and technical factors. Silicon devices are a highly matured PV product with over 90% of the PV market, owing to its potential for high efficiencies 25–27%, low-cost fabrication processes ($/Wp) and low LCOE.

A vast range of research, development, integration, commercialisation and demonstration activities are needed to realise a commercial silicon tandem product within the next decade. This work package will address the most pressing issues relating to design and development of the optimal bottom silicon cell structure incorporating passivated contacts, optimal optical light trapping schemes, and advanced interface contact technologies.

PP3.5 Characterisation

Tandem cell technologies present unique challenges in assessing the impact of interfaces, contacts, individual and combined cell performance, losses, standard measurements and field performance.

Our research will allow the separation of the effects of the individual cell technologies and their interaction in a tandem structure, taking into account cell materials, design, interface and contact technologies. We will investigate correlations with efficiency enhancement and losses with a view to optimising performance and engineering new processes and materials.

PP3.6 Laboratory Cell and Module Performance Testing

Tandem solar cells present new challenges in measurement and testing that reflect the diversity of materials combinations and device architectures. Since 2015 CSIRO has operated the only IEC 17025–accredited PV cell measurement laboratory in the southern hemisphere and has provided dozens of independent measurements on research solar cells, including certifying two Australian results for the world record efficiency tables.

CSIRO has recently developed a novel approach to measuring tandem solar cell devices, with the aid of a new solar simulator design that produces the best spectral match ever reported.

PP3.1 PEROVSKITE TANDEMS

ANU Team

Prof. Klaus Weber, Prof. Kylie Catchpole, Prof. Daniel Macdonald, Dr The Duong, Dr Heping Shen, Dr Viqar Ahmad, Dr Daniel Walter, Dr Hualin Zhan, Dr Sieu Pheng Phang, Dr Rabin Basnet, Dr Di Kang, Mr Stephane Armand

ANU Students

Mr Keqing Huang, Mr Li-Chun Chang, Mr Wei Wang, Mr Yihui Hou, Ms Grace Tabi, Mr Thuan Nguyen

University of Sydney Team

Prof. Anita Ho-Baillie, Dr Md Arafat Mahmud, Dr Jianghui Zheng, Dr Jueming Bing

University of Sydney Students

Mr Shi Tang, Mr Chwenhaw Liao, Mr Guoliang Wang, Mr Tik Lun Leung, Mr Jianpeng Yi

UNSW Team

Prof. Xiaojing Hao, Prof. Ziv Hameiri, Prof. Nicholas Ekins-Daukes, Dr Ziheng Liu, Dr Pengfei Zhang, Dr Caixia Li, Dr Meng Zhang, Dr Mingrui He, Prof. Martin Green, Brett Hallam, Li Wang

UNSW Students

Chen Qian, Jialin Cong, Minwoo Lee, Yihao Wang

CSIRO Team

Yong Li, Faiazul Haque, Adrian Element, Hareem Khan, Emma Holder, Ange Chen, Kenrick Anderson, Bruno Vicari Stefani, Benjamin Duck, Noel W. Duffy, Chris Fell, Gregory J. Wilson, Timothy W. Jones, Andre Cook, Callum Carroll

Academic Partners

University of Surrey
Korea Research Institute of Chemical Technology (KRICT)
University of Science and Technology of China
Macquarie University
Flinders University
Karlsruhe Institute of Technology (Germany)
Monash University
University of Oxford: Matthew Wright, Anastasia Soeriyadi, Ruy Sebastian Bonilla, Pietro Altermatt

Funding Support

ACAP, ARENA, ARC, ANU, UNSW, University of Sydney, SIEF, CSIRO Energy

Aim

Perovskite cells offer opportunities for several types of tandem cells, including four-terminal tandems and monolithic (two-terminal) tandems. In the latter category, both perovskite-silicon and perovskite-perovskite tandems are potentially highly attractive. At this stage, there are no clear technology winners. The project partners aimed to address key challenges associated with the different technologies to facilitate development to their full potential.

Progress

A. Efficient and stable methylammonium-free perovskite and perovskite-silicon tandem solar cells

Methylammonium (MA)-free perovskite solar cells generally have significantly better stability than their MA-containing counterparts but the efficiency of MA-free perovskite solar cells generally lags behind due to inferior bulk quality. The aim of this work (Duong et al. 2023) was to develop MA-free cells with high efficiency and improved stability, through the use of additives to help stabilise the perovskite.

4-methylphenethylammonium chloride (4M-PEACl) was added into an MA-free perovskite precursor, which resulted in greatly enhanced bulk quality. Quasi-two-dimensional (2D) perovskites are formed and passivate defects at the grain boundaries of the perovskite crystals. This facile approach led to a steady state efficiency of 23.7% for MA-free perovskite solar cells. The devices also show excellent light stability, retaining more than 93% of the initial efficiency after 1000 hours of constant illumination in a nitrogen environment.

We utilised this perovskite composition in four-terminal perovskite-silicon tandem solar cells. Semitransparent perovskite solar cells were fabricated using the structure glass/indium tin oxide (ITO)/SnO_2/perovskite/Spiro-MeOTAD/MoO3/indium zinc oxide (IZO)/Au fingers. A schematic of the four-terminal mechanically stacked perovskite-silicon tandem solar cells is illustrated in Figure PP3.1.1(A) and the cross-sectional SEM image of a semitransparent perovskite solar cell is shown in Figure PP3.1.1(B).

The performance of each sub-cell is presented in Figure PP3.1.1(C). The champion semitransparent perovskite top cell showed an efficiency of 22.9% in reverse scan, 22.2% in forward scan and a steady state efficiency of 22.6%. Under a semitransparent perovskite cell filter, which had all the layers similar to the active semitransparent perovskite cells, a bottom passivated emitter and rear locally-diffused (PERL) silicon cell with an original efficiency of 23.8% retained an efficiency of 7.7%. The external quantum efficiency (EQE) spectrum of the silicon cell, semitransparent perovskite cell and silicon cell under perovskite filter are presented in Figure PP3.1.1(D). Overall, the EQE results were in excellent agreement with the J-V results of the devices. The integrated J_{SC} of the semitransparent perovskite top cell was 23.6 $mAcm^{-2}$, which was 2% lower than the J_{SC} extracted from the J-V curves of the device. On the other hand, the integrated JSC of the silicon cell performing alone and under semitransparent perovskite were 41.7 $mAcm^{-2}$ and 13.7 $mAcm^{-2}$, respectively, in both the J-V and EQE results. Overall, the efficiency of a four-terminal perovskite-silicon tandem solar cell was calculated to be 30.3%, which is one of the highest values reported for this type of tandem devices using the perovskite top cells with comparable active areas.

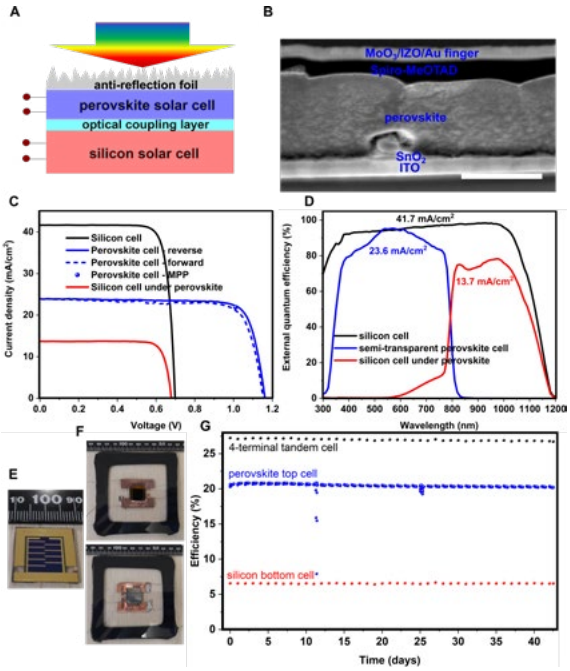

Figure PP3.1.1: (A) Schematic of four-terminal perovskite-silicon tandem solar cells; (B) cross-sectional SEM images of a semitransparent perovskite solar cell with a structure glass/ITO/SnO_2/perovskite/Spiro-MeOTAD/MoO_3/IZO/Au finger. The scale bar is 500 nm; (C) J-V curves of the sub-devices in the tandem configuration; (D) EQE of the sub-devices in the tandem configuration; (E) picture of a 1 cm2 semitransparent perovskite solar cell; (F) pictures of an encapsulated four-terminal perovskite-silicon tandem solar cell from top and bottom; (G) operational stability of the encapsulated four-terminal perovskite-silicon tandem solar cell for 42 day/night cycles.

The tandem devices were encapsulated using polyisobutylene (PIB) edge-seal method and the picture of the encapsulated cell can be seen in the inset of Figure PP3.1.1(F). The operational stability of the tandem device was examined by exposing the device under day/night cycles. The temperature of the devices was between 10°C and 60°C during the test. The efficiency of the perovskite top cell was measured continuously while the efficiency of the silicon bottom cell was checked periodically. The performance of the encapsulated device was lower than the non-encapsulated device due to the presence of the top cover encapsulating glass. After 42 day/night cycles in ambient, the tandem device showed excellent operational stability, retaining over 98% of the initial performance (reduced from 27.2% to 26.7%). To date, very few reports have demonstrated the operational stability of four-terminal perovskite-silicon tandem solar cells. The results demonstrate the state-of-the-art operational stability of four-terminal perovskite-silicon tandem solar cells, further affirming the benefit of using low–moderate bandgap perovskite compositions for tandem applications.

Highlights

- Demonstrated substantial stability improvement in MA-free perovskite solar cells.
- 30.3% calculated efficiency for four-terminal perovskite-silicon tandem solar cell.

B.Cation-diffusion-based simultaneous bulk and surface passivations for high bandgap inverted perovskite solar cell producing record fill factor and efficiency

High bandgap perovskite solar cells (bandgap ~1.7 eV) are integral to monolithic perovskite-based tandem solar cells but present challenges in terms of device efficiency and stability. We aimed to improve device performance through improved bulk and surface passivation.

We developed a cation-diffusion-based double-sided interface passivation scheme that simultaneously provides bulk passivation for a 1.75 eV perovskite cell that is also compatible with a p-i-n cell architecture (Mahmud et al. 2022). The champion cell achieved a record fill factor of 86.5% and a power conversion efficiency of 20.2% (Figure PP3.1.2). Results (not shown here but found in the paper) of ionic distribution profiling, Fourier transform infrared spectroscopy, and X-ray diffraction crystallography reveal evidence of cation diffusion from the surface perovskite passivation layer into bulk. The diffused cations reduce Shockley–Read–Hall recombination in the perovskite bulk and at the surfaces. This concurrent bulk and surface passivation scheme renders record fill factor and efficiency in the double-sided passivated cells at the time of reporting (Figure PP3.1.3). This provides new insights for future passivation strategies based on ionic diffusion of functionalised materials.

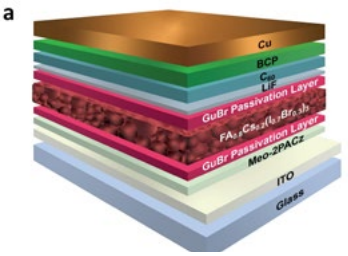

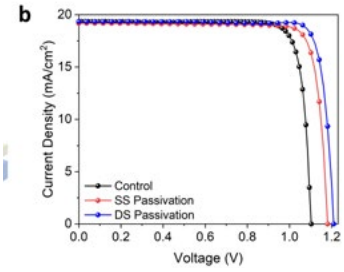

c

Device	Average/ Champion	V_{OC} (mV)	J_{SC} (mA/cm²)	FF (%)	PCE (%)	Series Resistance (Ω.cm²)	Shunt Resistance (Ω.cm²)
Control	Average	1085±11	19.3±0.1	84.3±0.5	17.6±0.2	1.42±0.16	3009±1216
	Champion	1104	19.4	84.7	18.1	1.46	4563
SS Passivation	Average	1179±7	19.2±0.2	84.5±0.6	19.1±0.1	1.34±0.08	3108±818
	Champion	1187	19.2	85.0	19.3	1.33	4602
DS Passivation	Average	1208±7	19.3±0.1	85.6±0.5	19.9±0.2	1.04±0.24	3335±1420
	Champion	1210	19.3	86.5	20.2	1.15	5445

Figure PP3.1.2: (a) Schematic diagram showing the cell structure for high bandgap p-i-n perovskite solar cell demonstration using SAM-based HTL and double-sided (DS) passivation layers sandwiching the bulk perovskite film. (b) J-V curves of the champion control, SS passivation and DS passivation cells (reverse scan). (c) Table listing photovoltaic parameters – averaged from 15 cells and measured for the champion device in each category: control (unpassivated), SS passivated and DS passivated perovskite solar cells. Figures from Mahmud et al. 2022.

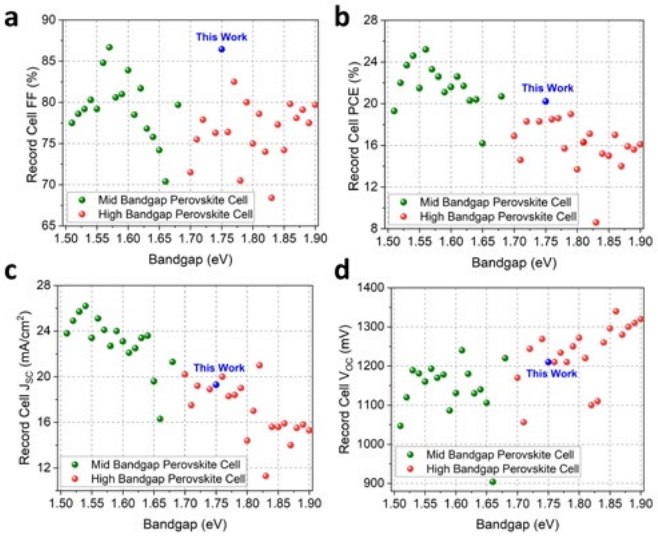

Figure PP3.1.3: (a) Fill factors (FF); (b) power conversion efficiency (PCE); (c) short-circuit current density (J_{SC}); and (d) open-circuit voltage (V_{OC}) of mid and high bandgap solar cells with record efficiencies reported in peer-reviewed articles at the time of the reporting of Mahmud et al. 2022. Figures from Mahmud et al. 2022.

Highlights

- Demonstrated significant improvement in the performance of high bandgap perovskite cells.
- Achieved best-in-class efficiency of 20.2% for a perovskite cell with a bandgap greater than 1.7 eV.

C.Water-free, conductive hole transport layer for reproducible perovskite-perovskite tandems with record fill factor

Many of the state-of-the-art perovskite-perovskite tandem solar cells incorporate a water-based poly(3,4-ethylenedioxythiophene):polystyrenesulfonate (PEDOT: PSS) hole transport layer in the low bandgap sub-cell. However, there is a limitation regarding its use due to the moisture sensitivity of perovskites and the insulating property of PSS. We aimed to overcome this limitation by using a water-free and PSS-free PEDOT-based hole transport layer for low bandgap single-junction perovskite solar cells (Figure PP3.1.6(a)) and in perovskite-perovskite tandems (Mahmud et al. 2023).

We successfully developed a suitable hole transport layer (HTL). After combining the high bandgap cell from Mahmud et al. 2022 with this new HTL, the champion monolithic perovskite-perovskite tandem produces an efficiency of 21.5% and a fill factor of 85.8%, the latter value was highest for any perovskite-based double-junction tandems at the time of reporting (Figure PP3.1.4(b)). Results of photoelectron spectroscopy, Fourier-transform infrared spectroscopy, and conductive atomic force microscopy reveal evidence of enhanced conductivity of water-free and PSS-free PEDOT compared to its conventional counterpart (not shown here but can be found in Mahmud et al. 2023). The use of water-free and PSS-free PEDOT also eliminates decomposition of the high bandgap sub-cell with its interfacing layer stack in a tandem that otherwise occurs with conventional PEDOT:PSS (Figure PP3.1.4(d, e)). This leads to enhanced reproducibility of perovskite-perovskite tandems (Figure PP3.1.4(c)).

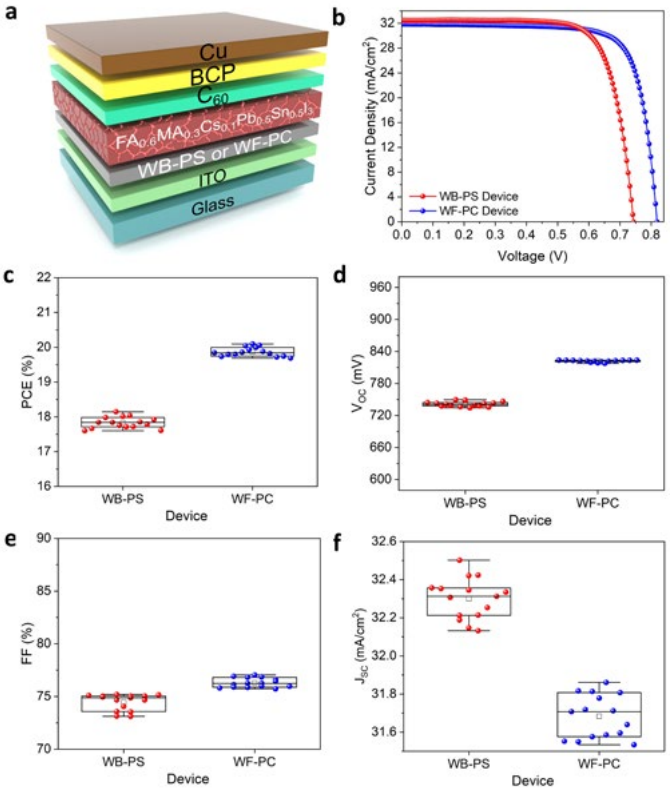

Figure PP3.1.4: (a) Schematic diagram showing the structure for a p-i-n low bandgap single-junction Sn–Pb (1.27 eV) perovskite solar cell. (b) J-V curves of the champion cells under reverse scan. Distributions of (c) PCE, (d) V_{OC}, (e) FF, and (f) current density J_{SC} of WB-PS- and WF-PC-based cells (15 cells of each kind). Figures from Mahmud et al. 2023.

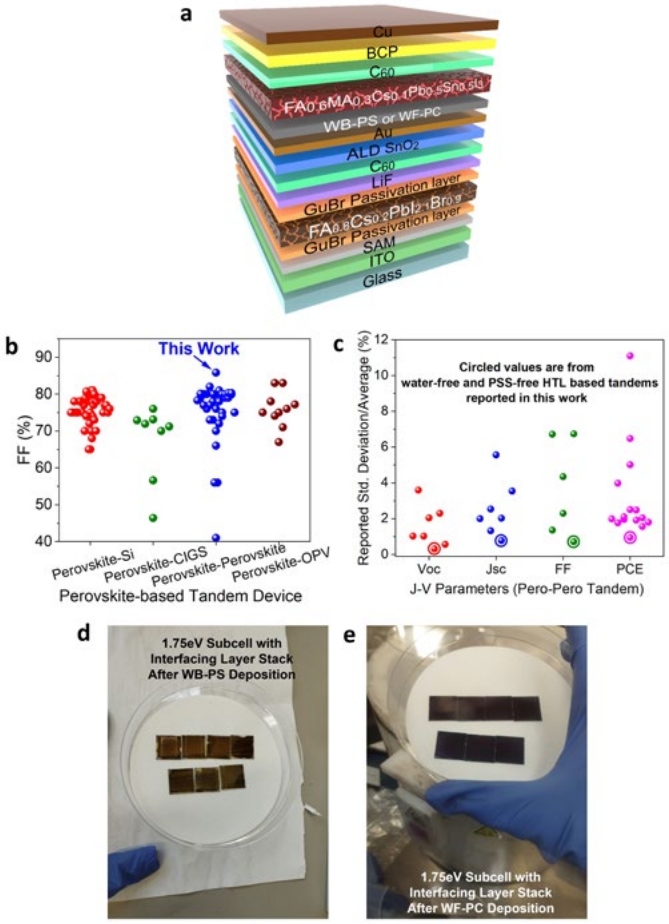

Figure PP3.1.5: (a) Schematic diagram showing the cell structure for a p-i-n perovskite-perovskite tandem solar cell consisting of low bandgap (1.27 eV) Sn–Pb-based and high bandgap (1.75 eV) Pb-based perovskite sub-cells. (b) Fill factors reported in peer-reviewed articles on perovskite-based tandem (perovskite-Si, perovskite-CIGS, perovskite-perovskite and perovskite-OPV) solar cells at the time of the reporting of Mahmud et al. 20232). (c) Ratios of standard deviation values to average values for cell parameters indicating their "spreads" for perovskite-perovskite tandems reported in peer-reviewed articles at the time of the reporting of Mahmud et al. 2023. All parameters of our WF-PC cells have narrower distributions than those reported showing high reproducibility. Photographs showing a 1.75 eV sub-cell with interfacing layer stack after (d) WBPS or (e) WF-PC deposition. Degradation can be seen on the sub-cell after (d) WB-PS deposition but not after (e) WF-PC deposition. Figures from Mahmud et al. 2023.

Highlights

- Developed a water-free hole transport layer to facilitate all-perovskite tandem cell fabrication.
- Successfully implemented the new HTL to fabricate all-perovskite tandems with an efficiency of 21.5% and a fill factor of nearly 86%, the best reported to date.

D.Phase-stable, high bandgap perovskite cells for monolithic tandems through A-site cation engineering

A significant challenge is adjusting the perovskite bandgap from 1.5 eV to the optimal 1.7 eV for its tandem application, given the fixed 1.1 eV bandgap of silicon. Efforts to increase the bandgap of perovskite by substituting 20%–40% iodine with bromine have faced issues of photo-instability due to the "halide phase segregation" under light exposure, thereby hindering its applications at the industrial level.

To fundamentally avoid halide phase segregation, we successfully developed a pure iodide wide bandgap perovskite, $APbI_3$, solar cell with a bandgap of 1.66 eV through A-site cation engineering via a solution-based sequential deposition method.

Our preliminary results in Figure PP3.2.6 show that the photoluminescence (PL) spectrum of the pure iodide wide bandgap perovskite film remains unchanged after exposure to ambient conditions with approximately 50% humidity for 15 hours, signifying excellent stability. In contrast, the PL spectrum of the mixed-halide wide bandgap perovskite film exhibits a clear red shift and enlarges full width at half maximum, providing clear evidence of phase segregation in the mixed-halide perovskite. The up-to-date Br-free perovskite with the n-i-p (ITO/SnO2/Perovskite/Spiro-OMeTAD/Au) cell architecture demonstrated an efficiency of over 17%.

Highlights

- Developed a bromide-free perovskite absorber with a bandgap of 1.66 eV; its application in solar cells demonstrated an efficiency of 17.1%.
- The moisture stability of the bromide-free perovskite thin film demonstrated better performance than that of the conventional mixed-halide wide bandgap perovskite.

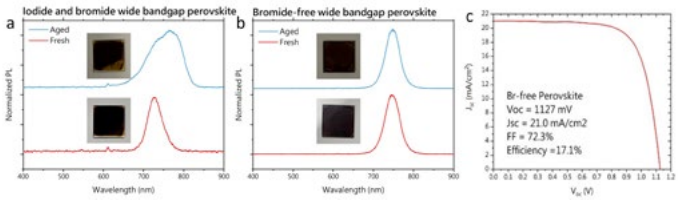

Figure PP3.1.6: PL spectrum changes exposure to ambient conditions with approximately 50% humidity for 15 hours of (a) pure iodide and (b) mixed-halide wide bandgap perovskite; and (c) the I-V curve of Br-free perovskite solar cells with 1.66 eV.

References

Duong, T., Nguyen, T., Huang, K. et al. (2023). Bulk Incorporation with 4-Methylphenethylammonium Chloride for Efficient and Stable Methylammonium-Free Perovskite and Perovskite-Silicon Tandem Solar Cells. Advanced Energy Materials, 2203607.

Ho-Baillie, A. W. Y., Zheng, J., Mahmud, M. A., Ma, F.-J., McKenzie, D. R. & Green, M. A. (2021). Recent progress and future prospects of perovskite tandem solar cells. Applied Physics Reviews 8 (4), 041307.

Mahmud, M. A., Zheng, J., Tang, S., Wang, G., Bing, J., Bui, A. D., Qu, J., Yang, L., Liao, C., Chen, H., Bremner, S. P., Nguyen, H. T., Cairney, J. & Ho-Baillie, A. W. Y. (2022). Cation-Diffusion-Based Simultaneous Bulk and Surface Passivations for High Bandgap Inverted Perovskite Solar Cell Producing Record Fill Factor and Efficiency. Advanced Energy Materials 12 (36), 2201672.

Mahmud, M. A., Zheng, J., Tang, S., Liao, C., Wang, G., Bing, J., Leung, T. L., Bui, A. D., Chen, H., Yi, J., Bremner, S. P., Nguyen, H. T. & Ho-Baillie, A. W. Y. (2023). Water-Free, Conductive Hole Transport Layer for Reproducible Perovskite–Perovskite Tandems with Record Fill Factor. ACS Energy Letters 8, 21-30.

E.Solution-less large-area perovskite deposition using CVD

The CSIRO-led perovskite CVD project is aimed at demonstrating a conformal, uniform and physically consistent (over large area 100 cm^2) perovskite layer using a novel (CSIRO patented) CVD process. The incorporation of the perovskite into a high efficiency perovskite-silicon tandem device is the long-term objective.

In the last 12 months a new iteration of the CVD reactor was designed to operate at sub-ambient pressures following the identification of chemical incompatibilities between materials in the ambient pressure system. The initial inverted structure (p-i-n) using an organic HTL (2PACz) showed limited stability and delamination during CVD and a more stable inorganic HTL (SnO_2) required reversion to the normal (n-i-p) structure to eliminate intrinsic stability of the interface. Observation of crystalline efflorescence in the intermediate Pb acetate intermediate was addressed with the use of an improved industrial gas mixture as carrier gas. The optimisation of a Pb seed layer thickness was also able to demonstrate control of starting film thickness 7 nm through to 60 nm, with an optimum chosen at 20 nm to limit side-reaction and efflorescence. Further optimisations included amount and chemical precursors in high temperature sublimators, control of chamber and substrate operating temperatures and introduction of rapid substrate cooling. Demonstration of uniformity over a large area (64 cm^2) with spatial uniformity and up to 144 cm^2 for material crystalline consistency was achieved.

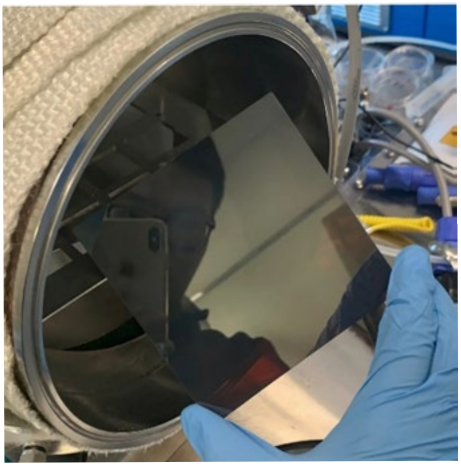

Figure 3.1.7: Example of large-area CVD deposition of perovskite using FAI precursors on a 12 cm × 12 cm substrate.

Highlights

- Materials deposition sequence engineered and validated with process optimisation demonstrated for reactor systems with at least 10 films with +/- 10% crystalline uniformity prepared on 3 × 3 cm ITO substrates with masked area of > 2 cm^2.
- Process optimised for scale-up with process scalability demonstrated with 20 x factor increase and at least 10 films with +/- 10% spatial uniformity prepared on 8 × 8 cm ITO substrates with masked area of 64 cm^2.

PP3.2 III-V ON SILICON TANDEMS

Aims

Four-terminal III-V / silicon tandem cells offer the potential for very high efficiency. The removal of the requirement for current matching in the two sub-cells in the four-terminal architecture enables thorough optimisation of each sub-cell. However, managing optical losses in four-terminal devices becomes critical, due to the presence of many interfaces which can act as scattering layers.

These intermediate scattering layers impact the generated currents, photon recycling (PR), as well as luminescent coupling (LC) in the device. Detailed optical modelling is required to understand the behaviour of these structures and fully optimise the individual layers. The III-V/Si efficiency can be simulated using expressions that involve a simplified and idealised intermediate layer structure but cannot accurately reflect its actual performance. This work aims to establish a systematic optical model for III-V/Si tandem cells with complicated intermediate layers.

Progress

A.A modelling framework to quantify the intermediate layer impact in III–V/Si multi-junction solar cells

A device-level optical model integrating a 3D nanostructure intermediate layer has been developed for III-V/Si tandem solar cells. This model allows the design of the intermediate layer by investigating its impact on the photocurrent of the individual junction, the photon recycling (PR), luminescent coupling (LC), and thus on the overall device performance.

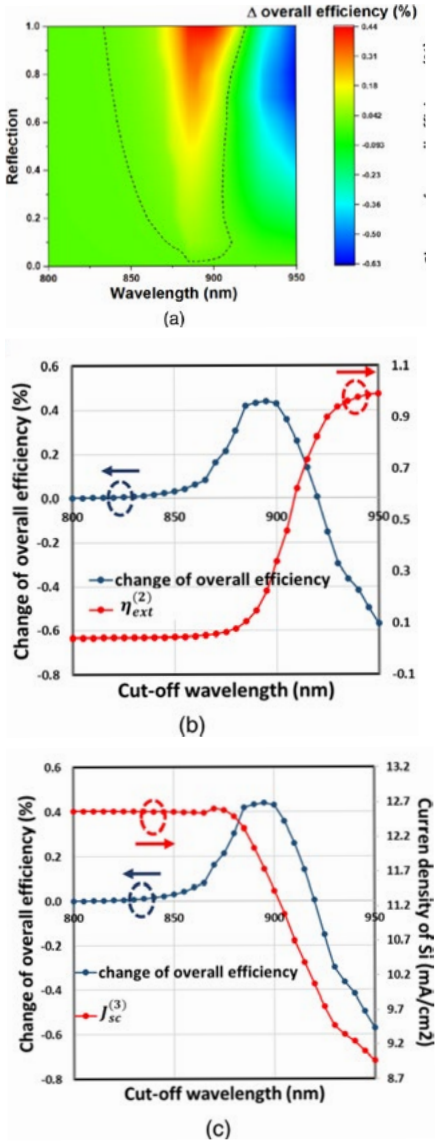

Figure PP3.2.1: (a) The change in the GaInP/GaAs//Si cells efficiency as a function of the cut-off wavelength and the reflection of the ideal reflector. The area framed by the black dash line indicates enhanced overall efficiency. (b) The change of the overall efficiency and next on the function of the λR , with the integration of the ideal reflector (R = 1). (c) The change of the overall efficiency and J_{SC} of the Si in the function of the λR , with the integration of the ideal reflector (R = 1).

Furthermore, this model provides a guide for introducing the more sophisticated intermediate layer in tandem cells. A three-dimensional metallic nanocylinder array is designed as the intermediate layer to improve device performance. With the model, high performance tandem cells can be designed and optimised by quantifying the impact of PR and LC on device parameters. This efficiency improvement can be further promoted by suppressing the parasitic absorption within the nanostructured intermediate layer, which weakens the LC effect. This theoretical model may also be applicable to other tandem cells, such as perovskite/Si and chalcogenide/Si tandem cells, guiding the design of the intermediate layer for the ultimate cell performance improvement.

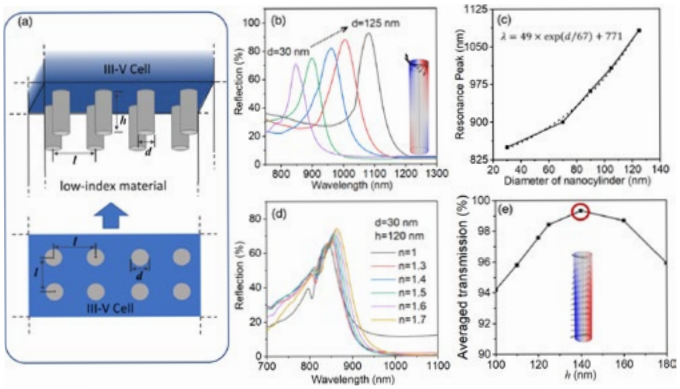

Figure PP3.2.2: (a) Structure of Ag nanocylinder under III-V top cell. (b) Reflection spectra with different diameters (30 nm, 70 nm, 90 nm, 105 nm, 125 nm). The inset shows the distribution of electric charge and electric field lines of the nanocylinder. (c) Dependency of resonance peak location on the nanocylinder diameter. (d) Reflection spectra of the nanocylinder surrounded by dielectrics with different refractive indices. (e) Averaged transmission at long-wavelength (950 nm–1300 nm) of nanocylinders with different heights. The inset shows the distribution of electric charge and electric field lines of the nanocylinder.

Highlights

- Developed a sophisticated optical model for four-terminal III-V/Si cells that incorporate LC and PR effects.
- Demonstrated the use of the model to achieve significant performance gains through the implementation of advanced intermediate scattering layers

References

Li, C., Pusch, A., Liu, Z., Zhang, P., Huang, J., Guo, H., Zhang, W., Wang, H., Gao, P., Sun, Q., Ekins-Daukes, N. & Hao, X. (2023). A modeling framework to quantify the intermediate layer impact in III−V//Si multijunction solar cells. Japanese Journal of Applied Physics 62, SK1053.

PP3.3 CHALCOGENIDE ON SILICON TANDEMS

Aims

$Sb_2(S,Se)_3$ has emerged as a promising new photovoltaic (PV) material for tandem applications for its high absorption coefficient, tunable bandgap, and non-toxic and Earth-abundant constituents. However, high-efficiency $Sb_2(S,Se)_3$ solar cells exclusively employ monofacial architectures, leaving a considerable gap towards large-scale application. We aim to develop bifacial and semitransparent $Sb_2(S,Se)_3$ solar cells and demonstrate their application in tandem solar cells.

Progress

A.Bifacial and semitransparent $Sb_2(S,Se)_3$ solar cells for tandem photovoltaic applications

Semitransparent cells with a device architecture of FTO/CdS/$Sb_2(S,Se)_3$/MnS/ITO were developed in this work (Qian et al. 2023). The chemical bath deposition (CBD) and hydrothermal method were respectively used for the deposition of the CdS electron transport layer (ETL) and $Sb_2(S,Se)_3$ absorber layer as described in our previous work. The obtained $Sb_2(S,Se)_3$ absorber layer is often significantly thinner than that deposited using the vapour thermal deposition (VTD) or rapid thermal evaporation (RTP) methods (350 nm vs 1 μm), resulting in a fully depleted absorber layer. MnS was employed as the HTL for its competitive performance, excellent stability and most importantly, great tolerance to the subsequent sputtering process compared with spiro-OMeTAD that is commonly used in high efficiency superstrate-configuration $Sb_2(S,Se)_3$ solar cells. The ITO layer then grew on top of MnS, serving as a back contact in our semitransparent cell.

All the fabrication processes prior to ITO or Au deposition were controlled to be identical for eliminating variates when comparing $Sb_2(S,Se)_3$ semitransparent and monofacial cells in our work. All layers, particularly MnS and ITO layers, have good coverage and thickness uniformity, which satisfies the technical requirements of large-area and upscaling manufacturing.

The bifacial and semitransparent $Sb_2(S,Se)_3$ solar cells developed in our work, with a sandwich structure of TCO/n-i-p architecture/TCO provide a great bifaciality with the aid of an ultra-thin fully depleted $Sb_2(S,Se)_3$ absorber layer. The exceptional transmittance of the resultant solar cell at long wavelengths enables its application in a pioneering four-terminal $Sb_2(S,Se)_3$/Si tandem with an 11.66% PCE (Figure PP3.3.1).

This finding highlights the significant potential of $Sb_2(S,Se)_3$ in tandem solar cell applications due to their adjustable bandgap, upscalable deposition methods, semitransparent properties, and ability to effectively absorb non-vertical incident light.

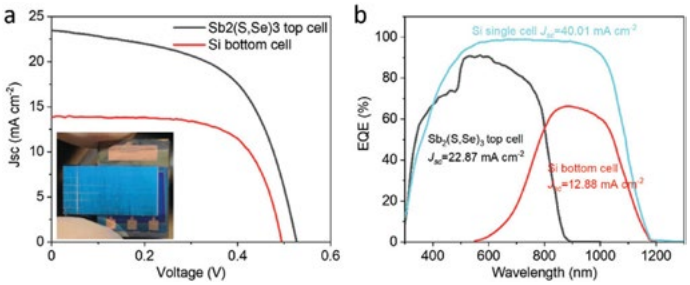

Figure PP3.3.1: (a) J-V curves of the $Sb_2(S,Se)_3$ semitransparent top cell and Si bottom cell. (b) EQE curves of the $Sb_2(S,Se)_3$ semitransparent top cell, Si bottom cell covered by the $Sb_2(S,Se)_3$ semitransparent top cell, and Si cell alone.

Highlights

- Developed semitransparent, upscalable $Sb_2(S,Se)_3$ solar cells suitable for use in four-terminal tandem configuration.
- Demonstrated a promising 11.66% efficiency for a $Sb_2(S,Se)_3$ / silicon tandem cell.

References

Qian, C., Sun, K., Cong, J., Cai, H., Huang, J., Li, C., Cao, R., Liu, Z., Green, M., Hoex, B., Chen, T. & Hao, X. (2023). Bifacial and Semitransparent Sb2(S,Se)3 Solar Cells for Single-Junction and Tandem Photovoltaic Applications. Advanced Materials 35, 2303936.

Zhang, P., Li, C., He, M., Liu, Z. & Hao, X. The Intermediate Connection of Subcells in Si-based Tandem Solar Cells. Small Methods 2300432. *https://doi.org/10.1002/smtd.202300432.*

PP3.4 TUNED BOTTOM SILICON DEVICES

Aims

The current baseline silicon bottom cells used in monolithic perovskite-silicon tandems have polished surfaces. As a result, tandem cells have sacrificed the J_{sc} due to less optimal light trapping conditions on the bottom Si-cells. In this work, we are developing textured surfaces compatible with the top perovskite layers. However, the passivation effectiveness of doped poly-Si contacts is compromised when incorporating doped-poly-Si layers on the textured surfaces. Therefore, rounding off vertices of pyramid and performing atomic hydrogenation using an AlO_x/SiN_x stack will perform to improve the poly-Si passivation on the textured surfaces.

Progress

A.Highly controllable sub-micrometer texturing method suitable for monolithic perovskite-silicon tandem cells

A highly reproducible metal-free silicon texturing process using a Tetramethylammonium (TMAH) and MonoTex solution is optimised to achieve a precisely controlled pyramid height and achieve relatively low overall reflectance (less than 15%) in the main tandem response AM1.5G wavelength range (300–1100 nm), as shown in Figure PP.3.4.1. The preliminary simulations and experimental evidence suggest that a pyramid height of 500–700 nm is the optimal for the tandem cells.

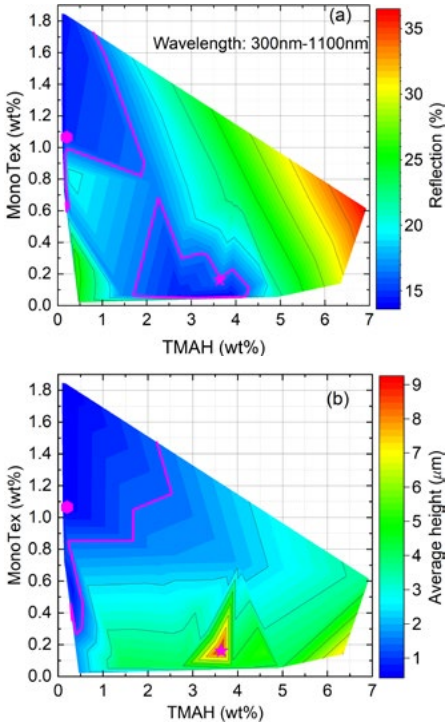

Figure PP3.4.1: Contour plots of the TMAH and MonoTex weight ratios used in different recipes achieving (a) reflection percentage integrated over 300–1100 nm range; and (b) average pyramid height.

The rounding of sharp edges, peaks, and valleys on standard pyramid structures can improve passivation quality without significant loss in optical benefits. The rounding off of the vertices of textured surfaces is achieved by an etch-back (EB) process using an alkaline solution for different durations, as shown in Figure PP.3.4.2.

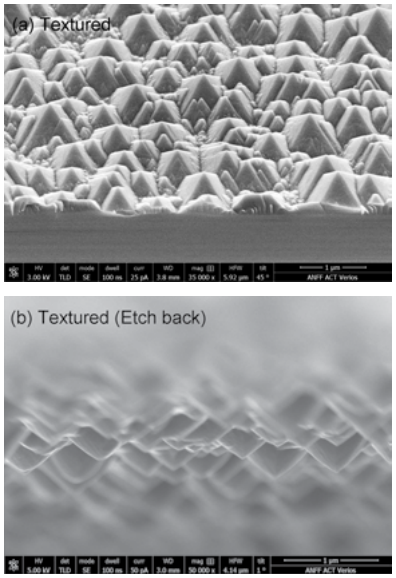

Figure PP3.4.2: SEM images of the (a) optimal sub-micron control samples; and (b) etch-back (rounded) samples.

Further, the passivation of doped poly-Si (p^+ and n^+) were tested on the symmetric lifetime samples with different surface morphology. The iV_{oc} of these samples were compared before and after atomic hydrogenation, as shown in Figure PP 3.4.3. The results clearly show that after atomic hydrogenation, the iV_{oc} of n^+ poly-Si contact passivated samples are similar on both textured surfaces (725 mV) and planar surfaces (725 mV). However, the iV_{oc} is still lower than 20 mV on the textured surfaces (699 mV) compared to planar (722 mV) when passivated by p+ poly-Si contacts.

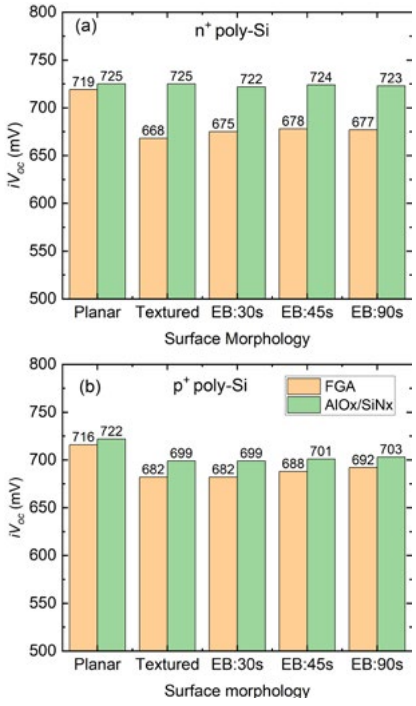

Figure PP3.4.3: Evolution of implied open-circuit voltages at one-sun conditions for n+ poly-Si and p+ poly-Si passivated samples on planar, textured and etch-back samples.

Highlights

- Developed a new texturing process that results in features of reduced height, compatible with monolithic perovskite-silicon tandems.

References

Wei, W., Basnet, R., Phang, P., Hou, Y., Macdonald, D., & Shen, H., Highly controllable sub-micrometer texturing method suitable for monolithic perovskite-silicon tandem cells. (under preparation).

PP3.5 CHARACTERISATION

Aims

The characterisation of tandem cells, particularly monolithic tandems, poses unique challenges due to the fact that a tandem cell consists of two cells connected in a series and physically inseparable from each other. Such cells also put significantly higher requirements on accurate solar cell testing and the use of accurate and uniform spectra, since the current response from each sub-cell depends intimately on the solar spectrum and intensity. The ACAP partners, led by CSIRO, are carrying out pioneering work on improved characterisation methods.

Progress in multi-junction testing and accreditation at Solar PV Performance Lab

CSIRO has continued activities across a number of areas to stay at the forefront of measurement and characterisation of emerging perovskite and perovskite-silicon devices and positioning for the next generation of commercial silicon modules.

Assessing encapsulation for durability/reliability of perovskite on silicon

A short study investigated the correlation of Ca resistance to optical measurements over time as an indicator for barrier effectiveness. The study developed protocols aligned with standard conditions for thermal cycling, damp heat, dry heat, photostability and incorporated an in situ kinetic imaging. The materials assessed included a top-cell transparent barrier and a dense edge-seal barrier for PVK-Si tandems.

Monolithic perovskite-on-silicon tandem solar cell historical data application

CSIRO Early Research Career (CERC) Fellow Bruno Vicari Stefani developed an interactive data application for perovskite-on-silicon solar cells. The application is designed to be an educational tool for students and researchers working in the field. It provides information regarding the design and performance of monolithic devices published in the literature. The main window displays the evolution of a given solar technology's conversion efficiency over the years, while the colour of the markers indicates the value of the selected solar cell parameter (e.g. open-circuit voltage). The marker size provides a qualitative representation of device area. Hovering over data points highlights the current-voltage characteristics and area of each device. Selecting a data point displays the silicon, perovskite and associated transport layer materials used in device fabrication and the corresponding reference. A side window displays the short-circuit current density of the perovskite (y-axis) and silicon (x-axis) solar cells, which allows the user to identify the current-limiting sub-cell in each device. The rear side menu allows the user to filter the results on display based on (1) perovskite polarity, (2) silicon doping type, (3) inter-layer, (4) perovskite hole transport layer and (5) perovskite electron transport layer. The measurement types and certification status can be selected via the radio items on the side menu. The data application can be accessed at http://pvdata.csiro.au.

The data application forms part of the supplementary information of the article "Design considerations for the bottom cell in perovskite/silicon tandems: a terawatt scalability perspective", published in Energy and Environmental Sciences. The article aims to bridge the communication gap between the perovskite and silicon solar cell communities and accelerate the development of sustainable and cost-effective silicon bottom cells for tandem applications in the terawatt scale.

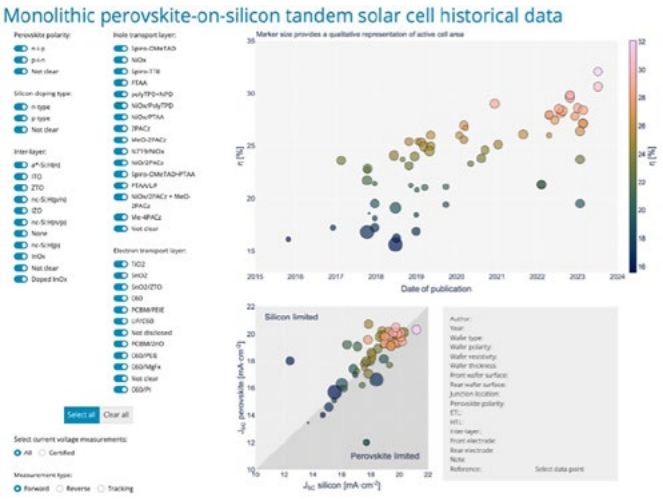

Figure 3.5.1: Interface of the data application, available at https://pvdata.csiro.au/.

Reference

Wright, M., Vicari Stefani, B., Jones, T. W., Hallam, B., Soeriyadi, A., Wang, L., Altermatt, P., Snaith, H. J., Wilson, G. J. & Bonilla, R. S. (2023). Design considerations for the bottom cell in perovskite/silicon tandems: a terawatt scalability perspective. Energy & Environmental Science 16, 4164-4190. https://doi.org/10.1039/D3EE00952A.

PP3.6 LABORATORY CELL AND MODULE PERFORMANCE TESTING

Tandem solar cells present new challenges in measurement and testing that reflect the diversity of material combinations and device architectures.

Methodologies towards multi-junction cell measurement accreditation

The year 2023 has seen the development of robust methods for durability and stability assessment (see above) and continued development of measurement protocols necessary to meet technical requirements for assessment of multi-junction cells. This has included uncertainty estimates, covariance analysis, metastability influence and culminated in proficiency testing via two round robins on perovskite cells. The studies have enabled implementation of an improved spectral-response capability for tandem cells, measurements performed for 10 ACAP participants, and an iterative design of standardised non-destructive test jigs to suit multiple research groups in Australia.

CSIRO PV Outdoor Research Facility (at Newcastle Energy Centre)

CSIRO is midway through an upgrade to the Photovoltaic Outdoor Research Facility, designed to make collaboration easier. It is anticipated ACAP partners will be able to put devices on the system and access detailed data themselves via a web interface. Improved capability for large-area modules (both indoor and outdoor) is anticipated to come online in mid-2024.

PVPL participation in bi-facial module round robin

The year 2023 saw the largest international round robin measurement campaign for PV ever attempted involving 24 PV testing laboratories in 12 countries, including key accredited labs. The activities had been in planning for over 12 months and took nearly two years for full execution, coordinated by SERIS (Singapore). The study involved eight commercial-scale modules (two monofacial and six bifacial) and required 24 parameters (per module) to be measured and reported. The aim was to test the suitability of the new IEC TS 60904-1-2 method and its integration into accredited measurement lab protocols.

Future Work

The ACAP partners have identified several areas of particular importance to accelerate the development of commercial tandem technology.

A.Accurate measurement of large-area tandem cells

Tandem cell measurements are highly complex. Tandem cells pose several additional challenges compared with single-junction cells. Perhaps most importantly, because tandem cells generally consist of two individual cells of different materials that are stacked on top of each other and connected in a series, the output of the tandem cell is more sensitive to spectral mismatch than single-junction cells. In addition, where the top cell is a perovskite cell, the challenges associated with the measurement of single-junction perovskite cells – in particular due to cell hysteresis – are inherited. Currently, accurate measurements of tandem devices are mainly confined to areas of ~1 cm^2.

The partners, led by CSIRO, will work to develop the capability to be able to measure tandem devices with significantly larger areas. This capability is critical given current efforts to develop commercial tandem cells, which invariably require upscaling to larger cell sizes.

B.Stability testing of perovskite-based solar cells, including perovskite tandems

The stability of perovskite cells, and therefore also of perovskite-based tandems, is widely recognised to be still insufficient for commercial application.

Typically, the IEC 61215 standard serves as the industry benchmark for assessing stability. However, the tests described in the standard are carried out on complete modules. In addition, there is strong evidence that the tests in the standard are not sufficient to establish with confidence whether or not a perovskite-based module will be stable for 20 years or more in the field. This is because the tests do not expose the cells or modules to several important stressors, which appear to result in degradation in perovskite cells, such as the changes in electrical bias within the cell as a result of day/night cycles, and the synergistic effects of heat and light.

To date, the results of stability tests reported on perovskite cells in the research literature suffer from a lack of standardisation. Tests use a wide range of temperatures, ambients and exposure times. Some cells are encapsulated while others are not. The lack of standardisation, and the often tenuous connection between testing conditions and conditions that are likely to represent a reasonable equivalence to 20 years of outdoor exposure, renders much of the reported stability data nearly useless. This is despite the fact that detailed protocols for the comprehensive and standardised stability assessment of perovskite cells have been developed.

One significant hurdle that may be preventing the more widespread adoption of standardised and appropriate stability tests is the fact that stability tests are often time and resource intensive, making it prohibitive to thoroughly test more than a very small number of cells. Proper stability tests require a controlled atmosphere, accurate temperature control, a well-calibrated, one-sun light source, the ability to cycle cells through a wide range of temperatures and encapsulation. Stability tests require long-term exposure of cells, for times of up to 1000 hours or more.

Another significant challenge is the fact that it is not clear which set of stability tests will ultimately replace IEC61215 for the testing of perovskite-based modules. For example, if it is necessary to incorporate light cycling into the test protocol, then the question arises how long the light on and light off cycles need to be, and how many such cycles will be sufficient for the test.

The ACAP partners will aim to address these challenges in a number of ways. First, we will aim to significantly improve the understanding of the physics of the degradation mechanisms underlying various stressors. Such understanding is necessary to enable the development of suitable test standards for perovskite-based cells. Second, we will seek to develop stability tests that are less resource intensive and provide a good initial assessment of stability. Such tests could help to screen out many materials and cells that are clearly not suitable because they are insufficiently stable. This will allow research efforts to be better focused on materials and cell architectures that display promising stability.

C.Novel hole transport materials

The hole transport layer (HTL) is a critical functional layer in perovskite solar cells. It has two main functions: to minimise recombination of light-generated carriers at the perovskite-HTL interface, and to facilitate the transport of holes across the perovskite-HTL interface. One factor holding back the limitation of perovskite-silicon tandems is the current lack of suitable HTLs for perovskite cells in the n-i-p configuration, where the HTL faces the sun.

The ACAP partners will develop novel hole transport materials and share them among ACAP nodes for further assessment and development, as well as disseminating the results to the wider research community to remove this bottleneck on perovskite tandem cell development. .

PP4
DEVICE TO MODULE

OVERVIEW

The Device to Module Program Package focuses on the opportunity to increase performance and reduce cost by optimising the device metallisation, interconnection and module fabrication within a more holistic solar module production framework.
Device-to-module research can deliver benefits at the cell-design level, reducing the use of materials such as silver, enabling large wafers and module sizes, new cell interconnection technologies, light trapping and manufacturing process efficiencies.
The learning gained from the growing maturity of the silicon PV industry can be applied to facilitate a faster transition of new, emerging materials and devices from the research phase to pilot-scale production, with relevance to tandem devices.
Explore the research programs being undertaken in this area:

PP4.1 Device Metallisation

PP4.2 Holistic Device-to-Module Modelling

PP4.3 Module Durability

PP4.5 Advanced Outdoor Testing

PP4.1 DEVICE METALLISATION

PP4.1.1 Advanced Screen Printing

UNSW Team
A/Prof. Brett Hallam, Prof. Bram Hoex, Dr Yuchao Zhang, Dr Li Wang, Dr Sisi Wang, Dr Yuan-Chih Chang, Dr Zhenyu Sun, Dr Ran Chen, Dr Catherine Chan

Partners
Trina Solar
Talesun Solar
Jolywood Solar
ORISolar
Hunan Redsun Solar
Changzhou Fusion New Materials
Toyo Aluminium K.K.

Funding Support
ARENA, ACAP, UNSW

Aims

As the world has passed 1 TW of solar installation and the PV industry is fast approaching a TW-scale annual production capacity, PV technologies are expected to play a central role in future decarbonisation and clean energy transition. However, one pressing issue for industrial silicon solar cells is high silver consumption in existing screen-printed contacts. This not only contributes significantly to the manufacturing costs of solar cells but also imposes great challenges to establishing TW-scale production without depleting the global silver supply. This project builds on previous work and knowledge to develop a series of advanced screen-printing technologies to greatly reduce silver consumption of various solar cell technologies, such as PERC, TOPCon and SHJ, while maintaining compatibility with existing industrial screen-printing and interconnection methods. The target for the end of this project is to achieve ultra-low silver consumption of less than 2 mgW^{-1}, enabling sustainable manufacturing of silicon solar cells on an upcoming TW-scale.

Progress

A comprehensive analysis of material consumption in existing industrial silicon solar cell technologies has been conducted in this work (Zhang et al. 2021). We identified the consumption of scarce metals, including silver, indium and bismuth, as a critical concern to the PV industry on a TW manufacturing scale. To enable a 3 TW annual production capacity, the silver consumption associated with screen-printed contacts must be reduced to less than 2 mgW^{-1} for any solar cell technologies, which is well below the average consumption level in current industrial silicon solar cells (see Figure PP4.1.1). Although ITRPV projections expect a 50–60% reduction in silver usage over the coming decade, by 2031, the projected silver consumption of industrial mainstream PERC, TOPCon and SHJ solar cells will still be well above the 2 mgW^{-1} target at 8.5, 13.8 and 14.3 mgW^{-1}, respectively. This highlights the need for more advancements and innovation in screen-printing technology to reduce silver consumption for sustainable manufacturing of silicon solar cells on an upcoming TW scale.

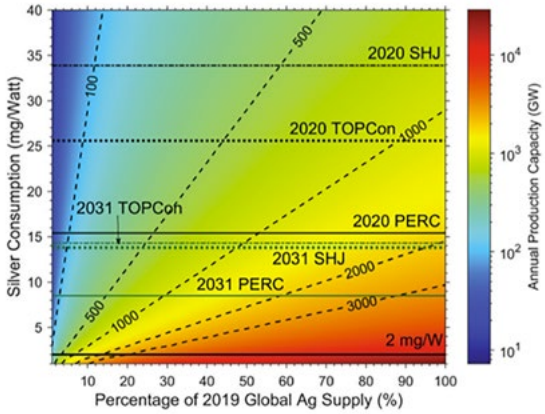

Figure PP4.1.1: Allowable annual production capacity as a function of the percentage of 2019 global silver supply available to the PV industry and silver consumption in mg/W for PERC, TOPCon and SHJ cells.

In 2023, we successfully demonstrated a silver-lean hybrid screen-printing contact design, which consists of a thin layer of plated copper on top of screen-printed silver fingers with reduced printed height (Chang et al. 2023). A cross-sectional scanning electron microscope (SEM) image of such contacts is shown in Figure

PP4.1.2. In conventional screen-printed contacts, a major drawback of reducing silver consumption is reduced finger conductivity, which subsequently translates into losses in fill factor and efficiency of solar cells. However, with our silver-lean hybrid screen-printing design, plated thin layers of copper will provide additional conductivity to fingers, allowing reductions in silver consumption of screen-printed fingers without compromising the performance of solar cells. We have achieved more than 40% reductions in silver consumption, while the finger line resistance was halved at the same time owing to the superior conductivity of plated copper layers. Another key advantage of our design is the use of screen-printed silver layers as seed layers for subsequent plating, which eliminates the need for a dedicated patterning step in the process. Such a self-aligned patterning-free process will significantly lower the capital expenditure and technical barriers of plating in mass production environments.

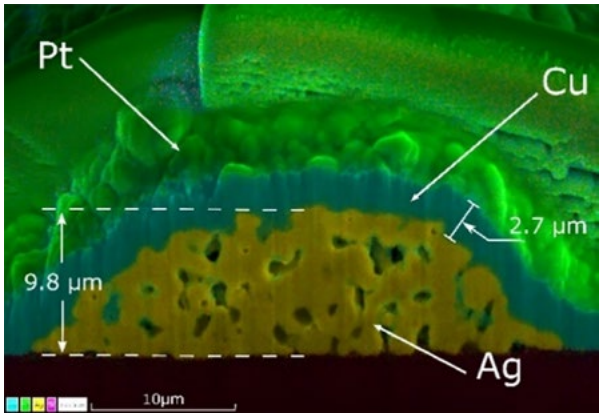

Figure PP4.1.2: Cross-sectional SEM-EDS image of a hybrid screen-printed finger.

To further reduce silver consumption in industrial solar cells, we have developed an ultra-low silver screen-printed contact relying on the use of an innovative pattern design and silver-free paste materials. Our design decouples the roles of contact formation and electrical conduction in finger regions, which allows the use of a wide range of silver-lean and silver-free paste materials in fingers without endangering the formation of high quality metal/Si interfaces on the silicon surface. By implementing such a design on the rear side of TOPCon solar cells, we have demonstrated over 40% reductions in silver consumption from 15.6 to 9.6 mgW^{-1} on large-area (166 × 166 mm) devices. In the meantime, a high efficiency of 23.5% has been achieved (see Figure PP4.1.3), which is comparable to the efficiency of reference cells fabricated with conventional screen-printed contacts. With further optimisations in the screen-printing process and implementation of such a design on both sides of solar cells, we expect the silver consumption of industrial TOPCon solar cells to be reduced to an ultra-low level of 2 mgW^{-1}. These results will be published in 2024. To accelerate technology development and deployment, a consortium with leading PERC, TOPCon and SHJ cell manufacturers and paste companies has been formulated in this project. Our silver-lean metallisation design is currently being evaluated and tested by several cell manufacturers on their R&D or pilot lines.

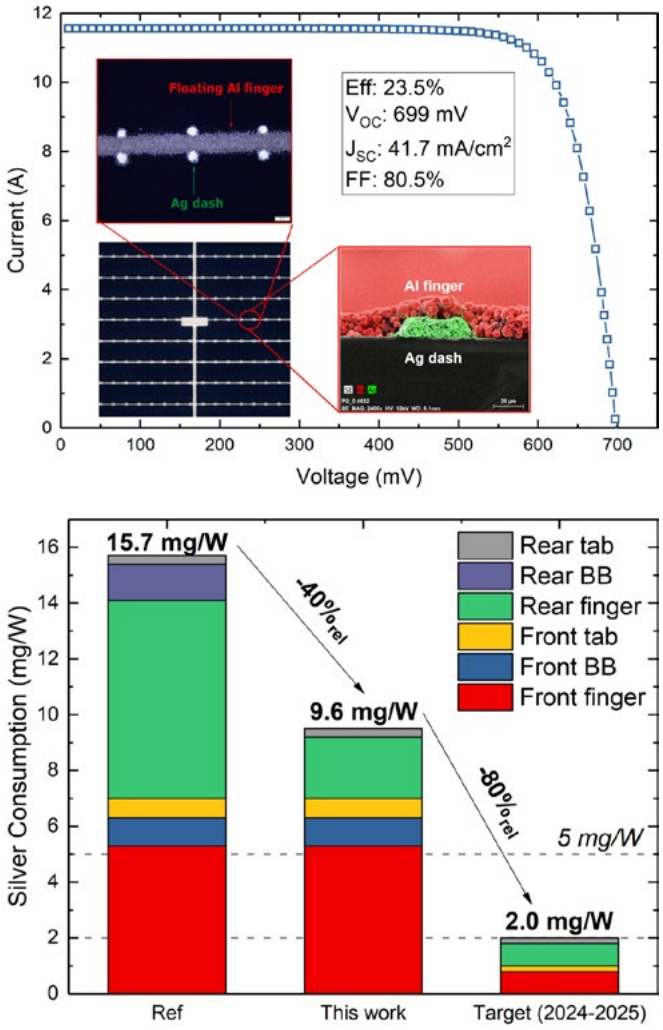

Figure PP4.1.3: Images and silver consumption of screen-printed silver-lean solar cells fabricated in this work (inset), measured IV results and (b) silver consumption.

References

Chang, Y.-C., Zhang, Y., Wang, L., Wang, H., Huang, C.-Y., Chen, R., Chan, C. & Hallam, B. (2023). Silver-lean Metallization and Hybrid Contacts via Plating on Screen-Printed Metal for Silicon Solar Cells Manufacturing. Progress in Photovoltaics: Research and Applications. (Under Review)

Zhang, Y., Kim, M., Wang, L., Verlinden, P. & Hallam, B. (2021). Design considerations for multi-terawatt scale manufacturing of existing and future photovoltaic technologies: challenges and opportunities related to silver, indium and bismuth consumption. Energy & Environmental Science. Royal Society of Chemistry 14, 5587–5610.

PP4.2 HOLISTIC DEVICE-TO-MODULE MODELLING

ANU Team
Dr Marco Ernst, Mr Xuesi Liu

Partners
SunDrive Solar Pty Ltd (Australia)

Funding Support
SunDrive, ANU

Aims

The aim of this project was to investigate the feasibility of using bifacial solar modules in rooftop applications. Despite significant uptake of bifacial solar modules in utility-scale photovoltaic systems, their potential in this area remains largely unexplored. The primary objectives were to assess the energy yield gains achievable by utilising bifacial modules on rooftops, considering real-world conditions and variations. The study aimed to fill the knowledge gap in this field by conducting a thorough analysis using Monte Carlo Ray Tracing (MCRT) techniques combined with detailed electrical modelling. The specific objectives were:

Investigate viability: The central aim of this study was to investigate the feasibility of implementing bifacial solar modules on rooftops, with a focus on a representative rooftop in Canberra, Australia. The study aimed to understand the practicality and potential challenges associated with this application, taking into account factors such as rooftop reflectivity, module orientation and tilt angle.

Accurately quantify energy yield gains: Further, the project aimed to quantify the energy yield gains that can be achieved by implementing bifacial modules in rooftop scenarios. The focus was on providing a detailed understanding of the gains, considering various factors such as mounting components, system design, and environmental conditions, to offer insights relevant to real-world applications.

Address existing modelling limitations: The project aimed to overcome existing limitations associated with View Factor (VF) modelling in accurately modelling bifacial systems in rooftop applications. To achieve this, a novel approach was developed by integrating MCRT simulations with a detailed electrical model. This enabled a more accurate and comprehensive analysis of bifacial energy yield potential.

Understand impact factors: The study aimed to investigate the main factors that impact energy yield gains, such as module tilt, rooftop reflectivity, and the use of individual module-level optimisers. The study focused on understanding how these factors influence bifacial module performance in rooftop applications.

Results

The analysis conducted on a 7.2° Equator-facing pitched rooftop in Canberra, Australia, demonstrates the benefits of integrating bifacial solar modules in rooftop applications. The study revealed an energy yield gain of up to 22.6%, particularly notable when implemented on highly reflective rooftops and in scenarios without shading obstructions from mounting structures. This finding highlights the considerable potential of bifacial technology in maximising solar energy production on rooftops, as highlighted in Figure PP4.2.1.

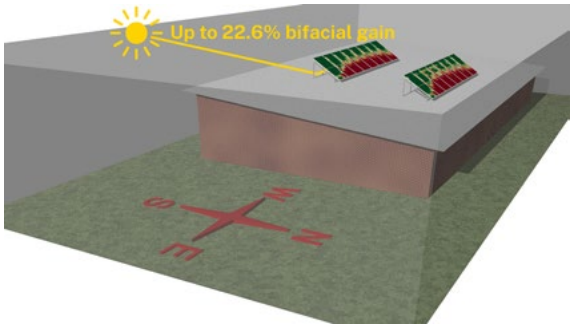

Figure PP4.2.1: Illustration of the photovoltaic system on the 7.2° pitched shed roof, highlighting the increased illumination at the rear of the module. © 2023 Marco Ernst. This figure was published in Ernst et al. (2024).

The implementation of module-level optimisation strategies is a critical aspect that influences the overall gain. It was found that fine-tuning at the module level accounted for 1.4% of the total 22.6% gain (see Figure PP4.2.2). To express this as a relative figure, module-level optimisation represents a substantial 6.6% improvement in the overall energy yield gain. This result underscores the importance of optimising individual modules to enhance the overall performance of bifacial modules on rooftops.

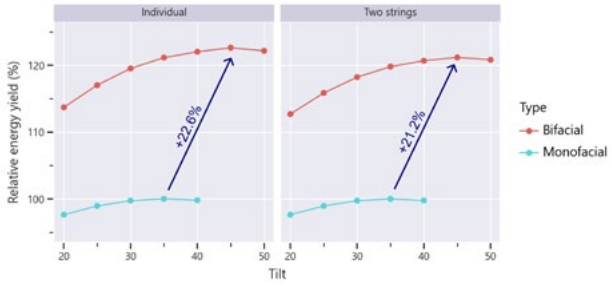

Figure PP4.2.2: Specific energy yield for a monofacial and a bifacial system as a function of module tilt angle, for systems with individually optimised modules (left) and two parallel eight-module strings (right). © 2023 Marco Ernst. This figure was published in Ernst et al. (2024).

Importantly, the study examined the effect of shading obstructions caused by mounting structures on energy yield. Figure PP4.2.3 summarises the key results. The results showed that with module-level optimisation, shading caused by mounting racking led to a significant increase of 20.3% in energy yield. Even without module-level optimisation, a substantial gain of 19.1% was achieved. These results emphasise the importance of considering mounting structure design to maximise the benefits of bifacial modules.

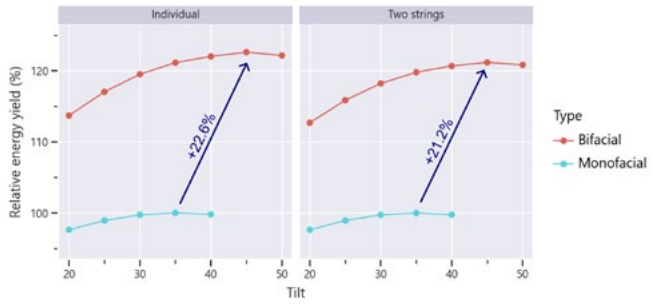

Figure PP4.2.3: Relative bifacial energy yield gain for systems with monofacial, bifacial and bifacial-coated modules, with and without mounting components, for modules with individual optimisation (left) and modules configured in two parallel strings (right). © 2023 Marco Ernst. This figure was published in Ernst et al. (2024).

The study explored the relationship between the optimal tilt angle of bifacial modules and rooftop reflectivity. It was found that as rooftop reflectivity increased, the optimal tilt angle for bifacial modules also increased. This highlights the importance of designing systems that consider both rooftop conditions and module orientation to maximise energy generation.

Further, it was examined how weather conditions affect the performance of bifacial solar modules, with a specific focus on the impact of clouds and time of day. The analysis of power output data from clear-sky and partly cloudy days in Figure PP4.2.4 shows a significant increase in the relative power output of the bifacial system, particularly during morning and evening periods. Cloudy days, which only make up 15% of the total monofacial annual yield, contribute approximately 28% to the annual bifacial yield gain.

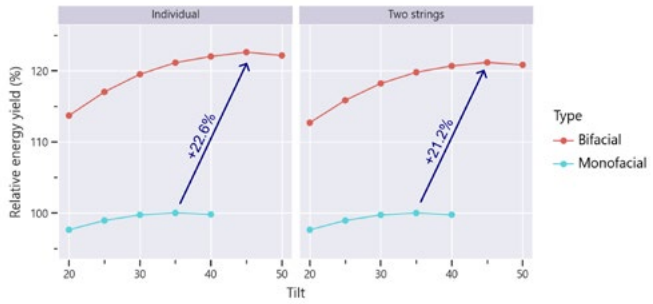

Figure PP4.2.4: Top: Absolute and Bottom: relative power of the 16-module monofacial and bifacial system configured in two parallel strings. © 2023 Marco Ernst. This figure was published in Ernst et al. (2024).

Discussion

In this study, it was found that bifacial modules have a high potential for rooftop applications due to their substantial energy yield gains of over 20%. It is important to note that the installation and maintenance costs for bifacial modules are almost the same as those for monofacial modules, with only a small increase in capital costs (Smith et al. 2020). The study shows that bifacial systems can achieve a significant yield gain, which is higher than the typical range of 4%–15% achieved by utility-scale solar farms. This could lead to substantial cost and installation footprint reductions or result in a significant economic gain over an equivalent monofacial system (Pelaez et al. 2019; Patel et al. 2017).

Additionally, the study indicates that highly reflective roof materials can further increase the yield gain of bifacial systems, similar to ground-mounted PV systems. In a rooftop context, highly reflective cool roof materials not only enhance the efficiency of bifacial modules but also reduce building temperatures, offering potential synergies between rooftop bifacial module systems and reflective roof materials. Further exploration of the techno-economic synergy between these elements could lead to simultaneous economical electricity production and reduced cooling energy needs in buildings (Killoran et al. 2017; Rawat & Singh 2022). This implies that the yield gains presented in this work have broader implications for sustainable and cost-effective energy solutions in the context of building-integrated photovoltaics.

References

Ernst, M., Liu, X., Asselineau, C. A., Chen, D., Huang, C. & Lennon, A. (2024). Accurate modelling of the bifacial gain potential of rooftop solar photovoltaic systems. Energy Conversion and Management 300, 117947. (*https://doi.org/10.1016/j.enconman.2023.117947*).

Smith, B. L., Woodhouse, M., Horowitz, K. A. W., Silverman, T. J., Zuboy, J. & Margolis, R. M. (2021). Photovoltaic (PV) Module Technologies: 2020 Benchmark Costs and Technology Evolution Framework Results. United States: U.S. Department of Energy, Office of Scientific and Technical Information. (*https://doi.org/10.2172/1829459*).

Pelaez, S. A., Deline, C., Greenberg, P., Stein, J. S. & Kostuk, R. K. (2019). Model and Validation of Single-Axis Tracking with Bifacial PV. IEEE Journal of Photovoltaics 9, 715-721. (*https://doi.org/10.1109/JPHOTOV.2019.2892872*)

Patel, M. T., Ahmed, M. S., Imran, H., Butt, N. Z., Khan, M. R. & Alam, M. A. (2021). Global analysis of next-generation utility-scale PV: Tracking bifacial solar farms. Applied Energy 290, 116478. (*https://doi.org/10.1016/j.apenergy.2021.116478*).

Killoran, C., Hespe, A. & Kovachevich, A. (2017) Microclimate Study: BlueScope Microclimate Thermal Study. ARUP Pty Ltd, Rep. 251927. [Online]. Available: *https://cdn.dcs.bluescope.com.au/download/bluescope-microclimate-thermal-study-stage-1a-microclimate-study-arup*.

Rawat, M. & Singh, R. N. (2022). A study on the comparative review of cool roof thermal performance in various regions. Energy and Built Environment 3, 327-347. (*https://doi.org/10.1016/j.enbenv.2021.03.001*).

PP4.3 MODULE DURABILITY

PP4.3.1 Thermomechanical Stress Modelling

Lead Partner
UNSW

UNSW Team
Dr Pei-Chieh Hsiao, Dr Arastoo Teymouri, Dr Alison Ciesla, Dr Michael Pollard, Dr Zibo Zhou, Dr Ran Chen, Dr Ning Song, Prof. Alison Lennon, Prof. Renate Egan

Funding Support
SunDrive
5B

Aims

The PP4.3.1 program aims to investigate the induced stress in solar cells and modules during thermal processing or mechanical loading conditions. The evaluated stress magnitude and locations in the cells and modules provide guidance for the development of cell metallisation and interconnection, module assembly architectures, module mounting systems, etc. This assists in achieving more reliable photovoltaic systems in their field operation.

Progress

The PP4.3 program is dedicated to improving the understanding of how stress is developed within solar cells that could potentially lead to cell fracture and module failure. Analysis of thermomechanical stress and modules under static wind loading is conducted using the finite element method to characterise the stress and verified by experimental measurements.

A. Annealing of copper-plated fingers on silicon heterojunction solar cells (UNSW)
Copper metallisation to silicon heterojunction (HJT) solar cells has been demonstrated by SunDrive Solar Pty Ltd to achieve world record cell efficiency. Annealing of copper-plated contacts occurs in processing steps such as hydrogenation, interconnect soldering and lamination. Due to the mismatch of the coefficient of thermal expansion (CTE) between Si and Cu, thermomechanical stress is induced. Figure PP4.3.1.1 shows the top and cross-sectional views of Si tensile stress mapping during annealing. It reveals the evolution of maximum stress locations, transited from the pyramidal apex at peak temperature to the plated contact edge after annealing.

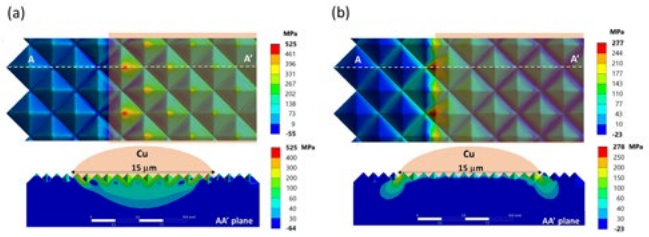

Figure PP4.3.1.1: Simulated Si tensile stress induced by a 15μm-wide Cu finger plated on a pyramidal (1.5 μm base) textured surface (a) at peak annealing temperature (200°C); and (b) after annealing (20°C).

The impact of Cu finger width on Si stress is shown in Figure PP4.3.1.2 The maximum Si tensile stress increases with the finger width, then stabilised when the finger width is greater than 50 μm. It highlights the benefits of narrow finger width, which reduces the optical shading loss as well as the stress developed in the solar cells.

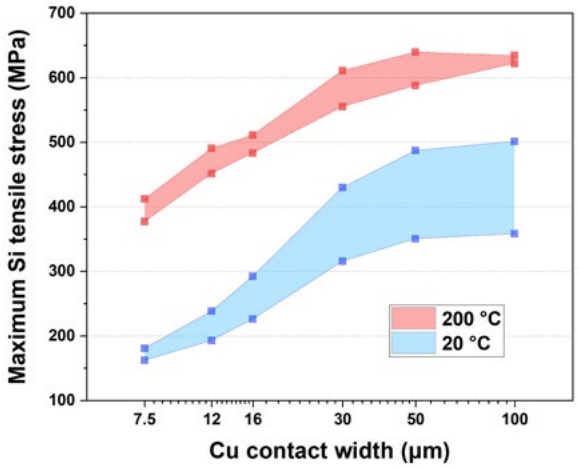

Figure PP4.3.1.2: Simulated maximum Si tensile stress as a function of Cu finger width. Red and blue curves represent the stress range at peak annealing temperature and after annealing, respectively.

B. Stress evolution in multi-busbar (MBB) interconnected half-cell tiled modules after soldering and lamination (UNSW)
In this study (Wang 2023), different module assembly architectures are evaluated. Tiled modules, in which solar cells are partially overlapped (width < 2 mm), have increased cell packing density by eliminating the cell gaps and hence module efficiency is increased. Figure PP4.3.1.3 illustrates the diagram of solar modules with solar cells interconnected in a cell gap and tiled approach. The higher module efficiency comes at the cost of additional local high stress regions in Si where cells are overlapped and under the Cu wires.

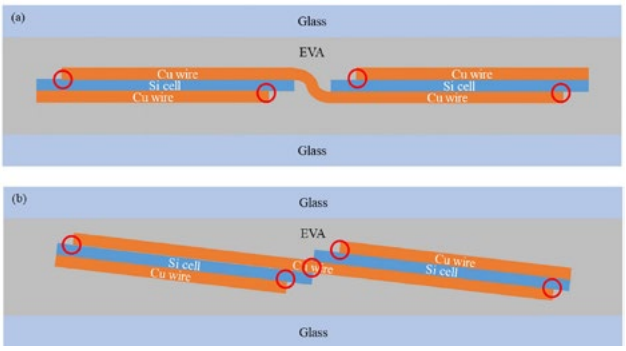

Figure PP4.3.1. 3: 2D diagram of a glass-glass module with two solar cells interconnected in (a) a cell gap; and (b) tiled approach. The red circles indicate the local high stress regions in the solar cells.

As shown in Figure PP4.3.1.4(a), after soldering solar cells have consistent tensile stress, which is influenced by the solders coated on the Cu wires. After modules are fabricated, the impact of cell gap on Si stress appears, with significant stress increase with the overlapping width. As the encapsulant EVA serves as a protective buffer layer between the solar cells and the stiff glass, thicker EVA alleviates the Si stress provided the overlapping width is ≤ 0.5 mm.

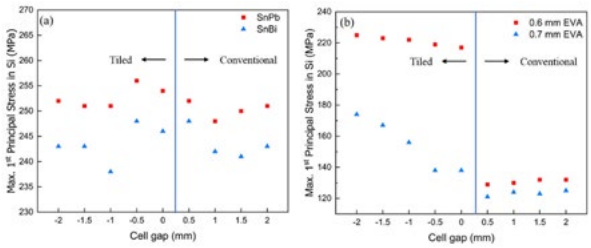

Figure PP4.3.1.4: (a) Maximum induced tensile stress in the Si cells after soldering with varied cell gaps and solders; and (b) after lamination with varied cell gaps and thicknesses of EVA based on SnPb solder.

C. Deflection of utility modules on 5B's mounting system under static wind conditions (UNSW)

The Maverick (MAV) system by 5B is a photovoltaic array prefabricated in a factory for rapid field installation. The system is not impacted by dynamic wind loads due to a resonant frequency > 1Hz, and experiences relatively low static wind loads due to its aerodynamic design. Therefore, it is essential to evaluate the deflection and mechanical stresses of modules using a hinged corner mounting. A finite element model is developed and calibrated by the measured deflection of a reference module under uplift loading and fixed on both module ends. The model assumes no separation between the module and the mounts, resulting in overestimated module deflection and stresses due to the increase in effective stiffness of the frame. Despite this overestimation, the stresses on the cells in worst case uplift scenarios are minimal as seen in Figure PP4.3.5(a). In comparison, Figure 4.3.1.5(b) shows the cell stresses are much higher on the same module mounted by standard quarter point fixing under a standard 1200 Pa load.

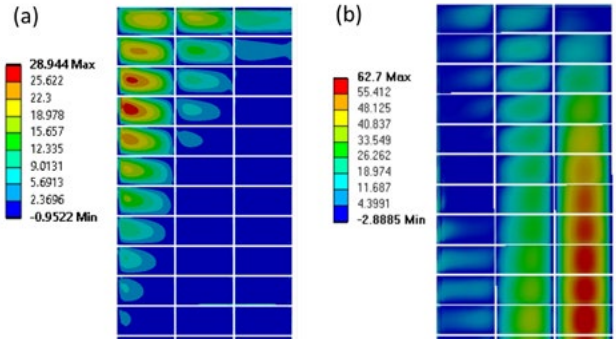

Figure PP4.4.1.5: Simulated tensile stress in the cells for the module on: (a) 5B's Maverick worst case uplift with safety factor Wind Region A (1053 Pa); and (b) a standard quarter point mount under 1200 Pa.

Summary

The PP4.3 program has continued to investigate module durability by quantifying the tensile stress developed in solar cells under various scenarios.

These have shown how thermal processes, module architectures and mounting systems can induce tensile stress on different scales. The identified stress magnitudes, locations and distribution reveal how the cell stress can be addressed, thereby developing approaches to minimise the stress and improve module reliability.

Highlights

- Local high-stress transition on pyramidal surfaces induced by annealing of Cu-plated HJT cells.
- Increased stress in solar cells in tiled modules.
- Distinct lower stress distribution in solar cells in modules on 5B's mounting system than standard quarter-point mounting.

Future Work

- Assessment of the probability of fracture using Weibull distribution.
- Development of new technologies reducing cell stress in tiled modules.
- Development of an accurate simulation model and assistance in module mounting system design.

References

Ciesla, A., Chen, R., Hsiao, P.-C., Teymouri, A., Evans, A., Rego, V., Horsley, J., Bhoopathy, R. & Evans, R. (2021). Static wind loading of utility sized modules mounted using 5B's rapid deployment system. Asia-Pacific Solar Research Conference. Sydney, Australia.

Hsiao, P.-C., Colwell, J., Chen, D., Huang, C., Lennon, A. & Egan, R. (2023). Analysis of Thermomechanical Stress Induced in Silicon Heterojunction Solar Cells by Copper Fingers. Asia-Pacific Solar Research Conference. Melbourne, Australia.

Teymouri, A., Russo, J., Pollard, M., Zhou, Z., Evans, R., Chen, R. & Ciesla, A. (2023). Deflection of utility modules on 5B's mounting system under static wind conditions. Asia-Pacific Solar Research Conference. Melbourne, Australia.

Wang, Z., Hsiao, P.-C., Song, N., Shen, X., Xu, C., Yi, H. & Lennon, A.. (2023). Use finite element modelling to characterise the stress evolution in Multi Busbar interconnected half-cell tiled modules after soldering and lamination. Solar Energy Materials and Solar Cells 252, 112166.

PP4.3.2 Morphological Analysis

Lead Partners
UNSW

Unsw Team
Dr Chandany Sen, Dr Muhammad Umair Khan, Prof. Bram Hoex

P artners
Tindo Solar, CSI Solar Co Ltd

UNSW Students
Haoran Wang, Xinyuan Wu, Jiexi Fu, Xutao Wang

Aims

The objective of the PP4.3.2 program is to evaluate the overall comprehension of the potential and humidity-induced degradation in PV modules. Additionally, we aspire to establish cell-level testing for all the identified failures that occurred in PV modules. The testing of non-encapsulated cells can be immensely valuable in identifying issues and is cost- and time-efficient. This process enables significantly faster identification of issues and more thorough characterisation, facilitating quicker implementation of mitigation measures.

Progress

A. Setting new test standards for cell-level PID testing

Potential-induced degradation of the shunting type (PID-s) is a well-known problem for photovoltaic modules. However, the standard International Electrotechnical Commission (IEC) PID test at the cell or module level takes 96 hours due to the time it takes for the sodium (Na) ions to diffuse from the glass to the solar cell through the ethylene-vinyl acetate (EVA) encapsulant (Figure PP4.3.2.1). This is too slow to monitor production quality in the fast-paced solar cell industry. Moreover, it results in the encapsulation of solar cells, significantly restricting characterisation options after PID testing. Therefore, our group has proposed a new standard for PID testing by modifying the polymer and setting a new testing standard, 'SEMI PV75-0823', which only takes 12 minutes to test PID in solar cells (Khan et al. 2023) (CSI-UNSW, 2023).

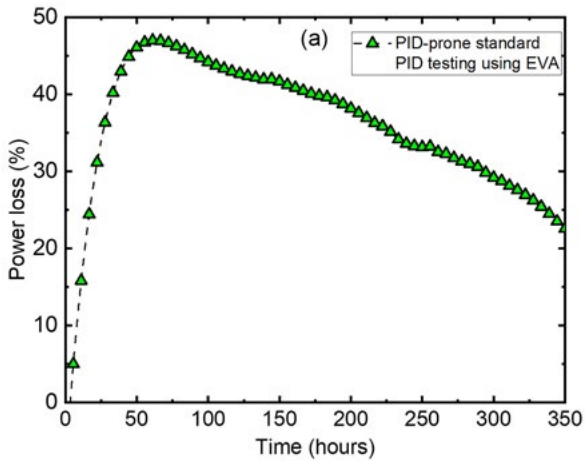

Figure PP4.3.2.1: Cell-level PID testing of solar cells using previous testing standard. Please note that it takes roughly 70 hours to reach the highest power loss, and typically, solar cells are not tested beyond 96 hours.

In this work, we replace the EVA in the PID testing setup with a salt-enriched hybrid polymer, which provides the solar cell with direct access to sodium (Na) ions while avoiding encapsulation during the testing process. Solar cells that underwent PID-s testing with the salt-enriched hybrid polymer showed a maximum degradation after only 12 minutes (Figure PP4.3.2.2), over two orders of magnitude faster than standard PID-s testing using EVA, which took 4,300 minutes (~72 hours) to reach maximum degradation.
Hence, PID-s testing using the salt-enriched hybrid is significantly faster than conventional techniques and avoids encapsulation, thus allowing for more detailed post-PID cell analysis. This new test shows that some solar cells can recover from PID-s, which was corroborated by extending the standard test to 300 hours (see Figure PP4.3.2.1). This important novel insight shines a new light on the PID-s mechanism and the impact of this failure mode in field operation.

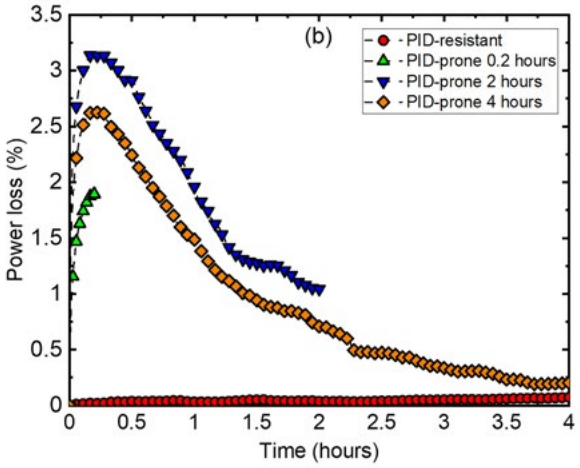

Figure PP4.3.2.2: Cell-level PID testing using new standard testing (SEMI PV75-0823), which was developed by UNSW in collaboration with Canadian Solar.

In addition to being significantly faster, this process also does not encapsulate the solar cell, thus allowing for a more detailed post-PID analysis. The dark lock-in thermography (DLIT) images showed maximum shunting for 0.2 hours of testing, and it recovered fully after prolonged testing (Figure PP4.3.2.3). The completely recovered sample showed no or minimal shunting, showing that the shunts formed due to PID can be fully recovered. This full recovery was never reported previously and this could have significant implications for asset owners whose PV farms suffer from PID-s. They now can allow for self-recovery in the field if that makes sense from a techno-economic perspective.

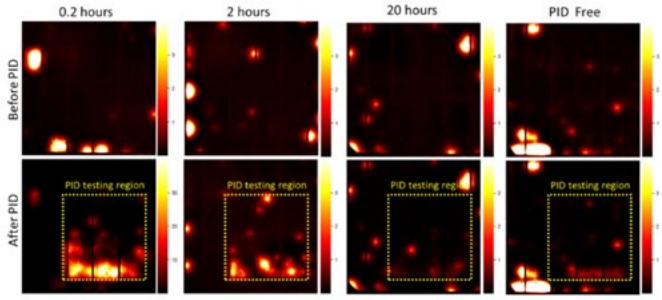

Figure PP4.3.2.3: DLIT images for samples before and after PID testing at various testing times.

B. Damp-heat-induced degradation in HJT modules Silicon heterojunction technology (HJT) has gained a significant market share due to its potential to deliver a low levelised cost of electricity (LCOE). In order for HJT to achieve a low LCOE, it needs to have a high initial efficiency and degrade less than 0.5% per year. However, damp heat can lead to severe degradation in HJT glass-backsheet modules, resulting in several failure modes. This study investigates the different types of failure modes that can occur and their impact on power output, which can range from 5% to 50% depending on the type of failure mode. The study identified four unique failure modes (Sen et al. 2023b):

- Type-1 failure mode: point localised failure.
- Type-2 failure mode: failure around the interconnection of busbars and ribbon wires.
- Type-3 failure mode: failure between busbars and/or whole areas of cells or modules.
- Type-4 failure mode: failure on the interconnection of busbars and ribbon wires.

Each failure mode is hypothesised to be caused by different root causes and requires different testing techniques at the cell level to generate a similar failure mode. Figure PP4.3.2.4 shows the electroluminescence (EL) images of the four failure modes in HJT glass-backsheet modules observed after damp heat (DH) testing.

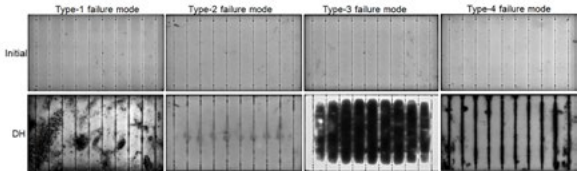

Figure PP4.3.2.4: EL images of HJT glass-backsheet modules before (initial) and after DH testing show four failure modes.

With concerted effort, all four failure modes identified in the HJT modules have been successfully reproduced at the cell level using non-encapsulated cells. Figure PP4.3.2.5 illustrates the photoluminescence (PL) and EL images of HJT cells after ~50 hours of DH testing. This cell-level testing procedure is approximately one to two orders of magnitude faster than module-level testing and greatly facilitates root cause analysis. The speculated causes for each failure mode are as follows:

- Type-1 failure may be attributed to inadvertent contamination introduced to the cells prior to encapsulation.
- Types 2 and 3 failures are likely linked to the presence of soldering flux utilised in the connection of ribbon wires to the busbars of cells.
- Type-4 failure is believed to be associated with the presence of acetic acid, which is generated from EVA encapsulation.

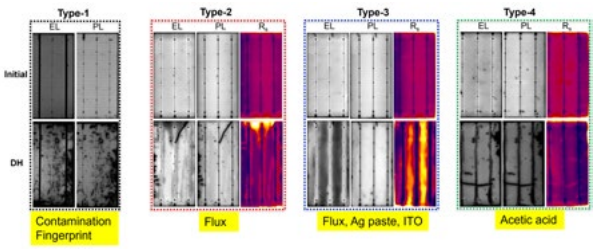

Figure PP4.3.2.5: PL and EL images of HJT cells after ~50 hours of damp heat testing show the reproduction of four failure modes at the cell level.

C. A novel approach to preventing humidity-induced failure in HJT modules

This work presents a method to mitigate all types of failure modes in HJT cells, as presented in Figure PP4.3.2.5 (Sen et al. 2023c;, Wu et al. 2024). Left unprotected, this failure can lead to both recombination and series resistance (Rs) losses, resulting in a power loss of up to 40% relative.

However, by implementing aluminium oxide (Al2O3) barrier layers on both sides of HJT cells, we have successfully eradicated all losses associated with these failure modes, rendering HJT solar cells inherently more stable. Both recombination and series resistance issues stemming from the chemical interaction between moisture and contaminants can be averted in HJT cells coated with ~10 nm thick Al2O3 barrier layers. Figure PP4.3.2.6 shows the PL and EL images of HJT cells with all failure modes, both with and without mitigation after the DH test.

To our knowledge, this represents the most effective approach in preventing damp-heat-induced failure in HJT cells and holds promise as a novel strategy to mitigate humidity-induced failure in glass-backsheet modules, a significant barrier impeding the prevalent adoption of HJT glass-backsheet modules in the market.

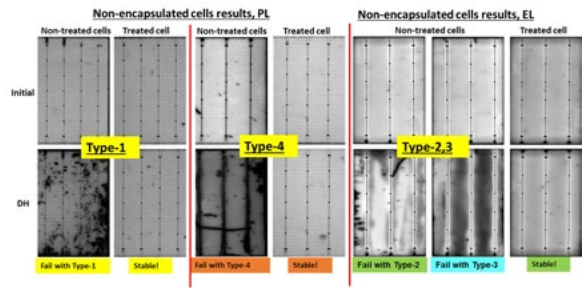

Figure PP4.3.2.6: All four failure modes shown in Figure PP4.3.2.4 are effectively prevented at the cell level by the application of Al2O3 barrier layers.

D. Accessing corrosion-induced degradation in PERC, HJT and TOPCon cells using NaCl

Metal contact corrosion is one of the most commonly observed causes of performance deterioration in indoor and outdoor humidity testing. This corrosion leads to an increase in R_s over time, resulting in a loss of performance. The corrosion is believed to be caused by electrochemical reactions that occur between moisture, various contaminants and the metal contacts of the solar cell. The contaminants can include acetic acid hydrolysis from EVA. In addition to this, residual solder flux has also been found to play a critical role in contact corrosion. This is primarily due to the presence of organic acid and/or halide materials, which chemically react with moisture and metal contacts, leading to an increase in Rs. These halide materials include chlorine (Cl), bromine (Br) and fluorine (F). Furthermore, sodium (Na) is a common contaminant released from the solar glass during high-voltage operation or due to leaching caused by exposure to high heat and humidity during damp heat conditions.

This study assesses the corrosion-induced degradation resulting from NaCl exposure in three mainstream cell technologies, including passivated emitter and rear cell (PERC), heterojunction (HJT), and tunnel oxide passivated contact (TOPCon) solar cells (Sen et al. 2023d).

Among the investigated cell technologies, TOPCon solar cells exhibit the highest degradation, with a maximum power loss (P_{max}) of approximately 75% after 20 hours of DH testing. HJT cells follow with a P_{max} drop of around 50%, while PERC cells experience only about a 10% drop (see Figure PP4.3.2.7). The degradation is primarily due to increased R_s on the front side of TOPCon cells, both sides of HJT cells, and the rear side of PERC cells, which is attributed to corrosion of the metal contact caused by high levels of Na^+ and Cl^- ions.

These results are crucial for all cell technologies as they highlight the potential failures that could occur in the field. Na^+ and/or Cl^- ions are common contaminants in solar glass, human fingerprints, soldering flux, rainwater, soil/dust and seawater. During field operation, these ions have the potential to penetrate and directly interact with solar cells. In our view, the preferred solution is for the solar cells to be corrosion-resistant, which can be rapidly assessed using the method presented in this work.

This research also highlights the significance of cell-level testing without encapsulation, which can lead to significant time and cost savings. It also enables efficient and accurate characterisation of failure mechanisms. The proposed test method offers a rapid alternative to module-level testing, making it possible to quickly screen cells that are sensitive to corrosion in PV production lines.

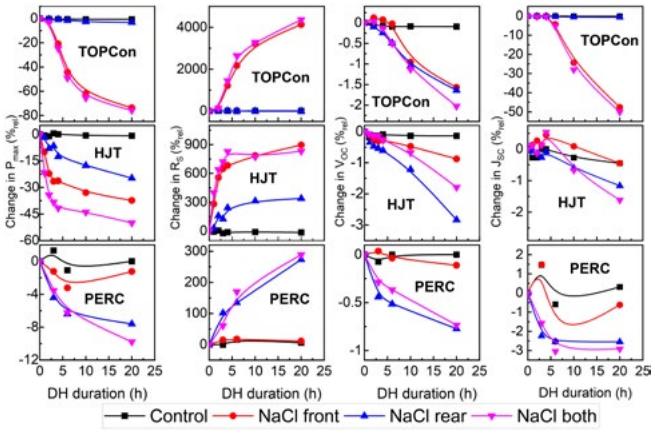

Figure PP4.3.2.7: Relative one-sun I-V parameters (P_{max}, R_s, V_{OC} and J_{SC}) of the TOPCon, HJT and PERC solar cells as a function of the humidity testing time of all cells tested with NaCl.

E. Damp-heat-induced failure in the TOPCon modules

N-type TOPCon technology is poised to capture a considerable market share in the near future. Despite significant technological advances, concerns persist regarding the reliability of TOPCon cells when deployed in the field. This is particularly true when encapsulated with a low-cost bill of materials. This research investigates the degradation

induced by humidity in TOPCon glass-backsheet modules. Various combinations of materials were examined, incorporating polyolefin elastomer (POE), EVA and diverse backsheet options (Sen et al. 2023a).

Our findings reveal that TOPCon modules can exhibit substantial degradation, resulting in a reduction in P_{max} ranging from 4% to 65% relative to baseline levels. This decline can be attributed to a notable increase in R_s. It appears that the elevated R_s observed post-DH testing is likely caused by an electrochemical reaction between moisture, soldering flux, and potential contaminants like sodium chloride, corroding the metallisation of solar cells. Hence, further research is imperative to deepen our understanding and bolster the resilience of TOPCon cells against the deleterious effects of moisture and other contaminants.

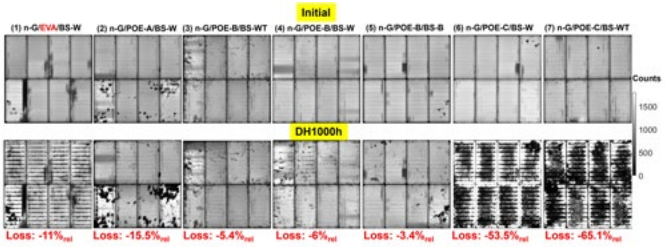

Figure PP4.3.2.8: Damp-heat-induced failure in TOPCon glass-backsheet modules.

Summary

The PP4.3.2 program assesses the comprehensive understanding of potential and humidity-induced degradation in PV modules. It seeks to revise and propose a new cell-level testing approach to promptly detect all failure modes within the modules. The proposed cell-level test method provides a swift alternative to module-level testing, enabling efficient screening of cells in PV production lines. Conducting cell-level testing can significantly aid in root cause analysis, offering cost and time savings. This approach facilitates faster issue identification and more thorough characterisation, expediting the implementation of mitigation measures.

Highlights

- A new testing standard PID, which only required 12 minutes to test PID in solar cells "SEMI PV75-082".
- Four failure modes were found in the HJT glass-backsheet modules after damp heat (humidity) testing.
- Al_2O_3 barrier layers: A novel approach to preventing humidity-induced failure in HJT modules.
- Accelerated damp-heat testing at the cell level of bifacial silicon HJT, PERC and TOPCon solar cells using sodium chloride.
- More severe degradation was found in the TOPCon glass-backsheet modules during damp heat testing.

Future Work

- Continue collaborations with the industry to examine the root cause of the failure in TOPCon modules.
- Work with industry to explore approaches to improve the reliability of the TOPCon modules, particularly for the glass-backsheet module structure.
- Continue to develop cell-level testing to detect all failure modes identified in the modules.
- Explore cell-level mitigation approach to protect TOPCon cells from humidity-induced degradation.

References

CSI-UNSW. (2023). SEMI PV75 - Test Method on Cell Level for Potential-Induced Degradation Susceptibility of Solar Cells and Module Encapsulation Materials. SEMI: semi.

Khan, M. U., Sen, C., Chan, C., Abbott, M., Poduval, G., Wu, Y., Lv, R., Zhang, G. & Hoex, B. (2023). Supercharging cell-level potential-induced degradation (PID) testing using a salt-enriched hybrid polymer layer. Solar Energy Materials and Solar Cells 260.

Sen, C., Wang, H., Khan, M. U., Fu, J., Wu, X., Wang, X. & Hoex, B. (2023a). Buyer Aware? TOPCon's Reliability Issues in Comparison with PERC PV Modules After Damp Heat Testing. Asia-pacific solar research conference.

Sen, C., Wang, H., Wu, X., Khan, M. U., Chan, C., Abbott, M. & Hoex, B. (2023b). Four failure modes in silicon heterojunction glass-backsheet modules. Solar Energy Materials and Solar Cells 257.

Sen, C., Wang, H., Wu, X., Khan, M. U., Mao, L., Jiang, F., Zhang, G., Chan, C. & Hoex, B. (2023c). Al2O3 Barrier Layers: A Novel Approach to Preventing Humidity-Induced Failure in Heterojunction Solar Modules. EU PVSEC.

Sen, C., Wu, X., Wang, H., Khan, M. U., Mao, L., Jiang, F., Xu, T., Zhang, G., Chan, C. & Hoex, B. (2023d). Accelerated damp-heat testing at the cell-level of bifacial silicon HJT, PERC and TOPCon solar cells using sodium chloride. Solar Energy Materials and Solar Cells 262.

Wu, X., Sen, C., Wang, H., Wang, X., Wu, Y., Khan, M. U., Mao, L., Jiang, F., Xu, T., Zhang, G. & Hoex, B. (2024). Addressing sodium ion-related degradation in SHJ cells by the application of nano-scale barrier layers. Solar Energy Materials and Solar Cells 264.

PP4.5 ADVANCED OUTDOOR TESTING

Lead Partners
UNSW, ANU

UNSW Team
Dr Jessica Yajie Jiang, Dr Zibo Zhou, Dr Yiyu Zeng, Dr Angus Gentle, Dr Milad Mohsenzadeh, Dr Ning Song, Dr Mark Keevers, Prof. Renate Egan, Prof. Martin Green

Partners
Jinko Solar, JA Solar, LONGi, Canadian Solar

Aims

This activity will explore the potential of new materials aimed at reducing the operating temperature of solar PV modules. The research will consider designs for Australian conditions and a future where border taxes are employed to reduce global emissions.

Progress

Outdoor PV module convective behaviour measurement setup
Passively cooling photovoltaic (PV) modules holds significant importance in enhancing system-level economic benefits and environmental impact. Despite advancements in cell technologies reducing temperature dependencies for output power, modules still experience notable efficiency losses at elevated temperatures. Effective cooling techniques not only mitigate these losses but also slow down material degradation within the PV module, maximising the total energy generation and reducing the need for module recycling.

Vortex generators (VGs) have previously demonstrated promising passive cooling potential under free convection conditions (indoor experiment). The VGs attached to the rear surface module achieved a cooling of up to 3°C, while the VGs designed for rooftop systems and attached to the roof provide more than 4°C of cooling. However, the wind conditions experienced by field-deployed systems are complex and dynamic, with free convection conditions being rare. Therefore, the shape and arrangement of the VGs need further optimisation to maximise effectiveness in practical use cases.

This requires an outdoor experiment setup which measures the full detailed weather and radiation data, the temperature and the electrical output of the module. Such a setup not only provides a platform for assessing the outdoor performance of VGs, but also an opportunity to gain insight into the complex wind-module interactions and the resulting convective heat transfer for a given system and site.

Figure PP4.5.1: The rear view of the outdoor convective measurement setup. The placement of the temperature sensor are indicated on module M4 in the red circle. Module M3 and M4 have aluminium and 3D-printed polymer VGs attached to the backsheet.

The open rack system located on top of a five-storey building has been built to fulfil such needs, as shown in Figure PP4.5.1. The weather and radiation data are measured in sub-minute intervals and then consequently processed using a Python program. The downwelling and upwelling for shortwave (solar radiation) and longwave (thermal emission) radiation are measured, along with the wind speed and directional data that are used to develop a thermal balance model. This model is based on the fact that the incoming radiation is mostly dissipated through convection and radiation or stored in the thermal mass of the module. It is then possible to evaluate the total convective flux for each timestep and derive the convective heat transfer coefficient. The commonly used two-component convective model is applied in the model, which decomposes the total convective coefficient into free and force convective components.

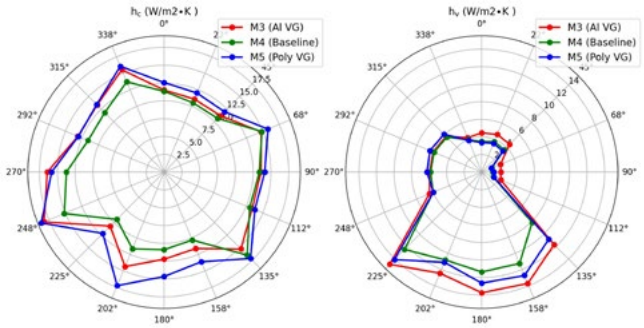

Figure PP4.5.2: The polar plot of the free convection heat transfer coefficient (left, hc) and force convection coefficient (right, hv) of the three testing modules derived from the thermal balance model for different wind directions.

The wind-directional-dependent, convection coefficients are presented with 10 months of data in Figure PP4.5.2. The modules with VG have shown greater convective efficiency, for both free and forced convection coefficients. The convective behaviour of the module is highly wind-direction-dependent, the hv value for the south wind is around three times of the north wind. The VG performances are also superior for the south wind, as both hc and hv values are higher for the VG-equipped module M3 and M5. This analysis provides valuable insights into the directional-dependent behaviour of the VG on PV modules, thus an essential step for future optimising the shape of the VGs for field operations.

Summary

An outdoor measurement setup has been established to evaluate the convective behaviour of PV modules under different weather conditions, which is an essential step for evaluating and optimising the design of VG for passive PV module cooling.

The measurement setup also brings insight into how a particular PV system behaves thermally under given wind conditions. This technique can be applied to different system layouts and locations (e.g. high-density system vs. tracker), where the convective efficiency can be compared.

Highlights

- Outdoor long-term measurement of the VG on PV modules.
- Thermal balance model for evaluating the convective heat transfer coefficient.

Future Work

- Install more wind sensors near the module surface for evaluating local wind effects.
- Separate convection effect on front and rear surfaces.
- Development of a portable measurement setup for field measurements.
- Develop an alternative method for evaluating the convective flux, for example heat flux sensor.

References

Zhou, Z., Bahl, P., Tkachenko, S., Hari, A., de Silva, C., Timchenko, V., & Green, M. A. (2023). Vortex Generators for Passive Cooling of Rooftop Photovoltaic Systems Under Free Convection. IEEE Journal of Photovoltaics. DOI: 10.1109/JPHOTOV.2023.3299752.

Zhou, Z., Tkachenko, S., Bahl, P., Tavener, D., de Silva, C., Timchenko, V., Jiang, J., Keevers, M. & Green, M. (2022). Passive PV module cooling under free convection through vortex generators. Renewable Energy 190, 319-329.

PP5
MANUFACTURING AND SUSTAINABILITY

OVERVIEW

This program package covers a wide range of activities that complement the other ACAP programs. The sub-packages are:

PP5.1 – Sustainable Manufacturing. This package seeks to identify any key material requirements and bottlenecks for TW-scale manufacturing, consider how cell and module designs can be improved for reduced material requirements, and how modules can be designed and manufactured for improved end-of-life outcomes. This year, we report on analysis of supply requirements and potential improvements for silicon, solar glass, silver and the aluminium frame.

PP5.2 – Techno-Economic Analysis and Life Cycle Analysis. This package carries out financial and environmental analysis of different technologies being developed by ACAP researchers. This year we report on cost analysis of a multi-layer sputtered AR coating, advances in silicon perovskite tandems and the cost of 100% renewables in Indonesia.

PP5.3 – Local Manufacturing and Supply Chain Analysis. This package looks at opportunities for Australian manufacturing and also considers risks in the PV supply chain. This year we report on ACAP's involvement with the APVI Silicon to Solar report, and detailed analysis of policy support options for Module Assembly manufacturing.

PP5.4 – Performance Analysis and Optimisation. This package aims to measure and validate field performance of module technologies and model/optimise for improved yield and levelised cost. This year we report on the completion of a testing and yield simulation/optimisation study of a Tractile product, and improved temperature and degradation modelling of yield for LCOE calculations.

PP5.5 – End-of-Life Management: Extend, Re-use, Repair, Recycle. This package aims to minimise waste through extending first-life, encouraging a second-life and recycling of modules. This year we report on an End-of-Life Management report commissioned by Neoen, a cost/benefit analysis of recycling in Australia, and a study on alternate solvents for use in chemical recycling.

PP5.6 – Novel Characterisation for Manufacturing and In-Field Performance. This package aims to develop characterisation techniques for use with in-field cells and modules and in manufacturing. This year we report on in-field testing and automated characterisation of cells and modules to inform end-of-life decision-making and the completion of a project to develop outdoor photoluminescence imaging.

PP5.1 SUSTAINABLE MANUFACTURING

Lead Partners

UNSW, CSIRO, ANU

UNSW Team

Brett Hallam, Richard Corkish, Li Wang, Moonyong Kim, Nathan Chang, Sisi Wang

PhD Students

Mohammad Dehghanimadvar, Tamal Chowdhury

Aims

This work package targets identifying material requirements for terawatt-scale PV deployment and critical material issues/bottlenecks that must be addressed. From this, technology roadmaps towards sustainable TW-scale PV manufacturing will be developed for existing and emerging solar cell technologies. Activities seek to address critical material issues to improve PV's sustainable manufacturing capacity, while ensuring low cost. This will include modified cell structures, metallisation schemes and interconnection methods to reduce the reliance on critical materials, and also target designs to improve recyclability.

This package has three streams with more specific aims:

5.1.1 Critical material challenges

- Progress early development of critical material challenges across the whole PV value chain for existing (PERC, TOPCon and SHJ) and emerging solar cell and module technologies. Assessments will be based on projected cell/module efficiencies, global material reserves and annual supply, expected material requirements for other clean energy technologies and will consider the impact of module recycling, and length of operation in the field.
- Develop technology roadmaps and compare with other roadmaps including ITPRV.

5.1.2 Modified cell and module designs

- Draw on findings from PP5.1A, target device and module fabrication changes to increase the sustainable manufacturing capacity of the respective technologies, while ensuring high performance and low LCOE values.
- Investigate alternative metallisation technologies, targeting reducing silver consumption to < 2 mg/W in collaboration with SunDrive.
- Assess two-terminal tandem devices, for the unique opportunity to greatly reduce silver by a factor of up to six compared to PERC.
- Investigate sustainability issues with passivating contacts the bottom cell of silicon-based tandems, moving away from ITO.
- Investigate opportunities for changes to cell metallisation and interconnection schemes in module level technology development for both screen-printed and plated cells to assist with the reduction of key materials such as silver, lead and bismuth.
- Investigate aluminium usage with reduced-frame or frame-less modules and changes to cell configurations. The activity will also develop low-weight modules to reduce emissions associated with transportation.

5.1.3 Design for recycling and end of life

- Investigate alternative encapsulant materials with improved ability to recycle.
- Investigate encapsulant-free module technologies such as the New Industrial Solar Cell Encapsulation (N.I.C.E) technology from Apollon Solar, a partner in the program.
- Develop modified cell architectures designed to integrate with module technologies for improved recyclability such as copper-plated contacts as cell technologies push towards lower silver consumptions, which could affect the economics of recycling.

Progress

Note: Some of the plans for this program package overlap with two related ARENA projects recently awarded to Brett Hallam (Lead CI) and other ACAP researchers – *https://arena.gov.au/projects/low-cost-and-sustainable-pv-systems-for-the-terawatt-scale/* and *https://arena.gov.au/projects/silver-lean-screen-printing-for-sustainable-low-cost-industrial-pv-manufacturing/*. Some of the activities and outputs of those projects are included in this report as there are ongoing ACAP resources allocated to that project in addition to the ARENA funding.

A.Poly-si consumption and production expansion for 3TW/year target (UNSW)

This work was reported at the APSRC, 2023 (Wang et al. 2023). Various estimates have been made of the amount of annual PV production the world requires. Using one such estimate of 3 TW/year, we estimate the poly-silicon required to meet this demand. Figure PP5.1.1(a) shows the process flow and material requirements to produce 1 kg of silicon wafers.

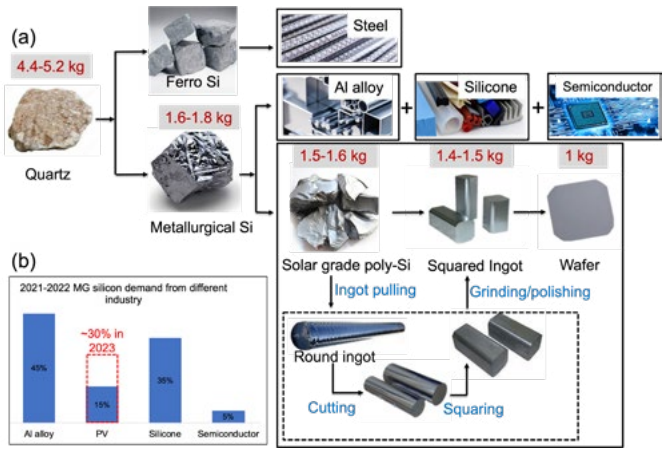

Figure PP5.1.1: (a) Material requirements to produce 1 kg of silicon wafers, (b) MG-Si demand from different industries in 2021–2022 with expected demand of near 30% from PV in 2023.

We estimate the current poly-Si consumption as 2–2.7 g/W (Si modules), which could reduce to ~1.5 g/W for future Si-based tandem cells. Current global solar grade poly-Si production is ~0.9 million tonne/year. To achieve 3 TW/year, poly-Si production will need to increase approximately seven-fold.

Technology improvements can reduce this requirement. Figure PP5.1.2 shows the amount of quartz, MG-Si and poly-Si required for 3 TW/year production under different technology improvement scenarios.

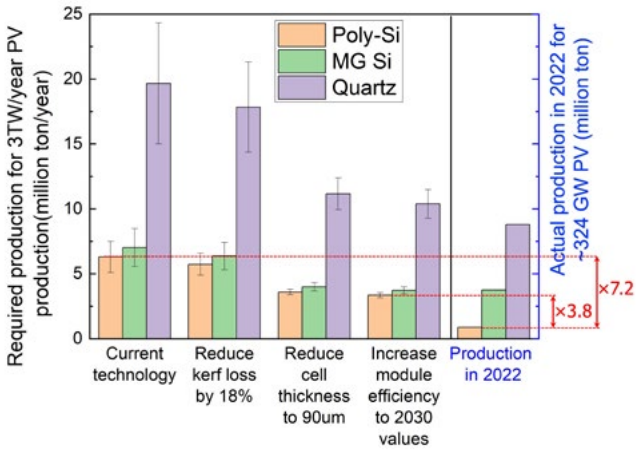

Figure PP5.1.2: Pathways to reduce poly-Si requirements to achieve 3 TW/year PV production.

B.PV glass needs low-iron sand

Recent work within ACAP on sand resource requirements has been reported (Chowdhury et al. 2023).

Glass constitutes 75% of a module by weight, and the majority of this is formed from sand. This sand needs to be high purity (in particular low in iron impurities) to allow high light transmission. We estimate the need for 120–125 Mt of glass per year, considering 22% efficiency, 3.2 mm glass thickness and production of 3.4 TW of PV per year (Haegel et al. 2023).

Mineral reserves are hard to ascertain, and statements of quantities are commonly unclear about iron content. Consequently, it is challenging to make definitive statements about adequacy of sand supply for glass for TW-scale PV production.

However, we can say that Australia has globally significant proven reserves (Figure 5.1.3), especially in Queensland and Western Australia.

The tentative conclusion of this study is that, while there may not be a global shortage of suitable sand there will probably be major challenges in supplying it at a sufficient rate for one or more TW/y PV production.

Therefore, looking for ways to reduce the pressure on this scarce source is necessary. Higher-iron-content sand may be used instead (reduced module efficiency). Sand with high iron content may be beneficiated, at the costs of additional chemical and energy consumption. Alternative materials to glass might be developed but they might generate other environmental issues. Thinner glass might be used but that runs the risk of providing insufficient mechanical support for the cells.

More attractively, clean and uncontaminated low-iron cullet may be recovered from modules at end-of-life and returned to glass factories to offset the demand for sand and other inputs. In many jurisdictions, recycling is required or strongly promoted in any case, so adopting recycling methods that maintain the highest possible quality in the

recovered materials, when of sufficiently low cost, will both reduce landfill and maximise opportunities for replacing new materials.

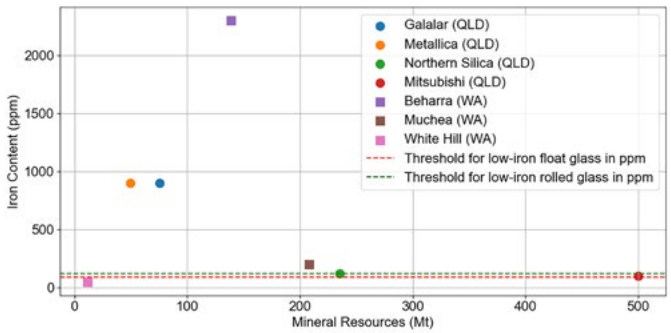

Figure PP5.1.3: Estimated reserves of low-iron silica sand within Australia.

C.Low-embodied energy module frame materials (UNSW)
In this work investigation has been made into options for reducing the material use and emissions from the modules' aluminium frames.

D.Reductions in silver use (UNSW)
In work also reported in section PP4.1.1 , which describe work aiming to achieve ultra-low silver consumption of less than 2 mg/W^{-1}, enabling sustainable manufacturing of silicon solar cells on an upcoming TW-scale

Summary

ACAP has spawned and continues to support ongoing work in this area under ARENA projects "Low-Cost and Sustainable PV Systems for the Terawatt Scale" and "Silver-lean Screen-printing for Sustainable Low-cost Industrial PV Manufacturing".

Highlights

- Review of needs and reduction alternatives for poly-silicon material.
- Understanding of the quality and volume requirements of low-iron sand for PV glass.
- Alternatives for reductions in embodied energy in Al frames.
- A comprehensive analysis of material consumption in existing industrial silicon solar cell technologies.

Future Work

- Ongoing identification and evaluation of material and energy needs for different materials.
- Assessment of opportunities for material reduction, replacement and/or lower emission supply (see F63 in the next (2024) annual report).

References

Chowdhury, T., Chang, N.L. & Corkish, R. (2023). Is There Enough Low-Iron Sand for TW PV Growth? 34th International Photovoltaic Science and Engineering Conference, Shenzhen, 6–10 November 2023.

Haegel, N. M., Verlinden, P., Victoria, M., Altermatt, P., Atwater, H., Barnes, T., Breyer, C., Case, C., De Wolf, S., Deline, C., Dharmrin, M., Dimmler, B., Gloeckler, M., Goldschmidt, J. C., Hallam, B., Haussener, S., Holder, B., Jaeger, U., Jaeger-Waldau, A., Kaizuka, I., Kikusato, H., Kroposki, B., Kurtz, S., Matsubara, K., Nowak, S., Ogimoto, K., Peter, C., Peters, I. M., Philipps, S., Powalla, M., Rau, U., Reindl, T., Roumpani, M., Sakurai, K., Schorn, C., Schossig, P., Schlatmann, R., Sinton, R., Slaoui, A., Smith, B. L., Schneidewind, P., Stanbery, B., Topic, M., Tumas, W., Vasi, J., Vetter, M., Weber, E., Weeber, A. W., Weidlich, A., Weiss, D. & Bett, A. W. (2023). Photovoltaics at multi-terawatt scale: Waiting is not an option. Science 380, 39-42.

Wang, L. (2023). Study on material requirement along the silicon production chain for terawatt scale PV deployment. 2023 Asia-Pacific Solar Research Conference. Melbourne 5–7 December 2023.

PP5.2 TECHNO-ECONOMIC ANALYSIS AND LIFE CYCLE ANALYSIS

Lead Partners
UNSW, ANU

UNSW Team
Nathan Chang, Rong Deng, Renate Egan, Richard Corkish, Ning Song

ANU Team
Andrew Blakers, David Silalahi, Heping Shen

Aims

Techno-economic and life cycle analyses are support activities that relate to all of the other Program Packages, which focus on the technical feasibility of new PV technologies.

Techno-economic analysis evaluates technical work carried out in all the Program Packages from a cost-benefit perspective, while life cycle analysis examines the technologies from an environmental impact perspective.

Progress

A.Durable multi-layer AR coating without module heating (UNSW)
Current porous AR coatings only last about five years, and because they increase coupling of certain wavelengths of light, tend to heat modules to a higher temperature. Because of the temperature coefficient of modules, this leads to reduced electricity yield.
This work (Song, under review) proposes the use of multi-layer sputter-coated AR layers that are more durable (~20-year lifetime), and can

have their properties tuned to avoid heating the modules. Estimated yield and cost modelling shows an improved LCOE with new AR coating, as shown in Figures PP5.2.1 and PP5.2.2.

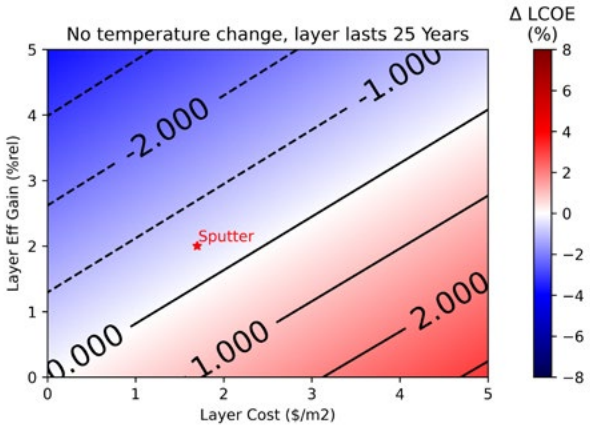

Figure PP5.2.1: The change in LCOE estimated from the addition of a traditional porous AR layer. The point labelled "Porous" shows the cost and efficiency gain expectations of this layer, which is expected to have a short lifetime (five years) and to heat the module by an average of 1K compared to the baseline (no AR coating) scenario.

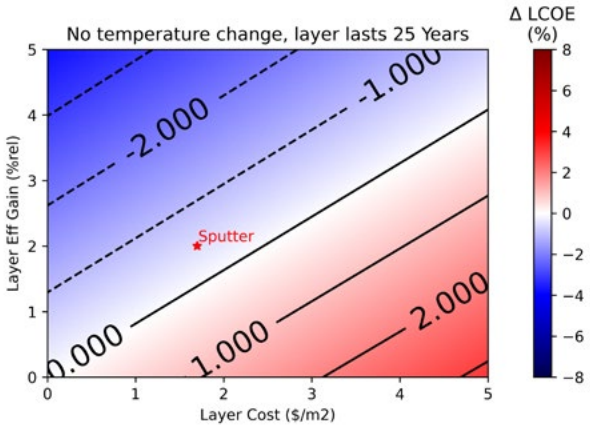

Figure PP5.2.2: The LCOE for the proposed multi-layer sputtered AR coating, which is expected to have a much longer lifetime, and is not expected to increase the module temperature compared to the baseline (no AR coating) scenario.

B.Cost improvements – silicon perovskite tandems (ANU, UNSW)

Silicon perovskite tandem cells are a promising method of improving solar cell efficiency. Recent improvements at ANU to this structure are reported (Duan, under review), with an increased efficiency. In that work, ACAP contributed to the cost analysis, showing that the combination of higher efficiency and reduced material costs (replacing SPIRO-OMeTAD) resulted in an improved cost of production (Figure PP5.2.3) and lower levelised cost of electricity (LCOE), as shown in Figure PP5.2.4.

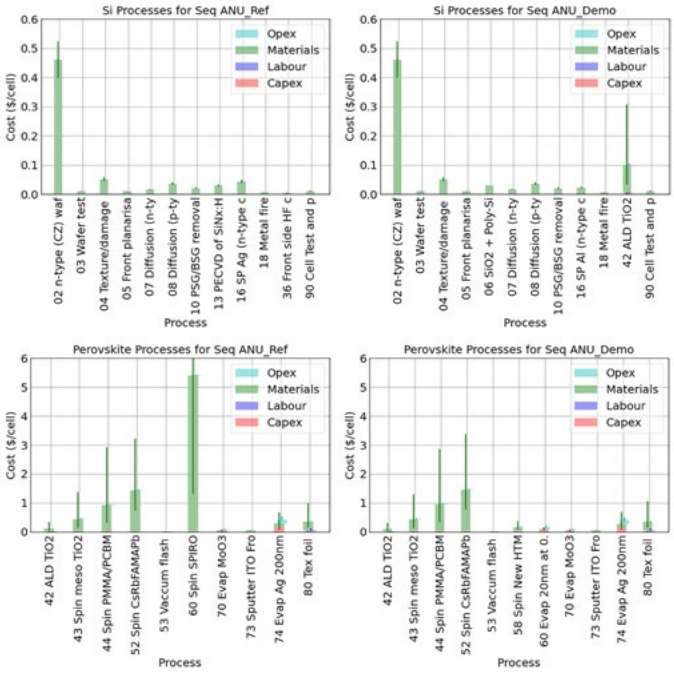

Figure PP5.2.3: Process cost for each step in tandem cell production. Compares previous ANU tandem cells (left) with new ANU tandem cells (right). The bottom Si cell processes (top) and top perovskite cell processes (bottom).

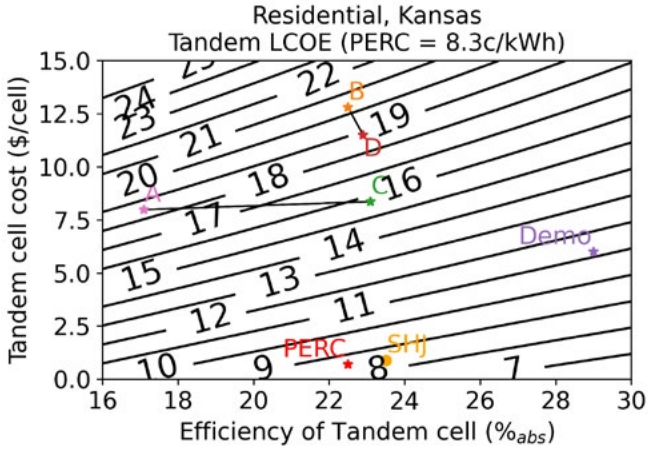

Figure PP5.2.4: LCOE analysis showing that improved efficiency and reduced cost of the demonstrated tandem ("Demo") leads to reduced LCOE compared to the previous reported tandems at UNSW (A, C) and ANU (B, D).

C.100% renewables LCOE in Indonesia (ANU)

Continuing on with previous years' work on the LCOE of 100% renewables, this report (Silalahi, 2024) updated and expanded on analysis of Indonesia.

This study assumed high-voltage inter-regional interconnections and calculated an hourly energy balance using 10 years of meteorological data. It calculated the LCOE of 100% renewables for different regions and the entire super grid (Figure PP5.2.5).

The vast potential of marine floating solar PV potential in Indonesia's calm sea (Silalahi et al. 2023)–- free from strong winds and large waves – is crucial for the transition to 100% renewables (Figure PP5.2.4).

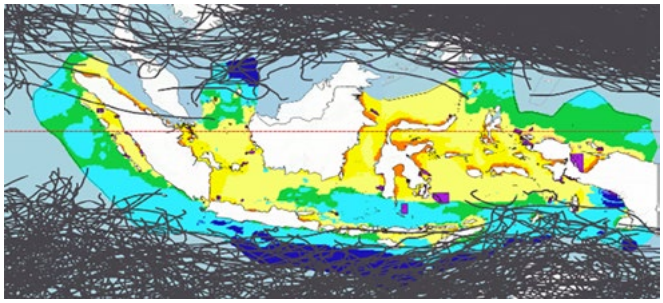

Figure PP5.2.5: Wind and wave assessment to determine the potential for floating solar in Indonesia.

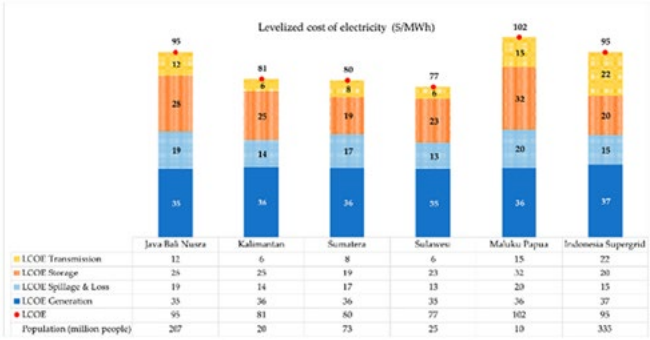

Figure PP5.2.6: 100% renewable LCOE analysis results for Indonesia.

This work showed that Indonesia's vast solar potential combined with capacity for off-river pumped hydro energy storage could readily achieve 100% renewable electricity at low cost.

Summary

Cost and life cycle analysis is an important parallel activity to technical improvements to assess and guide the impact of new technologies.

Highlights

- Financial assessment of new developments in antireflection coating and silicon perovskite tandems.
- Expansion of 100% renewable energy LCOE for Indonesia.

Future Work

- Ongoing commercial assessment of cell and module technologies under development within ACAP.
- Ongoing analysis of 100% renewable energy scenarios worldwide.

References

Duan, L. et al. (under review). Over 29%-efficient, stable n-i-p monolithic perovskite/silicon tandem solar cells based on double-sided poly-Si/SiO2 passivating contact silicon cells.

Silalahi, D. F. & Blakers, A. (2023). Global Atlas of Marine Floating Solar PV Potential. Solar 3(3), 416-433. https://doi.org/10.3390/solar3030023.

Silalahi, D. F., Blakers, A. & Cheng, C. (2024) 100% Renewable Electricity in Indonesia. Energies 17(1), 3. https://doi.org/10.3390/en17010003.

PP5.3 LOCAL MANUFACTURING AND SUPPLY CHAIN ANALYSIS

Lead Partner

UNSW

UNSW Team

Dr Michelle Vaqueiro Contreras, Dr Nathan Chang, Dr Rong Deng, Fred Qi, Prof. Renate Egan

Partners

APVI – Muriel Watt, ITP Renewables – Brett Hallam, Bright Dimension – Oliver Hartley, Deloitte – Will Rayward-Smith, Matt Walden, Elizabeth Boylan, Anna Thoran, Camille Malbrain

UNSW Student

Mohammad Dehghanimadvar

Aims

This activity aims to develop models to support techno-economic analysis of local module manufacturing and supply chain risk. The analysis will include consideration of policy, ethical and social impacts such as market development, risk management, waste handling, local employment and labour rates.

A.Silicon to solar – Australian manufacturing (APVI, UNSW)
ACAP is the major partner in this APVI project looking at silicon refining, wafer, cell and module manufacturing in Australia. This project included wide consultation with industry and government. The report from this work (APVI, 2024) examines in detail the bottom-up cost of manufacturing in each sector within Australia, and the policy support required to build a manufacturing industry for PV in Australia.

An example of the cost analysis results is shown in Figure PP5.3.1, which shows the breakdown of production cost (without profit) for a Chinese-based and Australian-based poly-silicon factory. This analysis was repeated for the other sectors of production – ingot/wafer, cell and module.

Figure PP5.3.1 shows the roadmap from the Silicon to Solar (S2S) report, outlining short-, medium- and long-term recommendations for production and policy to build an Australian PV manufacturing industry.

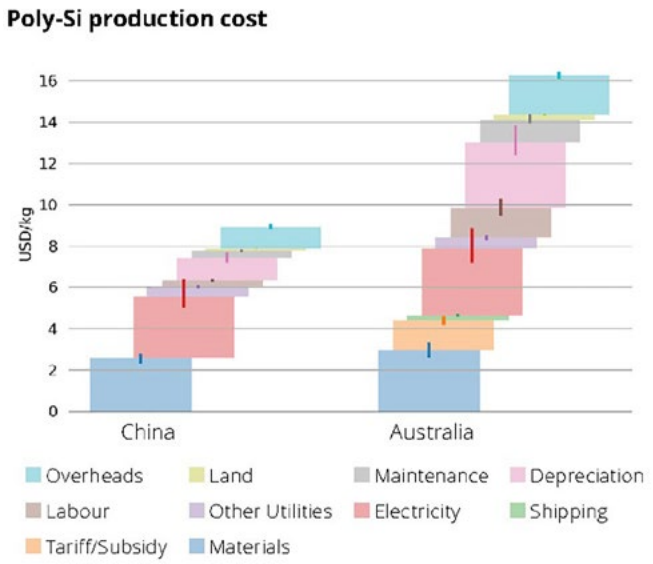

Figure PP5.3.1: Bottom-up cost analysis of Australian vs. Chinese production of poly-Si.

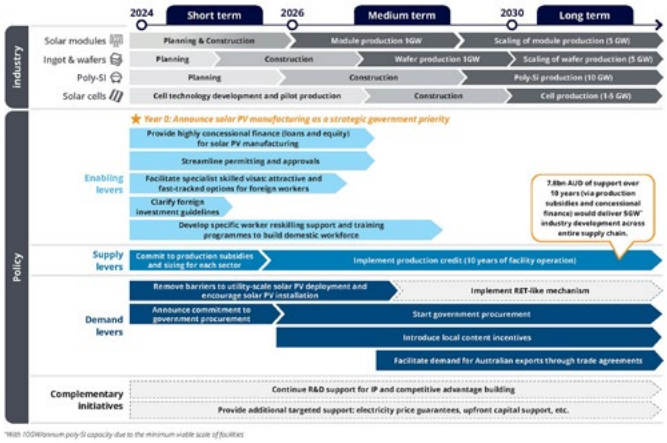

Figure PP5.3.2: Roadmap from the S2S report.

B.Australian module manufacturing – supportive vs. protective policies (UNSW)

In this work (Dehghanimadvar, 2024), a review of government policy options to support local manufacturing was completed. Quantitative modelling was then completed to calculate the level of support required from different policy alternatives that would allow Australian manufacturing to be competitive with imported modules. The policy options considered in this work were derived based on a comprehensive literature review on policies that have been used in PV industry particularly by Germany, China and the US. These options include supportive measures like production credits and investment incentives, among others, in addition to protective policies such as trade barriers.

The initial findings regarding the impact of a production credit on the Australian market are presented in Figure PP5.3.1. This shows the required Australian-made incentives on local module manufacturing by considering the range (10th, 50th and 90th percentile) of internal rate of return that would be achieved if locally produced modules were sold at the median imported PV cost. This research furthermore analyses and quantifies the impact of different ranges of tariffs, as a protective policy, on local manufacturing and PV markets.

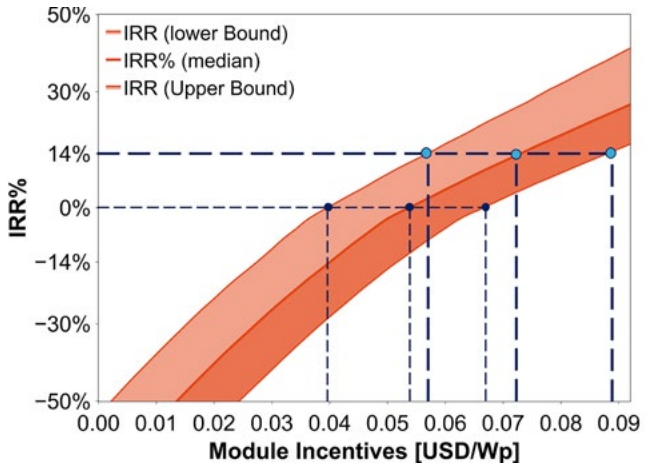

Figure PP5.3.3: The impact of locally-made incentives on 600 MWp Si PV module manufacturing.

The model was also applied to the US case study to quantify the impact of the current implemented policies in the country. Figure PP5.3.4 shows the local Si PV manufacturing with 2023 supportive and protective policies in the US and Figure PP5.3.5 shows how the money flows between government, consumers and suppliers.

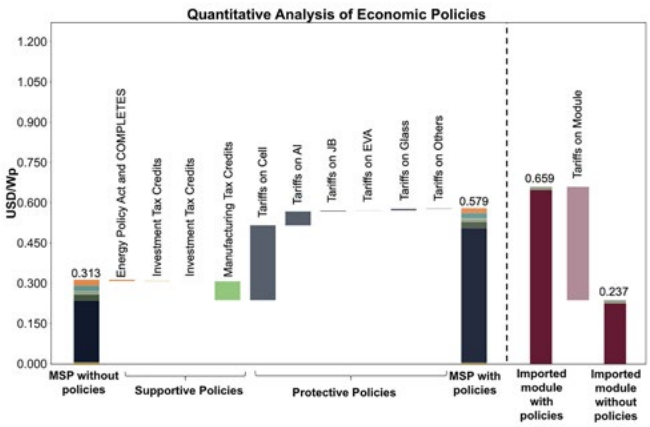

Figure PP5.3.4: Quantitative analysis of economic policies for USA

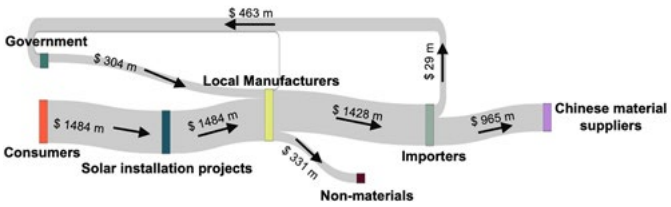

Figure PP5.3.5: Flow of cash between government, consumers and suppliers under different policy conditions.

Summary

ACAP involvement with the APVI S2S project has given a significant boost to this Program Package, complemented by policy work within UNSW ACAP.

Highlights

- Silicon to Solar Project – Detailed bottom-up cost analysis of Australian manufacturing across the PV value chain shared with government in late 2023, published February 2024
- Quantitative analysis of both supportive and protective policies to enable Australian module manufacturing.

Future Work

- Expected ongoing engagement with industry and government on Australian manufacturing – technical, financial and policy related.

References

APVI (2024). Silicon to Solar – Foundations for Solar PV Manufacturing in Australia. https://apvi.org.au/wp-content/uploads/2024/02/S2S-Foundations-for-Solar-PV-Manufacturing-in-Australia.pdf.

Dehghanimadvar, M., Egan, R. & Chang, N. L. (2024). Quantifying the Costs of Diversifying Silicon PV Module Assembly with Local Economic Policies. Joule (accepted).

PP5.4 PERFORMANCE ANALYSIS AND OPTIMISATION

Lead Partner
UNSW

UNSW Team
Phillip Hamer, Bram Hoex, Xutao Wang, Shukla Poddar, Svetlana Tkachenko

Partners
Tractile, 5B

Aims

This activity aims to validate field performance of module technologies and to seek to optimise performance and/or LCOE outcomes. Module performance is application and environment specific. Measurement, analysis, modelling and simulation of performance in Australian conditions is expected to yield improved performance through better module and system design.

Work to date, detailed below, includes analysis and modelling of a PV thermal product with industry partner Tractile, operations and maintenance (O&M) and levelised cost of electricity (LCOE) modelling of large-scale solar deployment options.

A. Tractile project
This ACAP project was completed this year. An integrated photovoltaic thermal product produced by Tractile was analysed and modelled for durability and performance.

For more details see project closing report in section 6.14.

B. O&M and LCOE modelling

As a follow-on from an ACAP small-grant project in LCOE modelling (partner Sun Cable), ACAP researchers have been awarded an ARENA grant TRAC 012 "Optimal O&M Strategy and LCOE-Modelling for Ground-Mounted PV" which focuses on modelling and optimising electrical yield and LCOE. In the past year the project has focused on improving models for cell temperature and module degradation. These two topics are closely linked as increased cell temperatures accelerate module degradation, as well as decreasing module performance in the short term.

In the first instance the industry standard Faiman model has been expanded to include the effects of radiative heat transfer with the sky, following the work of McIntosh et al. (2022) and Driesse and Stein (2022). Transient effects were also included. In this project this approach was applied to the 5B MAVERICK mounting system. This greatly improved the fit to data particularly during the morning and evening hours, with no additional fitting parameters required (Hamer et al. 2023).

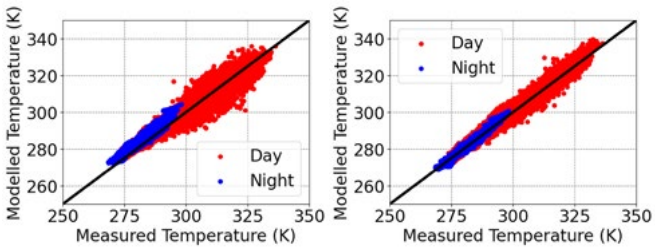

Figure PP5.4.1: Scatter plots comparing measured and modelled temperature data when using (left) industry standard temperature models and (right) models including sky radiation and transient effects.

It was also observed that different models for sky radiation impacted the fits, with best results observed when using the ERA-5 re-analysis data set.

A much more detailed approach is the use of computational fluid dynamics (CFD) to model the MAVERICK system. Using CFD allowed for the prediction of temperatures across the module (and associated mismatch losses), with differences of up to 10°C simulated. The impact of wind direction was also considered in detail, along with its effect on temperatures across the module (Tkachenko 2023).

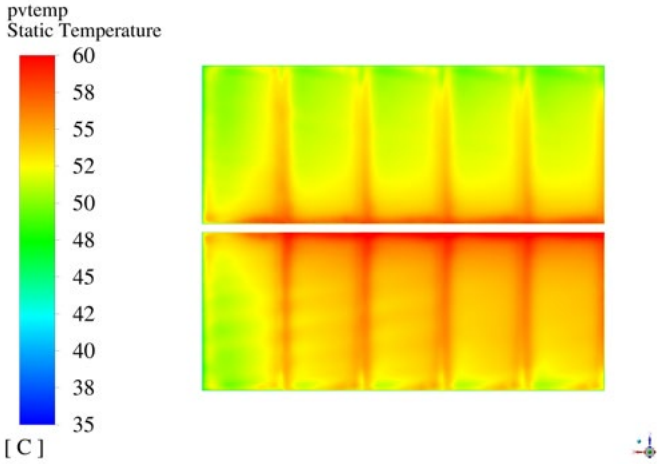

Figure PP5.4.2: Simulated temperatures across a 5B MAVERICK (10 modules) using CFD.

While temperature variations across a module can lead to mismatch losses in the short term (up to 0.4%), the greater impact is likely to be on degradation over time. System failure and degradation is a key concern for utility-scale solar plants, and improved modelling is clearly required. The current industry standard model is linear degradation with time, with no consideration for operating conditions.

During this project a modelling framework has been developed that considers both the operating conditions and the impact on module parameters for different degradation and failure modes (Poddar et al. 2023). The key environmental stressors have been identified as: module temperature, UV exposure, relative humidity, chemical reactions and soiling. These vary with location and with system design (higher DC:AC ratios lead to higher module temperatures, while SAT systems also run hotter due to increased plane-of-array irradiance). Our model captures these impacts and determines appropriate degradation rates across location, system design and time.

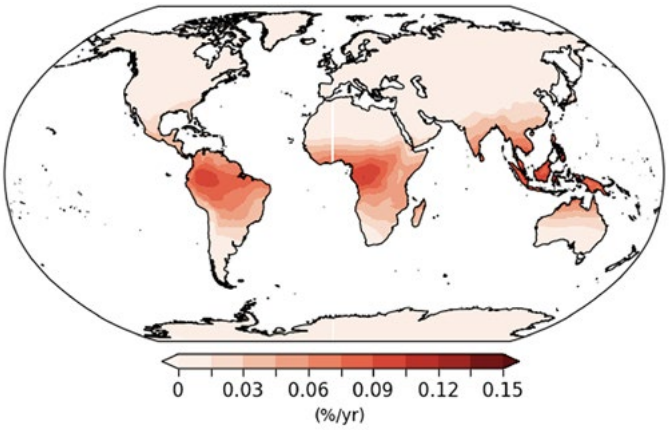

Figure PP5.4.3: Expected degradation rates for a mode dependent on temperature and humidity across the world.

The model also departs from the usual approach of simply de-rating the system DC output to account for degradation. Instead as degradation occurs the electrical characteristics, such as photocurrent, dark saturation current, series resistance etc. are altered. For example, degradation of EVA encapsulant has been observed to lead to reduced photocurrent (light is captured in the encapsulant rather than the cell) and increased series resistance (acetic acid is formed in the encapsulant and attacks the metal contacts). Using such a detailed model allows for simulation of non-linear interactions between different degradation modes.

The final model will allow for informed decisions to be made around the module bill-of-materials with clear visibility of the trade-off between higher cost materials and reduced degradation for any given location.

The focus of the project to date has been on the modelling side, with significantly more detailed models implemented for module operating temperature and system degradation. With this framework in place systems can be simulated with greater accuracy, and decisions around system design and operation can be made in an informed manner.

Highlights

- Completion of ACAP project with Tractile.
- 37% reduction in error when simulating module temperature for 5B MAVERICK prefabricated arrays.
- Development of a world-leading model for degradation.

Future Work

- Application of improved thermal and degradation models to evaluate and optimise system operation.
- Establish verified parameters for degradation modes.
- Simulation and optimisation of operation and maintenance.

References

Driesse, A., Stein, J. S. & Theristis, M. (2022). SANDIA REPORT Improving Common PV Module Temperature Models by Incorporating Radiative Losses to the Sky. [Online]. Available: https://classic.ntis.gov/help/order-methods/.

Hamer, P. et al. (2023). Improved thermal modelling of the 5B MAVERICK system: Impact of sky temperature. In Proceedings of the Asia-Pacific Solar Research Conference 2023, Australian PV Institute.

McIntosh, K.R. et al. (2022). The influence of wind and module tilt on the operating temperature of single-axis trackers. In 2022 IEEE 49th Photovoltaics Specialists Conference (PVSC), 1033-1036. doi: 10.1109/PVSC48317.2022.9938577.

Poddar, S. et al. (2023). Global-Scale Non-Linear Modelling of Photovoltaic Module Degradation. In Proceedings of the Asia-Pacific Solar Research Conference 2023, Australian PV Institute.

Tkachenko et al. (2023). CFD Modelling of the 5B MAVERICK system and temperature variations across PV modules. In Proceedings of the Asia-Pacific Solar Research Conference 2023, Australian PV Institute.

PP5.5 END-OF-LIFE MANAGEMENT: EXTEND, RE-USE, REPAIR, RECYCLE

Lead Partner
UNSW

UNSW Team
Rong Deng, Chence Niu, Richard Corkish, Renate Egan

Partner
Neoen

UNSW Students
Verity Tan, Olivia Bowen, Ricky Huang

Aims

This task aims to minimise waste and decrease barriers to re-use, repair and recycling by extending the lifetime of photovoltaics, by re-use and repair solutions that call for research around end-of-life classification and diagnostics. Recycling aims to process and extract all the materials contained in the end-of-life devices and feed these materials back into the supply chain that relies on research on how to best process the end-of-life devices to achieve high recovery rates, and low processing and environmental cost.

Work to date, described in detail in the following, includes completion of a scoping study on end-of-life management of solar panels in Australia, with partners Neoen, a cost-benefit analysis of solar panel recycling in Australia and an assessment of organic solvent processing in chemical recycling of solar panels.

A.Scoping solar panel end-of-life management in Australia (UNSW)

The study provides an in-depth analysis of the current PV recycling landscape, market opportunity, best practice and most cost-effective strategies to manage solar panels' end of life in Australia. The research was supported by Neoen, and conducted by ACAP (UNSW) in partnership with the Research Centre for Integrated Transport Innovation (rCITI UNSW). The project achieved the following outcomes:

- Assessed the volume and location of end-of-life solar panels in Australia from 2023 to 2035.
- Mapped the optimal locations, treatment capacities and associated logistic networks to for large-scale PV waste management facilities in Australia for the 2023–2035 period.
- Analysed the cost-benefits of module recycling and re-use technologies for Australia to understand the technical, investment and market requirements to establish a domestic PV recycling industry.
- Highlighted best practice of PV end-of-life management policy frameworks and businesses.
- Developed a case study for the ACT Region.
- Delivered a 12-year industry roadmap (2023–2035) bringing results from all above that the industry can take as a step-by-step guide to sustainably deal with PV waste in Australia.

More details of this report can be found in "Scoping study: Solar Panel End-of-life Management in Australia" (Deng 2024).

The trajectory for PV waste generation in Australia is evident, with forecasts indicating a potential total of 680,000 tonnes by 2030 and reaching 1 million tonnes between 2034 and 2035 (Figure PP5.5.1). On an annual scale, waste volume will surpass 50,000 tonnes in 2025 and will reach approximately 100,000 tonnes, equivalent to 1.2 GW per year, from 2030 to 2035 on a national scale. Significantly, more than 80% of the decommissioned solar panels by 2030 are projected to emanate from small-scale distributed PV systems, attributable to the earlier evolution of Australia's residential PV market.

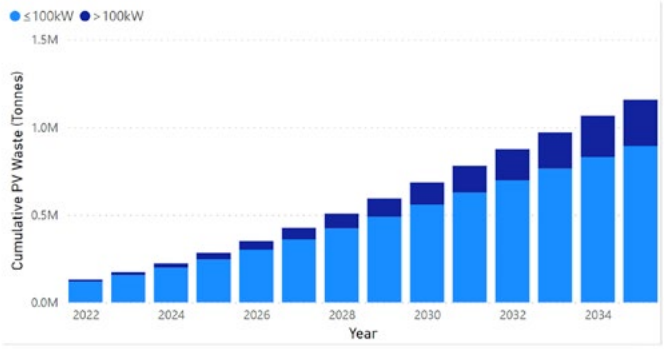

Figure PP5.5.1: Cumulative PV waste in tonnes in Australia from 2022 to 2035, comparison between small (< = 100 kW) and large-scale (> 100 kW) systems.

While large-scale solar farms in regional and remote Australia have no decommissioning plans before 2030, the bulk of this waste will cluster around major Australian cities: Sydney, Melbourne, Brisbane, Perth and Adelaide (Figure PP5.5.2). This issue is starting to manifest with plans to decommission Australia's first large-scale solar farm in 2024 . Australia needs facilities in major cities now to be taking feedstock already available and ramp up capacity for the large-scale volumes that will reach their end of life, and then progressively branch out to regional areas.

Figure PP5.5.2: 3D bar maps showing cumulative PV waste (in tonnes) generated in each LGA in 2030. The height of the blue bar indicates the expected volume, and the red region indicates a centralised area with a high waste volume. If there is no blue bar, it means there will be low or negligible waste solar panels in that area by 2030.

B.Cost-benefit analysis of PV module recycling technologies in the Australian context

The cost-benefit analysis was conducted on various PV recycling technologies within the Australian context (Huang 2023). The unit cost calculation factors in learning effects (LE) and economies of scale (EoS), by considering the PV waste projection in Australia. LE refers to cost reduction achieved through cumulative experience in waste processing, while EoS indicates decreased unit costs with increased operational scale. The initial high costs of PV recycling, currently requiring subsidies, are projected to decrease due to LE (Figure PP5.5.3).

A cost break-even point can be achieved in under three years for simple recycling methods such as electrostatic separation when the overall recycling rate across the country maintains over 50% (i.e. 50% retired modules can be collected and recycled at recycling centres rather than being stockpiled, landfilled or exported). Higher recycling rates further accelerate the cost reduction. Therefore, initiating large-scale recycling operations as soon as possible is key to achieving financial viability early.

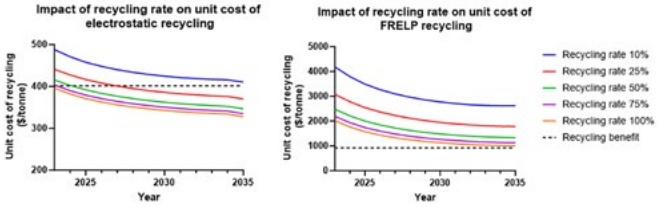

Figure PP5.5.3: Cost trajectory over time for PV module recycling using the electrostatic and FRELP methods, factoring in learning effects at various recycling rates.

C.Organic solvents for chemical recycling of photovoltaic panels

This study (Bowen 2023) investigates the efficacy of four organic solvents – toluene, pentane, hexane and D-limonene – in the chemical recycling of photovoltaic panels. Two sample types were subjected to treatment: samples that were manually dismantled and those processed with a hot-knife technique. Each solvent's ability to dissolve the ethylene-vinyl acetate (EVA), and separate the cells was assessed, followed by both alkaline and acidic etching processes. The resultant solutions were then analysed via inductively coupled plasma optical emission spectrometry (ICP-OES). Additionally, differential scanning calorimetry (DSC) was employed to evaluate alterations in the polymer structure of the EVA layer post-solvent dissolution.

Findings indicate that the hot-knife pretreatment (200°C for one minute) facilitates EVA delamination across all solvents. D-limonene proved to be the most effective in material extraction from manually dismantled panels, while toluene showed the highest efficacy for panels treated with the hot-knife. The results point to two potential mechanisms during organic solvent delamination: one that involves dissolution at the interface, allowing for the detachment of cells, and another that involves destruction of the bulk cross-linked EVA, which is supported by varying degrees of observed structural changes.

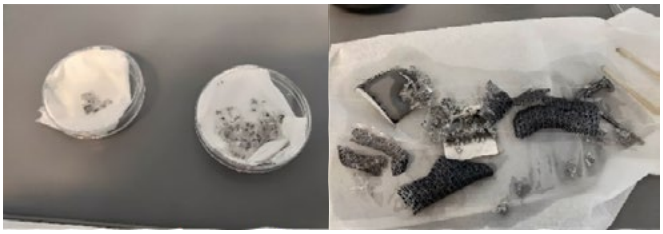

Figure PP5.5.4: Pictures of manually dismantled cells and hot-knife cells following submersion in organic solvents.

Summary

The emerging PV end-of-life challenge in Australia, representing a potential market opportunity exceeding $1 billion by 2035, brings both exciting prospects and significant hurdles. To manage this emerging but not well understood new waste stream, while achieving an 80% resource recovery rate under the National Waste Policy, our scoping study aims to provide some certainty as to when, what and where the problem is, in order to develop a 12-year roadmap for Australia to tackle the end-of-life PV challenge, to enable sustainable business

opportunities with positive economic, environmental and social outcomes. ACAP is committed to ongoing research in this field to bolster the local industry's capacity to build a robust domestic solar end-of-life management capability.

Highlights

- A detailed assessment of the volume of end-of-life solar panels in Australia was conducted, covering the period from 2023 to 2035.
- A comprehensive 12-year industry roadmap (2023–2035) for sustainable management of PV end-of-life materials in Australia has been established.
- The initial high cost of recycling, which presently necessitates subsidies, is projected to decrease significantly and reach a break-even point due to learning effects and improved efficiencies.
- Completed a cost-benefit analysis of various PV recycling technologies within Australia, showing a three-year cost break-even point, and the need for larger recycling volumes to access economies of scale.
- Preliminary studies of organic solvents for delamination in recycling of photovoltaic panels provide greater insight into delamination pathways.

Future Work

- Advance scalable, efficient and comprehensive recycling solutions through continuous R&D and industry collaboration.
- Further research is needed to explore the significant market potential in the re-use of solar panels.
- Investigate and understand the end-use applications of recycled materials within the Australian context to facilitate the establishment of new businesses in this sector.
- Continuous improvement and updating of modelling methodologies and results to reflect the evolving industry and technological advancements.

References

Bowen, O. & Deng, R. (2023). Comparison of organic solvents for chemical recycling of photovoltaic panels. (2023). APSRC, Melbourne, Australia, 5–7 December 2023.

Deng, R., Tan, V., Niu, C. & Egan, R. Scoping study: Solar Panel End-of-life Management in Australia. Expected release in 2024.

Huang, Z. & Deng, R. (2023). Cost benefit analysis of PV module recycling technologies in the Australian context. APSRC 2023, Melbourne, Australia, 5–7 December 2023.

PP5.6 NOVEL CHARACTERISATION FOR MANUFACTURING AND IN-FIELD PERFORMANCE

Lead Partner
UNSW

UNSW Team
Ziv Hameiri, Thorsten Trupke, Oliver Kunz, Brendan Wright, Rama Sharma

Partner
SolarCycle

UNSW Student
Yun Li

Aims

This work package aims to develop novel characterisation techniques, for applications in PV manufacturing, to monitor in-field performance of PV at scale and inform end-of-life decisions. A significant aspect, apart from the development of the associated methods and systems, is the development of a systematic approach for applying these techniques in routine operation and maintenance, with a view to optimise the performance of PV systems, while keeping the associated extra costs at a minimum.

Progress

A.Photovoltaic module end-of-life assessment (UNSW)

As reported in Wright, 2023, the objective of this project was to develop an automated module quality assessment pipeline to inform end-of-life (EOL) decisions based on in-field luminescence images.

Methods used included:

- luminescence image pre-processing (perspective correction and segmentation)
- machine learning-based cell image feature extraction and defect classification
- cell-level quality and risk assessment for module quality bin assignment.

Results included:

- successful robust image correction methodology for de-skew and cell-in-module segmentation
- validation of automated module quality assessment against manual domain experts
- preliminary calibration of module circuit simulation for power loss estimation.

See Figure 5.6.1 for an example of processed images.

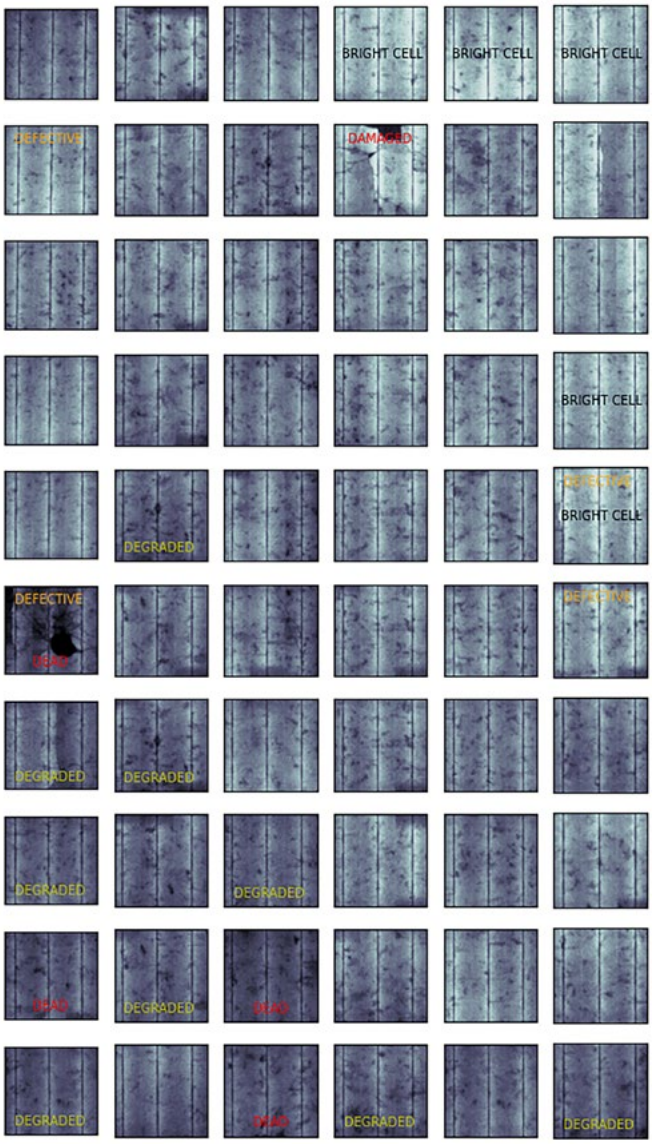

Figure PP5.6.1: Example module quality assessment from luminescence image after pre-processing and segmentation. Identified defects are labelled by class and severity.

B.Daylight photoluminescence imaging

The ACAP small grant: "Survey of Solar Module Quality on Australian Solar Farms using Outdoor Photoluminescence Imaging and Fourier Transform Infrared Spectroscopy" finished this year, and the final technical report is included in section 6.73.

That ACAP project formed the basis of a five-year ARENA grant: "Daytime Inspection Solutions for Advanced Operation and Maintenance of Solar Farms" to continue this work.

- Various daylight PL technologies are currently being developed for residential and utility-scale applications.
- Commercial aspects of these technologies will be developed in later years.

Summary

This year has seen ACAP make progress in automatic quality assessments of in-use modules and advances in daylight PL imaging.

Highlights

- Successful image correction and quality assessment of modules for EOL assessment.
- Enhanced collaboration with SolarCycle – the company will join as a SPREE CoOp scholarship sponsor in 2024.
- Successful completion of daylight PL project including award of five-year ARENA grant to follow-on this work.

Future Work

- Grant applications with a Sydney-based recycling company.
- ARENA grant for further development of Daytime Inspection Solutions.

References

Wright, B. et al. (2023). Automated Photovoltaic Module Quality Assessment: Defect Identification and Classification from Luminescence Images using Generative Representation Learning. In Proceedings of the Asia-Pacific Solar Research Conference 2023, Australian PV Institute.

PP6
PV FUTURES AND KNOWLEDGE SHARING

OVERVIEW

The PP6 PV Futures and Knowledge Sharing package includes technology perspectives, commercialisation activities, knowledge sharing and capacity building. ACAP is building on past success in knowledge sharing and communications and extending this to increase engagement, to raise the profile of research outcomes, to participate in the public conversation and to support the development and deployment of ultra-low-cost PV.

The knowledge sharing program has been extended to include technology roadmapping and PV futures. ACAP will monitor, model and report on global developments in PV devices, processes and applications, delivered through a series of authoritative reports with an over-the-horizon view of the future PV industry, facilitating informed decisions.

PP6.1 PV FUTURES

Lead Partners
UNSW, ANU

UNSW Team
Prof. Renate Egan, Dr Nathan Chang, Prof. Ziv Hameiri, Dr Richard Corkish

ANU Team
Prof. Andrew Blakers, Prof. Kylie Catchpole

CSIRO Team
Dr Anthony Chesman, Dr Régine Chantler

Monash Team
Jacek Jasieniak

UQ Team
Prof. Paul Burn, Dr Paul Shaw

UoM Team
Prof. David Jones

Industry Partners
Australian Photovoltaics Institute (APVI)

Funding Support
All partners, ACAP

Aims

This work package resources the continuous review of PV technologies, markets and opportunities and delivers an over-the-horizon perspective on developments in current and emerging PV technologies.

Progress

In engaging nationally and globally, ACAP has made significant contributions to the global conversation on PV futures, including in a number of peer-reviewed papers that review photovoltaics and related technologies, in contributions to roadmaps, including the significant Silicon to Solar report aimed at informing decision-makers on Australia's role in the solar supply chain and in the public conversation, including a large number of public outreach activities such as the annual ANU Solar Oration.

Roadmapping: ACAP partnered with the Australian Photovoltaics Institute (APVI) during 2023 to develop the important roadmap report, Silicon to Solar (Vaqueiro Contreras et al. 2023).

This report is an outcome of the APVI's Silicon to Solar Study (S2S Study) commissioned by ARENA and delivered by the APVI that builds on foundational research in ACAP's Manufacturing Issues program. The study was conducted over eight months between March 2023 and October 2023 in a collaboration with ACAP, Bright Dimension, ITP Renewables and Deloitte. The study analyses the solar value chain from poly-Si to module production, assessing whether Australia can play a role and what is required for the development of a domestic solar industry. The study uses tools including techno-economic analysis developed at UNSW ACAP and considers business rationale and policy, to develop a roadmap for establishing diversified PV supply chains. The report delivers recommendations for government and industry stakeholders and was delivered to ARENA in October 2023, and publicly released in February 2024.

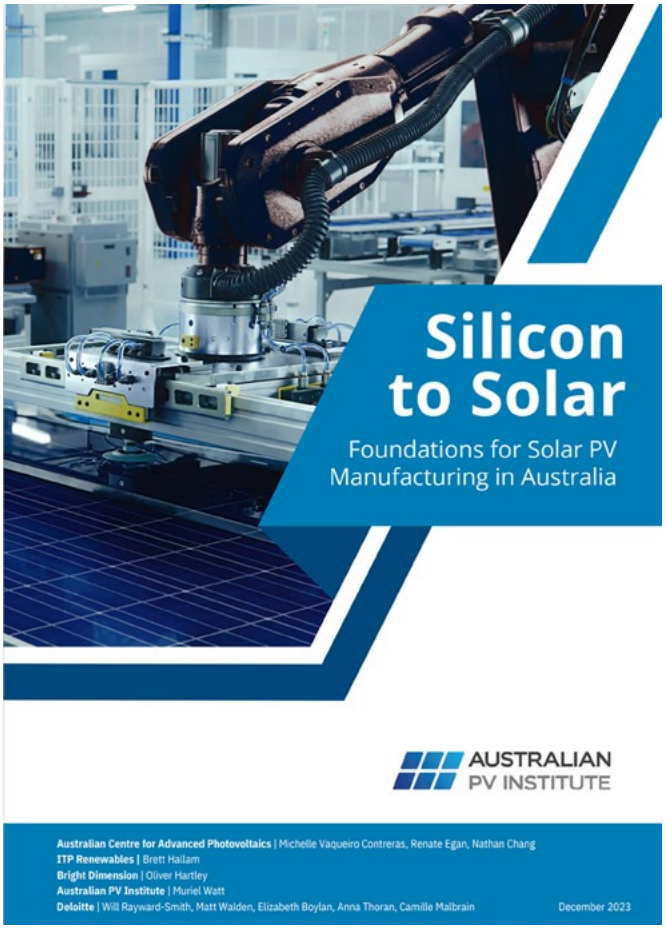

Figure PP6.1: ACAP researchers were key participants in the team that delivered the Silicon to Solar report in 2023.

Outreach: Professor Renate Egan delivered the ANU Solar Oration in 2023 entitled 'Generation Change – and the leading role of solar PV' and the path to ultra-low-cost solar.

Figure PP6.2: Solar Oration by Professor Renate Egan, Executive Director of ACAP

Technology Reviews: ACAP researchers published several reviews during 2023, including:

- Abdin, Z., Al Khafaf, N., McGrath, B., Catchpole, K. & Gray, E. (2023). A review of renewable hydrogen hybrid energy systems towards a sustainable energy value chain. Sustainable Energy & Fuels 7, 2042-2062.
- Cui, D., Wang, R., Qian, C., Shen, H., Xia, J., Sun, K., Liu, H., Guo, C., Li, J., Yu, F. & Bao, W. (2023). Achieving High Performance Electrode for Energy Storage with Advanced Prussian Blue-Derived Nanocomposites – A Review. Materials (Basel) 16(4) 16(4):1430. doi: 10.3390/ma16041430.
- Du, H.-Q., Jiang, Y., Rothmann, M. U., Bach, U., Cheng, Y.-B. & Li, W. (2023). Transmission electron microscopy studies of organic–inorganic hybrid perovskites: Advances, challenges, and prospects. Applied Physics Reviews 10, 021314
- Duan, L., Walter, D., Chang, N., Bullock, J., Kang, D., Phang, S. P., Weber, K., White, T., Macdonald, D., Catchpole, K. & Shen, H. (2023). Stability challenges for the commercialization of perovskite–silicon tandem solar cells. Nature Reviews Materials 8, 261-281.
- Herrando, M., Wang, K., Huang, G., Otanicar, T., Mousa, O. B., Agathokleous, R. A., Ding, Y., Kalogirou, S., Ekins-Daukes, N., Taylor, R. A. & Markides, C. N. (2023). A review of solar hybrid photovoltaic-thermal (PV-T) collectors and systems. Progress in Energy and Combustion Science 97.
- Howlader, A. H. & Uddin, A. (2023). Progress and Challenges of Chloride–Iodide Perovskite Solar Cells: A Critical Review. Nanomanufacturing 3, 177-216.
- Kamble, G. U., Shin, S. W., Park, S. W., Gaikwad, M. A., Karade, V. C., Jang, J. S., Park, Y., Ghorpade, U. V., Suryawanshi, M. P. & Kim, J. H. (2023). Germanium Selenide: A Critical Review on Recent Advances in Material Development for Photovoltaic and Photoelectrochemical Water-Splitting Applications. Solar RRL 7.
- Silalahi, D.F. & Blakers, A. (2023). Global Atlas of Marine Floating Solar PV Potential. Solar, 3(3), 416-433, 2023, https://www.mdpi.com/2673-9941/3/3/23.
- Silalahi, D. F.; Blakers, A. & Cheng, C. (2024).100% Renewable Electricity in Indonesia. Energies 17, 3. https://doi.org/10.3390/en17010003.
- Tarique, W. B. & Uddin, A. (2023). A review of progress and challenges in the research developments on organic solar cells. Materials Science in Semiconductor Processing 163.
- Vaqueiro-Contreras, M., Hallam, B. & Chan, C. (2023). Review of Laser Doping and its Applications in Silicon Solar Cells. IEEE Journal of Photovoltaics 13, 373-384.
- Wang, X., Zhang, M., Hou, T., Sun, X. & Hao, X. (2023). Extrinsic Interstitial Ions in Metal Halide Perovskites: A Review. Small 19, e2303060.
- u, Y., Bai, X., Li, S., Shi, J., Wang, L., Xi, F., Ma, W. & Deng, R. (2023). Review of silicon recovery in the photovoltaic industry. Current Opinion in Green and Sustainable Chemistry 44.

PP6.2 Current and Emerging Applications of PV

While ACAP research focuses on delivering ultra-low-cost solar, it does so with reference to current and emerging applications of photovoltaics.

Australia leads in the per capita deployment of solar, with over 1.3 kW of solar per person by the end of 2023. With 35 GW of solar installed, the majority is on rooftops. Large-scale, ground mount deployment will be needed to deliver ultra-low-cost solar but there is much to be learned from the successes in rooftop solar and integration. The falling cost of solar also creates new opportunities in applications of PV and ACAP continues to monitor and engage in developments as they relate to efficiency improvements, cost reductions, market opportunities and regulatory change that translate to applications in ultra-low-cost solar.

PP6.2.1 GROUND MOUNT PV

UNSW Team
Nathan Chang, Anna Bruce, Mike Roberts, Renate Egan

ANU Team
Andrew Blakers, Matthew Stocks

Aims

- Maintain a close and detailed watch on global developments on technological changes while also pursuing research including techno-economic analysis into the logistics of site delivery and in-field performance.
- Identify, assess and seek research partnerships to cut LCOE (levelised cost of energy) further through improved performance at low cost and high reliability and to adapt them to Australian circumstances.

Progress

Ground mount photovoltaics is where there is significant opportunity for cost reduction and performance improvement, in targeting a $20/MWh levelised cost of electricity from solar.

ACAP engages across the industry sector in Australia to support deployment, including with partner companies like 5B, in technology assessment with partner companies including SunCable and in performance and reliability of large-scale solar, with technology development, including the daylight photoluminescence capabilities, now funded independently through ARENA's TRAC R&D round.

Published project activity includes:

- Fluid dynamic (CFD) modelling of the 5B MAVERICK system and temperature variations across PV modules (Tkachenko et al. 2023)
- Improved thermal modelling of the 5B MAVERICK system: impact of sky temperature (Hamer et al. 2023)
- Impact of different PV mounting systems on yield, material consumption and emissions intensity. 2023 Asia-Pacific Solar Research Conference. Melbourne 5–7 December 2023 (Wang 2023)
- O. Kunz, Survey of Solar Module Quality on Australian Solar Farms using Outdoor Photoluminescence Imaging and Fourier Transform Infrared Spectroscopy (see section 6.73).

In a related activity, ANU researchers completed and published a global atlas of offshore floating solar PV that identified vast opportunities for Nigeria and Indonesia and surrounding countries to harvest up to 1 million terawatt-hours of electricity per year from calm equatorial seas that never see large waves nor strong winds.

PP6.2.2 ROOFTOP PV

UNSW Team
Anna Bruce, Mike Roberts, Richard Corkish

Industry Partner
Australian PV Institute

Aims

- Monitor market growth and global technology developments with potential applications to Australian problems.
- Extend collaboration with industry partners, to resolve technical barriers for lightweight PV modules for commercial and industrial roofs.
- Monitor innovative business models that will drive solar uptake including solving the split incentive challenge for landlords and roof leasing.

Progress

Australian solar deployment has been dominated by rooftop solar, developing world's best practice in deployment and integration. As a result of learning by doing, Australia has demonstrated the lowest cost of electricity at source from rooftop solar and has developed some of the most efficient practices and processes around solar integration. Challenges with grid integration of large volumes of distributed energy resources arise and continue to be managed.

ACAP supports research and progress in rooftop solar, where it relates and informs research into ultra-low-cost solar.

The UNSW-based ACAP project, "Mapping consumer outcomes of rooftop solar potential", concluded in 2023 (see the closing report in section 6.13 of this report). The project validated APVI's SunSPOT methodology against output data from real household PV systems, developed a novel method of generating synthetic residential load profiles based on climate zones, household characteristics and appliance ownership, and integrated it into the updated SunSPOT tool, rolled out nationally. The team also developed a high-level method for approximate PV system sizing, based on tariff and customer load profile. See section 6.13 for details.

ACAP has been monitoring innovative business models developing in 2023 that will drive solar uptake and promote equitable access, including solving the split incentive challenge for landlords/renters and roof leasing. Researchers at ANU published in May 2023 (Hammerle et al. 2023) on their study of the barriers perceived by investor-landlords to installing solar PV on domestic rental properties, including their expectation that renters will be unwilling to pay higher rents to compensate them for the expense.

PP6.2.3 AGRICULTURAL PV

ANU Team
Marco Ernst

UNSW Team
Jose Bilbao, Ziv Hameiri, Ivan Perez-Wurfl, Santosh Shrestha, Nathan Chang, Anna Bruce, Ian Thomas

Industry Partner
Tindo Solar

Aims

This task aims to identify opportunities to increase large-scale deployment of solar energy by addressing the challenges of system design for photovoltaics in agriculture. It will do so by undertaking detailed modelling and design to achieve an understanding of the role of mono- andbifacial photovoltaic and flexible technologies in the context of complex environmental factors and the impact on agricultural activities.

Progress

One promising approach to enhancing the benefits and reducing the problems of co-location of PV arrays and growing plants is to restrict the reduction by PV of tramsmission to plants of the range of wavelengths [in sunlight that drive photosynthesis, 400–700 nm. UNSW research (Thomas 2023) aims to make the PV modules spectrally selective, transmitting the photosynthetically active radiation to the plants and absorbing other wavelengths. The UNSW project (intends to partner partially populated c-Si modules with novel thin-film embedded optics to support a low level of concentration of the near-infrared spectral components, allowing them to be used for electricity generation.

UNSW and CSIRO have been collaborating with Australian PV module manufacturer Tindo since 2022 on development of commercial semi-transparent solar modules that could be used in fields or integrated into greenhouses. Silicon PV cells are enclosed within semi-transparent material embedded with nanoparticles, which allow transmission of the spectral fraction needed for photosynthesis, while diverting other spectral components to the rear of bifacial modules. Further, the modules create a micro-environment that provides crop protection from weather extremes for field application.

PP6.2.4 EMERGING APPLICATIONS

Aims

Photovoltaic deployment at TW scales will require ultra-low-cost photovoltaics that operate at high efficiency for decades. Complementing the TW scale deployment, there are emerging sectors where photovoltaics may not have the same potential for scale of deployment but will have an increasing and important role and at a higher value point. These areas include the transport, agriculture, space and building sectors. Each of these sectors presents distinct photovoltaic requirements, considered in Table PP6.1.

Application (Sector)	Scale	Ultra-low Cost <5c/kwhr	High Efficiency >20%	Low Weight >50W/kg	Tunable Colour	Flexibility	Light Transmission	Longevity +20yr	Recyclability
Large Scale Solar Farms (Electricity)	TW	✓	✓	•	×	×	×	✓	✓
PV in Vehicles (Transport)	MW	×	✓	•	✓	✓	•	×	•
Solar Greenhouses (Agriculture)	MW	×	•	•	•	×	•	•	•
Satellites (Space)	MW	×	✓	✓	×	×	×	✓	×
Rooftop Solar (Building)	GW	×	✓	•	×	×	×	✓	✓
Solar Windows (Building)	GW	×	•	×	•	×	✓	✓	✓

Table PP6.1: Empirical assessment of the desired photovoltaic properties across various applications and sectors. General considerations include colour (reflective or refractive colour); flexibility (non-rigid substrates that are at least partly flexible) and light transmission.

Progress

The development of photovoltaics built-for-purpose across these sectors presents a growing opportunity for Australia to continue to increase the uptake of renewables, drive reductions in carbon emissions across diverse sectors, increase energy resilience, develop new photovoltaic technologies, capture valuable IP, and diversify the photovoltaic industry in terms of technologies, skills and supply chains. The falling cost of solar also creates new opportunities in such applications, and ACAP continues to monitor and engage in developments as they relate to efficiency improvements, cost reductions, market opportunities and regulatory change that translate to applications in ultra-low-cost solar.

The Round 6 ACAP Collaboration Grant, Super-efficient Coloured PV for Vehicles, was completed in 2023 and is reported in detail in section 6.71 in the Appendix to this report. This project successfully fabricated and tested filters of four colours, red, yellow, blue and purple, which achieve super-efficient coloured PV mini-modules with efficiencies exceeding 30% and developed a new type of filter on textured glasses, highly suitable for indoor coloured PV applications. Refer to section 6.71 and Jiang et al. (2023) for detailed information.

ACAP researchers have also published in 2023 on the more general aspects of vehicle-integrated photovoltaics (VIPV), including performance prediction and energy generation modelling (Yang et al. 2023).

An ACAP Collaboration Grant project, awarded to UNSW, Development of III-V cells on GaAs and InP for a 50% Efficient Spectrum Splitting CPV Receiver, targets the historically significant value of 50% by spectrum splitting between two III-V three-junction cells grown on GaAs (high Eg) and InP (low Eg). See section 6.72 in the appendix of this report for progress and details.

PP6.3 INDUSTRY PARTNERSHIPS AND COMMERCIALISATION

New formal collaborations with industry and academia have been formed in ACAP2.0 in 2023, as noted in Chapter 4, and detailed discussions are underway with many more expected to be formalised in 2024. Current partners are Delphi Laser, Nutown Technologies, Federal University of Santa Catarina (UFSC), GreenDynamics, Green Energy Institute, Korea Research Institute of Chemical Technology (KRICT), Neoen Australia, Open Instruments, RayGen Resources, SunDrive Solar, Trina Solar, Scipher Technologies, University of Surrey and VRX Silica.

PP6.4 KNOWLEDGE SHARING

Lead Partners
All Program Participants

Industry Partner
Australian Photovoltaics Institute (APVI)

Funding Support
All partners, ACAP

ACAP has specific targets for high quality publications and for the number of researchers in different categories who benefit from the infrastructural support it provides, as well as for the number and length of researcher exchanges. A significant number of outreach events are also targeted for each year. As well as major events such as those reported in the PP6 section of this annual report, other outreach activities in 2023 included public lectures on material relevant to ACAP's activities, newspaper and magazine articles, visits, information papers and presentations for policy developers and their advisors. The ACAP nodes continue to educate future investors, industry partners, practitioners, researchers and educators to support the necessary rapid expansion of the national and global photovoltaics (PV) industry and to develop more effective educational tools.

Aim

The work described here is about promoting knowledge of the opportunities and successes of Australian photovoltaics research, adding to the global body of knowledge, engaging the next generation of researchers, and sharing knowledge with the broader community including industry, government and the general public.

Conferences

ACAP holds an annual research conference near the end of each year to keep ARENA and its National Steering Committee informed, to exchange research results, enhance collaboration and reinforce face-to-face contacts between students and staff from the different nodes. On 8 December 2023 at RMIT University, Melbourne, and online, ACAP held its half-day conference immediately after the Asia-Pacific Solar Research Conference (APSRC), which consisted of the director's welcome, presented by Professor Renate Egan, followed by the presentations of ACAP PP1–PP6 summaries.

Figure PP6.3: ACAP's 2023 conference was held at RMIT University, Melbourne, with additional attendees participating online.

Attending a conference provides a student or researcher an opportunity to present their work to a wider audience and receive valuable feedback on their findings. It also provides networking opportunities, enabling researchers to connect with their peers, form collaborations, stay up to date on the latest developments and develop new research ideas.

The Asia-Pacific Solar Research Conference (APSRC), organised by the Australian PV Institute (APVI) (5–7 December 2023), was also held at RMIT University. Staff and students from ACAP's various nodes participated in the APSRC in person, allowing them to present their research and engage in meaningful discussions with other members in attendance.

Figure PP6.4: Pablo Ribeiro Dias, UNSW alumnus and CTO of SolarCycle, presenting at the 2023 APSRC at RMIT University, Melbourne, with additional attendees participating online.

The APVI's APSRC aims to provide a forum for the development and discussion of content specific to Australia and its region, allow an opportunity to foster collaboration between institutes and promote engagement between industry and academics. ACAP partners with the APVI to support the development of the conference program through financial sponsorship, participation in its organisation and through encouraging ACAP presentations as contributions to the conference.

Figure PP6.5: Professor Vasilis Fthenakis, Founding Director of the Center for Life Cycle Analysis at Columbia University, New York, presenting his invited plenary presentation, "Photovoltaics Sustainability: Past, Present and Future", at the 2023 APSRC.

ACAP was a sponsor for the 2023 conference and representatives from UNSW and ACAP nodes helped with the organisation of the conference. Staff and students from all the nodes participated in academic review committees and contributed papers and posters to the conference.

ACAP supported the involvement of one of the world's leading researchers in PV sustainability, Professor Vasilis Fthenakis, Founding Director of the Center for Life Cycle Analysis at Columbia University, New York, as an invited plenary speaker. Professor Fthenakis presented on, "Photovoltaics Sustainability: Past, Present and Future". Professor Fthenakis also made a presentation at the UNSW node, as part of its seminar series, mentioned above.

Over the three days of the APSRC, ACAP members presented or attended presentations in the streams:

1. Photovoltaic Devices;
2. Renewable Electricity Deployment & Integration;
3. Solar Buildings and Solar Heating & Cooling;
4. Concentrating Solar Thermal; and
5. Process Heat & Chemistry.

ACAP also sponsored the fifth annual symposium of the Australasian Community for Advanced Organic Semiconductors (AUCAOS), held at Tweed Heads, New South Wales, from Wednesday 29 November to Friday 1 December 2023. The symposium included 41 oral presentations from keynote speakers (Professors Helen Huang and Rona Chandrawati), group leaders, early career researchers (ECRs), PhD, Honours and Masters students and a very active poster session. ACAP researchers were prominent among the organising committee and presenters.

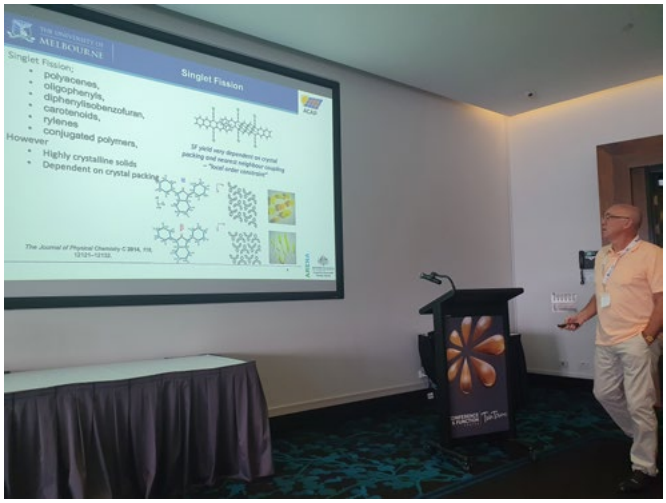

Figure PP6.6: ACAP's Principal Investigator of the University of Melbourne node, A/Professor David Jones presenting at the 2023 AUCAOS symposium.

The proceedings of the APSRC are available at the following url: *https://apvi.org.au/solar-research-conference/proceedings-apsrc-2023/*

Knowledge Sharing with ASEAN and South Asia

ACAP members from ANU are engaged in extensive overseas knowledge sharing with strong support from the Department of Foreign Affairs and Trade. The themes of the knowledge sharing include solar, wind and pumped hydro opportunities; Australia as a global renewable energy pathfinder; floating solar for Indonesia and surrounding countries; and high resolution modelling of 100% renewable energy. ANU teams are frequently visiting Nepal, Sikkim (India), Bhutan, Indonesia, Cambodia, Laos, Thailand and Malaysia, and are hosting delegations from those countries and other ASEAN members.

Professional Bodies

In addition to involvement in the APSRC, ACAP has continuing strong engagement with the APVI, one of the more effective vehicles for Australian policy development through its focus on data, analysis and collaborative research. ACAP was a founding "Large Organisation" member of the APVI and ACAP partners were active members of APVI throughout 2023.

Additionally, ACAP collaborators contributed to and participated in Australian representation on the Executive Committee for the International Energy Agency: Photovoltaic Power Systems (PVPS). ACAP institutions provided Australian leaders for the following PVPS Tasks:

- Executive Committee – Renate Egan (UNSW)
- Task 1 (Strategic PV Analysis & Outreach) – Renate Egan and Linda Koschier (UNSW)
- Task 12 (PV Sustainability Activities) – Rong Deng and Yansong Shen (UNSW)
- Task 14 (Solar PV in the 100% RES Power System) – Iain MacGill (UNSW)
- Task 16 (Solar Resource for High Penetration and Large Scale Applications) – Merlinde Kay (UNSW)
- Task 17 (PV & Transport) – Nicholas Ekins-Daukes (UNSW)

ACAP and other Australian researchers and practitioners contributed to these Tasks and also to Tasks 15 (Enabling Framework for the Development of BIPV) and 18 (Off-Grid and Edge-of-Grid Photovoltaic Systems).

A media release from the Prime Minister on 10 March 2023 announced a deepening partnership with India on "opportunities to accelerate the rollout of solar PV and clean supply chains". ACAP's Executive Director, Professor Renate Egan, was named as the Australian leader of the Taskforce.

Figure PP6.7: The Prime Ministers strengthening renewable energy partnership (Image credit: Australian Institute of International Affairs).

Researcher Exchanges

Researcher exchanges in 2023 included

- Roland, Clausing,
- ISFH, Germany,
- hosted by ANU node
- Leon Salomon, Leibniz University, Hannover, Germany, hosted by ANU
- Gabriel Bartholazzi, Aalto University, Finland, hosted by ANU
- Filippo Micharikopoulos, University of Padova, Italy, hosted by Monash University
- Anyao Liu, ANU, hosted by Leibniz University, and Fraunhofer ISE, Germany
- Zhongshu Yang, ANU, hosted by Leibniz University, Hannover, Germany
- Thuan Nguyen, ANU, hosted by Monash University
- Anh Bui, ANU, hosted by UNSW
- Khoa Nguyen, ANU, hosted by UNSW
- Lars-Erik Maurer, Justus Liebig University, Giessen, Germany, hosted by Monash University
- Simon Biberger, University of Bayreuth, Germany, hosted by Monash University
- Yihui Hou, ANU, hosted by Monash University.

New ACAP PhD, Masters and Honours Students

In 2023, we have welcomed:

- 49 Honours Students;
- 42 Masters Students; and
- 43 PhD students,

including some active but not listed included in earlier reports.

Education and Training

ACAP is a strong driver in education. Overall, to date, ACAP has supported at least in each category 196 early career researchers, 392 Honours students, 220 Masters students and 434 PhD students. More than 278 PhD graduates have come out of the ACAP program. See Chapter 8 for additional theses added in 2023.

News and Magazines

ACAP's research is driving the development of next generation solar cell technologies and is helping pave the way for a more sustainable and low-carbon future. As a result, ACAP attracts international attention and during 2023 there were over 280 news and magazine articles and tv and radio stories documented by ACAP.

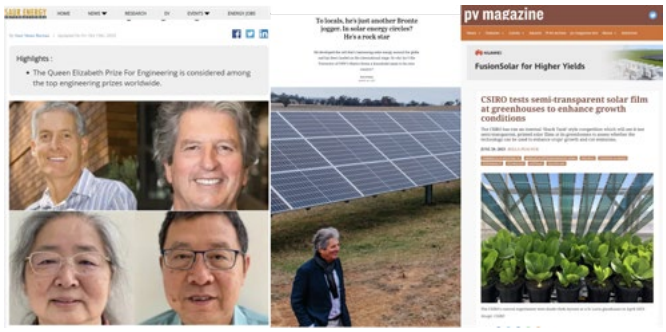

Figure PP6.8: A few of the high-profile stories that got significant press coverage in 2023.

Outreach

International Electrotechnical Commission (TC82)

On 1 November 2023 the UNSW node hosted a tour of its ACAP facilities for the participants of a Sydney meeting of the Technical Committee – Solar Photovoltaic Energy Systems (TC82) of the International Electrotechnical Commission (IEC). The meeting was hosted by the CSIRO Energy node in the Sydney CBD.

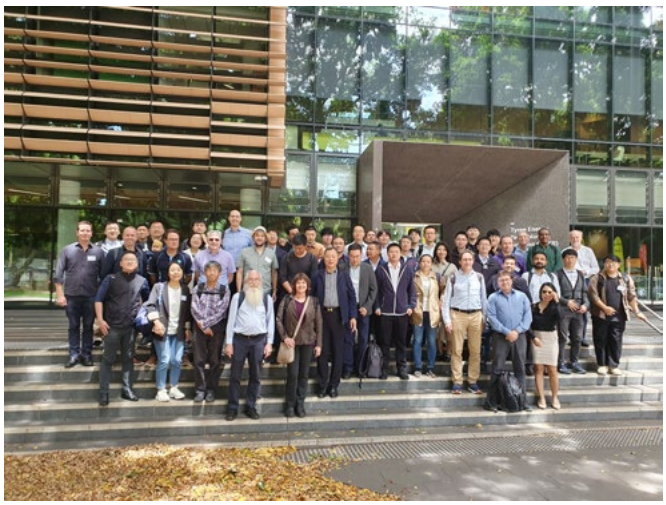

Figure PP6.9: Visit to UNSW of the Technical Committee –– Solar Photovoltaic Photovoltaic Energy Systems (TC82) of the International Electrotechnical Commission (IEC).

ACAP Characterisation Symposium

Dr Henner Kampwerth (UNSW) organised an ACAP Symposium on PV characterisation at UNSW on 9 August 2023.

Figure PP6.10: Attendees to the PV Characterisation Symposium at UNSW on 9 August 2023.

There were 32 attendees, 11 staff and students from the UNSW node and 21 from other nodes (Australian National University, CSIRO, Monash University, Sydney University), most of whom took the opportunity to deliver concise presentations on their specific research topics and characterisation needs and capacities. The symposium took half a day and laboratory tours at UNSW took up the other half. The day's activities enhanced inter-ACAP partnership opportunities and capacity to optimise usefulness of available equipment and connections beyond ACAP.

University of Sydney – Outreach

Figure PP6.11: The University of Sydney hosted laboratory tours for delegates from the 2023 Times Higher Education Global Summit.

Figure PP6.12: The University of Sydney hosted students from International Science School (ISS) 2023 "Meet a Researcher" event.

Figure PP6.13: The University of Sydney presented a "Show-and-Tell" to delegates attending the Sensor and Technology Conference in June.

Course Revision

The UNSW Bachelor of Engineering (Renewable Energy Engineering) program was revised and ratified in 2023. The revision supported additional flexibility (seven electives), updated courses, two new courses, and allows three new strands (minors): Humanitarian and Sustainability, Low Energy Systems and Renewable Energy Systems. The program now has enhanced compatibility with *Vertically Integrated Projects*. Revision of the pioneering Bachelor of Engineering (Photovoltaics Engineering) program is underway.

The UNSW teaching team is also developing new courses and improved teaching methods through several Working Groups, focused on topics including Data Science, Gamification, MSc in Energy Transition, PV modules, and others.

UNSW SPREE's Public Research Seminars

Featuring SPREE academics, ACAP members and internationally renowned visiting researchers, the SPREE weekly seminar series has over 200 video seminars available to researchers around the world via YouTube url: *https://www.youtube.com/unswspree*.

Additionally, webpages located at the short url: unsw.to/pvseminars show the seminar videos and also allow researchers and teachers to download the speaker's presentation in PDF format.

Figure PP6.14: The web page (short url: unsw.to/pvseminars) shows the video, slides, abstract and biography for the 2023 presentations in the Public Research Seminars series.

During 2023 there were 14 seminars for which permission was granted for online availability.

SunSprint Solar Challenge

ACAP supports the UNSW SunSprint Solar Challenge for students from Kindergarten to Year 12. The challenge is a series of solar-powered races that are both fun and suitable for each age group.

In 2023, the UNSW SunSprint event featured five different races, with students across primary and secondary years participating. The event was held on the UNSW campus in October.

Figure PP6.15: The UNSW SunSprint Solar Challenge occurs each year in October with schools from New South Wales and the ACT.

The aim of the challenge is to encourage students to use their imagination, develop their learning, enhance their academic skills and embrace challenges through age-appropriate science- and engineering-based events that involve planning, construction, experimentation and competition.

One of the main races is the SunSprint, which takes place on a 100-metre figure-eight track. Teams of up to four students (from Year 6 to Year 12) usually build the cars, which can take up to six months to design and construct.

Another race is the MiniSprint, which takes place on a 20-metre straight track. These cars are built from a kit made up of a solar module, motor, gears, wheels and corflute chassis.

There is also a Solar Boats race, which takes place in a 10-metre pool using fishing line for guidance and the Solar Pursuit race involving MiniSprint-style cars chasing each other around a single-lane oval track until one car catches up and touches the other.

Figure PP6.16: The Solar Boats race at UNSW campus.

6.5 Capacity Building

ACAP invests in capacity building to train the engineers, scientists, innovators and entrepreneurs needed to deliver the energy transition through:

- Funding scholarships and competitive research Fellowships offered for research projects based at the nodes.
- Financial support to competitively selected small collaboration grants, with the grantees working with industry and other research institutions.
- Collaboration with industry and international research partners targeting leveraged research outcomes and joint publications in line with delivering ultra-low cost solar.
- Support of learning through course development, running or hosting short courses and support for open education.

Fellowships

ACAP supported a fifth round of competitive Fellowships in 2023. These appointments are all short term, to be completed by 30 June 2024. The appointees and projects are:

- Naeimeh Mozaffari, Improving the stability and efficiency of high bandgap perovskite solar cells (Monash)
- Sudhaker Reddy Saripally, Development of efficient energy materials for stable photovoltaics (Monash)
- Alexander Corletto, IBC Silicon solar cell interface passivation (UniMelb)
- Cheng Cheng, Optimums in 100% Renewable Energy Systems (ANU)
- Rabin Basnet, Unlocking the full potential of doped poly-Si contacts on textured surface (ANU)
- Hualin Zhan, Development of a low-cost and quantitative materials analysis platform by physics-based machine learning (ANU)
- Mile Gao, Enhancing free carrier generation efficiency measurement in organic photovoltaic devices using optimised Photo-MIS-CELIV technique (UQ)
- Sisi Wang, Sustainable Low Bismuth Interconnects (UNSW)
- Huy Tuan Anh, Social and Ethical Aspects of PV Lifecycle Analysis (UNSW)
- Yiyu Zeng, Development of Multi-Functional 5-layer Anti Reflection Coatings (UNSW).

Additionally, UNSW appointed and funded two more short-term fellows:

- Mingrui He, Development of Rapid Cell Testing Methods
- Chandany Sen, Development of Stable Pure Iodide Wide Bandgap Perovskites Solar Cells.

References

Hamer, P., Wang, S., Juhl, M., Kim, M., Fletcher, J., McIntosh, K. R. & Hoex, B. (2023). Improved thermal modelling of the 5B MAVERICK system: impact of sky temperature. 2023 Asia-Pacific Solar Research Conference. Melbourne.

Hammerle, M., White, L. V. & Sturmberg, B. (2023). Solar for renters: Investigating investor perspectives of barriers and policies. Energy Policy 174, 113417.

Jiang, Y. & Ekins-Daukes, N. (2023). Ultra-Efficient Coloured Photovoltaic Devices for Buildings and Vehicles. 3rd Global Hydrogen and Renewable Energy Conference and Exhibition, Melbourne, 27–29 November 2023.

Thomas, I. (2023). Spectrally selective modules for Agrivoltaics. 2023 Asia-Pacific Solar Research Conference. Melbourne 5–7 December 2023.

Tkachenko, S., Hamer, P., Zhang, T., Klisser, R., Zhou, Z., de Silva, C., Timchenko, V. & Hoex, B. (2023). CFD modelling of the 5B MAVERICK system and temperature variations across PV modules. 2023 Asia-Pacific Solar Research Conference. Melbourne

Vaqueiro Contreras, M., Egan, R., Chang, N., Hallam, B., Hartley, O., Watt, M., Rayward-Smith, W., Walden, M., Boylan, E., Thoran, A. & Malbrain, C. (2023). Silicon to Solar. Foundations for Solar PV Manufacturing in Australia. Australian Centre for Advanced Photovoltaics, ITP Renewables, Bright Dimension, Australian PV Institute, Deloitte.

Wang, S. (2023). Impact of different PV mounting systems on yield, material consumption and emissions intensity. 2023 Asia-Pacific Solar Research Conference. Melbourne

Yang, Z., Perz-Wurfl, I., Jiang, J.Y., Gentle, A. & Ekins-Daukes, N.J. (2023) Vehicle-Integrated Photovoltaics (VIPV): Insights into Photovoltaic Performance & Energy Generation Modelling. 34th International Photovoltaic Science and Engineering Conference, Shenzhen, 6–10 November 2023.

COLLABORATIVE ACTIVITIES

The Australian Centre for Advanced Photovoltaics' international collaborations are directed at the highest level through an International Advisory Committee, with representatives from the key partners in Australia and from the world's most active PV R&D nations, with engagement fostered through the development of collaborative research programs, the annual ACAP conference and the major global research conferences.

Specific project activities that leverage the benefits of the international relationships include the following key projects:

- The collaboration on international cell performance standards, described in Section 6.4, is a longstanding one that records the status of a whole range of photovoltaic technologies in the maintenance and regular publication of the Solar Cell Efficiency Tables.
- Section 6.8 describes progress on a UNSW collaboration with SunDrive Solar Pty Ltd to analyse optical and electrical loss mechanisms for experimental mini-modules comprising two Cu-plated (Ag-free) bifacial M6 half cells encapsulated in glass-backsheet configuration. The study has shown that the main losses were front cover reflection, encapsulant absorption, interconnection shading and tabbing ribbon cabling.
- UNSW, Open Instruments and Tokyo University are working together in a project on the photothermal deflection spectroscopy (PDS) characterisation technique for ultra-sensitive characterisation of thin-film PV materials. Progress is described in Section 6.12.
- In Section 6.13 UNSW was validating the Australian Photovoltaics Institute's SunSPOT solar calculator tool; exploring the relationship between modelled PV output, based on shading calculations derived from 3D spatial data, and real-world PV system output; and generating realistic synthetic residential load profiles based on household and appliance characteristics for all Australian climate zones.

In addition to the specific activities captured in this section, many of the reports already presented as detailed research reports also involve collaborations with international partners.

Since late 2015 the organisation has had six rounds of small collaboration grants to researchers based at ACAP nodes. The progress reports for those still active in 2023 are presented online at https://www.acap.org.au/post/acap-s-annual-reports-2013-present and their titles and participants are listed there.

Many of the 67 ACAP Fellowships awarded in four rounds also involved collaborations and there is a report for each one that had 2023 activity included in https://www.acap.org.au/post/acap-s-annual-reports-2013-present and their titles and participants are listed here.

Additionally, this year, we are able to report on progress on Infrastructure Grants that were still active in 2023. These grants are supporting the renewal of the nation's PV research tools and equipment.

Finally, the education, training and outreach activities reported in PP6 include a wide range of international interactions, the ACAP Conference and regular and special public lectures.

6.4 SOLAR CELL PERFORMANCE DOCUMENTATION

Lead Partner
UNSW

UNSW Team
Prof. Martin Green, Prof. Xiaojing Hao

NREL Team
Dr Nikos Kopidakis

Academic Partners
CSIRO, Newcastle
NPVM, China
Fraunhofer Institute for Solar Energy Systems, Germany
ISFH, Germany
JRC, Ispra, Italy
AIST, Japan
JET, Japan

Funding Support
ACAP, UNSW, NREL

Aim

To improve accuracy and quality of photovoltaic device measurement and reporting.

Progress

A longstanding research collaboration between UNSW and NREL, now being conducted as an ACAP international collaborative project, involves the reliable documentation of the status of the whole range of photovoltaic technologies worldwide. This is by the biannual publication of the "Solar Cell Efficiency Tables" in the Wiley journal, Progress in Photovoltaics. More information about the scope and history of these Tables is given elsewhere (Green 2020).

By enforcing guidelines for the inclusion of solar cell efficiency results into these Tables, they not only provide an authoritative summary of the current state of the art but also ensure measurements are reported on a consistent basis. One criterion that has been important to enforce has been that results be independently certified at one of a limited but increasing number of "designated test centres", generally of a national facility status, with a certified measurement capability and additionally involved in international "round robin" testing. CSIRO (Newcastle) is the first test centre in the southern hemisphere that has been accepted as a designated test centre.

This rigour has been important particularly as new device technologies come to the fore and groups relatively inexperienced with cell testing suddenly are thrust into the limelight. The other important role has been in developing measurement standards to cover situations where international standards are not available. Figure 6.4.1 shows standards in this category developed for defining the area used for efficiency determination for experimental laboratory cells.

Several results from the ACAP program have set new world standards and are featured in these Tables. In 2023, these included the retention of UNSW record efficiencies for CZTS cell performance, with 10.0% confirmed for a 1 cm² device and a new record of 11.4% confirmed during the year for a smaller device, a 25% record for a UNSW silicon PERC cell, a 23.4% record for a GaAsP/Si monolithic tandem solar cell (UNSW with Ohio State University and SolAero), a 32.9% efficiency for a GaInP/GaAs multi-junction solar cell involving multiple quantum wells (UNSW with NREL), a 34.5% UNSW record for a GaInP/GaInAs/Ge plus Si spectral split mini-module, a UNSW 40.6% result for a concentrator submodule using a similar cell combination and 21.7% for a large-area UNSW Si concentrator cell.

The Tables are widely used and referenced by the photovoltaic research community. According to the ISI Web of Knowledge, the 20 versions prepared since 2013 under the ACAP banner have all been among the most cited papers published since then in the engineering discipline worldwide.

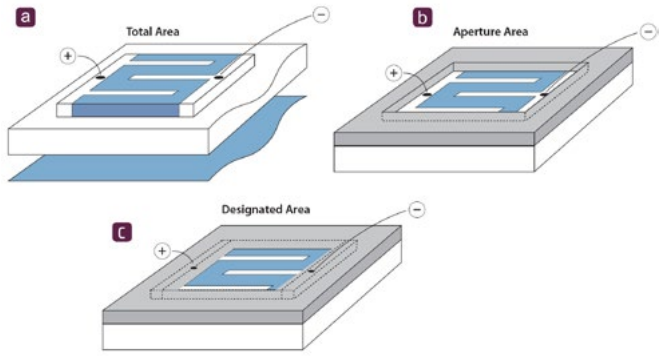

Figure 6.4.1: Cell area definitions: (a) total area; (b) aperture area; and (c) designated illumination area.

Highlight

Value and widespread use of Tables validated by exceptionally high citation rates.

Future Work

Publish two updated versions of the Tables during 2024.

Reference

Green, M.A. (2020). Tracking solar cell conversion efficiency. Nature Reviews Physics 2, 172-173.

6.8 COPPER-PLATED SILICON HETEROJUNCTION MODULES WITH EFFICIENCIES EXCEEDING 23%

Lead Partner
SunDrive

UNSW Team
Dr Pei-Chieh Hsiao

Funding Support
ACAP, UNSW

Aim

The highest single-junction cell efficiency of crystalline cells has been obtained using silicon heterojunction (SHJ) technology. To convert the high cell efficiency into a high module efficiency, the two main factors to be considered in module design are optical and electrical losses. Optical losses arise from reflection at the material interfaces and absorption by the materials are evaluated, whereas electrical losses are incurred from the power resistive loss occurring in the interconnect ribbons/wires and tabbing ribbons. This project aims to analyse these for mini modules comprising two Cu-plated bifacial M6 half cells encapsulated in glass-backsheet configuration. Module efficiencies were independently measured at SERIS's ISO/IEC 17025 accredited laboratory, and the cell-to-module (CTM) losses of the modules were analysed.

Progress

Glass is typically used as the front cover to provide the primary mechanical support for the modules. The reflectance of three glass candidate materials is compared in Figure 6.8.1(a). Planar glass without an antireflection coating (ARC) and a thickness of 2 mm showed higher reflectance in the mid wavelength range. The average 0.2% reflectance decrease in the 300–1000 nm region of 2 mm textured glass with no ARC was possibly due to different manufacturers and the scattering effect from the rear textured surface. Textured glass with an ARC showed broadband reduction in measured reflectance, with an average of 8.2% in the 300–1000 nm region. However, improvement in reflection with ARC appeared significantly lower than the expected 3–4% which is reported in the literature (Helsch & Deubener 2022; Priyadarshini & Sharma 2016). As the absorption in glass is minimal, the 3 mm thick ARC-coated textured glass was selected as the front cover for the mini-modules.

Ethylene-vinyl acetate (EVA) is the most widely used encapsulant in PV modules with over 80% world market share in 2021 according to the ITRPV 2022 report. The acetic acid generated from EVA decomposition can potentially lead to Cu corrosion which has been attributed to power degradation in modules subjected to a damp heat test (Gawlinska-Necek et al. 2021). Polyolefin elastomers (POE) are an alternative encapsulant commonly used for SHJ modules, bifacial applications and when Cu metallisation is employed. Based on the compatibility with Cu cell metallisation, along with the advantage of increased transmittance in the UV wavelengths and lower water vapour transmission rates over EVA (Oreski et al. 2020), POE was used for these experimental modules.

Interconnected ribbons affect module performance both optically and electrically. Optical shading and resistive loss resulting from the ribbons should be minimised simultaneously. Figure 6.8.1(b) plots the reflectance measured on cells interconnected by three types of ribbons with similar cross-sectional area (i.e. electrical loss was controlled). Structured ribbons presented ~1.6% higher reflectance owing to their larger 1 mm ribbon width. Theoretically triangular ribbons can achieve higher optical gain than circular wires by redirecting the incident light to the cell surface, however this advantage is compromised by the round apex and curved solder coating in the actual ribbons. Consequently, reflectance of triangular ribbons and circular wires were optically comparable, except for wavelengths > 1000 nm where the triangular ribbons reflected less light. Ribbon geometry is also related to cell spacing in the modules. Ribbons with low aspect are typically used for high packing density modules which implement zero cell gap or tiled configuration. For these modules they can reduce both the encapsulant thickness and the thermomechanical stress which is induced during lamination. Sectional ribbons using different geometries (e.g. triangular/circular at the front and flat at the rear) can provide the benefits of increased front surface optical performance and reduced encapsulant cost and induced Si stress. The process temperature for stringing/interconnection is determined by the solder composition. As SHJ cells are sensitive to thermal processes > 200°C, low melting temperature solders are more ideal to prevent potential damage to the a-Si:H passivation layers. As such circular wires coated with SnBiAg solder were used for interconnection with a 1 mm cell gap.

Selection of back cover material is mainly determined by the electrical insulation and moisture protection. The mainstream white backsheet was used as it provides higher optical coupling than a black backsheet

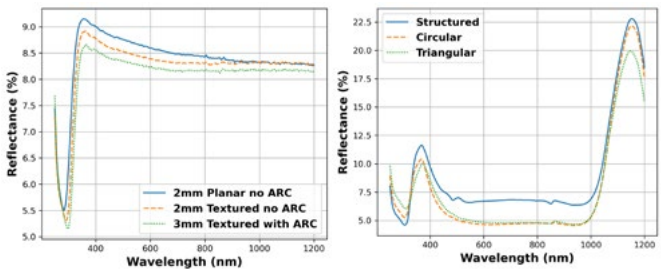

Figure 6.8.1: (a) Measured reflectance of glass; and (b) measured reflectance of SHJ cells interconnected by different ribbons and laminated in AR-coated textured glass-glass modules.

Five mini-modules were fabricated by interconnecting two Cu-plated bifacial M6 half cells. Module I-V was characterised using a Class A+A+A+ 100 ms h.a.l.m. cetisPV-XF2-M pulsed solar simulator. The measurement uncertainty for maximum output power (P_{MAX}) was ± 1.4%. Due to the total internal reflection in the mini-modules (200 ± 200 mm in dimension), masking was applied to avoid light being reflected by the white backsheet into the cells. A module area of 277.22 cm^2 was used to calculate the module efficiencies. The measured I-V performance is summarised in Table 6.8.1. The average P_{MAX} was 6.327 ± 0.085 W and calculated efficiency was 22.82 ± 0.31%. The best module achieved an efficiency of 23.17% with the certified I-V curve shown in Figure 6.8.2.

Table 6.8.1: Module I-V performance of five mini-modules (with an active area of 277.22 cm2)

	V_{oc} (V)	I_{sc} (A)	FF (%)	P_{MAX} (W)	h (%)
Average	1.487± 0.002	5.257± 0.026	80.96± 0.81	6.327± 0.085	22.82± 0.31
Best	1.489	5.292	81.52	6.423	23.17

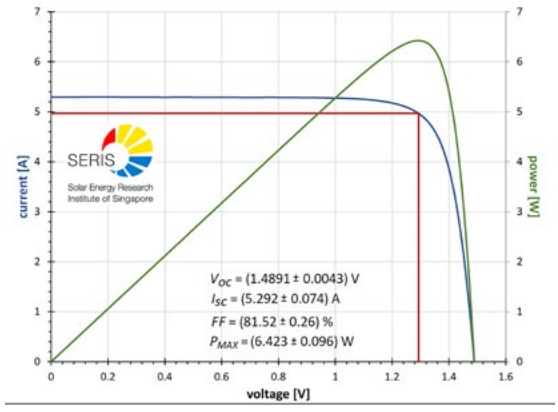

Figure 6.8.2: Certified I-V curve from SERIS ISO/IEC 17025 accredited laboratory.

To investigate the optical and electrical losses of fabricated modules and provide guidance for future improvement, a CTM analysis using SmartCalc.CTM version 1.3 (Haedrich et al. 2014; Mittag & Ebert 2017) was conducted. Since the software allows user-defined material information, the measured cell I-V parameters, spectral response and reflection were used. The glass reflection was adopted from the measured data (green curve in Figure 6.8.1(a)). The optical parameters of POE and white backsheet from the software database were used. The circular wires had a diameter of 0.35 mm with 15 µm of solder coating. The size of the tabbing ribbons was 7 x 0.3 mm. Because the glass (200 x 200 mm) was significantly larger than the cells, the resistive loss in the tabbing ribbons was calculated in "junction box and cabling" (k15), presuming the distance from the connector of the solar simulator to the centre busbar was 150 mm.

The resulting waterfall diagram is shown in Figure 6.8.3. The analysis started with a half-cell efficiency of 25%, assuming an absolute 0.3% loss from the cell cutting process. Figure 6.8.3 clearly shows that the greatest loss (1.04%) resulted from front cover reflection (k3), probably because the ARC was not optimally deposited on small-sized glass. This cover reflection loss is expected to be 0.43% if the average glass reflectance can be reduced by 3% to a similar value reported in the literature. The second largest loss was "encapsulant absorption" (k6). Reduction of light absorption by POE is possible if circular wires with decreased diameter are used, which may require adjustment of the busbar numbers. The next largest optical loss arose from "interconnection shading" (k7), despite using circular wires. This highlights that interconnected ribbons are one of the most crucial components of a module's design as they also contribute to non-negligible electrical loss (k12) in the modules. The largest electrical loss of 0.34% resulted from "junction box and cabling" (k15), i.e. the resistive loss in the tabbing ribbons. This loss, which is typically insignificant in full-sized modules, can be reduced by using thicker tabbing ribbons or matching the glass size to the cells in the mini-modules. The estimated module efficiency was 23.31%, 0.14% greater than the highest mini-module efficiency. The difference may at least be partly due to (i) variation in cell efficiencies; and/or (ii) the electrical mismatch between the two half cells that was not evaluated in the analysis.

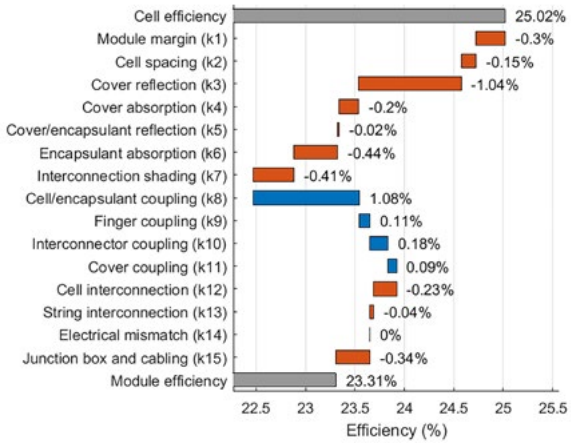

Figure 6.8.3: Waterfall diagram of CTM analysis of glass-backsheet modules with two Cu-plated M6 half SHJ cells.

Highlights

- Mini-modules with two Cu-plated bifacial M6 half cells were fabricated using AR-coated textured glass, POE, white backsheet and circular wires for cell interconnection with 1 mm gap.
- The average and highest module efficiency, measured at SERIS's ISO/IEC 17025 accredited laboratory, were 22.82 ± 0.31% and 23.17%, respectively.
- A CTM analysis revealed that the main losses were front cover reflection, encapsulant absorption, interconnection shading and tabbing ribbon cabling.

References

Gawlinska-Necek, K., Socha, R. P., Balawender, P., Stodolny, M. K., Van Aken, B. B., Starowicz, Z. & Panek, P. (2021). Silicon solar cells and modules with front contact paste containing copper-based component. Progress in Photovoltaics: Research and Applications 29, 1008-1019.

Haedrich, I., Eitner, U., Wiese, M. & Wirth, H. (2014). Unified methodology for determining CTM ratios: Systematic prediction of module power. Solar Energy Materials and Solar Cells 131, 14-23.

Helsch, G. & Deubener, J. (2012). Compatibility of antireflective coatings on glass for solar applications with photocatalytic properties. Solar Energy 86, 831-836.

Mittag, M. & Ebert, M. (2017). Systematic PV-module optimization with the cell-to-module (CTM) analysis software. Photovoltaics International, 36th edition, 97-105.

Oreski, G., Omazic, A., Eder, G. C., Voronko, Y., Neumaier, L., Mühleisen, W., Hirschl, C., Ujvari, G., Ebner, R. & Edler, M. (2020). Properties and degradation behaviour of polyolefin encapsulants for photovoltaic modules. Progress in Photovoltaics: Research and Applications 28, 1277-1288.

Priyadarshini, B. G. & Sharma, A. K. (2016). Design of multi-layer anti-reflection coating for terrestrial solar panel glass. Bulletin of Materials Science 39, 683-689.

6.12 ADVANCING THE PDS TECHNIQUE FOR ALL PHOTOVOLTAIC THIN-FILMS

Lead Partner
UNSW

UNSW Team
Prof. Xiaojing Hao, Dr Henner Kampwerth, Prof. Gavin Conibeer

Industry Partners
Open Instruments

Academic Partner
Tokyo University: Prof. Masakazu Sugiyama, Prof. Yoshitaka Okada, Meita Asami

Funding Support
Open Instruments, ACAP (UNSW Node)

Summary

The ARENA / ASI-USAEC Project RG172866-D, titled "Advancing the PDS Technique for Photovoltaic Thin-Films," was a collaborative initiative with Japanese researchers to promote academic collaboration and knowledge exchange. The project commenced with an initial emphasis on refining the photothermal deflection spectroscopy (PDS) technique at SPREE, the School of Photovoltaics and Renewable Energy Engineering laboratory.

Aim

This cutting-edge system has its roots in the University of New South Wales (UNSW), where it was initially developed during the years 2013–2015, with the support from an ARENA Fellowship. Over time, it evolved and matured towards commercialisation in stages with industrial collaborator Open Instruments and support from ACAP (ACAP Collaboration Grant Round 3) and ARENA (ARENA Commercialisation of R&D), see Figure 6.12.1.

The instrument operates by measuring the photo-absorption spectrum through the detection of the minuscule heat generated by absorbed photons. The technique is particularly useful for photovoltaic thin-film measurements, due to two characteristics:

(a) Exceptional Sensitivity: It can measure absorption data spanning up to five orders of magnitude, enabling the analysis of even the weakest absorbing films.

(b) "Dark" Recombination Capability: This remarkable feature allows the measurement of recombination in the absence of photoluminescence signals, eliminating the need for such signals in the assessment.

The initial objective of this project was to expand the range of applications for this technique. One aspect considered for exploring was the simultaneous electrical biasing of the cell during measurements.

Figure 6.12.1: The first commercial beta version of a PDS unit was presented at the Asia-Pacific Solar Research Conference (APSRC) at UNSW in December 2018.

Progress

The collaborative grant was initially drafted during Dr Kampwerth's visit to Tokyo University, where he established connections with Prof. Sugiyama and his research team. Following the approval of funding, Prof. Sugiyama reciprocated by attending the Asia-Pacific Solar Research Conference (APSRC) at UNSW in December 2018.

Subsequently, a series of samples featuring thin-film quantum structures were dispatched from Tokyo University to UNSW for biased photothermal deflection spectroscopy (PDS) measurements. The specific project requirements and the characteristics of the samples necessitated adaptations to our measurement equipment at UNSW. However, it is worth noting that, despite promising initial results, we encountered growing incompatibility issues with subsequent samples. Furthermore, the emergence of the COVID-19 pandemic mandated a re-evaluation of the exact PDS topics under investigation.

The visits of PhD student Meita Asami (now Associate Professor) in August and September 2022, followed by another visit in March 2023, accompanied by Prof. Watanabe, brought about a recalibration of the project's direction. This recalibration primarily emphasised the enhancement of PDS data to render it even more insightful. One key focus area related to the development of data correction methods to include the influence of reflections. The excellent results can be found in the submitted article by M. Asami at Physica Status Solidi (a), reference number 202300585R1.

Additionally, during the project's progression, the original commercial prototype of Open Instruments, as depicted in Figure 6.12.1, was succeeded by an upgraded commercial prototype, depicted in Figure 6.12.2. This upgrade notably bolstered measurement accuracy (see Figure 6.12.3), contributing to the project's overall success.

Figure 6.12.2: The second industrial prototype of the PDS system, called AURA, from Open Instruments.

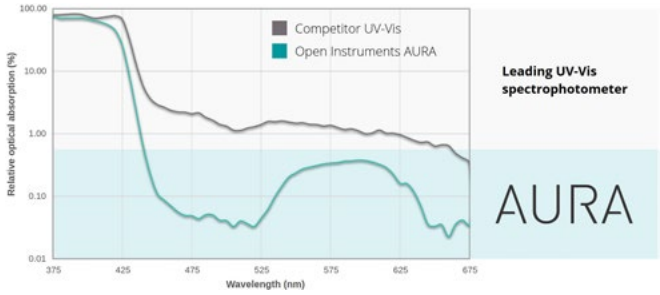

Figure 6.12.3: The graph shows the absorption spectrum of a perovskite flake measured on an R&T absorption spectrometer and on the PDS AURA. The direct comparison of both measurement principles highlights the superiority of PDS in regard to dynamic range and lack of data compression. The sub-bandgap absorption band from 525 to 625 was only detectable with the PDS system as too weak for the R&T technique.

Throughout the project's duration, four visits were conducted, five conference presentations given, with two of them at international conferences. In addition, three talks were given at the UNSW recorded seminar series, and three journal publications have been produced, of which one is currently in the review process.

Moreover, the PDS system is now accessible to all members of ACAP for measurement purposes, and inquiries regarding measurements can be directed to Dr Kampwerth.

The overarching goal of this project was twofold: firstly, to forge new research connections with Tokyo University, and secondly, to lay the foundation for future, more extensive projects. It is worth noting that the project has achieved notable success in both aspects, not only strengthening the ties with Tokyo University but also contributing to the refinement of the PDS technique itself.

Deliverables and Outcomes

1. Joint publication of at least one publication at an international conference on the newly developed characterisation technique
   - Dr Kampwerth presented at 2020 Asia-Pacific Solar Research Conference on 30 November – 3 December 2020.
   - Prof. Sugiyama and Prof. Okada attended 2018 Asia-Pacific Solar Research Conference (APSRC) in December 2018 at UNSW as guest speakers.

2. Publication of at least three journal articles and one conference article where this technique is applicable
   - He, M., Huang, J., Li, J., Jang, J. S., Suryawanshi, U. P., Yan, C., Sun, K., Cong, J., Zhang, Y., Kampwerth, H., Suryawanshi, M. P., Kim, J., Green, M. A. & Hao, X. (2021). Systematic Efficiency Improvement for Cu2ZnSn(S,Se)4 Solar Cells By Double Cation Incorporation with Cd and Ge. Advanced Functional Materials 31, 2104528.
   - Zhang, Y., Huang, J., Zhang, X., Chin, R. L., Nielsen, M. P., Rey, G., Zeng, Y., Kampwerth, H., Hameiri, Z., Ekins-Daukes, N. J. & Hao, X. (2020). Deep-Level Defect in Quasi-Vertically Oriented CuSbS2 Thin Film. Solar RRL 4, 2000319.
   - Asami, M., Nakano, Y., Sugiyama, M., Kampwerth, H., Pollard, M., Hao, X., Komaba, S., Ikari, T. & Fukuyama, A. (n.d.). Refining Photothermal Deflection Spectroscopy: Incorporating Reflectance for Enhanced Accuracy in Light Absorption Measurements, PSSA (submitted)
   - Oral presentation at CSW2023 (Jeju, Korea).
     Asami, M., Kampwerth, H., Pollard, M., Watanabe, K., Nakano, Y. & Sugiyama, M. (2023). Investigation of Light Absorption Properties of InGaAs/GaAsP Quantum Wells using Photothermal Deflection Spectroscopy. Compound Semiconductor Week 2023, TuD1-5, Jeju, Republic of Korea, 30 May 2023.

3. Make this characterisation technique available at UNSW for all ACAP researchers and project members by the end of this project.
   It is available now. Please contact Henner Kampwerth (h.kampwerth@unsw.edu.au) to have your samples measured.

4. Three visits of academic scholars to UNSW from Tokyo University with at least one recorded talk to be made public on SPREE

YouTube channel later on.

- December 2018, APSRC Prof. Sugiyama, presentation given.
- August/September 2022, Meita Asami, a school seminar talk was given.
- March 2023, A/Prof. Meita Asami, a recorded school seminar talk was given.
- March 2023, A/Prof. Watanabe, a recorded school seminar talk was given.

6.13 MAPPING CONSUMER OUTCOMES OF ROOFTOP SOLAR POTENTIAL

Funding Support
ACAP

Lead Partner
UNSW

UNSW Team
Prof. Anna Bruce, Dr Mike Roberts, Dr Rob Passey, Dr Navid Haghdadi, Zahra Rahimpour, Russell Kindler, Nargess Nourbakhsh, Ellie Kallmier

Aim

To better understand the relationship between modelled PV output, based on shading calculations derived from 3D spatial data, and real-world PV system output.

To generate realistic synthetic residential load profiles based on household and appliance characteristics for all Australian climate zones.

Progress

Validation of SunSPOT solar potential tool

The APVI's SunSPOT solar calculator tool is designed to support households and small businesses in decision-making around investment in rooftop solar. It includes a model of solar generation, based on local typical year weather data and the orientation, slope and shading of a proposed solar array. The premium version of the tool accesses a 1 m gridded data set (generated from point-cloud LiDAR data), containing the average orientation and slope of the sampled surface and an array describing the near shading throughout the year.

To validate the outputs of the SunSPOT algorithm, three analyses were performed using data from real solar systems, collected through ACAP's Energy Data Platform.

1. 1. Comparison of the roof slope and orientation derived from SunSPOT with that measured from Nearmap, created from "oblique" aerial imagery, which has reported a ground sample distance of 7.6 cm and vertical accuracy of 15 cm.

   Figure 6.13.1 shows high correlation between measured and modelled orientation but inconsistent results for slope.

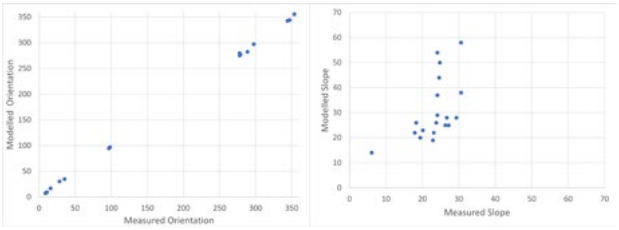

Figure 6.13.1: Modelled orientation (l) and slope (r) compared with measured.

More detailed analysis showed that SunSPOT overestimates roof slope when the array area is close to the building edge. This is because the slope is averaged across a 1 m2 area, which at roof edges may include vertical walls. Subsequent to this analysis, the averaging method was changed from using the mean to using the median, which has significantly reduced the error.

2. Comparison of solar generation modelled using the SunSPOT algorithm with actual solar generation data.

Figure 6.13.2 shows a comparison of SunSPOT modelled solar generation with measured output for a single site.

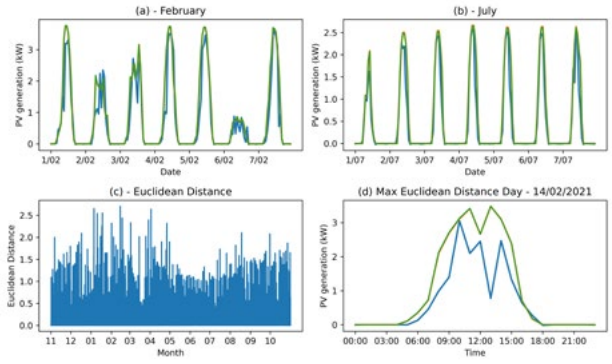

Figure 6.13.2: Comparison of SunSPOT modelled solar generation with measured values:
a), (b) PV generation over the first week of February and July respectively
(c) Euclidean distance over the year
(d) PV generation curve for the day with the maximum Euclidean distance occurring.

Table 6.13.1 presents the summarised statistics across 10 sites, showing good correlation for most sites. The detailed analysis (see appendix) suggests a range of issues causing discrepancies, including inverter faults, local differences in weather patterns between sites and their nearest BOM weather station and panel degradation.

Site	*Pearson cor.*	*Spearman cor.*	*Mean Bias Error*	*Euclidean Distance*	*Max Euclidean Distance*
A	0.94	0.87	0.0004	26.3	2.7
B	0.96	0.87	0.27	50.27	3.08
C	0.97	0.86	0.031	26.17	2.53
D	0.7	0.74	-0.12	55.23	2.83
E	0.93	0.84	-0.83	141.21	6.48
F	0.97	0.88	0.07	22.93	1.93
G	0.83	0.81	0.43	69.78	3.87
H	0.86	0.84	-0.12	51.36	3.37
J	0.72	0.55	0.31	47.4	2.52
K	0.94	0.89	-0.12	34.07	2.7
Average	0.88	0.82	+0.19, -0.39	52.47	3.20

Table 6.13.1: Comparison of modelled and measured generation – summary statistic.

3. Analysis of the shading data calculated from SunSPOT with visual analysis of shading on arrays using Nearmap aerial imagery.

   Detailed analysis of shading was carried out for six sites, with four showing good agreement between the SunSPOT-calculated shading array and an array generated through visual analysis of aerial imagery. The remaining two sites showed discrepancies likely caused by rounding errors due to the granularity of SunSPOT's shading array (five degree increments for both azimuth and zenith angles).

Synthetic load profiles

Informed household decision-making around installation of rooftop solar PV (and batteries) relies on understanding the financial costs and benefits. The bill savings (and therefore payback period and return on investment) delivered by solar are highly dependent on the proportions of generation that are self-consumed and exported. While many analyses (including commercial solar calculators) use high level approximations, the actual proportions are specific to individual household load profiles. Given the low penetration of residential smart meters (for non-solar households outside Victoria) this presents a need to generate synthetic load profiles from limited data including total energy use and household characteristics including appliance ownership and usage.

The APVI's SunSPOT solar calculator tool uses a machine learning model to generate synthetic load profiles for household users. The model is trained using the Smart Grid, Smart City (SGSC) data set (Australian Government, 2014), which comprises timeseries 30-minute load data linked to survey responses for around 2000 NSW households. Analysis of this data was used to identify which household characteristics are the most important predictors of household load profile. Using this information, different machine learning models were built and tested.

Two versions of a Random Forest (RF) model were built and trained, the first using actual load data and predicting load profiles based on household characteristics only; the second (NRF) using normalised load data and predicting normalised load profiles that are subsequently scaled using known total electricity consumption data.

The normalised model demonstrated improved performance, as shown in Figure 6.13.1 and Table 6.13.1.

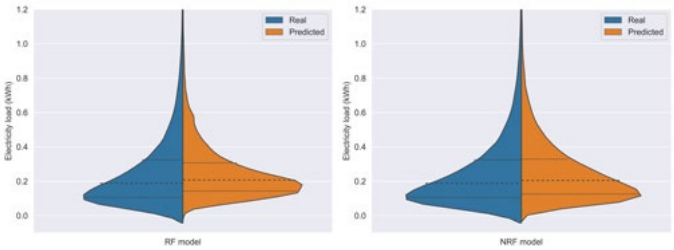

Figure 6.13.3: Predicted vs modelled 30-minute load (l) normalised RF (r) RF.

Notably, ownership of a pool has reduced importance in predicting the normalised load, while ownership of air-conditioning (regardless of type) dominates.

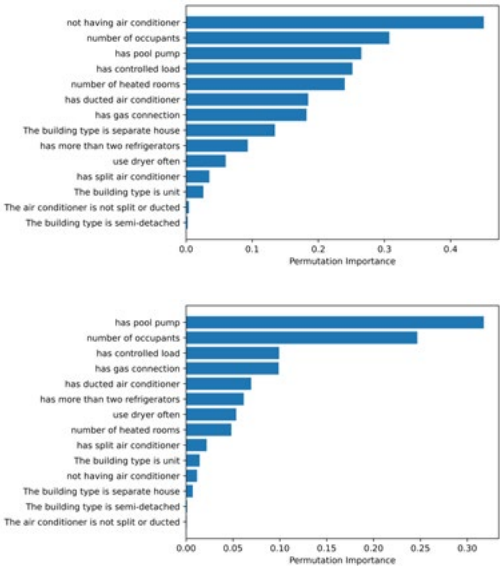

Figure 6.13.4: Feature importance using permutation method (l) normalised RF (r) RF.

Further extension of the model is ongoing, including developing the methodology to enable training with multiple data sets collected in different climate zones. There are only three available data sets that combine timeseries electricity consumption data with household surveys of occupancy, appliance ownership and use. These are SGSC, CSIRO's Energy Use Data Model (EUDM) data set and ACAP's Energy Data Platform (EDP). This development work will enable these data sets to be combined, increasing the accuracy of the model across different Australian climate zones.

PV system size recommendations

To inform development of a PV system size recommendation function in SunSPOT, a broad analysis was undertaken of the impacts that variations in tariffs and upfront system costs can have on the estimated optimal PV system size for residential households.

Data from 1146 Victorian residential sites collected by Solar Analytics[1] was used to analyse the effects of changing tariff rates and initial PV system costs on both PBP and ROI. Each site had a half-hourly load profile and PV profile for a minimum of one year, and the PV profiles for each site were scaled to estimate output of the same system at varying capacities between 1 and 15 kW[2]. Three rates (low, medium and high) for each tariff type were considered, using typical values for residential feed in tariffs (FiT), flat rate (FR) and time of use (ToU) tariffs in Australia. A typical all-year 2–8 pm peak, 10 pm–7am off-peak and a 7am–2pm and 8–10pm shoulder was also applied to each site when evaluating ToU tariffs. System cost data from Solar Choice in August 2022 was used to provide average system prices by state and territory[3] noting that some $/W prices for systems between 1 and 2 kW were derived by simple extrapolation from 1.5 kW system prices (Solar Choice, 2022). For Tasmania, the Northern Territory, the Australian Capital Territory and Western Australia, < 3 kW system prices were extrapolated from 3 kW systems, and for systems between 8 and 9 kW and > 10 kW, prices were also derived by extrapolation from 7 kW and 10 kW systems (Solar Choice, 2022).

When considering both minimum PBP and maximum ROI, results under FR tariffs and ToU tariffs showed significant variation in optimal system capacity ranges (Figure 6.13.5), ultimately suggesting that systems between 1 and 10 kW serve the best chance of optimising both metrics. This study confirmed the need for more detailed comparative studies examining the impact of PV production and consumer load in optimising PV system size. These results can be used to suggest a starting point for would-be PV users looking to find the most financially viable PV system and demonstrate the importance of customer-specific load data and tariff information to optimal system design.

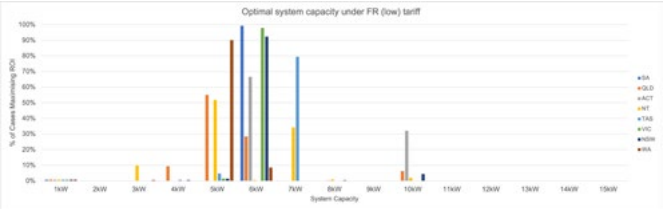

Figure 6.13.5: Optimal PV system sizes under flat rate tariffs by minimising payback period.

Financial

EXPENSES (Cash)	2021	2022	2023	TOTAL
Salaries	$150,000	$150,000		$300,000
Total expenses (AUD)	$150,000	$150,000		$300,000
REVENUES				
ACAP	$150,000	$150,000		$300,000
Total revenues (AUD)	$150,000	$150,000		$300,000

. Accessed through the UNSW Data Resource Time-series Hub (DARTH) Energy Database.

. This may result in some overestimation of output from larger residential systems, due to the likelihood of larger systems using less optimal roof areas alongside areas with the greatest solar insolation.

. Prices are quoted as total retail prices after STCs and GST.

Highlights

- Validation of SunSPOT methodology against output data from real household PV systems.
- New methodology for creating synthetic residential load profiles based on climate zone, household characteristics and appliance ownership and use and integration of these methods into updated SunSPOT tool, rolled out nationally.
- High level method for suggesting PV system size based on tariff and customer load profile.
- Two conference articles presented at Asia Pacific Solar Research Conference
- (Rahimpour et al. 2022; Kallmier et al. 2022).
- Forthcoming journal article comparing different machine loading methodologies for synthetic load profile generation.
- Validation report will be published on APVI's SunSPOT website (www.sunspot.org.au).

Future Work

- •Ongoing development of the machine learning model for generation of synthetic load profiles to incorporate multiple linked energy data and household survey data sets, including data from CSIRO's EUDM project and ACAP's Energy Data Platform, in addition to SGSC.
- •Analysis of commercial load profiles, including identification of temperature-dependent components, to develop approaches for generating synthetic load profiles across different climate zones.
- •This work has been funded through UNSW's Digital Grid Futures Institute seed funding.

References

Australian Government Department of the Environment and Energy. (2014). Smart Grid Smart City Customer Trial Data.

Rahimpour, Z., Haghdadi, N., Roberts, M., Nourbakhsh, N. & Bruce, A. (2022). Generating synthetic residential electricity load profiles using household characteristics. Asia Pacific Solar Research Conference, Newcastle, Australia.

Kallmier, E., Bruce, A., Roberts, M. & Haghdadi, N. (2022). Impact of tariffs and system costs on optimal PV system size. Asia Pacific Solar Research Conference, Newcastle, Australia.

Solar Choice, 2022, Solar System Prices, www.solarchoice.net.au/solar-panels/solar-power-system-prices/.

6.14 PERFORMANCE MODELLING OF TRACTILE'S SOLAR TILE IN VARIOUS CONFIGURATIONS AND LOCATIONS

Lead Partner
UNSW

UNSW Team
Bram Hoex, Osama Bany Mousa, Xinyuan Wu, Shaozhou Wang, Xutao Wang

Industry Partner
Tractile

Funding Support
ACAP small project

Aim

The aims of the project were as follows:

- Quantifying the performance of PVT versus standard roof-mounted PV in terms of electricity generation and operating temperature.
- Simulate the system performance of PVT when used to produce hot water and electricity.
- Quantifying the performance of the Tractile Solar Roof Tile in various climates.
- Identify areas of improvement to improve the electrical performance of the Tractile Solar Roof Tile.

Progress

The energy transition to renewables is in full swing. Photovoltaics (PV) is the lowest cost option for electricity generation in many places globally, with the lowest power purchasing agreements now below 0.02 $/kWh. Solar thermal presents an alternative for hot water, either for use in the house or for a pool, with economic payback periods down to two years in some parts of Australia. In this project, ACAP is working with industry partner Tractile who is developing a product that provides for the factory integration of PV and solar thermal directly in the roofing material, anticipating that highly automated factory integration will eventually be cheaper than manual add-on installations on rigid structures. While several companies provide standard roofing material with integrated PV, Tractile is unique by integrating both PV and solar thermal in a composite roofing system. Joint integration of thermal and PV can further improve the PV performance by up to 10% relative due to a lower operating temperature. The current worldwide markets for roofing and rooftop solar are USD 153 billion and are forecast to grow to USD 233 billion by 2025, and the move to net-zero (or net positive) buildings will further increase its market potential.

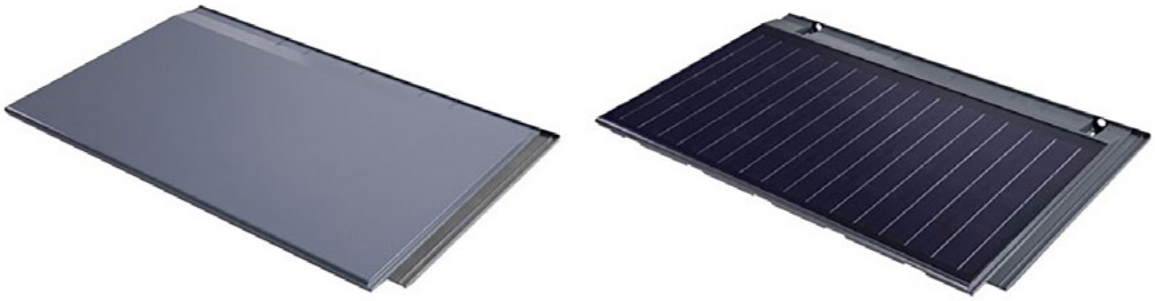

Figure 6.14.1: Picture of the standard Tractile Roof Tile (left) and Tractile Solar Roof Tile (right).

Tractile has already released a first-generation solar tile with integrated PV and solar thermal (see Figure 6.14.1). The current cost at low volume production however, is at too much of a premium for the mass market and sales are limited to a niche of high-end consumers. To make the product more competitive effort is needed in the following areas: Reducing the solar tile's weight from 20 kg to 15 kg, increasing the PV performance by 20%, and reducing the costs by at least 20%. This project focuses on the improvement in PV performance as well as an increased understanding of the benefits of the thermal performance of the product.

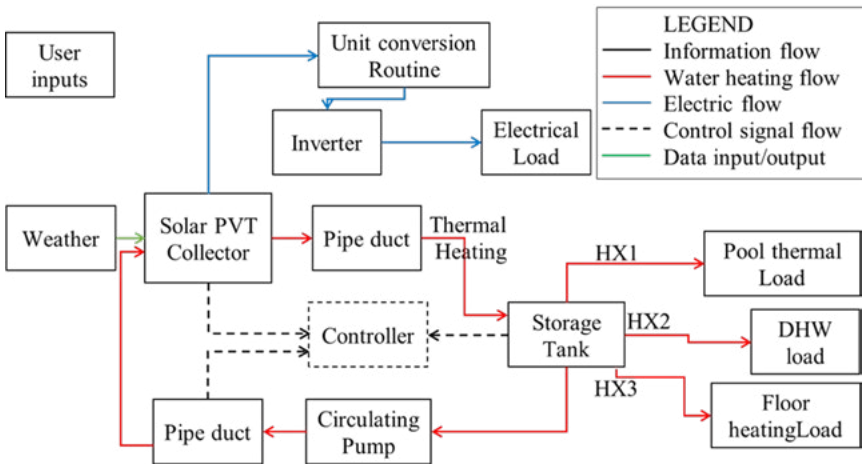

Figure 6.14.2: Schematic of the model constructed in TRNSYS.

Figure 6.14.2 shows the model constructed in TRNSYS ("TRNSYS,"), a transient system simulation software, which was designed to simulate and analyse the performance of a hybrid photovoltaic-thermal (PVT) energy system. This model incorporates a PVT module, which combines PV cells and a thermal energy collector to generate electricity and thermal energy from solar radiation concurrently. The thermal energy generated by the PVT module is transferred to a storage tank, characterised by parameters provided by thermal energy solutions.

The storage tank serves as an intermediary for distributing the collected heat energy to various applications, such as domestic hot water supply, swimming pool heating, and hydronic floor heating systems. This heat transfer process is facilitated through the utilisation of heat exchangers, pumps and control mechanisms to maintain desired temperature levels and system efficiency.

The TRNSYS model is equipped with the capability to simulate and assess the performance of the PVT system for different geographic locations and time zones by altering input parameters such as solar radiation, ambient temperature and load profiles. This flexibility enables users to evaluate the feasibility and optimisation of the PVT system for site-specific conditions and energy requirements, thus facilitating informed decision-making in the design, implementation and management of hybrid renewable energy systems. Figure 6.14.3 shows an example result from the model for Adelaide, clearly highlighting that the panel runs at a lower temperature, thus higher electrical performance, when water is flowing through the system.

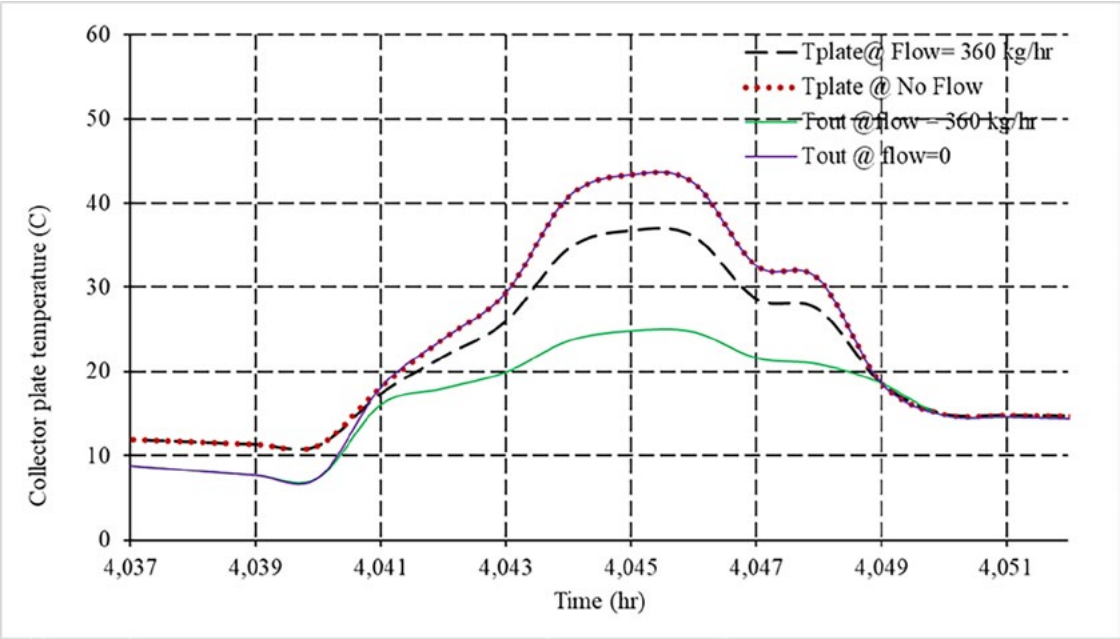

Figure 6.14.3: PVT and output water temperature simulated in TRNSYS for a typical winter day in Adelaide.

In addition to the TRNSYS model, a new PV module design was simulated using a Griddler module ("Griddler"), a versatile solar cell and module simulation tool. This new design demonstrated the potential to improve the performance of the PVT module from its current output of 100 W to nearly 150 W within the same module area. This enhancement is primarily achieved through the use of cut solar cells that employ advanced passivating contact technologies, such as silicon heterojunction (SHJ) and tunnel oxide with passivating contact (TOPCon). Silicon heterojunction technology involves the integration of thin layers of amorphous silicon (a-Si) with crystalline silicon (c-Si) substrates (Yoshikawa et al. 2017), forming a high quality passivating contact that significantly reduces carrier recombination losses. This results in improved cell efficiency and performance. TOPCon technology, on the other hand, is the natural successor of the PERC (passivated emitter and rear cell), which combines a diffused boron emitter with a rear passivating layer consisting of a poly-silicon layer on oxide, further minimising recombination losses in the solar cell and increasing overall cell efficiency (Feldmann et al. 2014).

The incorporation of these advanced cell technologies in the PVT module design not only increase the power output but also lowers temperature coefficients. This improvement can be attributed to the superior passivation properties of SHJ and TOPCon, which lead to reduced temperature coefficients and a higher overall energy yield. The adoption of such innovative solar cell technologies can substantially boost the performance and cost-effectiveness of the PVT system, making it a more attractive solution for diverse applications and locations.

Highlights

- A TRNSYS model was built for a PVT model with various potential use cases for the thermal energy that can be used for assessing the performance of the Tractile PVT system in various climate conditions.
- A new module layout with passivated contact solar cells was identified that could improve the performance of the Tractile Solar Roof Tile by 50% to 150 W.
- The new solar roof tile will have a lower temperature coefficient further boosting its yearly yield.

Future Work

In light of the promising results obtained from the simulations and modelling, we will seek additional funding to pursue the following objectives:

- Collaborate with Tractile to develop a next generation solar roof tile with enhanced performance: Building upon the insights gained from the advanced solar cell technologies, we aim to create a more efficient solar roof tile that combines both photovoltaic and thermal capabilities. This innovative product will provide higher energy yields and improved performance, making it a compelling option for residential and commercial applications.
- Enhance the existing model for Tractile to provide tailored thermal and electrical performance predictions: By refining and expanding the modelling capabilities, we will enable Tractile to offer customised performance estimations to clients based on

their unique requirements and site-specific conditions. This will facilitate informed decision-making and optimise system design for maximum efficiency.

- Incorporate full life cycle analysis into the model: Extending the model to include a comprehensive life cycle assessment will allow us to evaluate the environmental impacts of the PVT system from the cradle to the grave. This holistic approach will consider factors such as raw material extraction, manufacturing, transportation, operation, maintenance, and end-of-life management, providing valuable insights for improving the overall sustainability of the system.
- Develop the PVT system to include cooling capabilities in addition to heating: By integrating cooling functions into the existing PVT system, we can further enhance the technology's overall energy efficiency and versatility. This expansion will allow the PVT system to provide both heating and cooling solutions, making it a more comprehensive and attractive option for various applications, particularly in regions with fluctuating temperature extremes.

References

Feldmann, F., Simon, M., Bivour, M., Reichel, C., Hermle, M. & Glunz, S. W. (2014). Efficient carrier-selective p- and n-contacts for Si solar cells. Solar Energy Materials and Solar Cells 131, 100-104. doi:10.1016/j.solmat.2014.05.039.

Griddler. Retrieved from http://griddlersolar.com/.

TRNSYS. Retrieved from http://www.trnsys.com/.

Yoshikawa, K., Kawasaki, H., Yoshida, W., Irie, T., Konishi, K., Nakano, K. et al. (2017). Silicon heterojunction solar cell with interdigitated back contacts for a photoconversion efficiency over 26%. Nature Energy 2, 17032.

COLLABORATION GRANTS

ACAP's competitively selected Collaboration Grants, whose titles are shown below, are reported online at *acap.org.au/post/acap-s-annual-reports-2013-present*.

6.52 MICROSTRUCTURE CHARACTERISATION OF THERMALLY EVAPORATED PEROVSKITE SOLAR CELLS FOR THE APPLICATION OF MONOLITHIC PEROVSKITE-SILICON TANDEM SOLAR CELLS

Lead Partner

Monash University

Monash University Team

Prof. Udo Bach

Academic Partner

Wuhan University of Technology (WHUT), China: Dr Wei Li, Prof. Yi-Bing Cheng

Funding Support

ARENA, Monash, WHUT

6.60 SILICON SOLAR CELLS WITH SILICON CARBIDE PASSIVATED CONTACTS

Lead Partner

UNSW

UNSW Team

Dr Ning Song, Dr Udo Römer, Dr Fiacre Rougieux, Prof. Alison Lennon, Mr Shuo Deng, Mr Carlin Ng

Funding Support

ACAP

6.69 SCALABLE LAMINATION TECHNIQUES FOR LOW-COST PEROVSKITE SOLAR CELLS

Lead Partner

Monash University

Monash Team

Prof. Udo Bach, A/Prof. Alexandr N. Simonov, Dr Gaveshana Sepalage

Industry Partners

CSIRO (Clayton): Dr Anthony Chesman, Dr Hasitha Weerasinghe

RLA Polymers-Nan Pao: Mr Frank Lord, Mr Sin Chang, Terry Tsai

Funding Support

ACAP

6.71 SUPER-EFFICIENT COLOURED PV FOR VEHICLES

Lead Partner

UNSW

UNSW Team

Dr Jessica Yajie Jiang, Dr Yuanxun Liao, Dr Mark Keevers, Prof. N.J. Ekins-Daukes, Scientia Prof. Martin Green

Industry Partners

AZUR SPACE Solar Power, ACE Electric Vehicle Group

Funding Support

ACAP

6.72 DEVELOPMENT OF III-V CELLS ON GAAS AND INP FOR A 50% EFFICIENT SPECTRUM SPLITTING CPV RECEIVER

Lead Partner

UNSW

UNSW Team

Dr Mark Keevers, Dr Jessica Yajie Jiang, Dr Phoebe Pearce, Dr Anastasia Soeriyadi, Dr Angus Gentle, Dr Mengdi Liu, Sam Eui Ho Kim, Wenxin Shi, Prof. Ned Ekins-Daukes, Scientia Prof. Martin Green

Industry Partners

RayGen Resources Pty Ltd (Australia): Dr John Lasich

IQE plc (UK): Dr Andrew Johnson

SolAero Technologies Corp. (USA): Dr Daniel Derkacs

ANU, Department of Electronic Materials Engineering (Australia): Prof. Hoe Tan, Dr Julie Tournet

Funding Support

ACAP, UNSW

6.73 SURVEY OF SOLAR MODULE QUALITY ON AUSTRALIAN SOLAR FARMS USING OUTDOOR PHOTOLUMINESCENCE IMAGING AND FOURIER TRANSFORM INFRARED SPECTROSCOPY

Lead Partner

UNSW

UNSW Team

Dr Oliver Kunz (Lead)

Academic Partner

Australian National University: Dr Marco Ernst

Industry Partners

ScanPro: Luke Magon

5B Solar: Rhett Evans

Impact Investment Group: Stephen Callis

SolarShare Community Energy Ltd: Nicolas Fejer

Funding Support

ACAP

FELLOWSHIPS

ACAP's competitively selected Fellowships, whose titles are shown below, are reported online at *acap.org.au/post/acap-s-annual-reports-2013-present*.

F15 DEVICE ARCHITECTURE DESIGN FOR COMMERCIAL KESTERITE SINGLE-JUNCTION AND MULTI-JUNCTION SOLAR CELLS

Lead Partner

UNSW

UNSW Team

Dr Kaiwen Sun, Prof. Xiaojing Hao, Prof. Martin Green, Dr Jialiang Huang, Dr Chang Yan, Dr Jianjun Li, Dr Xin Cui, Dr Heng Sun, Ao Wang, Guojun He

Academic Partners

Shenzhen University: Prof. Zhenghua Su

Nanyang Technological University (NTU): Prof. Lydia Helena Wong

Duke University: Prof. David B. Mitzi, Dr Betul Teymur

Funding Support

ACAP

F29 HYDROGEN PASSIVATION OF SI1-XGEX FOR SI1-XGEX/SI TANDEM SOLAR CELLS

Lead Partner

UNSW

UNSW Team

Dr Li Wang, Dr Zhenyu Sun, Mr Hao Luo, and A/Prof. Brett Hallam

Funding Support

ACAP Fellowship

F31 INTERFACE ENGINEERING BY ATOMIC LAYER DEPOSITION FOR HIGH PERFORMANCE EARTH-ABUNDANT SOLAR CELLS

Lead Partner

UNSW

UNSW Team

Dr Xin Cui, Prof. Xiaojing Hao, Prof. Bram Hoex, Dr Kaiwen Sun, Dr Chang Yan, Dr Jialiang Huang, Ao Wang, Xiaojie Yuan, Guojun He

Funding Support

ACAP Fellowship

F41 APPLICATION OF STABLE LEAD-FREE ABSORBER LAYERS IN PHOTOVOLTAICS

Lead Partner

Monash University

Monash University Team

Dr Nadja Glueck (Giesbrecht), Prof. Udo Bach

Funding Support

ACAP Fellowship

F46 CHARACTERISING THE PERFORMANCE, CONTRIBUTION, AND IMPACT OF DISTRIBUTED PV SYSTEMS IN AUSTRALIA'S ELECTRICITY GRIDS

Lead Partner

UNSW

UNSW Team

Dr Navid Haghdadi, A/Prof. Anna Bruce, Prof. Iain MacGill

Funding Support

ACAP Fellowship

F59 OPTIMUMS IN 100% RENEWABLE ENERGY SYSTEMS

Lead Partner

ANU

ACAP Fellow

Dr Cheng Cheng

Supervisor

Prof. Andrew Blakers

Funding Support

ACAP fellowship

F60 UNLOCKING THE FULL POTENTIAL OF DOPED POLY-SI CONTACTS ON TEXTURED SURFACES

ACAP Fellow

Dr. Rabin Basnet

Supervisor

Prof. Daniel Macdonald

Funding Support

ACAP

F61 DEVELOPMENT OF A LOW-COST AND QUANTITATIVE MATERIALS ANALYSIS PLATFORM BY PHYSICS-BASED MACHINE LEARNING

Lead Partner

ANU

ACAP Fellow

Dr Hualin Zhan

Supervisor

Prof. Kylie Catchpole

Funding Support

ACAP Fellowship

F64 THE SOCIAL AND ETHICAL ASPECTS OF THE PHOTOVOLTAIC LIFE CYCLE SUPPLY CHAIN

Lead Partner

UNSW

UNSW Team

Dr Huy Tuan Anh Le

Prof. Ziv Hameiri

University of Sydney Team

A/Prof. Susan Banki

Funding Support

ACAP R4 Fellowship

F66 DEVELOPMENT OF STABLE PURE IODIDE WIDE BANDGAP PEROVSKITES SOLAR CELLS

Lead Partner

UNSW

UNSW Team

Mingrui He

Funding Support

ACAP Fellowship

F67 DEVELOPING A RAPID CELL-LEVEL TESTING METHOD TO IDENTIFY SOLDERING FLUX-INDUCED DEGRADATION IN HIGH-EFFICIENCY SOLAR CELLS

Lead Partner

UNSW

UNSW Team

Dr Chandany Sen (Lead), Prof. Bram Hoex

Funding Support

ACAP Fellowship and $40K cash support from industry partners, UNSW

INFRASTRUCTURE GRANTS

ACAP's competitively selected Infrastructure Grants, whose titles are shown below, are reported online at *acap.org.au/post/acap-s-annual-reports-2013-present*.

AIF101 HIGH-THROUGHPUT SOLUTION-PROCESSABLE PHOTOVOLTAIC MATERIALS DISCOVERY FACILITY (HPDF)

Lead Partner

Monash University

Monash University Team

Udo Bach, Jacek Jasieniak, Yi-Bing Cheng, Douglas MacFarlane, Mainak Majumder

Funding Support

ACAP, Monash University, ANFF, CSIRO, ARC Centre of Excellence in Exciton Science

AIF102 CLIMATE CHAMBER WITH INTEGRATED SOLAR SIMULATOR AND IN SITU CURRENT-VOLTAGE MEASUREMENTS

Lead Partner

UNSW

UNSW Team

Bram Hoex, Muhammad Umair Khan, Michael Pollard, Nino Borojevic

Industry Partners

Eternalsun Spire

Funding Support

ACAP

AIF104 COMBINATORIAL SPUTTERING FACILITY

Lead Partner

Monash

Monash University Team

Jacek Jasieniak, Udo Bach

Funding Support

ACAP

AIF107 NEXT GENERATION SI AND TANDEM HETERO-CONTACT LABORATORY

Lead Partner

ANU

ANU Team

Dr Kean Chern Fong, Dr Lachlan Black, Dr Thien Truong, Prof. Andrew Blakers, Prof. Daniel Macdonald, A/Prof. Klaus Weber, A/Prof. Thomas White, Prof. Kylie Catchpole, Dr Matthew Stocks, Dr Di Yan, Dr Pheng Phang, Dr Wensheng Liang, Dr Osorio Mayon

Funding Support

ACAP

AIF108 TANDEM CLUSTER

UNSW Team

Prof. Xiaojing Hao, Prof. Bram Hoex, A/Prof. Nicholas J. Ekins-Daukes, A/Prof. Ziv Hameiri

Funding Support

ACAP

AIF205 ENERGY DATA PLATFORM (EDP)

Funding Support

ACAP

Lead Partner

UNSW

UNSW Team

A/Prof. Anna Bruce (Principal), Dr Navid Haghdadi (ACAP Fellow), Dr Mike Roberts, Dr Nargess Nourbakhsh, Dr Baran Yildiz, Dr Rob Passey, Dr Merlinde Kaye, Dr Jose Bilbao, Dr Alison Ciesla, Dr Catherine Chan, Prof. Renate Egan, Prof. Bram Hoex, Prof. Alistair Sproul

AIF206 ROLL-TO-ROLL PV FILM PRINTING/LAMINATING FACILITY

Lead Partner

Commonwealth Scientific and Industrial Research Organisation (CSIRO)

CSIRO Team

Dr Mei Gao, Dr Andrew Scully, Dr Christopher Dunn, Karl Weber

Funding Support

ACAP, CSIRO

AIF209 SINGLE-SIDE ETCHING TOOL

Lead Partner

UNSW

UNSW Team

Bram Hoex, Fred Qi, Chukwuka Uzochukwu Madumelu

Funding Support

ACAP

AIF210 LARGE AREA MULTI-ZONE SOLAR SIMULATOR

Lead Partner

UNSW

UNSW Team

Prof. Nicholas Ekins-Daukes, Dr Mark Keevers, Prof. Xiaojing Hao, Prof. Stephen Bremner, Prof. Gavin Conibeer

Industry Partners

TS-Space Systems, AZUR SPACE Solar Power GmbH

Funding Support

ACAP

AIF211 ATMOSPHERICALLY CONTROLLED PV PROCESSING AND ACCELERATED TESTING FACILITY

Lead Partners

UNSW, Monash University

UNSW Team

Prof. Xiaojing Hao, Prof. Bram Hoex, A/Prof. Nicholas J. Ekins-Daukes, A/Prof. Ziv Hameiri

Monash University Team

Prof. Jacek Jasieniak, Prof. Udo Bach

Funding Support

ACAP

FINANCIAL SUMMARY

In December 2012, a grant of $33.2 million from the Australian Government through ARENA was announced to support an initial eight-year program of the Australian Centre for Advanced

Photovoltaics (ACAP). This support leveraged an additional $55.4 million cash and in-kind commitment from ACAP participants taking the total value of the project to $88.6 million.

ACAP commenced on 1 February 2013 after the signing of the Head Agreement between ARENA and UNSW, and with the receipt of letters of confirmation of participation under the terms of the Head Agreement by the other project participants. Collaboration Agreements with the Australian participants in the Australian Centre for Advanced Photovoltaics (ACAP) were completed on 1 July 2013.

An extension to the program, to undertake an Australian Solar PV Cell and Module Research Infrastructure Plan and Feasibility Study was signed in October 2014, generating an additional milestone, 4A. This project was completed and Milestone 4A was paid in October 2015. A further extension was formalised through Variation #4, executed in February 2016. It extended perovskites research in ACAP and generated two new Milestones for each year 2016–2019. Disbursements were made to each node following confirmation of institutional cash contributions for each completed year.

Variation #5 in June 2016 added a new partner, Dyesol Pty Ltd (subsequently known as Greatcell Solar Pty Ltd) and pooled the cash and in-kind contributions of most of the collaborating international research institutions and of the collaborating industry participants.

RayGen Resources Pty Ltd joined as a new collaborating industry participant during 2017 and Tindo Operations Co. Pty Ltd joined in 2019. Greatcell Solar Pty Ltd, ceased to trade during Q4 of 2018 and is no longer a collaborating industry participant in ACAP. 5B Australia Pty Ltd, Evolving Energy, Microsolar Energy Pty. Ltd., SunCable Pty Ltd, SunDrive Solar Pty Ltd and the University of Sydney joined in 2021 and Australian Photovoltaics Institute, CubicPV Inc. (USA), Green Energy Institute (Korea), Neoen Australia Pty Ltd, One Stop Warehouse Pty. Ltd. and Scipher Technologies Pty Ltd all became collaborating industry participants in 2022.

Variation #6 in October 2017 and #6A in December 2017 implemented many of the changes proposed by the Mid-Term Review Panel in 2016, including the provision of additional funding for Capacity Building (Fellowships) and Small Grants, and made several minor updates and corrections. These variations brought the total funds granted to $46.0 million. A robust and transparent process to distribute Small (Collaboration) Grants was developed in 2015 and implemented in a small first funding round in that year. Since 2015, five rounds of small project / collaboration grant funding have been started, releasing amounts of $20,000 to $66,000 over a total of 63 small projects and $3,108,105 to 2020. A further eight grants, valued at $422,655, were offered through Round 6 in Q4 of 2020.

Twenty ACAP Fellowships were all taken up during 2018. The fourth round of Small Grants were selected in Q2 of 2018, offering a total of 17 projects sharing $821,800. A further, fifth, round was offered late in 2018 (for projects to start in 2019). Again, 17 projects were successful and shared $856,305.

Variation #7 was executed on 4 April 2019. This provided additional funding of $19.0 million in the overall budget to extend the life of ACAP for an extra two years (its ninth and tenth) until the end of 2022, an additional two rounds each of 15 Fellowships – Round 2 in 2019 and Round 3 in 2020, and an additional round of Small Grants in 2020.

Partnerships with Sandia National Laboratories and the University of California, Santa Barbara were formally ended through Variation #7.

Variation #7 also included an agreement for support for infrastructure funding up to $19 million, which has led to two funding rounds. This brought the total cash support from ARENA to $84.0 million.

The Collaboration Agreement, between UNSW and the five Collaborating Australian Research Institutions was renegotiated during 2019 and was executed in Q4 of 2020.

A final round, the sixth, of short-term Fellowships was initiated in 2023. The initial ten-year program of ACAP, outlined above, is now termed "ACAP1.0".

Since the completion of several infrastructure projects, some fellowships and a few small grants were delayed by COVID-generated disruptions to such an extent that they could not be finished in 2022 and ARENA allowed the financial closure of ACAP1.0 to be postponed until November 2024 (Variation 14, 5 June 2023).

As reported in Chapter 2 of the 2022 ACAP Annual Report, Minister Chris Bowen announced in that year at UNSW that ACAP would be extended for a further eight years, including a stage-gate review, with an additional $45m of Australian Government funding to be provided through ARENA.

This extension to 2030, now known as ACAP2.0, was implemented through Variation 13 (3 January 2023), effectively a new Funding Agreement between ARENA and UNSW. This revision permitted the inclusion of two additional Project participants, CSIRO Energy and The University of Sydney. A stage-gate review of ACAP2.0 will be held in 2025. The present report covers the first year of operation of ACAP2.0.

All technical milestones for 2023 were achieved.

Accounts for ACAP1.0 and ACAP2.0 in 2023 are both presented here. There was no new revenue for ACAP1.0 in 2023. The actual total 2023 cash expenditure and in-kind contributionsfor all categories was $11.7 million and its breakdown is shown in Figure 7.1(b).

The breakdown by institution of the $13.4 million total cash and in-kind budget for ACAP2.0 in 2023 is shown in Figure 7.2(a). The actual total 2023 cash expenditure and in-kind contributionsfor all categories was $12.1 million and its breakdown is shown in Figure 7.2(b).

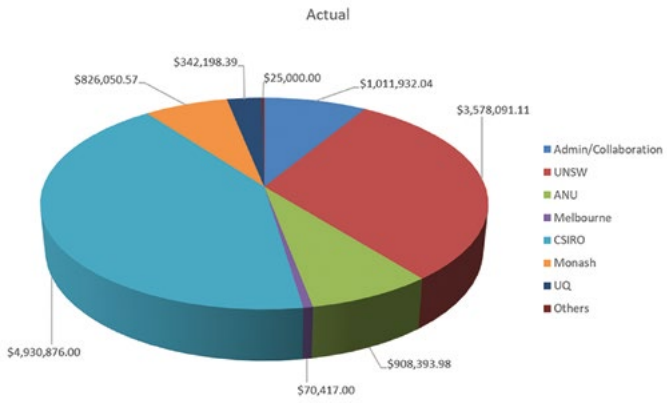

Figure 7.1: Actual ACAP 1.0 cash and in-kind expenditure ($m) breakdown by institution for 2023.

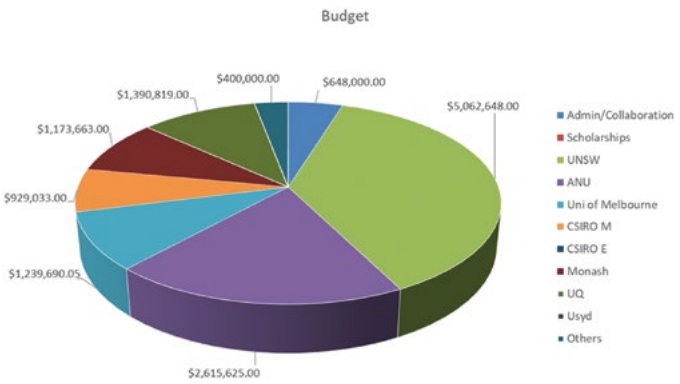

Figure 7.2(a): Total ACAP 2.0 cash and in-kind expenditure budget ($m) for 2023 broken down by institution.

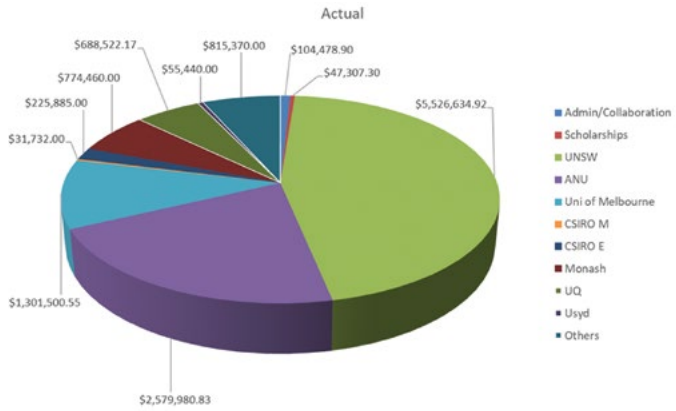

Figure 7.2(b): Actual ACAP 2.0 cash and in-kind expenditure ($m) breakdown by institution for 2023.

PUBLICATIONS

8.2. BOOK CHAPTERS

Bilbao, J., Young, S. & Hoex, B. (2023). PV systems in Australia: Market evolution and performance in desert applications. In Photovoltaic Technology for Hot and Arid Environments. IET Digital Library. DOI: 10.1049/PBPO144E_ch9

Corkish, R., Kumar, S. & Korinihona, J. (2024). Energy Transitions, in The Water, Energy and Food Security Nexus in Asia/Pacific. Vol. III: The Pacific, Dansie, A., Alleway, H. & Böer, B. (eds.), Springer Cham, May 2024. https://link.springer.com/book/9783031254628

Rougieux, F., Coletti, G. ; Gaal, S. Guo, B.(H.), Fu, N. (F.), Veirman, J., Liu, A. & Øvrelid, E.J. (2022). n-type silicon material. In n-Type Crystalline Silicon Photovoltaics: Technology, applications and economics. IET Digital Library. DOI: 10.1049/PBPO175E_ch2

8.3. PATENTS AND PATENT APPLICATIONS

Armin, A., Burn, P. L. Lin, Q. & Meredith, P. (2015). "Narrowband Photodetector", Patent Application AU2015/903564 (WO2017035589A1, PCT/AU2016/050819), AU2015/903705.

Bach, U. & Kashif, M.K.(2023). Electroactive materials. Provisional Australian patent. Application No. 2023901091. Filing date: 13/4/2023.

Bram Hoex, B., Sen, C. & Wu, X. A method for protecting solar cells from contaminants. Filed PCT

Cheng, Y.-B., Bach, U., Spiccia, L., Huang, F. & Xiao, M. (2017). Precipitation process for producing perovskite-based solar cells. US Patent Application No. 15/126,459. (Lapsed)

Ciesla, A., Chan, C., Chong, C.M., Chen, D., David Payne, D., Ly Mai, L., Abbott, M., Kim, M., Wenham, S. & Fung, T.H. A method for improving wafer performance for photovoltaic devices. Granted 201780071912.X China, 10-2019-7016969 South Korea, 17/287966 USA

Ciesla, A., Hallam, B., Chan, C., Chong, C.M., Chen, D., David Payne, D., Ly Mai, L., Abbott, M., Kim, M., Wenham, S. & Fung, T.H. Advanced hydrogen passivation that mitigates hydrogen-induced recombination (HIR) and surface passivation deterioration in PV devices. 201780072249.5 Granted, China

Dias, P.R. Method for recycling silicon photovoltaic modules. PCT/AU2022/051545

Edwards, M. & Slade, A. Bifacial PERC solar cells and methods for the production thereof. Reassigned Australia.

Green, M., Hao, X., Liu, Z., Li, C. Mehrvarz, H. & Zhang, Y. A method to generate conductive polymer. Filed PCT

Green, M., Hao, X., Liu, Z., Li, C. Mehrvarz, H. & Zhang, Y. An apparatus for perovskite fabrication. Filed Australia, provisional

Green, M., Hao, X., Liu, Z., Li, C. Mehrvarz, H. & Zhang, Y. Method of producing monograin membranes. Filed PCT

Green, M., Zhou, Z. & Deng, R. Delaminating of a photovoltaic module. Filed, Australia, provisional

Hallam, B., Chan, C., Chen, D., Zhang, Y. & Wright, B. Metallization for silicon solar cells. Filed Australia, India, examination requested China, Europe and USA

Hallam, B., Chan, C., Mahboubi Soufiani, A. & Zhang, Y. A solar cell structure and a method of forming a solar cell structure. Filed Australia, examination requested China and USA

Huang, J., Sun, K. & Green, M. A copper-based chalcogenide photovoltaic device and a method of forming the same. 201780039014.6. Granted, China

Lennon, A., Hsiao, P.-C., Roemer, C., Li, Y. & Song, N. Solar cell structure. Assigned China, Europe

Lennon, A., Ouyang, Z. & Hall, C. A method of forming a device structure. Assigned Australia, China, Europe, USA

Lennon, A., Ouyang, Z., Song, N., Hsiao, P.-C. & Yang Li, Y. A structured connector for interconnecting device components. Assigned Australia, China, Europe, USA

Trupke, T., Juhl, M., Kunz, O. & Rey, G. Outdoor photoluminescence imaging of photovoltaic arrays via optical string modulation. Filed Australia, China, India, Singapore and USA

Trupke, T., Kunz, O., Rey, G. & Paduthol, A.R. Outdoor photo-luminescence imaging of photovoltaic modules. Filed Australia, examination requested China, Singapore and USA

Uddin, A. & Dipta, S. Solution processable phenolic encapsulation of articles. Filed, Australia, provisional

8.4 PAPERS IN REFEREED SCIENTIFIC AND TECHNICAL JOURNALS

Abad, B., Alberi, K., Ayers, K. E., Badhulika, S., Ban, C., Béa, H., Béron, F., Cairney, J., Chang, J. P., Charles, C., Creatore, M., Dong, H., Du, J., Egan, R., Everschor-Sitte, K., Foley, C., Fontcuberta i Morral, A., Jung, M.-H., Kim, H., Kurtz, S., Lee, J., Leitao, D. C., Lemmer, K., Marschilok, A. C., Mitu, B., Newman, B. K., Owens, R., Pappa, A.-M., Park, Y., Peckham, M., Rossi, L. M., Shim, S.-H., Siddiqui, S. A., Son, J.-W., Spiga, S., Tsikata, S., Vianello, E., Wilson, K., Yuasa, H., Zardo, I., Zenyuk, I., Zhang, Y. & Zhao, Y. (2023). The 2022 applied physics by pioneering women: a roadmap. Journal of Physics D: Applied Physics 56.

Abdin, Z., Al Khafaf, N., McGrath, B., Catchpole, K. & Gray, E. (2023). A review of renewable hydrogen hybrid energy systems towards a sustainable energy value chain. Sustainable Energy & Fuels 7, 2042-2062.

Abdullah-Vetter, Z., Dwivedi, P., Buratti, Y., Sowmya, A., Trupke, T. & Hameiri, Z. (2023). Advanced analysis of internal quantum efficiency measurements using machine learning. Progress in Photovoltaics: Research and Applications 31, 790-802.

Ahmed, M. I., Hibbert, D. B. & Zhao, C. (2023). Rational catalyst design and mechanistic evaluation for electrochemical nitrogen reduction at ambient conditions. Green Energy & Environment 8, 1567-1595.

Almora, O., Baran, D., Bazan, G. C., Cabrera, C. I., Erten-Ela, S., Forberich, K., Guo, F., Hauch, J., Ho-Baillie, A. W. Y., Jacobsson, T. J., Janssen, R. A. J., Kirchartz, T., Kopidakis, N., Loi, M. A., Lunt, R. R., Mathew, X., McGehee, M. D., Min, J., Mitzi, D. B., Nazeeruddin, M. K., Nelson, J., Nogueira, A. F., Paetzold, U. W., Rand, B. P., Rau, U., Snaith, H. J., Unger, E., Vaillant-Roca, L., Yang, C., Yip, H.-L. & Brabec, C. J. (2023). Device Performance of Emerging Photovoltaic Materials (Version 3). Advanced Energy Materials 13, 2203313.

Almora, O., Cabrera, C. I., Erten-Ela, S., Forberich, K., Fukuda, K., Guo, F., Hauch, J., Ho-Baillie, A. W. Y., Jacobsson, T. J., Janssen, R. A. J., Kirchartz, T., Loi, M. A., Mathew, X., Mitzi, D. B., Nazeeruddin, M. K., Paetzold, U. W., Rand, B. P., Rau, U., Someya, T., Unger, E., Vaillant-Roca, L. & Brabec, C. J. (2023). Device Performance of Emerging Photovoltaic Materials (Version 4). Advanced Energy Materials 14.

Asami, M., Kampwerth, H., Pollard, M., Hao, X., Komaba, S., Ikari, T., Fukuyama, A., Watanabe, K., Nakano, Y. & Sugiyama, M. (2023). Refining Photothermal Deflection Spectroscopy: Incorporating Reflectance for Enhanced Accuracy in Light-Absorption Measurements. physica status solidi (a).

Ashfaq, S., Zhang, D., Zhang, C. & Dong, Z. Y. (2023). Load flow investigations for regionalized islanded microgrid considering frequency regulation with high renewable penetration. Electric Power Systems Research 214.

Baek, M. C., Jang, J. S., Suryawanshi, M. P., Karade, V. C., Kim, J., He, M., Park, S. W., Kim, J. H. & Shin, S. W. (2023). Rear interface engineering via a facile oxidation process of Mo back contact for highly efficient CZTSSe thin film solar cells. Journal of Alloys and Compounds 935.

Bailey, C. G., Gillan, L. V., Lee, M., Sloane, N., Liu, X., Hao, X., Soufiani, A. M. & McCamey, D. R. (2023). Influence of Organic Spacer Cation on Dark Excitons in 2D Perovskites. Advanced Functional Materials.

Bao, W., Shen, H., Wang, R., Qian, C., Cui, D., Xia, J., Liu, H., Guo, C., Yu, F., Li, J. & Sun, K. (2023). Photo-assisted rechargeable batteries: principles, performance, and development. Journal of Materials Chemistry A 11, 18605-18625.

Bao, W., Wang, R., Liu, H., Qian, C., Liu, H., Yu, F., Guo, C., Li, J. & Sun, K. (2023). Photoelectrochemical Engineering for Light-Assisted Rechargeable Metal Batteries: Mechanism, Development, and Future. Small 19, e2303745.

Bao, W., Wang, R., Qian, C., Shen, H., Yu, F., Liu, H., Guo, C., Li, J. & Sun, K. (2023). Light-Assisted Lithium Metal Anode Enabled by In Situ Photoelectrochemical Engineering. Small, e2307179.

Bartholazzi, G., Shehata, M. M., Basnet, R., Samundsett, C., Macdonald, D. H. & Black, L. E. Novel Interlayer Boosting the Performance of Evaporated Cu2O Hole-Selective Contacts in Si Solar Cells. Solar RRL n/a, 2300727.

Bartholazzi, G., Shehata, M. M., Macdonald, D. H. & Black, L. E. (2023). Atomic layer deposition of Cu2O using copper acetylacetonate. Journal of Vacuum Science & Technology A 41.

Basnet, R., Sun, C., Le, T., Yang, Z., Liu, A., Jin, Q., Wang, Y. & Macdonald, D. (2023). Investigating Wafer Quality in Industrial Czochralski-Grown Gallium-Doped p-Type Silicon Ingots with Melt Recharging. Solar RRL 7, 2300304.

Bati, A. S. R. et al. (2023). Atomically Doped 2D Black Phosphorus for Efficient and Stable Perovskite Solar Cells. Small Structures. Wiley.

Bati, A. S. R., Jiang, W., Chu, R., Mallo, N., Burn, P. L., Gentle, I. R. & Shaw, P. E. (2023). Fluorinated Cation-Based 2D Perovskites for Efficient and Stable 3D/2D Heterojunction Perovskite Solar Cells. ACS Applied Materials & Interfaces. American Chemical Society (ACS).

Belongeay, M., Shirkey, G., Lunardi, M. M., Rodriguez-Garcia, G., Sinha, P., Corkish, R., Stewart, R. A., Anctil, A., Chen, J. & Celik, I. (2023). Photovoltaic Systems through the Lens of Material-Energy-Water Nexus. Energies 16.

Bing, J., McKenzie, DR., Stals, T., Kypriotis, M., Zheng, J. & Ho-Baillie, A. (2023). Total equivalent energy efficiency metric for building-integrated photovoltaic windows. Joule, https://doi.org/10.1016/j.joule.2023.11.010

Bui, A. D., Nguyen, D.-T., Fell, A., Mozaffari, N., Ahmad, V., Duong, T., Li, L., Truong, T. N., Wibowo, A. A., Nguyen, K., Fischer, O., Schindler, F., Schubert, M. C., Weber, K. J., White, T. P., Catchpole, K. R., Macdonald, D. & Nguyen, H. T. (2023). Spatially resolved power conversion efficiency for perovskite solar cells via bias-dependent photoluminescence imaging. Cell Reports Physical Science 4, 101641.

Chai, Q. Z., Cuo; Xu, Yan; Dong, Zhao Yang; Zhang, Rui. (2023). Pareto Front Analysis Method for Optimization of PV Inverter Based Volt/Var Control Considering Inverter Lifetime. CSEE Journal of Power and Energy Systems.

Chao, I. H., Yang, Y. T., Yu, M. H., Chen, C. H., Liao, C. H., Lin, B. H., Ni, I. C., Chen, W. C., Ho-Baillie, A. W. Y. & Chueh, C. C. (2023). Performance Enhancement of Lead-Free 2D Tin Halide Perovskite Transistors by Surface Passivation and Its Impact on Non-Volatile Photomemory Characteristics. Small 19, e2207734.

Cheng, S., Sun, Z., Lim, K. H., Wibowo, A. A., Zhang, T., Du, T., Liu, L., Nguyen, H. T., Li, G. K., Yin, Z. & Kawi, S. (2023). Dual-Defective Two-Dimensional/Two-Dimensional Z-Scheme Heterojunctions for CO2 Reduction. ACS Catalysis 13, 7221-7229.

Chin, R. L., Soufiani, A. M., Fassl, P., Zheng, J., Choi, E., Ho-Baillie, A., Paetzold, U. W., Trupke, T. & Hameiri, Z. Surface saturation current densities of perovskite thin films from Suns-photoluminescence quantum yield measurements. Progress in Photovoltaics: Research and Applications n/a.

Choi, E., Lee, J.-W., Anaya, M., Mirabelli, A., Shim, H., Strzalka, J., Lim, J., Yun, S., Dubajic, M., Lim, J., Seidel, J., Agbenyeke, R. E., Kim, C. G., Jeon, N. J., Soufiani, A. M., Park, H. H. & Yun, J. S. Synergetic Effect of Aluminum Oxide and Organic Halide Salts on Two-Dimensional Perovskite Layer Formation and Stability Enhancement of Perovskite Solar Cells. Advanced Energy Materials, 13 2301717.

Choi, M. J., Lee, S. W., Lee, M., Shin, S. J., Kim, M., Jeon, G. G., Yoon, S. E., Xiangyang, F., Lee, B. R., Seidel, J., Yun, J. S., Chang, D. W. & Kim, J. H. (2023). Strategic approach for achieving high indoor efficiency of perovskite solar Cells: Frustration of charge recombination by dipole induced homogeneous charge distribution. Chemical Engineering Journal 454.

Chowdhury, T., Chowdhury, H., Islam, K. S., Sharifi, A., Corkish, R. & Sait, S. M. (2023). Resilience analysis of a PV/battery system of health care centres in Rohingya refugee camp. Energy 263.

Coddington, O. M., Richard, E. C., Harber, D., Pilewskie, P., Woods, T. N., Snow, M., Chance, K., Liu, X. & Sun, K. (2023). Version 2 of the TSIS-1 Hybrid Solar Reference Spectrum and Extension to the Full Spectrum. Earth and Space Science 10.

Collins, M. I., Campaioli, F., Tayebjee, M. J. Y., Cole, J. H. & McCamey, D. R. (2023). Quintet formation, exchange fluctuations, and the role of stochastic resonance in singlet fission. Communications Physics 6.

Cordaro, A., Tabernig, S. W., Pollard, M., Yi, C., Alarcon-Llado, E., Hoex, B. & Polman, A. (2023). Nanopatterned SiNx Broadband Antireflection Coating for Planar Silicon Solar Cells. physica status solidi (a) 220.

Cui, D., Wang, R., Qian, C., Shen, H., Xia, J., Sun, K., Liu, H., Guo, C., Li, J., Yu, F. & Bao, W. (2023). Achieving High Performance Electrode for Energy Storage with Advanced Prussian Blue-Drived Nanocomposites-A Review. Materials (Basel) 1616(4) 16(4):1430. doi: 10.3390/ma16041430.

Cui, X., Sun, K., Huang, J., Sun, H., Wang, A., Yuan, X., Green, M., Hoex, B. & Hao, X. (2023). Low-Temperature Plasma-Enhanced Atomic Layer Deposition of ZnMgO for Efficient CZTS Solar Cells. ACS Materials Letters 5, 1456-1465.

de Clercq, D. M., Yang, J., Hanif, M., Alves, J., Feng, J., Nielsen, M. P., Kalantar-Zadeh, K. & Schmidt, T. W. (2023). Exciton Dissociation, Charge Transfer, and Exciton Trapping at the MoS2/Organic Semiconductor Interface. The Journal of Physical Chemistry C 127, 11260-11267.

Du, H.-Q., Jiang, Y., Rothmann, M. U., Bach, U., Cheng, Y.-B. & Li, W. (2023). Transmission electron microscopy studies of organic–inorganic hybrid perovskites: Advances, challenges, and prospects. Applied Physics Reviews 10, 021314.

Duan, L., Walter, D., Chang, N., Bullock, J., Kang, D., Phang, S. P., Weber, K., White, T., Macdonald, D., Catchpole, K. & Shen, H. (2023). Stability challenges for the commercialization of perovskite–silicon tandem solar cells. Nature Reviews Materials 8, 261-281.

Duong, T., Nguyen, T., Huang, K., Pham, H., Adhikari, S. G., Khan, M. R., Duan, L., Liang, W., Fong, K. C., Shen, H., Bui, A. D., Mayon, A. O., Truong, T., Tabi, G., Ahmad, V., Surve, S., Tong, J., Kho, T., Tran-Phu, T., Lu, T., Zheng, J., Paetzold, U. W., Lemmer, U., Baillie, A. H., Liu, Y., Andersson, G., White, T., Weber, K. & Catchpole, K. (2023). Bulk Incorporation with 4-Methylphenethylammonium Chloride for Efficient and Stable Methylammonium-Free Perovskite and Perovskite-Silicon Tandem Solar Cells. Advanced Energy Materials 13, 2203607.

Dwivedi, P., Weber, J. W., Lee Chin, R., Trupke, T. & Hameiri, Z. (2023). Deep learning method for enhancing luminescence image resolution. Solar Energy Materials and Solar Cells 257.

Ernst, M., Liu, X., Asselineau, C. A., Chen, D., Huang, C. & Lennon, A. (2024). Accurate modelling of the bifacial gain potential of rooftop solar photovoltaic systems. Energy Conversion and Management 300, 117947.

Ernst, M., Wagner-Mohnsen, H., Wasmer, S., Klöter, B. & Altermatt, P. P. (2023). Predicting Module Performance from Cell and Module Parameters Using Machine Learning. Advanced Photonics Congress 2023. Busan: Optica Publishing Group, JW2E.5.

Farooq, U., Zhang, M., Chi, D., Wang, J., Idris, A. M., Huang, S., Pan, Z. & Li, Z. (2023). Surface Defects Passivation with Organic Salt for Highly Stable and Efficient Lead-Free Cs3Sb2I9 Perovskite Solar Cells. ACS Applied Energy Materials 6, 10294-10302.

Fischer, C., Schmid, A., Herguth, A., Zuschlag, A., Altermatt, P. P., Hamer, P. & Hahn, G. (2023). Influence of highly doped layers on hydrogen in-diffusion into crystalline silicon. Solar Energy Materials and Solar Cells 250.

Fischer, O., Bui, A. D., Schindler, F., Macdonald, D., Glunz, S. W., Nguyen, H. T. & Schubert, M. C. Versatile implied open-circuit voltage imaging method and its application in monolithic tandem solar cells. Progress in Photovoltaics: Research and Applications n/a.

Ford, E., Peters, I. M. & Hoex, B. (2024). Quantifying the impact of wildfire smoke on solar photovoltaic generation in Australia. 27(2) 108611. iScience 27.

Forecast, R., Gholizadeh, E. M., Prasad, S. K. K., Blacket, S., Tapping, P. C., McCamey, D. R., Tayebjee, M. J. Y., Huang, D. M., Cole, J. H. & Schmidt, T. W. (2023). Power Dependence of the Magnetic Field Effect on Triplet Fusion: A Quantitative Model. J Phys Chem Lett 14, 4742-4747.

Fu, K., Yang, Z., Sun, H., Chen, X., Li, S., Ma, W. & Chen, R. (2023). Multiple modification on nanoporous silicon derived from photovoltaic silicon cutting waste for extraction of PbⅡ in industrial effluents. Materials Today Communications 35.

Fürer, S. O., Rietwyk, K. J., Pulvirenti, F., McMeekin, D. P., Surmiak, M. A., Raga, S. R., Mao, W., Lin, X., Hora, Y., Wang, J., Shi, Y., Barlow, S., Ginger, D. S., Marder, S. R. & Bach, U. (2023). Naphthalene-imide Self-assembled Monolayers as a Surface Modification of ITO for Improved Thermal Stability of Perovskite Solar Cells. ACS Applied Energy Materials 6, 667-677.

Gaikwad, M. A., Ghorpade, U. V., Suryawanshi, U. P., Kumar, P. V., Jang, S., Jang, J. S., Tran, L., Lee, J. S., Bae, H., Shin, S. W., Suryawanshi, M. P. & Kim, J. H. (2023). Rapid Synthesis of Ultrathin Ni:FeOOH with In Situ-Induced Oxygen Vacancies for Enhanced Water Oxidation Activity and Stability of BiVO(4) Photoanodes. ACS Appl Mater Interfaces 15, 21123-21133.

Gao, C., Li, W., Jing, L., Wang, Z., Shi, L., Sheng, J., Wang, L., Zhao, Y. & Fei, W. (2023). Enhanced photovoltaic and piezo-photovoltaic effects in flexible oxide ferroelectric film directly coated on polyimide substrate. Nano Energy 117.

Gayot, F., Bruhat, E., Bouttemy, M., Frégnaux, M., De Vito, E., Kleider, J.-P., Cros, S. & Manceau, M. (2023). Elucidating Interfacial Limitations Induced by Tin Oxide Electron Selective Layer Grown by Atomic Layer Deposition in N–I–P Perovskite-Based Solar Cells. ACS Applied Energy Materials 6, 11849-11860.

Gilmore, N., Koskinen, I., Burr, P., Obbard, E., Sproul, A., Konstantinou, G., Bilbao, J., Daiyan, R., Kay, M., Corkish, R., Macgill, I., Lovell, E., Menictas, C. & Bruce, A. (2023). Identifying weak signals to prepare for uncertainty in the energy sector. Heliyon 9. https://doi.org/10.1016/j.heliyon.2023.e21295

Gour, K. S., Karade, V. C., Parmar, R., Jang, J. S., Kazim, S., Jang, S., Gunnella, R., Park, J., Yun, J. H. & Kim, J. H. (2023). In Search of Disorder Transitions and Defects Within Cu2ZnSn(S,Se)4-Based Absorber Layers via Temperature-Dependent Raman Spectroscopy Technique. Solar RRL 7.

Grandhi, G. K., Hardy, D., Krishnaiah, M., Vargas, B., Al-Anesi, B., Suryawanshi, M. P., Solis-Ibarra, D., Gao, F., Hoye, R. L. Z. & Vivo, P. (2023). Wide-Bandgap Perovskite-Inspired Materials: Defect-Driven Challenges for High-Performance Optoelectronics. Advanced Functional Materials.

Green, M. A. (2023). Silicon solar cells step up. Nature Energy 8, 783-784.

Green, M. A., Dunlop, E. D., Yoshita, M., Kopidakis, N., Bothe, K., Siefer, G. & Hao, X. (2023). Solar cell efficiency tables (version 62). Progress in Photovoltaics: Research and Applications 31, 651-663.

Green, M. A., Dunlop, E. D., Yoshita, M., Kopidakis, N., Bothe, K., Siefer, G. & Hao, X. (2023). Solar cell efficiency tables (Version 63). Progress in Photovoltaics: Research and Applications 32, 3-13.

Gunawan, D., Yuwono, J. A., Kumar, P. V., Kaleem, A., Nielsen, M. P., Tayebjee, M. J. Y., Oppong-Antwi, L., Wen, H., Kuschnerus, I., Chang, S. L. Y., Wang, Y., Hocking, R. K., Chan, T.-S., Toe, C. Y., Scott, J. & Amal, R. (2023). Unraveling the structure-activity-selectivity relationships in furfuryl alcohol photoreforming to H2 and hydrofuroin over ZnxIn2S3+x photocatalysts. Applied Catalysis B: Environmental 335.

Guo, Q., Zhang, T., Li, W., Li, W., Tan, W. L., McMeekin, D., Xu, Z., Fang, X.-Y., McNeill, C. R., Etheridge, J. & Bach, U. (2023). Toward Uniaxially Textured CsPbIBr2 Perovskite Thin Films with Twin Domains by Potassium Incorporation. ACS Energy Letters 8, 699-706.

Gupta, B., Shehata, M. M., Lee, Y., Black, L. E., Ma, F., Hoex, B., Jagadish, C., Tan, H. H. & Karuturi, S. (2023). Unveiling the Role of H2 Plasma for Efficient InP Solar Cells. Solar RRL 7.

Gusken, N. A., Fu, M., Zapf, M., Nielsen, M. P., Dichtl, P., Roder, R., Clark, A. S., Maier, S. A., Ronning, C. & Oulton, R. F. (2023). Emission enhancement of erbium in a reverse nanofocusing waveguide. Nat Commun 14, 2719.

Habibur Rahaman, M., Sang, B., Anower Hossain, M., Hoex, B., Mota-Santiago, P., Mitchell, V. D., Uddin, A. & Stride, J. A. (2023). Impact of the bilayer electron transport layer in the donor acceptor bulk heterojunctions for improved inverted organic photovoltaic performance. Applied Surface Science 612.

Hamadani, B. H. (2023). 2.11 - Accurate characterization of indoor photovoltaic performance. JPhys Mater 6.

Hameiri, Z. (2023). Editorial: Passivating contact solar cells. Progress in Photovoltaics: Research and Applications 31, 309-309.

Han, E. Q., Lyu, M., Choi, E., Zhao, Y., Zhang, Y., Lee, J., Lee, S. M., Jiao, Y., Ahmad, S. H. A., Seidel, J., Yun, J. S., Yun, J. H. & Wang, L. (2024). High-Performance Indoor Perovskite Solar Cells by Self-Suppression of Intrinsic Defects via a Facile Solvent-Engineering Strategy. Small 20, e2305192.

Hao, X. (2023). Phase evolution under pressure. Nature Energy 8, 429-430.

Herrando, M., Wang, K., Huang, G., Otanicar, T., Mousa, O. B., Agathokleous, R. A., Ding, Y., Kalogirou, S., Ekins-Daukes, N., Taylor, R. A. & Markides, C. N. (2023). A review of solar hybrid photovoltaic-thermal (PV-T) collectors and systems. Progress in Energy and Combustion Science 97.

Holzhey, P., Prettl, M., Collavini, S., Chang, N. L. & Saliba, M. (2023). Toward commercialization with lightweight, flexible perovskite solar cells for residential photovoltaics. Joule 7, 257-271.

Howlader, A. H. & Uddin, A. (2023). Progress and Challenges of Chloride–Iodide Perovskite Solar Cells: A Critical Review. Nanomanufacturing 3, 177-216.

Hsiao, P.-C., Wang, Z., Li, Y., Song, N., Lv, J., Zhu, C. & Lennon, A. (2023). Strategies for minimizing induced thermomechanical stress in glass–glass PV modules with half cells identified using finite element modelling. Solar Energy 255, 60-70.

Hu, B., Wang, Y., Shen, Z., Wang, X., Zhang, M., Chen, Y., Bu, L., Ma, W. & Lu, G. (2023). Polycyclic Aromatic Lactam-Like Donors Synthesized upon C—H Activation Strategy for High-Efficiency Ternary Organic Solar Cells. Solar RRL 7.

Hu, J., Wang, Y., Jia, H., Hu, W., Hassan, M., Kusy, B., Uddin, A. & Youssef, M. (2023). Iris. Proceedings of the ACM on Interactive, Mobile, Wearable and Ubiquitous Technologies 7, 1-27.

Hu, T., Hou, H., Peng, J., Wu, Q., He, J., Yu, H., Liu, R., Hou, T., Zhou, X., Zhang, M., Zhang, X., Yang, X., Sun, Y., Li, X. & Bai, Y. (2023). 4-tert-butylpyridine induced Ni3+/Ni2+ ratio modulation in NiO hole transport layer towards efficient and stable inverted perovskite solar cells. Materials Today Energy 32.

Hughes, K. M., Ito, M., Vaquero-Stainer, A., Ekins Daukes, N. J. & Phillips, C. C. (2023). Room Temperature Operation of a Quantum Ratchet Intermediate Band Solar Cell. Solar RRL 7.

Ishwara, T., Feng, J., de Clercq, D. M., Geng, R., Alves, J., McCamey, D. R., Nielsen, M. P. & Schmidt, T. W. (2023). Nanoporous Solid-State Sensitization of Triplet Fusion Upconversion. ACS Energy Letters 8, 4078-4084.

Jafari, S., Figg, M. & Hameiri, Z. (2023). Investigation of light-induced degradation in gallium- and indium-doped Czochralski silicon. Solar Energy Materials and Solar Cells 251.

Jang, J. S., Karade, V. C., Suryawanshi, M. P., Lee, D. M., Kim, J., Jang, S., Baek, M. C., He, M., Kim, J. H. & Shin, S. W. (2023). Improving Long-Term Stability of Kesterite Thin-Film Solar Cells with Oxide/Metal/Oxide Multilayered Transparent Conducting Electrodes. Solar RRL 7.

Jang, S., Karade, V. C., Jang, J. S., Jo, E., Shim, H., Kim, S. G., Patil, K., Gour, K. S. & Kim, J. H. (2023). Achieving over 10% device efficiency in Cu2ZnSn(S,Se)4 thin-film solar cells with modifications of window layer properties. Journal of Alloys and Compounds 930.

Javier, G. M. N., Dwivedi, P., Buratti, Y., Perez-Wurfl, I., Trupke, T. & Hameiri, Z. (2023). Improvements and gaps in the empirical expressions for the fill factor of modern industrial solar cells. Solar Energy Materials and Solar Cells 253.

Jing, Y., Liu, X., Xu, Y., Zhang, M., Li, R., Wang, S., Yan, Z., Sun, W., Wu, J. & Lan, Z. (2023). Amorphous antimony sulfide nanoparticles construct multi-contact electron transport layers for efficient carbon-based all-inorganic CsPbI2Br perovskite solar cells. Chemical Engineering Journal 455.

Juhl, M. K., Heinz, F. D., Coletti, G., Rougieux, F. E., Sun, C., Contreras, M. V., Niewelt, T., Krich, J. & Schubert, M. C. (2023). On the Conversion Between Recombination Rates and Electronic Defect Parameters in Semiconductors. IEEE Journal of Photovoltaics 13, 524-534.

Jung, H. Y., Oh, E. S., Kim, D. J., Shim, H., Lee, W., Yoon, S. G., Lim, J., Yun, J. S., Kim, T. S. & Yang, T. Y. (2023). Adjusted Bulk and Interfacial Properties in Highly Stable Semitransparent Perovskite Solar Cells Fabricated by Thermocompression Bonding between Perovskite Layers. ACS Appl Mater Interfaces 15, 31344-31353.

Kaleem, A., Tayebjee, M., Nielsen, M. P., Schmidt, T., Musser, A. J. & Baran, D. (2023). Concentration, polarization and power dependence study of TIPS-pentacene concentrated solutions using femtosecond stimulated Raman spectroscopy. Physical Chemistry of Semiconductor Materials and Interfaces XXII.

Kamble, G. U., Shin, S. W., Park, S. W., Gaikwad, M. A., Karade, V. C., Jang, J. S., Park, Y., Ghorpade, U. V., Suryawanshi, M. P. & Kim, J. H. (2023). Germanium Selenide: A Critical Review on Recent Advances in Material Development for Photovoltaic and Photoelectrochemical Water-Splitting Applications. Solar RRL 7.

Karade, V. C., Sutar, S. S., Shin, S. W., Suryawanshi, M. P., Jang, J. S., Gour, K. S., Kamat, R. K., Yun, J. H., Dongale, T. D. & Kim, J. H. (2023). Machine Learning Assisted Analysis, Prediction, and Fabrication of High-Efficiency CZTSSe Thin Film Solar Cells. Advanced Functional Materials 33.

Karade, V., Sutar, S., Jang, J., Gour, K., Shin, S., Suryawanshi, M., Kamat, R., Dongale, T., Kim, J. & Yun, J. (2023). Unraveling the Effect of Compositional Ratios on the Kesterite Thin-Film Solar Cells Using Machine Learning Techniques. Crystals 13.

Khan, M. U., Sen, C., Chan, C., Abbott, M., Poduval, G., Wu, Y., Lv, R., Zhang, G. & Hoex, B. (2023). Supercharging cell-level potential-induced degradation (PID) testing using a salt-enriched hybrid polymer layer. Solar Energy Materials and Solar Cells 260.

Kim, D., Yun, JS., Sagotra, A., Mattoni, A., Sharma P., Kim, J., Lim, S., O'Reilly, P., Brinkman, L., Green, M. A., Huang, S., Ho-Baillie, A., Cazorla,C., & Seidel J. (2023). Charge carrier transport properties of twin domains in halide perovskites. Journal of Materials Chemistry A, 11, 16743-16754

Kim, H., Lee, D. Y., Lim, J., Kim, J., Park, J., Seidel, J., Yun, J. S. & Seok, S. I. (2023). Enhancing Stability and Efficiency of Perovskite Solar Cells with a Bilayer Hole Transporting Layer of Nickel Phthalocyanine and Poly(3-Hexylthiophene). Advanced Energy Materials 13.

Kim, M., Drury, S., Altermatt, P., Wang, L., Zhang, Y., Chan, C., Dias, P. & Hallam, B. (2023). Identifying methods to reduce emission intensity of centralised Photovoltaic deployment for net zero by 2050: Life cycle assessment case study of a 30 MW PV plant. Progress in Photovoltaics: Research and Applications 31, 1493-1502. doi:10.1002/pip.3747

Le, A. H. T., Bonilla, R. S., Black, L. E., Seif, J. P., Allen, T. G., Dumbrell, R., Samundsett, C. & Hameiri, Z. (2023). Recombination in Passivating Contacts: Investigation Into the Impact of the Contact Work Function on the Obtained Passivation. Solar RRL 7.

Le, A. H. T., Srinivasa, A., Bowden, S. G., Hameiri, Z. & Augusto, A. (2022). Temperature and illumination dependence of silicon heterojunction solar cells with a wide range of wafer resistivities. Progress in Photovoltaics: Research and Applications 31, 536-545.

Le, T., Cai, Y., Yang, Z., Chen, R., Macdonald, D. & Liu, A. (2024). Industrial Czochralski n-type Silicon Wafers: Gettering Effectiveness and Possible Bulk Limiting Defects. Solar Rrl 8, 2300928.

Le, T. T., Phang, S. P., Yang, Z., Macdonald, D. & Liu, A. (2023). Impact of Depth-Wise Inhomogeneous Iron Distributions on the Accuracy of Lifetime-Based Interstitial Iron Measurements on Silicon Wafers. IEEE Journal of Photovoltaics 13, 495-502.

Li, C., Pusch, A., Liu, Z., Zhang, P., Huang, J., Guo, H., Zhang, W., Wang, H., Gao, P., Sun, Q., Ekins-Daukes, N. & Hao, X. (2023). A modeling framework to quantify the intermediate layer impact in III–V//Si multijunction solar cells. Japanese Journal of Applied Physics 62.

Li, H., Chu, R., Bati, A. S. R., Gupta, S., Burn, P. L., Gentle, I. R. & Shaw, P. E. (2023). Efficient Inverted Perovskite Solar Cells Using Dual Fluorinated Additive Modification. Advanced Materials Interfaces. Wiley.

Li, J., Sun, K., Yuan, X., Huang, J., Green, M. A. & Hao, X. (2023). Emergence of flexible kesterite solar cells: progress and perspectives. npj Flexible Electronics 7.

Li, P., Wu, Z., Zhang, C., Xu, Y., Dong, Z. & Hu, M. (2023). Multi-timescale Affinely Adjustable Robust Reactive Power Dispatch of Distribution Networks Integrated with High Penetration of PV. Journal of Modern Power Systems and Clean Energy 11, 324-334.

Li, X., Liu, H., Li, C., Chen, G., Zhang, C. & Dong, Z. Y. (2023). Deep Reinforcement Learning-Based Explainable Pricing Policy for Virtual Storage Rental Service. IEEE Transactions on Smart Grid 14, 4373-4384.

Li, Y., Li, R., Jia, Z., Yu, B., Yang, Y., Bai, S., Pollard, M., Liu, Y., Ma, Y., Kampwerth, H. & Lin, Q. (2023). Precursor Engineering of Solution-Processed Sb(2) S(3) Solar Cells. Small, e2308895.

Li, Z., Jia, C., Wan, Z., Xue, J., Cao, J., Zhang, M., Li, C., Shen, J., Zhang, C. & Li, Z. (2023). Hyperbranched polymer functionalized flexible perovskite solar cells with mechanical robustness and reduced lead leakage. Nat Commun 14, 6451.

Li, Z., Wan, Z., Jia, C., Zhang, M., Zhang, M., Xue, J., Shen, J., Li, C., Zhang, C. & Li, Z. (2023). Cross-linked polyelectrolyte reinforced SnO2 electron transport layer for robust flexible perovskite solar cells. Journal of Energy Chemistry 85, 335-342.

Liang, J., Rawal, A., Yu, M., Xiao, K., Liu, H., Jiang, Y., Lennon, A. & Wang, D.-W. (2023). Low-potential solid-solid interfacial charging on layered polyaniline anode for high voltage pseudocapacitive intercalation Li-ion supercapacitors. Nano Energy 105.

Liao, C. H., Mahmud, M. A. & Ho-Baillie, A. W. Y. (2023). Recent progress in layered metal halide perovskites for solar cells, photodetectors, and field-effect transistors. Nanoscale 15, 4219-4235.

Liao, CH., Mahmud, MA., Ho-Baillie AWY. (2023). Recent progress in layered metal halide perovskites for solar cells, photodetectors, and field-effect transistors. Nanoscale 15, 4219 – 4235

Liao, Q., Li, S., Xi, F., Tong, Z., Chen, X., Wan, X., Ma, W. & Deng, R. (2023). High-performance silicon carbon anodes based on value-added recycling strategy of end-of-life photovoltaic modules. Energy 281.

Liu, G., Dwivedi, P., Trupke, T. & Hameiri, Z. (2023). Deep Learning Model to Denoise Luminescence Images of Silicon Solar Cells. Adv Sci (Weinh) 10, e2300206.

Liu, K., Rafique, S., Musolino, S. F., Cai, Z., Liu, F., Li, X., Yuan, Y., Bao, Q., Yang, Y., Chu, J., Peng, X., Nie, C., Yuan, W., Zhang, S., Wang, J., Pan, Y., Zhang, H., Cai, X., Shi, Z., Li, C., Wang, H., Deng, L., Hu, T., Wang, Y., Wang, Y., Chen, S., Shi, L., Ayala, P., Wulff, J. E., Yu, A. & Zhan, Y. (2023). Covalent bonding strategy to enable non-volatile organic cation perovskite for highly stable and efficient solar cells. Joule 7, 1033-1050.

Liu, X., Luo, D., Lu, Z. H., Yun, J. S., Saliba, M., Seok, S. I. & Zhang, W. (2023). Stabilization of photoactive phases for perovskite photovoltaics. Nat Rev Chem 7, 462-479.

Liu, Z., Chen, D., Han, H., Xiang, J., Liu, Z., Xu, G., Zhang, X., Verlinden, P. J., Shen, H., Chen, Y. & Liang, Z. (2023). Simulation, Experimental Evaluation, and Characterization of a Novel Grid Line Design for TOPCon Solar Cells With Reduced Silver Consumption. IEEE Journal of Photovoltaics 13, 213-223.

Lu, H., Uddin, N., Sun, Z., Chen, Z., Mahfoud, Z., Wu, Y., Wibowo, A. A., Su, Z., Yin, X., Tang, C. S., Liao, X., Ringer, S. P., Zhao, X. S., Nguyen, H. T., Wee, A. T. S., Bosman, M. & Yin, Z. (2023). Stabilized bismuth nanoplasmonics for selective CO2 reduction to methanol at a heterointerface. Nano Energy 115, 108684.

Lu, X., Qiu, J., Zhang, C., Lei, G. & Zhu, J. (2023). Assembly and Competition for Virtual Power Plants With Multiple ESPs Through a "Recruitment–Participation" Approach. IEEE Transactions on Power Systems, 1-14.

Ma, L., Chen, X., Tang, C., Li, S., Xi, F., Lan, H., Ma, W. & Chang, Y. (2023). Effect of Silicon Wafer Surface Stains on Copper-Assisted Chemical Etching. Metals 13.

MacDonald, T. S. C., Tayebjee, M. J. Y., Collins, M. I., Kumarasamy, E., Sanders, S. N., Sfeir, M. Y., Campos, L. M. & McCamey, D. R. (2023). Anisotropic Multiexciton Quintet and Triplet Dynamics in Singlet Fission via Pulsed Electron Spin Resonance. J Am Chem Soc 145, 15275-15283.

Madumelu, C., Cai, Y., Hollemann, C., Peibst, R., Hoex, B., Hallam, B. J. & Soeriyadi, A. H. (2023). Assessing the stability of p+ and n+ polysilicon passivating contacts with various capping layers on p-type wafers. Solar Energy Materials and Solar Cells 253.

Majewski, P., Deng, R., Dias, P. R. & Jones, M. (2023). Product stewardship considerations for solar photovoltaic panels. AIMS Energy 11, 140-155.

Malavekar, D. B., Gaikwad, M. A., Patil, K. D., Jang, S., Park, S. W. & Kim, J. H. (2023). Nanoarchitectonics of self-grown copper selenide on copper for solid-state asymmetric supercapacitor. Journal of Energy Storage 68.

Mallo, N., McAnally, S., Chu, R., Babazadeh, M., Jin, H., Burn, P. L., Gentle, I. R. & Shaw, P. E. (2023). The effect of fluorination on the low and high frequency dielectric constants of non-polymeric organic semiconductors – towards homojunction solar cells. Journal of Materials Chemistry C. Royal Society of Chemistry (RSC), 14382–14394.

McMeekin, D. P., Holzhey, P., Fürer, S. O., Harvey, S. P., Schelhas, L. T., Ball, J. M., Mahesh, S., Seo, S., Hawkins, N., Lu, J., Johnston, M. B., Berry, J. J., Bach, U. & Snaith, H. J. (2023). Intermediate-phase engineering via dimethylammonium cation additive for stable perovskite solar cells. Nature Materials 22, 73-83.

Meftahi, N., Surmiak, M. A., Fürer, S. O., Rietwyk, K. J., Lu, J. F., Raga, S. R., Evans, C., Michalska, M., Deng, H., McMeekin, D. P., Alan, T., Vak, D., Chesman, A. S. R., Christofferson, A. J., Winkler, D. A., Bach, U. & Russo, S. P. (2023). Machine Learning Enhanced High-Throughput Fabrication and Optimization of Quasi-2D Ruddlesden–Popper Perovskite Solar Cell, Adv. Energy Maters, 13, 2203859

Meftahi, N., Surmiak, M. A., Fürer, S. O., Rietwyk, K. J., Lu, J., Raga, S. R., Evans, C., Michalska, M., Deng, H., McMeekin, D. P., Alan, T., Vak, D., Chesman, A. S. R., Christofferson, A. J., Winkler, D. A., Bach, U. & Russo, S. P. (2023). Machine Learning Enhanced High-Throughput Fabrication and Optimization of Quasi-2D Ruddlesden–Popper Perovskite Solar Cells. Advanced Energy Materials 13, 2203859.

Michel, J. I., Le, A. H. T., Yan, D., Berghuis, W. J., Korte, L., Liu, A., Phang, S. P., Chen, W., Macdonald, D., Macco, B., Hameiri, Z. & Bullock, J. (2023). Electron contact interlayers for low-temperature-processed crystalline silicon solar cells. Progress in Photovoltaics: Research and Applications.

Michel, J. I., Le, A. H. T., Yan, D., Berghuis, W.-J., Korte, L., Liu, A., Phang, S. P., Chen, W., Macdonald, D., Macco, B., Hameiri, Z. & Bullock, J. Electron contact interlayers for low-temperature-processed crystalline silicon solar cells. Progress in Photovoltaics: Research and Applications n/a.

Michel, J. I., Yan, D., Phang, S. P., Zheng, T., Johnson, B. C., Yang, J., Zhang, X., Chen, W., Wan, Y., Truong, T., Stuckelberger, J., Pan, Y., Macdonald, D. & Bullock, J. (2023). Poly-Si passivating contacts prepared via phosphorus spin-on-doping: A comparison between different silicon deposition methods. Solar Energy Materials and Solar Cells 255, 112290.

Motamedi, M., Jia, G., Yao, Y., Shanks, K., Yousefi, P., Hewakuruppu, Y. L., Rafeie, M., Lindner, F., Patterson, R., Christiansen, S., Plentz, J., Koshy, P. & Taylor, R. A. (2023). Nanopatterned indium tin oxide as a selective coating for solar thermal applications. Renewable Energy 210, 386-396.

Munro, P. G., Samarakoon, S., Kearnes, M. & Paisley, C. (2023). The right to repairable energy: A political ecology of off-grid solar repair in Zambia. Political Geography 106.

Mussakhanuly, N., Soufiani, A. M., Bernardi, S., Gan, J., Bhattacharyya, S. K., Chin, R. L., Muhammad, H., Dubajic, M., Gentle, A., Chen, W., Zhang, M., Nielsen, M. P., Huang, S., Asbury, J., Widmer-Cooper, A., Yun, J. S. & Hao, X. (2023). Thermal Disorder-Induced Strain and Carrier Localization Activate Reverse Halide Segregation. Adv Mater, e2311458.

Nath, S. K., Sun, X., Nandi, S. K., Chen, X., Wang, Z., Das, S. K., Lei, W., Faraone, L., Rickard, W. D. A. & Elliman, R. G. (2023). Harnessing Metal/Oxide Interlayer to Engineer the Memristive Response and Oscillation Dynamics of Two-Terminal Memristors. Advanced Functional Materials 33, 2306428.

Nguyen, D.-T., Walter, D., Weber, K. J., Duong, T. & White, T. P. (2023a). Simulating Proton Radiation Tolerance of Perovskite Solar Cells for Space Applications. Advanced Energy and Sustainability Research 4, 2300085.

Nguyen, K., Bui, A. D., Mayon, A. O., Nguyen, T., White, T., Truong, T., Ho-Baillie, A., Duong, T., Shen, H., Weber, K., Catchpole, K., Macdonald, D. & Nguyen, H. T. (2023). Correlative imaging of optoelectronic properties for perovskite solar cells via hyperspectral luminescence imaging. Cell Reports Physical Science 4, 101585.

Nielsen, M. P., Sazzad, M. H., Pusch, A., Pearce, P. M., Reece, P. J., Ekins-Daukes, N. J., Munday, J. N. & Bermel, P. (2023). A direct comparison between thermoradiative and thermophotovoltaic operation of HgCdTe photodiodes. New Concepts in Solar and Thermal Radiation Conversion V.

Othman, M., Zhang, T., McMeekin, D. P., Fürer, S. O., Mao, W., Li, W., Scully, A. D., Chesman, A. S. R., Nakashima, P. N. H., Bach, U. & Etheridge, J. (2023). Structural and Photophysical Properties of Guanidinium–Iodide-Treated Perovskite Solar Cells. Solar RRL 7, 2200852.

Packman, L., Mallo, N., Raynor, A., Gao, M., Babazadeh, M., Jin, H., Huang, D. M., Burn, P. L., Gentle, I. R. & Shaw, P. E. (2023). The impact of film deposition and annealing on the nanostructure and dielectric constant of organic semiconductor thin films. Physical Chemistry Chemical Physics 25, 23867-23878.

Perera, W. H. K., Masteghin, M. G., Shim, H., Davies, J. D., Ryan, J. L., Hinder, S. J., Yun, J. S., Zhang, W., Jayawardena, K. D. G. I. & Silva, S. R. P. (2023). Modification of Hydrophobic Self-Assembled Monolayers with Nanoparticles for Improved Wettability and Enhanced Carrier Lifetimes Over Large Areas in Perovskite Solar Cells. Solar RRL 7.

Poddar, S., Evans, J. P., Kay, M., Prasad, A. & Bremner, S. (2023). Assessing Australia's future solar power ramps with climate projections. Sci Rep 13, 11503.

Poddar, S., Kay, M., Prasad, A., Evans, J. P. & Bremner, S. (2023). Changes in solar resource intermittency and reliability under Australia's future warmer climate. Solar Energy 266.

Posar, J. A., Liao, C., Tegg, L., Ho-Baillie, A., Petasecca, M. & Griffith, M. J. (2023). Solution Processable Metal-Halide Perovskites for Printable and Flexible Ionizing Radiation Detectors. Metal-Halide Perovskite Semiconductors, 141-167.

Privat, K., Chang, S., Fernandez, T., Li, J., Huang, J. & Hao, X. (2023). Application of Spectral Cathodoluminescence to Multi-Modal Research at the Nano-Scale: Case Studies from the UNSW Electron Microscope Unit. Microsc Microanal 29, 1946-1948.

Pusch, A., Römer, U., Culcer, D. & Ekins-Daukes, N. J. (2023). Energy Conversion Efficiency of the Bulk Photovoltaic Effect. PRX Energy 2.

Puthen Veettil, B., Zhang, Y., Payne, D., Juhl, M., Huang, S., Hallam, B. & Bagnall, D. (2023). Microwave annealing of silicon solar cells. Applied Physics Letters 122.

Qian, C., Sun, K., Cong, J., Cai, H., Huang, J., Li, C., Cao, R., Liu, Z., Green, M., Hoex, B., Chen, T. & Hao, X. (2023). Bifacial and Semitransparent Sb(2) (S,Se)(3) Solar Cells for Single-Junction and Tandem Photovoltaic Applications. Adv Mater 35, e2303936.

Qian, C., Wang, R., Shen, H., Xia, J., Cui, D., Sun, K., Liu, H., Guo, C., Yu, F., Li, J. & Bao, W. (2023). Computational-Guided Design of Photoelectrode Active Materials for Light-Assisted Energy Storage. Small 19, e2304045.

Rietwyk, K. J., Lin, X., Tan, B., Warnakula, T., Holzhey, P., Zhao, B., Deng, S., Surmiak, M. A., Jasieniak, J. & Bach, U. (2023). Ideality Factor Mapping of Back-Contact Perovskite Solar Cells. Advanced Energy Materials 13, 2200796.

Sen, C., Wang, H., Wu, X., Khan, M. U., Chan, C., Abbott, M. & Hoex, B. (2023). Four failure modes in silicon heterojunction glass-backsheet modules. Solar Energy Materials and Solar Cells 257.

Sen, C., Wu, X., Wang, H., Khan, M. U., Mao, L., Jiang, F., Xu, T., Zhang, G., Chan, C. & Hoex, B. (2023). Accelerated damp-heat testing at the cell-level of bifacial silicon HJT, PERC and TOPCon solar cells using sodium chloride. Solar Energy Materials and Solar Cells 262.

Sharma, A. S., Hanif, M., Bremner, S. P., Nielsen, M. P., Tayebjee, M. J. Y., Rougieux, F. E., Ekins-Daukes, N. J. & Pusch, A. (2023). Heat Flow through Nonideal Contacts in Hot-Carrier Solar Cells. Physical Review Applied 20.

Sharma, A., Longden, T., Catchpole, K. & Beck, F. J. (2023). Comparative techno-economic analysis of different PV-assisted direct solar hydrogen generation systems. Energy & Environmental Science 16, 4486-4501.

Shehata, M. M., Bartholazzi, G., Macdonald, D. H. & Black, L. E. (2023a). Engineering Silicon Interfaces with Transparent AlyTiOx/ZnO/TiO2 Stack Exhibiting Exceptional Passivating Contact Performance. Advanced Energy Materials 13, 2300251.

Shehata, M. M., Macdonald, D. H. & Black, L. E. (2023b). Dramatic Reduction of Silicon Surface Recombination by ALD TiOx Capping Layer from TiCl4 and H2O: The Role of Chlorine. ACS Applied Materials & Interfaces 15, 46504-46512.

Shehata, M. M., Truong, T. N., Basnet, R., Nguyen, H. T., Macdonald, D. H. & Black, L. E. (2023c). Impedance spectroscopy characterization of c-Si solar cells with SiOx/ Poly-Si rear passivating contacts. Solar Energy Materials and Solar Cells 251, 112167.

Shutt, R. R. C., Ramireddy, T., Stylianidis, E., Di Mino, C., Ingle, R. A., Ing, G., Wibowo, A. A., Nguyen, H. T., Howard, C. A., Glushenkov, A. M., Stewart, A. & Clancy, A. J. (2023). Synthesis of Black Phosphorene Quantum Dots from Red Phosphorus. Chemistry – A European Journal 29, e202301232.

Singh, M., Datta, K., Amarnath, A., Wagner, F., Zhao, Y., Yang, G., Bracesco, A., Phung, N., Zhang, D., Zardetto, V., Najafi, M., Veenstra, S. C., Coletti, G., Mazzarella, L., Creatore, M., Wienk, M. M., Janssen, R. A. J., Weeber, A. W., Zeman, M. & Isabella, O. (2023). Crystalline silicon solar cells with thin poly-SiOx carrier-selective passivating contacts for perovskite/c-Si tandem applications. Progress in Photovoltaics: Research and Applications 31, 877-887.

Sio, H. C., Stuckelberger, J., Basnet, R. & Macdonald, D. (2023). Improving doped polycrystalline silicon passivating contacts with magnesium fluoride. Solar Energy Materials and Solar Cells 254, 112251.

Song, W., Wang, X., Hou, T., Li, X., Chen, H., Yu, Y., Sun, X., Singh, A. & Zhang, M. (2023). Formate Additive for Efficient and Stable Methylammonium-Free Perovskite Solar Cells by Gas-Quenching. Chemistry 29, e202300576.

Soufiani, A. M., Lee-Chin, R., Fassl, P., Mahmud, M. A., Pollard, M. E., Zheng, J., Weber, J. W., Ho-Baillie, A., Trupke, T. & Hameiri, Z. (2022). Implied Open-circuit Voltage Imaging via a Single Bandpass Filter Method—Its First Application in Perovskite Solar Cells. Advanced Functional Materials 33.

Stuckelberger, J., Yan, D., Phang, S. P., Samundsett, C., Wang, J., Antognini, L., Haug, F.-J., Wang, Z., Yang, J., Zheng, P., Zhang, X. & Macdonald, D. (2023). Pre-annealing for improved LPCVD deposited boron-doped poly-Si hole-selective contacts. Solar Energy Materials and Solar Cells 251, 112123.

Sun, Q., Zhao, Y., Tan, X., Jia, C., Su, Z., Meyer, Q., Ahmed, M. I. & Zhao, C. (2023). Atomically Dispersed Cu–Au Alloy for Efficient Electrocatalytic Reduction of Carbon Monoxide to Acetate. ACS Catalysis 13, 5689-5696.

Sun, X., Yang, X., Wang, X., Hou, T., Chen, H., Liu, J., Fu, Z., Yu, W., Zhang, W., Ma, Z., Huang, Y., Liu, X. & Zhang, M. (2023). The effect of pyrrolidone-based ligands in gas-quenching fabrication of FA0.9Cs0.1PbI3 perovskite films and solar cells. Journal of Alloys and Compounds 960.

Sun, Z., Wang, L., Luo, H., Hamer, P., Ye, H. & Hallam, B. (2023). Study of the Hydrogen Passivation Effect of Low-Temperature-Deposited Amorphous Silicon Layers on SiGe Solar Cells Grown on a Silicon Substrate. ACS Applied Energy Materials 6, 12064-12071.

Suryawanshi, M. P., Ghorpade, U. V., Toe, C. Y., Suryawanshi, U. P., He, M., Zhang, D., Jang, J. S., Shin, S. W., Kim, J. H., Hao, X. & Amal, R. (2023). Earth-abundant photoelectrodes for water splitting and alternate oxidation reactions: Recent advances and future perspectives. Progress in Materials Science 134.

Ta, X. M. C., Nguyen, T. K. A., Bui, A. D., Nguyen, H. T., Daiyan, R., Amal, R., Tran-Phu, T. & Tricoli, A. (2023). Optimizing Surface Composition and Structure of FeWO4 Photoanodes for Enhanced Water Photooxidation. Advanced Materials Technologies 8, 2201760.

Tang, S., Peracchi, S., Pastuovic, Z., Liao, C., Xu, A., Bing, J., Zheng, J., Mahmud, M. A., Wang, G., Townsend-Medlock, E. D., Wilson, G. J., Lakhwani, G., Brenner, C., McKenzie, D. R. & Ho-Baillie, A. W. Y. (2023). Effect of Hole Transport Materials and Their Dopants on the Stability and Recoverability of Perovskite Solar Cells on Very Thin Substrates after 7 MeV Proton Irradiation. Advanced Energy Materials 13.

Tang, W., Liu, T., Zhang, M., Yuan, F., Zhou, K., Lai, R., Lian, Y., Xing, S., Xiong, W., Zhang, M., Gao, F., Zhao, B. & Di, D. (2023). The roles of metal oxidation states in perovskite semiconductors. Matter 6, 3782-3802.

Tarique, W. B. & Uddin, A. (2023). A review of progress and challenges in the research developments on organic solar cells. Materials Science in Semiconductor Processing 163.

Truong, T., Kang, D., Wang, E.-C., Wang, J., Phang, S. P., Macdonald, D. & Stuckelberger, J. (2023). Ex-situ phosphorus-doped polycrystalline silicon passivating contacts for high-efficiency solar cells by physical vapour deposition. Solar Energy 255, 285-291.

Uddin, N., Sun, Z., Langley, J., Lu, H., Cao, P., Wibowo, A., Yin, X., Tang, C. S., Nguyen, H. T. & Evans, J. D. (2023). Ultrabroadband plasmon driving selective photoreforming of methanol under ambient conditions. Proceedings of the National Academy of Sciences 120, e2212075120.

Vaqueiro-Contreras, M., Hallam, B. & Chan, C. (2023). Review of Laser Doping and its Applications in Silicon Solar Cells. IEEE Journal of Photovoltaics 13, 373-384.

Vicari Stefani, B., Kim, M., Zhang, Y., Hallam, B., Green, M. A., Bonilla, R. S., Fell, C., Wilson, G. J. & Wright, M. (2023). Historical market projections and the future of silicon solar cells. Joule 7, 2684-2699.

Wang, A., Huang, J., Cong, J., Yuan, X., He, M., Li, J., Yan, C., Cui, X., Song, N., Zhou, S., Green, M. A., Sun, K. & Hao, X. (2024). Cd-Free Pure Sulfide Kesterite Cu(2) ZnSnS(4) Solar Cell with Over 800 mV Open-Circuit Voltage Enabled by Phase Evolution Intervention. Adv Mater 36, e2307733.

Wang, G., Zheng, J., Duan, W., Yang, J., Mahmud, M. A., Lian, Q., Tang, S., Liao, C., Bing, J., Yi, J., Leung, T. L., Cui, X., Chen, H., Jiang, F., Huang, Y., Lambertz,A., Jankovec,M., Topič,M., Bremner,S., Zhang,Y.-Z., Cheng,C., Ding,K. & Ho-Baillie, A. (2023). Molecular engineering of hole-selective layer for high band gap perovskites for highly efficient and stable perovskite-silicon tandem solar cells. Joule 7(11) 2583-2594 .

Wang, L., Jiang, Y., Li, S.-Y., Chen, X.-H., Xi, F.-S., Wan, X.-H., Ma, W.-H. & Deng, R. (2023). Scalable synthesis of N-doped Si/G@voids@C with porous structures for high-performance anode of lithium-ion batteries. Rare Metals 42, 4091-4102.

Wang, Q., Hu, Y., Zhang, M. & Tao, Z. (2023). Directional fracturing of granite cylinder via nitromethane-based energetic materials driven by electrical wire explosion. AIP Advances 13.

Wang, R., Qian, C., Zhang, Z., Shen, H., Xia, J., Cui, D., Sun, K., Liu, H., Guo, C., Yu, F., Li, J. & Bao, W. (2023). Advance of Prussian Blue-Derived Nanohybrids in Energy Storage: Current Status and Perspective. Small 19, e2206848.

Wang, X., Zhang, M., Hou, T., Sun, X. & Hao, X. (2023). Extrinsic Interstitial Ions in Metal Halide Perovskites: A Review. Small 19, e2303060.

Wang, Y., Hu, J., Jia, H., Hu, W., Hassan, M., Uddin, A., Kusy, B. & Youssef, M. (2023). Spectral-Loc. Proceedings of the ACM on Interactive, Mobile, Wearable and Ubiquitous Technologies 7, 1-26.

Wang, Z., Hsiao, P.-C., Song, N., Shen, X., Xu, C., Yi, H. & Lennon, A. (2023). Use finite element modelling to characterise the stress evolution in Multi Busbar interconnected half-cell tiled modules after soldering and lamination. Solar Energy Materials and Solar Cells 252.

Wei, Y., Tong, H., Li, S., Chen, X., Xi, F., Li, W., Ma, W. & Chang, Y. (2023). Research on silicon wafer surface phase under the Ultra-thin slicing process and its etching hindrance behavior during metal-assisted chemical etching. Surfaces and Interfaces 43.

Wibowo, A. A., Tebyetekerwa, M., Bui, A. D., Truong, T. N., Saji, S., Kremer, F., Yang, Z., Yin, Z., Lu, Y., Macdonald, D. & Nguyen, H. T. (2023). Hybrid Alkali Salt Catalysts-Promoted CVD Growth of 2D MoSe2–WSe2 and WSe2–MoSe2 Lateral Heterostructures. Advanced Materials Technologies 8, 2300143.

Wright, M., Vicari Stefani, B., Jones, T. W., Hallam, B., Soeriyadi, A., Wang, L., Altermatt, P., Snaith, H. J., Wilson, G. J. & Bonilla, R. S. (2023). Design considerations for the bottom cell in perovskite/silicon tandems: a terawatt scalability perspective. Energy & Environmental Science 16, 4164-4190.

Wu, Y., Wang, R., Lin, R., Xu, X., Zhang, X., Alsalman, O., Qiu, Y., Uddin, A. & Ouyang, X. (2023). Excited-state intramolecular proton transfer emitter for efficient violet-blue organic light-emitting diodes with hybridized local/charge transfer channel. Chemical Engineering Journal 465.

Xie, D., Xu, Y. & Zhang, C. (2023). Robust service restoration of distribution systems towards coordinated parallel network reconstruction and cold load pick-up. International Journal of Electrical Power & Energy Systems 152.

Xie, T., Wan, Y., Wang, H., Ostrom, I., Wang, S., He, M., Deng, R., Wu, X., Grazian, C., Kit, C. & Hoex, B. (2023). Opinion Mining by Convolutional Neural Networks for Maximizing Discoverability of Nanomaterials. J Chem Inf Model.

Xu, F., Zhang, M., Li, Z., Yang, X. & Zhu, R. (2023). Challenges and Perspectives toward Future Wide-Bandgap Mixed-Halide Perovskite Photovoltaics. Advanced Energy Materials 13.

Yan, D., Cuevas, A., Stuckelberger, J., Wang, E.-C., Phang, S. P., Kho, T. C., Michel, J. I., Macdonald, D. & Bullock, J. (2023a). Silicon solar cells with passivating contacts: Classification and performance. Progress in Photovoltaics: Research and Applications 31, 310-326.

Yang, J., Zhang, M., Zhang, Q., Qin, C., Qin, R., Jain, S. M. & Liu, H. (2023). Enhanced Performance of CsPbIBr(2) Perovskite Solar Cell by Modified Zinc Oxide Nanorods Array with [6,6]-Phenyl C(61) Butyric Acid. Chemistry 29, e202300566.

Yang, Z., Krügener, J., Feldmann, F., Polzin, J.-I., Steinhauser, B., Aleshin, M., Le, T. T., Macdonald, D. & Liu, A. (2023). Comparing the Gettering Effect of Heavily Doped Polysilicon Films and Its Implications for Tunnel Oxide-Passivated Contact Solar Cells. Solar RRL 7, 2200578.

Yi, C., Zhou, Z., Juhl, M. K., Tong, J., Fong, K. C., Rougieux, F. E. & Bremner, S. (2023). Nature of contaminants introduced in silicon wafers during molecular beam epitaxy chamber annealing. AIP Advances 13.

Yin, H., Sun, Z., Liu, K., Wibowo, A. A., Langley, J., Zhang, C., Saji, S. E., Kremer, F., Golberg, D., Nguyen, H. T., Cox, N. & Yin, Z. (2023). Defect engineering enhances plasmonic-hot electrons exploitation for CO2 reduction over polymeric catalysts. Nanoscale Horizons 8, 1695-1699.

Yu, C., Gao, K., Peng, C.-W., He, C., Wang, S., Shi, W., Allen, V., Zhang, J., Wang, D., Tian, G., Zhang, Y., Jia, W., Song, Y., Hu, Y., Colwell, J., Xing, C., Ma, Q., Wu, H., Guo, L., Dong, G., Jiang, H., Wu, H., Wang, X., Xu, D., Li, K., Peng, J., Liu, W., Chen, D., Lennon, A., Cao, X., De Wolf, S., Zhou, J., Yang, X. & Zhang, X. (2023). Industrial-scale deposition of nanocrystalline silicon oxide for 26.4%-efficient silicon heterojunction solar cells with copper electrodes. Nature Energy 8, 1375-1385.

Yu, Y., Bai, X., Li, S., Shi, J., Wang, L., Xi, F., Ma, W. & Deng, R. (2023). Review of silicon recovery in the photovoltaic industry. Current Opinion in Green and Sustainable Chemistry 44.

Yu, Y., Li, S., Xi, F., Lan, H., Wu, D., Chen, Z., Ma, W. & Deng, R. (2023). Influence of the structural differences between end-of-life Al-BSF and PERC modules on the Al leaching separation behavior. Solar Energy 263.

Zeng, Q., Ma, F., Guo, G., Meng, H., Zhou, L. & Wei, X. (2023). A study of improvement of HJT solar cells by electro-thermal processing. Materials Science in Semiconductor Processing 168.

Zeng, Y., Song, N., Lim, S., Keevers, M., Wu, Y., Yang, Z., Pillai, S., Jiang, J. Y. & Green, M. (2023). Comparative durability study of commercial inner-pore antireflection coatings and alternative dense coatings. Solar Energy Materials and Solar Cells 251.

Zhang, D., Li, H., Lu, H., Yin, Z., Fusco, Z., Riaz, A., Reuter, K., Catchpole, K. & Karuturi, S. (2023). Unlocking the performance of ternary metal (hydro)oxide amorphous catalysts via data-driven active-site engineering. Energy & Environmental Science 16, 5065-5075.

Zhang, M., Gong, S., Hakobyan, K., Gao, Z., Shao, Z., Peng, S., Wu, S., Hao, X., Jiang, Z., Wong, E. H., Liang, K., Wang, C. H., Cheng, W. & Xu, J. (2023). Biomimetic Electronic Skin through Hierarchical Polymer Structural Design. Adv Sci (Weinh), e2309006.

Zhang, P., Li, C., He, M., Liu, Z. & Hao, X. (2023). The Intermediate Connection of Subcells in Si-based Tandem Solar Cells. Small Methods, e2300432.

Zhang, Y., Liu, X., Sun, X., Huang, Y., Yu, J., Hou, T., Shi, L., Green, M. A., Hao, X. & Zhang, M. (2023). Barrier Strategy for Strain-Free Encapsulation of Perovskite Solar Cells. J Phys Chem Lett 14, 10754-10761.

Zhang, Y., Xiang, W., Wang, R., Zhang, J. & Conibeer, G. (2023). Study of the mechanisms of the phonon bottleneck effect in CdSe/CdS core/shell quantum dots and nanoplatelets and their application in hot carrier multi-junction solar cells. Nanoscale Adv 5, 5594-5600.

Zhang, Y., Zhou, S. & Sun, K. (2023). Cu(2)ZnSnS(4) (CZTS) for Photoelectrochemical CO(2) Reduction: Efficiency, Selectivity, and Stability. Nanomaterials (Basel) 13.

Zhao, B., Gillan, L. V., Scully, A. D., Chesman, A. S. R., Tan, B., Lin, X. F., Liu, J. Y., Rietwyk, K. L., Deng, S. Q., Bailey, C., Cheng, Y. B., McCamey, D. R. & Bach, U. (2023), Enhanced Carrier Diffusion Enables Efficient Back-Contact Perovskite Photovoltaics", Angew. Chem. Int. Ed., 62, e2022181

Zhao, B., Gillan, L. V., Scully, A. D., Chesman, A. S. R., Tan, B., Lin, X., Liu, J., Rietwyk, K. J., Deng, S., Bailey, C., Cheng, Y.-B., McCamey, D. R. & Bach, U. (2023a). Enhanced Carrier Diffusion Enables Efficient Back-Contact Perovskite Photovoltaics. Angewandte Chemie International Edition 62, e202218174.

Zhao, J., Chesman, A. S. R., Yan, J., Sutherland, L. J., Jasieniak, J., Lu, J., Mao, W. X. & Bach, U. (2023). Precursor Engineering of Lead Acetate-Based Precursors for High-Open-Circuit Voltage Wide-Bandgap Perovskite Solar Cells, ACS Appl. Mater. Interfaces, 15, 18800−18807

Zhao, J., Chesman, A. S. R., Yan, J., Sutherland, L. J., Jasieniak, J., Lu, J., Mao, W. & Bach, U. (2023b). Precursor Engineering of Lead Acetate-Based Precursors for High-Open-Circuit Voltage Wide-Bandgap Perovskite Solar Cells. ACS Applied Materials & Interfaces 15, 18800-18807.

Zhao, J., Fürer, S. O., McMeekin, D. P., Lin, Q., Lv, P., Ma, J., Tan, W. L., Wang, C., Tan, B., Chesman, A. S. R., Yin, H., Scully, A. D., McNeill, C. R., Mao, W., Lu, J., Cheng, Y.-B. & Bach, U. (2023c). Efficient and stable formamidinium–caesium perovskite solar cells and modules from lead acetate-based precursors. Energy & Environmental Science 16, 138-147.

Zheng, F., Li, X., Gaikwad, M. A., Jang, S. & Kim, J. H. (2023). FeOOH-induced electronic modulation of metal–organic framework-derived CoNi-ZLDH for overall water splitting. Surfaces and Interfaces 42.

Zheng, J., Duan, W., Guo, Y., Zhao, Z. C., Yi, H., Ma, F.-J., Granados Caro, L., Yi, C., Bing, J., Tang, S., Qu, J., Fong, K. C., Cui, X., Zhu, Y., Yang, L., Lambertz, A., Arafat Mahmud, M., Chen, H., Liao, C., Wang, G., Jankovec, M., Xu, C., Uddin, A., Cairney, J. M., Bremner, S., Huang, S., Ding, K., McKenzie, D. R. & Ho-Baillie, A. W. Y. (2023). Efficient monolithic perovskite–Si tandem solar cells enabled by an ultra-thin indium tin oxide interlayer. Energy & Environmental Science 16, 1223-1233.

Zheng, J., Ma, FJ., Liao, C., Bing J., Tang, S., Soufiani, A.M., Chin, R.L., Xue, C., Qu, J., Yang, L., Mahmud, Md A., Sun, Z., Leung, T. L,. Wang, G., Cairney, J. M., Bremner, S., McKenzie, D. R., Huang, S. & Ho-Baillie A. W. Y. (2023). Efficient perovskite solar cell on steel enabled by diffusion barrier and surface passivation. Cell Reports Physical Science 4, 101543

Zheng, P., Phang, S. P., Yang, J., Wang, Z., Chen, J., Wang, E. C., Stuckelberger, J., Sio, H. C., Zhang, X., Macdonald, D. & Jin, H. (2024). Polysilicon Passivating Contacts in Mass Production: The Pursuit of Higher Efficiencies. IEEE Journal of Photovoltaics 14, 80-84.

Zhi, R., Yang, C.-Q., Rothmann, M. U., Du, H.-Q., Jiang, Y., Xu, Y.-Y., Yin, Z.-W., Mo, Y.-P., Dong, W., Liang, G., Bach, U., Cheng, Y.-B. & Li, W. (2023). Direct Observation of Intragrain Defect Elimination in FAPbI3 Perovskite Solar Cells by Two-Dimensional PEA2PbI4. ACS Energy Letters 8, 2620-2629.

Zhou, Z., Bahl, P., Tkachenko, S., Hari, A., de Silva, C., Timchenko, V. & Green, M. A. (2023). Vortex Generators for Passive Cooling of Rooftop Photovoltaic Systems Under Free Convection. IEEE Journal of Photovoltaics 13, 743-749.

Zou, Y., Xu, Y. & Zhang, C. (2023). A Risk-Averse Adaptive Stochastic Optimization Method for Transactive Energy Management of a Multi-Energy Microgrid. IEEE Transactions on Sustainable Energy 14, 1599-1611.

8.5 CONFERENCE PAPERS AND PRESENTATIONS

Abdullah-Vetter, Z., Dwivedi, P., Ekins-Daukes, N.J., Trupke, T., & Hameiri, Z. (2023). Automated analysis of internal quantum efficiency measurements of GaAs solar cells using machine learning. IEEE 50th Photovoltaics Specialists Conference (PVSC), Puerto Rico, 11 June 2023.

Abdullah-Vetter, Z., Kearney, F., Dwivedi, P., Chin, R.L., Wright, B., Trupke, T. & Hameiri, Z. (2023). Predicting damp heat degradation in heterojunction PV modules using machine learning. IEEE 50th Photovoltaics Specialists Conference (PVSC), Puerto Rico, 11 June 2023.

Abdullah-Vetter, Z., Wright ,B., Trupke, T. & Hameiri, Z. (2022). Advanced analysis of internal quantum efficiency measurements of GaAs solar cells using machine learning. 2023 Asia-Pacific Solar Research Conference. Melbourne 5 – 7 December 2023.

Abdullah-Vetter, Z., Wright, B., Lee Chin, R., Trupke, T. & Hameiri, Z. (2023). Using latent ordinary differential equation neural networks to predict the degradation of HJT PV modules at the end of damp heat tests. 2023 Asia-Pacific Solar Research Conference. Melbourne 5 – 7 December 2023.

Andres, J., Ocampo, R., Bown, O., Hill, C., Pegram, C., Schmidt, A., Shave, J. & Wright, B. (2023). The Human-Built Environment-Natural Environment Relation - An Immersive Multisensory Exploration with 'System of a Sound'. 28th International Conference on Intelligent User Interfaces, 8-11.

Asami, M., Kampwerth, H., Pollard, M., Watanabe, K., Nakano, Y. & Masakazu Sugiyama, M. (2023). Investigation of Light Absorption Properties of InGaAs/GaAsP Quantum Wells using Photothermal Deflection Spectroscopy. Compound Semiconductor Week 2023, TuD1-5, Jeju, Republic of Korea, 30th May 2023.

Bach, U. (2023). High-Throughput Energy Materials Discovery, The effects of global warming are calling for a rapid transition from fossil to renewable energy sources. MRS Conference. San Francisco, California, 10 - 14 April, 2023.

Bailey, C.B. (2023). Effect of Organic Spacer Cation on Dark Excitons in 2D Perovskites via Magneto-Optical Spectroscopy. 2023 Asia-Pacific Solar Research Conference. Melbourne 5 – 7 December 2023.

Bartholazzi, G. (2023). Alternative interlayer boosting the performance of MoOx holeselective contacts. 2023 Asia-Pacific Solar Research Conference. Melbourne 5 – 7 December 2023.

Basnet, R., Le, T., Yang, Z., Ismael, M. & Macdonald, D. (2023). Material Quality of Industrial Czochralski-Grown Gallium-Doped p-Type Wafers with Melt Re-Charging. 40th European Photovoltaic Solar Energy Conference, Lisbon, 18-22 September 2023.

Bing, J. (2023). The synergistic effect of thermal and light stresses on perovskite solar cells. 2023 Asia-Pacific Solar Research Conference. Melbourne 5 – 7 December 2023.

Bowen, O. & Deng, R. (2023). Experimental Characterisation of Photovoltaic Panels for Recycling in Australia. 40th European Photovoltaic Solar Energy Conference, Lisbon, 18-22 September 2023.

Bowen, O. (2023). Comparison of Organic Solvents for Chemical Recycling of Photovoltaic Panels. 2023 Asia-Pacific Solar Research Conference. Melbourne 5 – 7 December 2023.

Brooks, E., McAnally, S., Burn, P. L., Gentle, I. R., Shaw, P. E. (2023). The Impact of Solvents of Y6 Homojunction Photophysics. 2023 Australasian Community for Advanced Organic Semiconductors (AUCAOS) Symposium.

Chang, Y., Wang, L., Zhang, Y., Wang, H., Huang, C.-Y., Chan, R., Chan, C. & Hallam, B. (2023). Silver-Lean Metallization for Sustainable PV Manufacturing at the TW Scale. 40th European Photovoltaic Solar Energy Conference, Lisbon, 18-22 September 2023.

Chen, Q., Kaiwen, S., Martin, G., Bram, H., Tao, C., Xiaojing, H. (2023). Single-junction bifacial and semitransparent Sb2(S,Se)3 solar cells. 13th Kesterite+ Workshop, Barcelona, Spain.

Chen, Q., Kaiwen, S., Martin, G., Bram, H., Xiaojing, H. (2023). Single-junction bifacial and semitransparent Sb2(S,Se)3 solar cells. IEEE 50th Photovoltaics Specialists Conference (PVSC), Puerto Rico, 11 June 2023.

Chen, Q., Kaiwen, S., Martin, G., Bram, H., Xiaojing, H. (2023). Single-junction bifacial Sb2(S,Se)3 solar cells. 40th European Photovoltaic Solar Energy Conference, Lisbon, 18-22 September 2023.

Chowdhury, T., Chang, N.L. & Corkish, R. (2023). Is There Enough Low-Iron Sand for TW PV Growth? 34th International Photovoltaic Science and Engineering Conference, Shenzhen, 6-10 November 2023.

Chowdhury, T., Chang, N.L., Dehghanimadvar, M. & Corkish, R. (2023). Reuse of Whole Glass Sheets from End-of-Life Waste in Making New PV Panels. 2023 Asia-Pacific Solar Research Conference. Melbourne 5 – 7 December 2023.

Cong, J., He, M., Jang, J.S., Huang, J., Privat, K., Chen, Y.S., Li, J., Yang, L., Green, M.A., Kim, J., Cairney, J. & Hao, X. (2023). Using advanced micro-to-atomic scale characterizations to explore the role of Ge in CZTSSe solar cells. 34th International Photovoltaic Science and Engineering Conference, Shenzhen, 6-10 November 2023.

Conibeer, G. & Shrestha, S. (2023). Third Generation Approaches for Low Cost, Radiation Tolerant, Efficienct Space Solar Cells. IEEE 50th Photovoltaics Specialists Conference (PVSC), Puerto Rico, 11 June 2023.

Corkish, R. Chowdhury, T., Chang, N. & Dehghanimadvar, M. (2023). Resource Demands for Glass for TW-scale PV. 3rd Global Hydrogen and Renewable Energy Conference and Exhibition, Melbourne, 27-29 November 2023. (invited).

Cui, X., Wang, A., Huang, J. Yuan, X., He, G., Sun, K., Green, M.A., Hoex, B & Hao, X. (2023). CZTS solar cells with bilayer electron selective contact. 34th International Photovoltaic Science and Engineering Conference, Shenzhen, 6-10 November 2023.

Das, N. (2023). End-of-Life Solar Panel Recycling by Using Organic Solvents. 2023 Asia-Pacific Solar Research Conference. Melbourne 5 – 7 December 2023.

Dehghanimadvar, M., Egan, R. and Chang, N. (2023). A Policy Framework for Promoting Local PV Manufacturing in Australia. 2023 Asia-Pacific Solar Research Conference. Melbourne 5 – 7 December 2023.

Ekins-Daukes, N. (2023). The Strain-Balanced Quantum Well Solar Cell – Enabling Record Efficiency Tandem Devices. 34th International Photovoltaic Science and Engineering Conference, Shenzhen, 6-10 November 2023.

Ekins-Daukes, N. Jiang, J.Y. & Perez-Wurfl, I. (2023). Pathways to low-cost III-V photovoltaic solar cells. 34th International Photovoltaic Science and Engineering Conference, Shenzhen, 6-10 November 2023.

Ekins-Daukes, N.J. Fundamentals of photovoltaics. Tutorial AM1. (2023). IEEE 50th Photovoltaics Specialists Conference (PVSC), Puerto Rico, 11 June 2023.

Feng Y., Burn, P. L., Shaw, P. E. (2023). Exploring factors that affect scaling of perovskite solar cells. 2023 Australasian Community for Advanced Organic Semiconductors (AUCAOS) Symposium.

Fischer, O., Schindler, F., Glunz, S.W. & Schubert, M.C., Bui, A.D. & Nguyen, H.T. (2023). Spatially Resolved and SubcellSelective Implied Open-Circuit Voltage Measurements on Perovskite Silicon Tandem Solar Cells. 40th European Photovoltaic Solar Energy Conference, Lisbon, 18-22 September 2023. (Student Awards Finalist Presentation)

Gao, M., McAnally, S., Jin, H., Shaw, P. E., Burn, P. L., Pivrikas, A. (2023). Mobility and Free carrier generation efficiency determined using Photo-MIS-CELIV. 2023 Australasian Community for Advanced Organic Semiconductors (AUCAOS) Symposium.

Gayot, F., Bruhat, E., Manceau, M., De Vito, E., Mariolle, D., Nguyen, N. & Cros, S. (2023). ALD-grown tin oxide as an electron selective layer for perovskite/silicon tandem cells. SiliconPV 2022, the 12th International Conference on Crystalline Silicon Photovoltaics.

Green, M. (2023). History and Future of the PV Industry. 3rd Global Hydrogen and Renewable Energy Conference and Exhibition, Melbourne, 27-29 November 2023.

Green, M. (2023). How close can we get to 29% silicon cell efficiency. 34th International Photovoltaic Science and Engineering Conference, Shenzhen, 6-10 November 2023. (Plenary/Keynote)

Gupta, S., Zhang. G., Etchells. I., Shaw, P., Kumar, S., Burn, P. L. (2023). Unravelling the carrier dynamics of hybrid perovskite films through ultrafast spectroscopy. 2023 Australasian Community for Advanced Organic Semiconductors (AUCAOS) Symposium.

Güsken, N. A., Fu, M., Zapf, M.; Nielsen, M. P., Dichtl, P., Röder, R., Clark, A. S., Maier, S. A., Ronning, C. & Oulton, R. F. Emission enhancement of erbium in a reverse nanofocusing waveguide. META 2023, the 13th International Conference on Metamaterials, Photonic Crystals and Plasmonics, 18 - 21 July 2023, Paris, France

Hamer, P. (2023). Global-Scale Non-Linear Modelling of Photovoltaic Module Degradation. 2023 Asia-Pacific Solar Research Conference. Melbourne 5 – 7 December 2023.

Hamer, P. Improved thermal modelling of the 5B MAVERICK system: impact of sky temperature. 2023 Asia-Pacific Solar Research Conference. Melbourne 5 – 7 December 2023.

Hanif, M., Bremner, S., Nielsen, M. P., Dubajic, M. & Conibeer, G. J. (2023). Ultrafast Dynamics of Photoexcited Carriers and Phonons in Tailored 1D Acoustic Phonon Potentials. IEEE 50th Photovoltaics Specialists Conference (PVSC), Puerto Rico, 11 June 2023.

Hanif, M., Dubajic, M., Bremner, S. P., Nielsen, M. P., Shrestha, S. & Conibeer, G. J. (2023). Controlling Photoexcited Carrier Relaxation Through Phonon Management in GaAs/AlAs Superlattices. IEEE 50th Photovoltaics Specialists Conference (PVSC), Puerto Rico, 11 June 2023.

Hao, X. (2023), A greener future: top cell routes for Si-based tandem cells, 1st Australian Conference on Green and Sustainable Chemistry and Engineering, Cairns (Plenary).

Hao, X. (2023), Design efficient photocathode green kesterite solar cells for Photoelectrochemical solar fuels, Global Energy Meet (virtual) (invited).

Hao, X., (2023). Emerging chalcogenide solar cells – design for next-gen PV Si-based tandem cells. The 1st Middle East and North Africa Solar Conference, Dubai (Keynote).

Hao, X., (2023). Emerging earth-abundant absorber materials for next-generation solar cells, International Conference on Materials Innovation, Brisbane (Keynote).

Hao, X., (2023). Modified spiro HTL for improved stability of perovskite solar cells. PACRIM15/CICC-13: Symposium 15, Perovskites for Solar Cells, LEDs, and other Applications, Shenzhen

Hao, X., (2023). The Path Towards High-Efficiency High Bandgap Kesterite Solar Cells, 13th European Kesterite Workshop, Barcelona (Keynote)

Hao, X., (2023). Thin film solar cells: the future of PV. Renewable energy generation and storage Xiaongjiang international forum, Changsha (plenary).

Hao, X., (2023). Towards High Efficiency High Bandgap Kesterite Solar Cells, The 10th Solar PV Materials and Devices Research Conference, Beijing (Plenary)

Harrison, J. (2023). Computational Optimization of Bragg Reflectors for InGaP/GaAs/Ge triple-junctions. 2023 Asia-Pacific Solar Research Conference. Melbourne 5 – 7 December 2023.

He, M. & Hao, X. (2023). Revealing the role of Ag alloying in metal precursors in kesterite thin films and solar cells. 34th International Photovoltaic Science and Engineering Conference, Shenzhen, 6-10 November 2023.

He, M., Li, J., Hao, X. & Kim, J.H. (2023). Revealing the Role of Ag Alloying in Metal Precursors in Kesterite Thin Films and Solar Cells. 40th European Photovoltaic Solar Energy Conference, Lisbon, 18-22 September 2023.

Ho-Baillie, A. (2023) 12th Asian Photochemistry Conference, 27 Nov – 1 Dec 2023, Melbourne, Australia. (Keynote)

Ho-Baillie, A. (2023) Asia-Pacific International Conference on Perovskite, Organic Photovoltaics and Optoelectronics, 23-24 January 2023. Kobe, Japan. (Invited)

Ho-Baillie, A. (2023) iCANX Volume 155, 4 Aug 2023. (Invited)

Ho-Baillie, A. (2023) International Conference on Materials for Advanced Technologies (ICMAT) 2023 Satellite Workshop on Perovskite Materials Stability, 30 June 2023, Singapore. (Keynote)

Ho-Baillie, A. (2023) N4SNano Global Summit 2023, 27 -29 Nov 2023, Sydney, Australia. (Invited)

Ho-Baillie, A. (2023) Symposium N: Halide Perovskite Materials for Photovoltaics, Lighting and Beyond, 11th International Conference on Materials for Advanced Technologies (ICMAT 2023), 26-30 Jun 2023, Singapore. (Invited)

Ho-Baillie, A. (2023). Perovskite multi-junction solar cell. 2023 Asia-Pacific Solar Research Conference. Melbourne 5 – 7 December 2023. (Plenary)

Hoex, B. (2023). Quality Risks of New PV Cell Technologies: TOPCon and HJT. 34th International Photovoltaic Science and Engineering Conference, Shenzhen, 6-10 November 2023.

Huang, H., Ata, S. & Rougieux, F.E. (2022). Prospects of off-grid green mining opportunities in Australia. World Renewable Energy Congress 2022. Perth 4 - 9 December 2022.

Huang, H., Ata, S. & Rougieux, F.E. (2023). Decarbonising Australia Off-grid Mining via Hybrid Microgrid. World Renewable Energy Congress 2023. Kuala Lumpur, Malaysia. 16 - 20 July 2023.

Huang, H., Ata, S. & Rougieux, F.E. (2023). The role of demand-side flexibility in decarbonising copper ore processing. World Mining Congress 2023. Brisbane, 26–29 June

Huang, J., Li, J., Sun, H., Conga, J., Privat, K., Yaob, Y., Chin, R.L., Yuan, X., He, M., Sun, K., Green, M.A. & Hao, X. (2023). Loss Mechanism Analysis on High-Efficiency Kesterite Solar Cell Using Multi-Platform Electron Microscopy based Characterization techniques. 34th International Photovoltaic Science and Engineering Conference, Shenzhen, 6-10 November 2023.

Huang, K. (2023). Structural and Chemical Crosslinking Interface for Efficient and Stable Perovskite Solar Cells. 2023 Asia-Pacific Solar Research Conference. Melbourne 5 – 7 December 2023.

Ibarra Michel, J.D.J., Yan, D., Bullock, J., Tuan Le, A.H. & Hameiri Z. (2023). Ionic-Compounds as Work Function Modifier Layers for Electron Extraction in Crystalline Silicon Solar Cells

Ismael, M. (2023). Exceptional Si Surface Passivation of Metal-Oxide Contacts Achieved by Chlorination Using TiCl4. 2023 Asia-Pacific Solar Research Conference. Melbourne 5 – 7 December 2023.

Javier, G.M. (2023). Enhancing luminescence images through deep learning-based point spread function correction. 2023 Asia-Pacific Solar Research Conference. Melbourne 5 – 7 December 2023.

Javier, G.M., Bucquet. H., Wright, B., Zhu Y., Wu, T.-C., Trupke ,T. & Hameiri, Z. (2023). Al-extraction of spatial photoluminescence and series resistance from electroluminescence images. 2023 Asia-Pacific Solar Research Conference. Melbourne 5 – 7 December 2023.

Javier, G.M.N., Dwivedi, P., Trupke, T. & Hameiri, Z. (2023). Decoupling open-circuit voltage and series resistance in electroluminescence images through deep learning. IEEE 50th Photovoltaics Specialists Conference (PVSC), Puerto Rico, 11 June 2023.

Javier, G.M.N., Evans, R., Dwivedi, P. Trupke, T. & Hameiri, Z. (2023). Advanced production line monitoring with time-lag sequential analysis. IEEE 50th Photovoltaics Specialists Conference (PVSC), Puerto Rico, 11 June 2023.

Jialin, C., Mingrui, H., Jialiang, H., Karen, P., Jun Sung, J., Yi-sheng, C., Jianjun, L., Limei, Y., Jinhyeok, K., Julie, C., Martin, G., Xiaojing,H.(2023). Unveiling the mystery role of Ge in CZTSSe solar cells by advanced micro-to-atom scale characterizations. The 27th Australian Conference on Microscopy and Microanalysis, Perth

Jiang, Y. & Ekins-Daukes, N. (2023). Ultra-Efficient Coloured Photovoltaic Devices for Buildings and Vehicles. 3rd Global Hydrogen and Renewable Energy Conference and Exhibition, Melbourne, 27-29 November 2023.

Johns, A. (2023). Mechanical Load Testing for High Wind Load on Novel PV Deployment Technology. 2023 Asia-Pacific Solar Research Conference. Melbourne 5 – 7 December 2023.

K. Sun, (2023). Kesterite-based photocathode for photoelectrochemical CO2 reduction and NH3 production, Materials for Sustainable Development Conference (MATSUS), València, Spain.

K. Sun, A. Wang, X. Hao, (2023). Record-level Cd-free kesterite Cu2ZnSnS4 solar cell with over 800 mV open-circuit voltage enabled by Ge incorporation, 13th European Kesterite+ Workshop, Barcelona, Spain.

Kasher, T., Kalizewski, L. M., Baan, M., Yi, C., Soeriyadi, A. H., Chang, A., Römer, U., Coletti, G., Bremner, S. P., Grassman, T. J. & Ringel, S. A. (2023). Advances in GaAsP Top Cells for Use in GaAsP/Si Tandems. IEEE 50th Photovoltaics Specialists Conference (PVSC), Puerto Rico, 11 June 2023.

Kessel, A. (2023). Perovskite Patterning via Printed Molecular Templates Towards Scalable Semi- Transparent Solar Cells. 2023 Asia-Pacific Solar Research Conference. Melbourne 5 – 7 December 2023.

Khan, M.U. (2023). Understanding potential-induced degradation (PID) degradation of the shunting type and its recovery. 2023 Asia-Pacific Solar Research Conference. Melbourne 5 – 7 December 2023.

Kim, M., Wang, L., Zhang, Y., Underwood, R., Drury, S. & Hallam, B. (2023). Roadmap towards sustainable SHJ solar cell design. SiliconPV 2022, the 12th International Conference on Crystalline Silicon Photovoltaics.

Le, A. H. T., Temperature-dependent performance of 50 µm thick SHJ solar cells for space applications. 2023 Asia-Pacific Solar Research Conference. Melbourne 5 – 7 December 2023.

Le, A.H.T. Balaji, P., Augusto, A. & Hameiri, Z. (2023). Temperature-dependent performance of ultra-thin silicon heterojunction solar cells for space applications. IEEE 50th Photovoltaics Specialists Conference (PVSC), Puerto Rico, 11 June 2023.

Le, A.H.T., Balaji, P., Rodriguez, J., Augusto, A. & Hameiri, Z. (2023). Temperature-dependent performance of 50 µm thick silicon heterojunction solar cells for space applications. 2023 Asia-Pacific Solar Research Conference. Melbourne 5 – 7 December 2023.

Le, A.H.T., Hameiri, Z. & Augusto, A. (2023). Lightly doped silicon heterojunction solar cells in relevant field conditions of illumination and temperature', SiliconPV, Konstanz. 10 – 14 April 2023.

Le, A.H.T.. Industrial (2023). Czochralski n-type Si wafers: gettering effectiveness and possible bulk limiting defects. 2023 Asia-Pacific Solar Research Conference. Melbourne 5 – 7 December 2023.

Lee Chin, R., Soufiani, A.M., Zheng, J., Pusch, A., Choi, E., Ho-Baillie, A., Trupke, T., Hameiri Z., Fassl, P. & Paetzold, U. (2023). Surface Saturation Current Densities of Perovskite Thin Films from Suns-Photoluminescence Quantum Yield Measurements. 40th European Photovoltaic Solar Energy Conference, Lisbon, 18-22 September 2023.

Leung, Tik Lun,et al (2023), Analysis of the circularity for PV recycling aiming at net-zero in 2050. 2023 Asia-Pacific Solar Research Conference. Melbourne 5 – 7 December 2023.

Li, C. (2023). Comparative study on the prediction of photovoltaic power output between physical and machine learning. 2023 Asia-Pacific Solar Research Conference. Melbourne 5 – 7 December 2023.

Li, C., Liu, Z., Zhang, P. & Hao, X. (2023). Transparent conductive adhesive (TCA) intermediate layers for tandem solar cells. 34th International Photovoltaic Science and Engineering Conference, Shenzhen, 6-10 November 2023.

Li, C., Liu, Z., Zhang, P., Xiao, B., Zhang, S. & Hao, X. (2023). Evaluation of prediction models for forecasting photovoltaic power output. 34th International Photovoltaic Science and Engineering Conference, Shenzhen, 6-10 November 2023.

Li, G., Wang, X., Madumelu, C., Toth, P., van den Hengel, L., Grozema, F., Conibeer, G. & Hoex, B. (2023). Revisiting Silicon Solar Cells for Space - Electron Irradiation of TOPCon Si Solar Cells. 34th International Photovoltaic Science and Engineering Conference, Shenzhen, 6-10 November 2023.

Li, Y, Wright, B. & Hameiri, Z. (2023). Distortion correction for real-world solar panel images based on deep learning. Melbourne, Australia, presented at Asia-Pacific Solar Research Conference, Melbourne, Australia, 05 December 2023

Li, Y., Johns, T., Haque, F., Element, A., Anderson, K., Duck, B., Duffy, N. & Wilson, G. (2023). Perovskite fabrication using chemical vapour deposition (CVD) technology. 34th International Photovoltaic Science and Engineering Conference, Shenzhen, 6-10 November 2023.

Liao, C.-W. (2023). Quasi-two-dimensional perovskites for stable single junction and perovskitesilicon double junction. 2023 Asia-Pacific Solar Research Conference. Melbourne 5 – 7 December 2023.

Liao, Y. (2023). Super-Efficient Coloured PV for Vehicles. 2023 Asia-Pacific Solar Research Conference. Melbourne 5 – 7 December 2023.

Liao, Y., Keevers, M., Ekins-Daukes, N.J., Green, M. & Jiang, Y.Super-Efficient Coloured PV for Vehicles. 34th International Photovoltaic Science and Engineering Conference, Shenzhen, 6-10 November 2023.

Liu, A. (2023). Silicon Materials for Photovoltaic Applications. 3rd Global Hydrogen and Renewable Energy Conference and Exhibition, Melbourne, 27-29 November 2023.

Liu, M. (2023). Electroplated Copper Metal Contact for GaAs Solar Cells. 2023 Asia-Pacific Solar Research Conference. Melbourne 5 – 7 December 2023.

Liu, X., Hao, X., Green, M.A. et al. (2-23). Perovskite solar cells based on spiro-OMeTAD stabilised with an alkylthiol additive. 34th International Photovoltaic Science and Engineering Conference, Shenzhen, 6-10 November 2023.

Liu, Y. Challenges of Implementing Performance-to-Peers Algorithms for Fault Detection in Distributed Commercial PV Systems. 34th International Photovoltaic Science and Engineering Conference, Shenzhen, 6-10 November 2023.

Liu, Y., Duran, E., Bruce, A., Yildiz, B., Martell, C. & Rougieux, F. (2023). Challenges of Implementing Performance-to-Peers Algorithms for Fault Detection in Distributed Commercial PV Systems. IEEE 50th Photovoltaics Specialists Conference (PVSC), Puerto Rico, 11 June 2023.

Lu, B. (2023). All-Electric Australia. 3rd Global Hydrogen and Renewable Energy Conference and Exhibition, Melbourne, 27-29 November 2023.

Macdonald, D. (2023). Towards 26% Efficient Silicon Solar Cells in Mass Production. 3rd Global Hydrogen and Renewable Energy Conference and Exhibition, Melbourne, 27-29 November 2023.

Macdonald, D. Industrial silicon solar cells with passivating contacts – TOPCon versus silicon heterojunctions. 2023 Asia-Pacific Solar Research Conference. Melbourne 5 – 7 December 2023.

Mahboubi, A., Soufiani Chin, R.L., Fassl, P., Mahmud, M.A., Pollard, M., Zheng, J., Weber, J., Ho-Baillie, A., Trupke, T., Hameiri, Z. (2023). Implied open-circuit voltage imaging of solar cells and cell precursors: Single bandpass filter method. SiliconPV, Konstanz. 11 – 14 April 2023.

Mahmud, M.A. (2023). Halogenated Polycyclic Aromatic Hydrocarbon Treatment for Perovskite-OPV Tandem with Record FF. 2023 Asia-Pacific Solar Research Conference. Melbourne 5 – 7 December 2023.

Mao, W., Hall, C.R., Bernardi, S. et al. (2023). Light-induced reversal of ion segregation in mixed-halide perovskites. Nat. Mater. 20, 55–61 (2021). ICMAT Conference. Singapore, 26 - 30 June, 2023

Meng, Z., Xiaojing, H et al. (2023) Methylammonium-free perovskite inks for gas-quenching fabrication of perovskite films and solar cells. 2023 Asia-Pacific Solar Research Conference. Melbourne 5 – 7 December 2023.

Meng, Z., Xiaojing, H et al. (2023) Gas-quenching inks for methylammonium-free perovskite solar cells, The International Conference on Materials Innovation 2023, Brisbane.

Michel JI; Le HTA; Yan D; Berghuis W-J; Macco B; Hameiri Z; Bullock J. (2023). Ionic compounds for electron extraction in low-temperature-processed crystalline silicon solar cells. 40th European Photovoltaic Solar Energy Conference, Lisbon, 18-22 September 2023.

Michel, J.I., Yan, D., Chen, W. & Bullock, J. (2023). Towards low-damage transparent conductive oxide sputtering for high-efficiency photovoltaics. 2023 Asia-Pacific Solar Research Conference. Melbourne 5 – 7 December 2023.

Mingrui, H., Xiaojing, H et al. (2023). Revealing the role of Ag alloying in metal precursors in kesterite thin films and solar cells. 13th European Kesterite+ Workshop, Barcelona.

Mingrui, H., Xiaojing, H et al. (2023). Controlling formation of kesterite thin film through pre-alloying Ag in metal precursor. 34th International Photovoltaic Science and Engineering Conference, Shenzhen, 6-10 November 2023.

Nguyen, D.-T. (2023). A Research on Perovskite Solar Cells' Tolerance under Proton Radiations. 2023 Asia-Pacific Solar Research Conference. Melbourne 5 – 7 December 2023.

Ni, S., Zheng, J., Ho-Baillie, A., Trupke, T. & Hameiri, Z. (2023). Zand, S., Chin, R.L., Zhu, Y., Weber, J.W., Wang, G., Luminescence-based implied voltage imaging of tandem solar cells via bandpass filter method. 34th International Photovoltaic Science and Engineering Conference, Shenzhen, 6-10 November 2023.

Nielsen, M. P., Sazzad, M. H., Pusch, A., Pearce, P. M., Reece, P. J. & Ekins-Daukes, N. J. (2023). A Direct Comparison of Thermoradiative and Thermophotovoltaic Operation of HgCdTe Photodiodes. IEEE 50th Photovoltaics Specialists Conference (PVSC), Puerto Rico, 11 June 2023.

Ouyang, Z. (2023). Outdoor PL imaging applications for module performance testing in PV power plants. 34th International Photovoltaic Science and Engineering Conference, Shenzhen, 6-10 November 2023.

Pai, N., Sutherland, L. J., Scully, A., Gao, M. & Angmo, D. (2023). Low-temperature and ambient processable all-inorganic solar cells. 2023 Asia-Pacific Solar Research Conference. Melbourne 5 – 7 December 2023.

Pan, Y. Kang, D., Yan, D., Wang, J., Zheng, P., Yang, J., Zhang, X. & Bullock, J. (2023). Ex-situ Doping of Polysilicon Hole Contacts via Electron-Beam Boron Evaporation. 2023 Asia-Pacific Solar Research Conference. Melbourne 5 – 7 December 2023.

Pearce, P. M., Halme, J., Jiang, J. Y., Elsehrawy, F. & Ekins-Daukes, N. J. (2023). Efficiency Limits for Multi-Junction Coloured Photovoltaics. IEEE 50th Photovoltaics Specialists Conference (PVSC), Puerto Rico, 11 June 2023.

Poddar, S., Kay, M., Prasad, A., Evans, J.P. & Bremner, S.P. (2023). Impact of Climate Change on Future Solar Resource Variability and Intermittency across Australia. 40th European Photovoltaic Solar Energy Conference, Lisbon, 18-22 September 2023.

Qian, C. Sun, K., Green, M.A., Hoex, B. & Hao, X. (2023). Single-Junction Bifacial Sb2(S,Se)3 Solar Cells. 40th European Photovoltaic Solar Energy Conference, Lisbon, 18-22 September 2023.

Qian, C., Sun, K., Green, M., Hoex, B. & Hao, X. (2023). Single-Junction Bifacial and Semitransparent Sb2(S,Se)3 Solar Cells. IEEE 50th Photovoltaics Specialists Conference (PVSC), Puerto Rico, 11 June 2023.

Rougieux, F. (2023). Actionable Insights: A Multi-algorithm approach to PV Performance Diagnostics. 2023 Asia-Pacific Solar Research Conference. Melbourne 5 – 7 December 2023.

Rougieux, F. E., Hossain, M. A. & Hoex, B. (2023). Density functional theory to calculate accurate defect energy levels in silicon. Siliconpv 2022, the 12th International Conference on Crystalline Silicon Photovoltaics.

Sarsour, M., Wright, B. & Hameiri, Z. 2023, Photovoltaic module performance and degradation analysis. 2023 Asia-Pacific Solar Research Conference. Melbourne 5 – 7 December 2023.

Sazzad, M.H. (2023). Power extraction from a thermoradiative operation and its possible applications. 2023 Asia-Pacific Solar Research Conference. Melbourne 5 – 7 December 2023.

Schmidt, T. W., Ekins-Daukes, N. J., Tayebjee, M., Nielsen, M. P., McCamey, D. R., Jiang, J. Y., Hoex, B., Ciesla, A., Pearce, P. M., Chang, N., Beves, J. E., Munday, J. N. & Bermel, P. (2023). Organic multiple exciton generation and silicon (OMEGA Si). New Concepts in Solar and Thermal Radiation Conversion V.

Sen, C. (2023). Buyer Aware? TOPCon's Reliability Issues in Comparison with PERC PV modules after Damp Heat Testing. 2023 Asia-Pacific Solar Research Conference. Melbourne 5 – 7 December 2023.

Chandany Sen, C., Chan, C., Wu, X., Wang, H., Umair Kha, M.,Mao, L., Jaubert, J.-N., Jiang, F., Zhang, and Hoex, B. (2023). The role of Na+ contamination in humidity-induced degradation in silicon HJT cells. 2023 Asia-Pacific Solar Research Conference. Melbourne 5 – 7 December 2023.

Sen, C. (2023). Hidden Fingerprints: How Solar Cell Handling Leads to Damp Heat Failures in Silicon Heterojunction Technology. 34th International Photovoltaic Science and Engineering Conference, Shenzhen, 6-10 November 2023.

Sen, C., Wang, H., Wu, X., Khan, M.U., Chan, C., Hoex,B., Mao, L., Jiang, F. & Zhang, G. (2023). L2O3 Barrier Layers: a Novel Approach to Preventing Humidity-Induced Failure in Heterojunction Solar Modules. 40th European Photovoltaic Solar Energy Conference, Lisbon, 18-22 September 2023.

Seo, G. (2023). A highly effcient perovskite solar cells via improved carrier management. 2023 Asia-Pacific Solar Research Conference. Melbourne 5 – 7 December 2023.

Sepalage, G. (2023). Scalable Lamination Techniques for Low- Cost Perovskite Solar Cells. 2023 Asia-Pacific Solar Research Conference. Melbourne 5 – 7 December 2023.

Sharma, A.S., Bremner, S.P., Nielsen, M.P., Tayebjee, M.J.Y., Rougieux, F.E., Ekins-Daukes, N.J. & Andreas Pusch, A. (2023). The Role of Carrier-Carrier Equilibration in Hot Carrier Solar Cells. EDISON 22 - The 22nd International Conference on Electron Dynamics in Semiconductors, Optoelectronics and Nanostructures. Münster, Germany. 14 - 18 August 2023.

Shi, X., Li, W., Zhang, M., Liu, Y., Chen, X., Zhang, C., Zhao, W., Zhong, L. & Gao, J. (2023). Space Charge Distribution in Submarine Cable Factory Joint Insulation. 2023 IEEE 4th

Song, N. (2023). Multilayer Antireflection Coating for Solar Module Glass. 34th International Photovoltaic Science and Engineering Conference, Shenzhen, 6-10 November 2023.

Song, N., Chang, N., Zeng, Y., Jiang, Y., Wu, Y., Zhou, Z., Keevers, M., Egan, R., Green, M. & Gentle, A. (2023). Multifunctional Coatings for Solar Module Glass. 40th European Photovoltaic Solar Energy Conference, Lisbon, 18-22 September 2023.

Sun, K. (2023). The path towards high efficiency high bandgap Cu 2 ZnSnS 4 solar cells. 3rd Global Hydrogen and Renewable Energy Conference and Exhibition, Melbourne, 27-29 November 2023.

Sun, K., Qian, C., Green, M., Hoex, B. & Hao, X. (2023). High Efficiency Bifacial and Semitransparent Sb2(S,Se)3 Solar Cells. 34th International Photovoltaic Science and Engineering Conference, Shenzhen, 6-10 November 2023.

Sutherland, L. J., Benitez-Rodriguez, J. F., Vak, D., Yan, S., Pai, N., Jasieniak, J., Gao, M., Simon, G. P. & Weerasinghe, H. (2023). Revolutionizing Scalable Perovskite Solar Cells with Isostatically Deposited Carbon Electrodes. 2023 Asia-Pacific Solar Research Conference. Melbourne 5 – 7 December 2023.

Sutherland, L. J., Benitez-Rodriguez, J. F., Vak, D., Yan, S., Pai, N., Jasieniak, J., Gao, M., Simon, G. P. & Weerasinghe, H. (2023). Versatile carbon electrodes for highly efficient small, large, rigid, and flexible perovskite solar cells. 1st International Conference on Carbon Electrode-based Perovskite Solar Cells, Online, 11-12 October.

Sutherland, L. J., Benitez-Rodriguez, J. F., Vak, D., Yan, S., Pai, N., Jasieniak, J., Gao, M., Simon, G. P. & Weerasinghe, H. (2023). Scalable fabrication of highly efficient perovskite solar cells using vacuum-free, solvent-free, and roll-to-roll compatible printed electrodes. 15th International Conference on Hybrid and Organic Photovoltaics (HOPV), London, 12-14 June 2023.

Tabi, G.D., Daniel Walter, D., Jun Peng, J., Duong, T., Naeimeh Mozaffari, N., Catchpole, K.R., Weber, K.J. and White, T.P.(2023). Simulation of nanohole point contacts for perovskite solar cells with insulating passivation layers. 2023 Asia-Pacific Solar Research Conference. Melbourne 5 – 7 December 2023.

Tan, V., Deng, R. & Egan, R. (2023). Solar Photovoltaic Waste and Resource Potential Projections in Australia, 2022-2050. 40th European Photovoltaic Solar Energy Conference, Lisbon, 18-22 September 2023.

Teymouri, A. (2023). Deflection of utility modules on 5B™s mounting system under static wind conditions. 2023 Asia-Pacific Solar Research Conference. Melbourne 5 – 7 December 2023.

Thomas, I. (2023). Spectrally selective modules for Agrivoltaics. 2023 Asia-Pacific Solar Research Conference. Melbourne 5 – 7 December 2023.

Truong, T., Kang, D., Wang, E.-C., Wang, J., Phang, S.P., MacDonald, D. & Stuckelberger, J. (2023). Ex-situ Phosphorus-doped Poly-Si Passivating Contacts for High Efficiency Solar Cells via Sputtering. 34th International Photovoltaic Science and Engineering Conference, Shenzhen, 6-10 November 2023.

Trupke, T. (2023). Photoluminescence imaging applications across the PV value chain: from ingots to systems. 34th International Photovoltaic Science and Engineering Conference, Shenzhen, 6-10 November 2023.

Vak, D. (2023). Automatic Roll-to-Roll Experiments and Fully Roll-to-Roll Fabricated Perovskite PV Modules. ChinaNano 2023, Beijing, 26-28 August.

Vaqueiro Contreras, M. (2023). Solar PV Supply Chain and Australia's Bottom-up Cost Model. 2023 Asia-Pacific Solar Research Conference. Melbourne 5 – 7 December 2023.

Verlinden, P.J. (2023). Going to multi-terawatt annual production with which cell technology? 34th International Photovoltaic Science and Engineering Conference, Shenzhen, 6-10 November 2023. (Plenary/ Keynote)

Wagner-Mohnsen, H., Wasmer, S., Klöter, B., Altermatt, P.P. & Ernst, M. (2023). Using Machine Learning to Predict Module Performance from Cell and Module Parameters. 40th European Photovoltaic Solar Energy Conference, Lisbon, 18-22 September 2023.

Wang, A., Sun, K., Huang, J., Green, M.A. & Hao, X. (2023). Over 11% Efficiency Cd-free High Bandgap Cu2ZnSnS4 Solar Cells Enabled by Bulk and Interface Engineering. 34th International Photovoltaic Science and Engineering Conference, Shenzhen, 6-10 November 2023.

Wang, G. (2023). Hole-selective contact engineering for perovskite single-junction and tandem solar cell. 2023 Asia-Pacific Solar Research Conference. Melbourne 5 – 7 December 2023.

Wang, G., Zhen, J., Duan, W., Yang, J., Mahmud, M.A., Lian, G., Cheng, C., Ding, K. & Ho-Baillie, A. (2023). Molecular engineering of self-assembled monolayer hole selective layer for high bandgap perovskite and highly efficient and stable perovskite-silicon tandem solar cells. 34th International Photovoltaic Science and Engineering Conference, Shenzhen, 6-10 November 2023.

Wang, J., Phang, S.P., Truong, T.N., Li, Z., Nguyen, H.T., MacDonald, D. & Stuckelberger, J. (2023). Phosphorus- and Boron-Doped Poly-Si/SiO_x Passivating Contacts via Inkjet Printing. 34th International Photovoltaic Science and Engineering Conference, Shenzhen, 6-10 November 2023.

Wang, L. (2023). Study on material requirement along the silicon production chain for terawatt scale PV deployment. 2023 Asia-Pacific Solar Research Conference. Melbourne 5 – 7 December 2023.

Wang, L.,Sun, Z., Perez-Wurfl, I., Chang, Y., Pollard, M., Qi., F., Kim, M., Chen, R. & Hallam,B. (2023). Impacts of Silicon Thickness on Cell Efficiency and Sustainable Deployment for Terawatt Scale Silicon Solar Cell Production. 34th International Photovoltaic Science and Engineering Conference, Shenzhen, 6-10 November 2023.

Wang, R, Zhang, Y., Zhang, C., Zhang, J. & Conibeer, G. (2023). Study the thermalization mechanisms in CdSe/CdS core/shell low-dimensional systems for hot carrier multi-junction solar cells. 34th International Photovoltaic Science and Engineering Conference, Shenzhen, 6-10 November 2023.

Wang, S. (2023). A roadmap towards emission lean and low-cost PV module manufacturing using decarbonised electricity. 2023 Asia-Pacific Solar Research Conference. Melbourne 5 – 7 December 2023.

Wang, S. (2023). Impact of different PV mounting systems on yield, material consumption and emissions intensity. 2023 Asia-Pacific Solar Research Conference. Melbourne 5 – 7 December 2023.

Wang, Y., Zhou, S., Liu, X., Sun, K.Lee, M., Liu, Z., Zhang, M.Bai, Y.,Hameiri, Z. & Hao, X. (2023). Multifunctional Interfacial Layers for Reproducible and Efficient p-i-n Perovskite Solar Cells. 34th International Photovoltaic Science and Engineering Conference, Shenzhen, 6-10 November 2023.

Weber, T. (2023). Estimating Intra-Day to Long-Term Energy Storage Needs for Grids Dominated by Solar. 2023 Asia-Pacific Solar Research Conference. Melbourne 5 – 7 December 2023.

Wilson, G. (2023). Tuning the chemistry of solution-less perovskite processes for PVK-silicon tandem cells. 34th International Photovoltaic Science and Engineering Conference, Shenzhen, 6-10 November 2023.

Wilson, T. & Ekins-Daukes, N. (2023). Suitability of GaAsBi as a Candidate Junction in a III-V Multi-Junction Solar Cell. IEEE 50th Photovoltaics Specialists Conference (PVSC), Puerto Rico, 11 June 2023.

Wright, B., Petesic, J., Dawson, T. & Hameiri, Z. (2023). Automated photovoltaic module quality assessment: defect identification and classification from luminescence images using generative representation learning. IEEE 50th Photovoltaics Specialists Conference (PVSC), Puerto Rico, 11 June 2023.

Wright, B., Sharma, R., Petesic, J., Dawson, T. & Hameiri, Z. 2023, 'Automated photovoltaic module quality assessment from luminescence images: defect classification using unsupervised machine learning. 2023 Asia-Pacific Solar Research Conference. Melbourne 5 – 7 December 2023.

Wu, X. (2023). Addressing Sodium Ion-Related Degradation in SHJ Cells by the Application of nanoscale barrier layer. 2023 Asia-Pacific Solar Research Conference. Melbourne 5 – 7 December 2023.

Wu, X., Sen, C., Wang, H., Wang, X., Wu, Y., Khan, M.U., Mao, L., Jiang, F., Xu, T., Zhang, Q. & Hoex, B. (2023). Addressing Sodium Ion-Related Degradation in SHJ Cells by the Application of Nano-Scale Barrier Layers. 34th International Photovoltaic Science and Engineering Conference, Shenzhen, 6-10 November 2023.

Xiaojie Y., Jianjun L., Kaiwen S., Jialiang H., Xin C., Ao W., Bram H., Martin G. and Xiaojing H. (2023) Improved Carrier Collection Efficiency in CZTS Solar Cells by Li-enhanced Liquid-Phase-Assisted Grain Growth. 34th International Photovoltaic Science and Engineering Conference, Shenzhen, 6-10 November 2023.

Xu Liu, Xiaojing, H et al. (2023). Perovskite solar cells based on spiro-OMeTAD stabilised with an alkylthiol additive. 34th International Photovoltaic Science and Engineering Conference, Shenzhen, 6-10 November 2023.

Yamaguchi, M., Araki, K., Zhang, Y., Hallam, B., Kojima, N. & Ohshita, Y. (2023). Consideration for importance of concentrating photovoltaics (PV) toward TW-scale PV production. In: Martin, R. H., Viallon, R., Araki, K., Datas, A., Nishioka, K. & Shimizu, M. (eds.) 18th International Conference on Concentrator Photovoltaic Systems (CPV-18) 13th World Conference on Thermophotovoltaic Generation of Electricity (TPV-13). Miyazaki, Japan. 25 – 27 April: AIP Conf. Proc. 2842(1), 020005.

Yamaguchi, M., Araki, K., Zhang, Y., Hallam, B., Kojima, N. & Ohshita, Y. (2023). Consideration for importance of concentrating photovoltaics (PV) toward TW-scale PV production. 18th International Conference on Concentrator Photovoltaic Systems (Cpv-18) and 13th World Conference on Thermophotovoltaic Generation of Electricity (TPV-13).

Yan, D., Michel, J. I., Pan, Y., Phang, S. P., Macdonald, D., Shen, H., Duan, L., Catchpole, K., Yang, J., Zheng, P., Zhang, X., Jin, H. & Bullock, J. (2023b). Improving the Stability of Polycrystalline Silicon Passivated Contacts Using Titanium Dioxide. IEEE 50th Photovoltaics Specialists Conference (PVSC), Puerto Rico, 11 June 2023.

Yang, Z., Perz-Wurfl, I., Jiang, J.Y., Gentle, A. & Ekins-Daukes, N.J. (2023) Vehicle-Integrated Photovoltaics (VIPV): Insights into Photovoltaic Performance & Energy Generation Modelling. 34th International Photovoltaic Science and Engineering Conference, Shenzhen, 6-10 November 2023.

Yi, J. (2023). CO2 laser-assisted ultrafast crystallization for highly efficient perovskite solar cells. 2023 Asia-Pacific Solar Research Conference. Melbourne 5 – 7 December 2023.

Yuan, X., Li, J., Sun, K., Huang, J., Hoex, B., Green, M.A. & Hao, X. (2023). Improved Carrier Collection Efficiency in CZTS Solar Cells Enabled by Li-enhanced Liquid-phase-assisted Grain Growth. 34th International Photovoltaic Science and Engineering Conference, Shenzhen, 6-10 November 2023.

Yun, J. S. (2023). Microstructural Inhomogeneity and Defect Sites in Wide Bandgap Mixed Perovskites: A Scanning Probe Microscopy Study. Proceedings of the International Conference on Perovskite Thin Film Photovoltaics and Perovskite Photonics and Optoelectronics.

Zandi, S., Nie, S., Lee Chin, R., Zhu, Y., Weber, J., Zheng, J., Ho-Baillie, A., Trupke, T. & Hameiri, Z. (2023). Implied voltage images of each subcell in perovskite/Si tandem solar cells using luminescence measurements. 2023 Asia-Pacific Solar Research Conference. Melbourne 5 – 7 December 2023.

Zandi, S., Soufiani, A.M., Hameiri, Z. & Trupke, T. (2023). Novel Method for the Extraction of the Implied Voltages of Silicon Wafers and Solar Cells from Luminescence-Based Measurements. 40th European Photovoltaic Solar Energy Conference, Lisbon, 18-22 September 2023. (Student Awards Presentation Winner).

Zeng, Y., Green, M.A. & Jiang, J.Y. (2023). Advanced Multi-layer AR Coatings to Improve Durability of Solar Modules. 34th International Photovoltaic Science and Engineering Conference, Shenzhen, 6-10 November 2023.

Zeng, Y., Green, M. & Jiang, J. Y. (2023). Multi-Layer Dense Antireflection Coatings. 2023 IEEE 50th Photovoltaic Specialists Conference (PVSC), 1-3.

Zhang, M. (2023). Methylammonium free perovskite inks for gas-quenching fabrication of perovskite films and solar cell. 2023 Asia-Pacific Solar Research Conference. Melbourne 5 – 7 December 2023.

Zhang, Y., Wang, L., Chang, Y.-C., Chen, R., Chan, C. & Hallam, B. (2023). Silver-Lean Screen-Printed Contacts for Industrial Silicon Solar Cells. 34th International Photovoltaic Science and Engineering Conference, Shenzhen, 6-10 November 2023.

Zhao, J. (2023). Formamidinium-Caesium Perovskite Solar Cells and Modules from Lead Acetate-Based Precursor. 2023 Asia-Pacific Solar Research Conference. Melbourne 5 – 7 December 2023.

Zhao, J., Fürer, S. O., McMeekin, D. P., Lin, Q., Lv, P., Ma, J., Tan, W. L., Wang, C., Tan, B., Chesman, A. S. R., Yin, H., Scully, A. D., McNeill, C. R., Mao, W., Lu, J., Cheng, Y.-B. & Bach, U. (2023). Efficient and stable formamidinium–caesium perovskite solar cells and modules from lead acetate-based precursors. Energy & Environmental Science 16, 138. HOPV Conference. London, UK, 12 - 14 June, 2023.

Zhao, J., Fürer, S. O., McMeekin, D. P., Lin, Q., Lv, P., Ma, J., Tan, W. L., Wang, C., Tan, B., Chesman, A. S. R., Yin, H., Scully, A. D., McNeill, C. R., Mao, W., Lu, J., Cheng, Y.-B. & Bach, U. (2023). Efficient and stable formamidinium–caesium perovskite solar cells and modules from lead acetate-based precursors. Energy & Environmental Science 16, 138. APC Conference. Melbourne, 27 November – 1 December, 2023

Zheng, J. (2023). Exploring the Role of ITO Interlayer to Accelerate the Perovskite Commercialization Prospective. 2023 Asia-Pacific Solar Research Conference. Melbourne 5 – 7 December 2023.

Zheng, J., Duan, W., Ma, F., Ding, K. & Ho-Baillie, A. (2023). The Role of Indium Tin Oxide in Interfacing Perovskite with Steel and Silicon Solar Cells. 34th International Photovoltaic Science and Engineering Conference, Shenzhen, 6-10 November 2023.

Zhu, Y., Chin, R.L., Mussakhanuly, N., Trupke, T. & Hameiri, Z. (2023). Dynamic calibration of injection dependent carrier lifetime from time-resolved photoluminescence. IEEE 50th Photovoltaics Specialists Conference (PVSC), Puerto Rico, 11 June 2023.

8.6 THESES

Ahluwalia, G. (2021). Amphiphilic Block Copolymers for Morphological Control in Bulk Heterojunction Solar Cells. PhD UniMelb

Al-Farsi, M. (2022). Computational materials discovery: Ab initio modelling of new, high-performance semiconductors for top cells in multi-junction tandems on silicon solar cells. PhD UNSW

Buratti, Y. (2023). Machine learning for advanced characterisation of silicon solar cells. PhD UNSW

Chen, Q. (2023). Fabrication of high-efficiency all-inorganic antimony chalcogenide solar cells via architecture modification. PhD UNSW

Choi, E. (2023). Exploring Nanoscale Optoelectronic Properties of Kesterite- and Perovskite-based Devices. PhD UNSW

Dehghanimadvar, M. (2023). Multi-objective Optimization of PV Module Assembly Supply Chain, Concerning Economic, Environmental and Social Impacts. PhD UNSW

Deng, S. (2019). Polysilicon contacts for next-generation industrial silicon solar cells. Masters UNSW

Deng, S. (embargoed). Microfabrication and Design Techniques for Back-Contact Perovskite Solar Cells. PhD Monash

Dubajic, M. (2023). Understanding the structure and dynamics of hybrid lead halide perovskites for photovoltaics. PhD UNSW

Ellis, Ryan. (2020). Synthesis and Ligand Engineering of Colloidal Metal Chalcogenide Nanoparticles for Scalable Solution Processed Photovoltaics. PhD Purdue (hosted by CSIRO)

Guo, Q. (embargoed). Microstructure Characterization of CsPbIBr2 perovskite material with potassium incorporation. PhD Monash

Hosseinabadi, P. (2023). Building Towards Singlet Fission Solar Cells - from photophysics to application. PhD UNSW

Hu, Y. (2018). Moisture Stability of Hybrid Perovskite Solar Cells. PhD Ludwig-Maximilians-Universität München (hosted by CSIRO)

Jafari, Saman. (2022). Investigation of Bulk Defects in p-type Silicon Wafers and Solar Cells. PhD UNSW

Jang, H. (2023). Compositional Modulation of Photoactive Layer for Sn-based Organometal Halide Perovskite Solar Cells. PhD Ulsan National Institute of Science and Technology (embargoed) (hosted by CSIRO)

Kaleem, A. (2023). Changing the Colour of the Sun - Femtosecond Stimulated Raman Spectroscopy Unravels the Photophysics Of Singlet Fission in Polyacene Molecules. PhD UNSW

Le, Huy Tuan Anh (2023). Solar Cells with Passivating Contacts – Investigation of Their Temperature- and Illumination-Dependent Performance and Surface Passivation. PhD UNSW

Lee, M. (2023). Fabrication of High Efficiency Wide Bandgap Perovskite Solar Cells. Masters UNSW

Lee, M. (2023). Fabrication of High Efficiency Wide Bandgap Perovskite Solar Cells. Masters UNSW

Liao, A. (2018). A novel room temperature contacting technique applied to silicon solar cells. Masters UNSW

Lin, Q. (2022). Study of Perovskite Single Crystals for Optoelectronic Applications. PhD Monash

Liu, M. (2023). Cost-effective Copper-plated Metallisation for III-V Solar Cells: A Development Path. PhD UNSW

Madumelu, C.U. (2023). Degradation in next-generation passivating contact solar cells. PhD UNSW

Poduval, G.K. (2022). Indium-free transparent conductive oxides for improved solar cell performance and reliability. PhD UNSW

Samadi, A. (2023). Hydrogenation of Cast-Mono Silicon Solar Cells. PhD UNSW

Sharma, A. (2023). The role of remote valleys in photovoltaic devices. PhD UNSW

Sun, Z. (2023). Low-temperature passivating carrier selective contacts for single-junction silicon solar cells and silicon-based tandem solar cells. PhD UNSW

Tan, X. (2020). Insights into the Mechanisms of Bulk and Surface Related Degradation in Monocrystalline Silicon Solar Cells. Masters UNSW

Tan, Xingru. (2023). Insights into the Mechanisms of Bulk and Surface Related Degradation in Monocrystalline Silicon Solar Cells. PhD UNSW

The, Z. (2018). Optimization of PbS Hole Transport Layer using Hybrid Ligand Treatment. Masters UNSW

Yuan, X. (2023). Developing high-efficiency Cu2ZnSnS4 (CZTS) solar cells by controlling element distribution. PhD UNSW

Zhang, Y. (2023). Novel Metallization Designs to Overcome Challenges of Screen-Printed Contacts in Silicon Solar Cells. PhD UNSW

Zhao, B. (2023). Concepts Toward Efficient Back-Contact Perovskite Solar Cells. PhD Monash

Zhao, J. (embargoed). Strategies for Efficient and Stable Perovskite Solar Cells and Modules. PhD Monash

Zhou, S. (2023). Optimising Cu2ZnSnS4 based Photocathodes for Photoelectrocatalytic Reactions. PhD UNSW

8.7 REPORTS/SUBMISSIONS

Deng, R., Corkish, R., Hallam, B., Thompson, D. (2023). Questions on "Regulation for small electrical products and solar photovoltaic system waste" for public consultation with DCCEEW 2023.

AUSTRALIAN CENTRE FOR ADVANCED PHOTOVOLTAICS

UNSW SYDNEY NSW
2052 AUSTRALIA

Email: acap@unsw.edu.au
Website: acap.org.au

Executive Director: Professor Renate Egan